Organic Rankine cycle as waste heat recovery system for marine application

Screening methodology, modeling and analysis

Sai B. Thimmanoor

SDPO.18.003.m

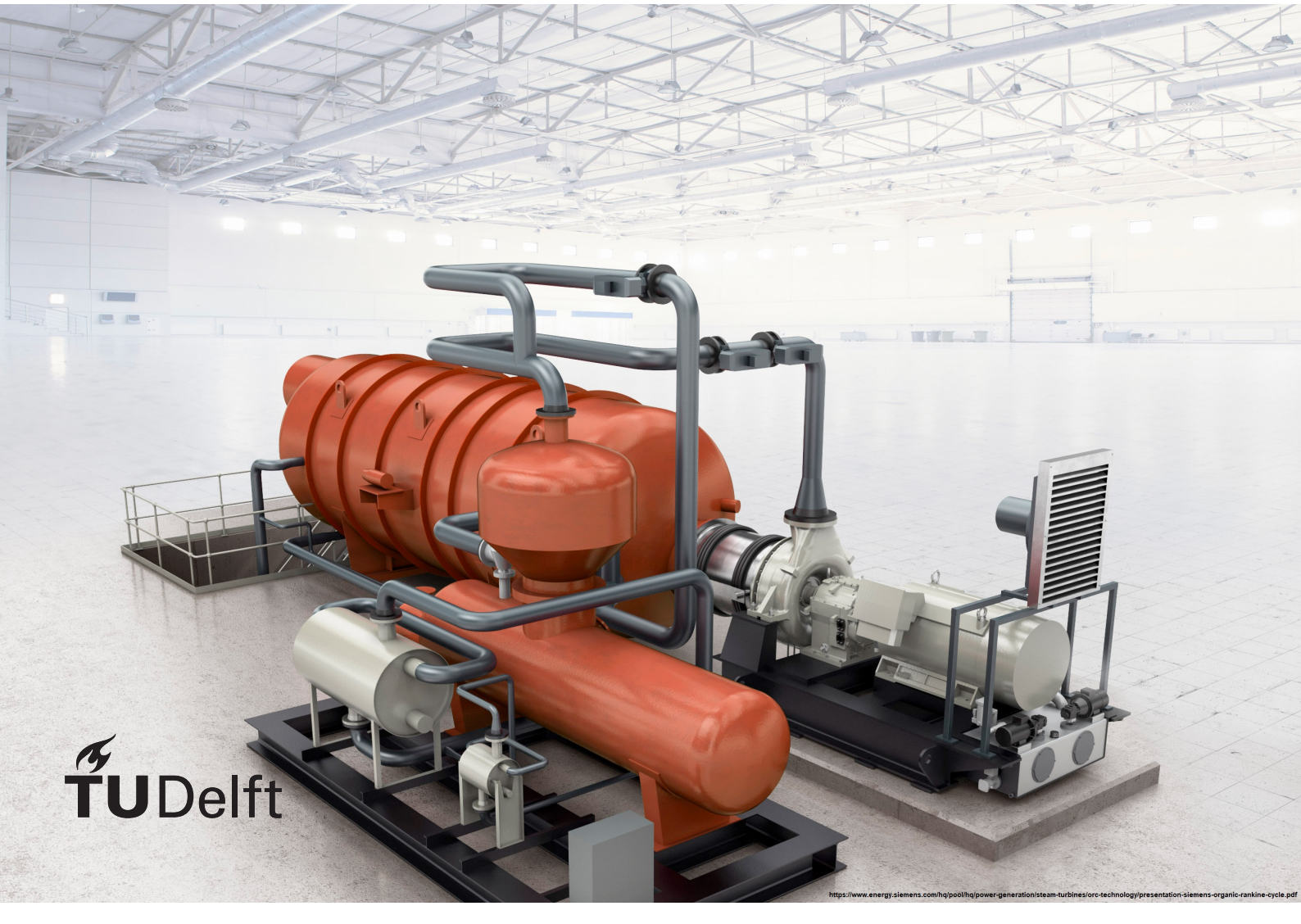

Organic Rankine cycle as waste heat recovery system for marine application

Screening methodology, modeling and analysis

by

Sai B. Thimmanoor

to obtain the degree of Master of Science
at the Delft University of Technology,
to be defended publicly on Monday January 15, 2018 at 09:30 AM.

Student number:	4463994	
Thesis number:	SDPO.18.003.m	
MTI report number:	AO 154	
Thesis duration:	November 01, 2016 – January 15, 2018	
Thesis committee:	Rear-Admiral (ME) ret. ir. K. Visser,	TU Delft, Chairman
	Ir. I. Georgescu,	TU Delft, Daily Supervisor
	Ir. B. T. W. Mestemaker,	IHC MTI, Daily Supervisor
	Dr. ir. C. A. Infante Ferreira	TU Delft, External

An electronic version of this thesis is available at `http://repository.tudelft.nl/`.

TU Delft

This thesis was carried out in collaboration with IHC MTI B.V., a part of Royal IHC of the Netherlands.
Their support and cooperation is hereby gratefully acknowledged.

Preface

Marine technology has always been my field of interest, which was the primary reason that inspired me to pursue this topic, in addition to its potential use as an environment friendly solution to ships.

I thank Rear-Admiral (ME) ret. ir. Klaas Visser for introducing me to this topic and for also heading the thesis committee. The critical review given by him has directed this thesis onto the right path. I am also very grateful to my daily supervisor Ir. Ioana Georgescu for providing guidance at every crucial step. The discussions with her gave me vital insights to resolve the obstacles. Furthermore, I extend my gratitude to Ir. Benny Mestemaker of IHC MTI B.V. for adding the practical dimension to this topic. Finally, I thank the external committee member Dr. ir. C . A. Infante Ferreira for taking out time to be part of the thesis committee.

I specially thank Ir. Theo Woudstra for introducing and teaching the thermodynamic software Cycle-Tempo. His support was significant to shape a major part of this work.

Finally, I cannot thank my parents and my sister enough for being a constant source of motivation and moral support throughout. I thank all my friends for their support as well.

Sai B. Thimmanoor
Delft, January 2018.

Abstract

Carbon dioxide emission into the earth's atmosphere by maritime activities are a concern for the people within and outside the industry. This is because of the environmental impacts that are caused by these greenhouse gas emissions which changes the very chemistry of this planet. These impacts can be mitigated by reducing the CO_2 emissions which can be achieved by several design and/or operational means. Waste heat recovery (WHR) technology is one such means that is capable of reducing emissions. This is achieved by improving the overall fuel efficiency of marine engines which reduces the fuel consumption of the vessel. This improvement is realized by harnessing the heat energy that is expelled by the engine through waste heat sources such as exhaust gas, etc.

Organic Rankine cycle (ORC) is one of many WHR technologies that is capable of harnessing that waste heat energy from the fuel which cannot be utilized by the engine operation alone. ORC as a WHR system (WHRS) is widely implemented in land based applications due to its fluid choice flexibility, plant simplicity and net efficiency. However, it is rather new to the maritime industry because WHRS on-board ships are predominantly based on steam Rankine cycle or turbo-compounding. These systems have their own advantages but ORC-WHRS may outweigh them in certain applications on-board ships. This is especially for electrical power generation from low and medium temperature waste heat sources. However, ORC in marine application encounters challenges unlike seen in land based applications. These challenges are caused by the physical & geometrical constraints, operational profile of the vessel or uncertainties caused at sea.

In this thesis, the implementation of ORC-WHRS to marine engines for exhaust gas is investigated and studied to understand how such an application can be beneficial. Unlike steam Rankine cycle, an ORC system has flexibility in choosing an organic fluid that is suitable based on the application. This flexibility in fluid choices are confronted by the above mentioned maritime related challenges. Hence, a screening methodology is devised in this thesis that finds a suitable fluid based on the waste heat source profile and selection parameters. These selection parameters are necessary to filter out functioning organic fluids that can be limited due to the mentioned challenges. In this thesis, the power density of the ORC plant is the selection parameter used.

As mentioned earlier, the ORC-WHRS may often be subjected to off-design conditions due to the operational profile of the vessel or by uncertainties at sea. Hence, off-design performance is analyzed to study the ORC system when designed at several discrete engine load points. These analysis are carried out in plant models modified from an existing steam based dynamic model and developed into a simple-ORC and a recuperative-ORC dynamic plant models. Sensitivity analysis of these models are also performed to understand uncertainties in the model output corresponding to uncertainties in model input parameter. This analysis is followed by analysis of the dynamic behavior of the ORC plant model to varying load step functions and step duration for plants designed at discrete engine load points.

This thesis can be extended, not only to study how ORC can be used to meet future regulations on CO_2 emissions, but also on operability limitations imposed on ships. The fluid screening approach used here can also be modified based on parameters, such as toxicity, flammability, cost, specific power etc. This can present a realistic approach to an end product that can be safely and economically operated on board.

Contents

List of Figures

List of Tables

Nomenclature

Constants

C_1	$= 9.35 \times 10^{-4}$	Constant	[-]
g	$= 9.81$	Acceleration due to gravity	[m/s^2]
Pr	$= \frac{C_p \cdot \mu}{k}$	Prandtl number	[-]

Variables

A	Area	[m^2]
C_p	Specific heat	[J/(kg· K)]
D	Diameter of tube/impeller	[m]
F	Correction factor	[-]
H	Pump head	[m]
H_0	Pump head at zero volumetric flow rate	[m]
h	Enthalpy	[J/kg]
k	Thermal conductivity	[W/(m·K)]
L	Length	[m]
m	Mass	[kg]
$\dot{m}$	Mass flow rate	[kg/s]
n	Rotational speed	[rps]
N	Number of rows or columns	[-]
p	pressure	[Pa]
$\dot{q}$	Heat	[W]
s	Entropy	[J/(kg· K)]
S_L	Vertical distance between adjacent tubes	[m]
S_T	Horizontal distance between adjacent tubes	[m]
T	Temperature	[$^\circ$C] or [K]
u	Specific internal energy	[J/kg]
U	Overall heat transfer coefficient	[W/(m^2·K)]
V	Volume	[m^3]
$\dot{V}$	Volumetric flow rate	[m^3/s]
$\dot{V}_0$	Pump volumetric flow rate at zero head	[m^3/s]
W	Work done	[W]
x	Vapour quality/Dryness factor	[-]

Symbols

α	Convective heat transfer coefficient	[W/(m^2·K)]
Δ	Difference	
λ	Conductive heat transfer coefficient	[W/(m^2·K)]
η	Efficiency	[-]
μ	Dynamic viscosity	[kg/(s· m)]
ν	Specific volume	[m^3/kg]
ρ	Density	[kg/m^3]
ϕ_m	Mass flow rate	[kg/s]
ϕ_q	Heat transfer	[W]
τ	Torque	[N· m]
υ	Kinematic viscosity	[m^2/s]
ω	Angular velocity	[rad/s]

Subscripts

0	Environment Condition
$cold$	Cold Fluid
$cond$	Condenser
$crit$	Critical
cw	Cooling water
D	Design
eg	Exhaust gas
est	Estimated
$evap$	Evaporator
Gen	Generator
hot	Hot fluid
in	Inlet/Inner
$isen$	Isentropic
liq	Fluid in liquid form
$mean$	Mean/Average
m, el	Mechanical and electrical
M	Metal
nd	non-dimensional
out	Outlet/Outer
row	Rows of tubes
sat	Saturated
SW	Sea Water
th	Thermal
vap	Fluid in vapour form
$wall$	Tube wall
wf	Working fluid

1 Introduction

This chapter covers the introduction of this thesis which includes the background and relevance of the subject, mainly focusing on the reasons of introducing organic Rankine cycle into marine application. This is followed by problem description, objective and thesis outline.

1.1. Background

Most energy consumers on board a ship demand energy in electrical form. These demands are usually satisfied by means of generator sets. The prime mover of such generator sets convert chemical energy of the fuel into heat energy and mechanical energy, that drives the generator. Whereas the heat energy is usually expelled as waste heat to the environment through exhaust gas, cooling water, etc. The heat energy from these expelled sources can be recovered to produce electrical energy to support or relieve the generator sets to meet those electrical energy demands. This not only increases the overall efficiency of the system but also leads to obvious reductions in fuel consumption and carbon dioxide emissions.

There are several promising waste heat recovery (WHR) technologies that are capable of converting waste heat energy into electrical energy. However, all of those may not be feasible for marine application primarily due to volume and weight constraints. Such a WHR system (WHRS) for marine purpose, should not only be relatively smaller and lighter but also simple in operation and operable for a wide range of waste heat source profile (i.e. engine load).

Rankine cycle (RC) based technology is one such system whose operation is simple and capable of satisfying these constraints and conditions. The type of working fluid used in this system is one of the most important parameters that determines the operation simplicity, plant layout and size. The selection of a suitable working fluid is primarily based on the temperature range of the waste heat source of the marine engine at varying operating loads. This fluid should also have a better thermal match between the waste heat and cooling water temperatures to have the maximum possible Carnot efficiency.

Based on the heat balance of marine engines, exhaust gas is the largest source of waste heat energy with relatively higher temperature. The high source temperature is beneficial because, it leads to relatively larger difference between the evaporation and condensation temperatures of the working fluid. Thus leading to relatively higher Carnot efficiency of the system.

Most cargo ships have steam based RC (SRC) as the WHRS for the engine exhaust gas. The steam in such systems are usually used for expansion in heating coils to meet heating demands and not for expansion in turbines for generating electricity. This is because for electricity generation, SRC is beneficial when the source temperatures are relatively higher (as in coal thermal power plants) than the available waste heat sources on-board. Despite this challenge, if SRC-WHRS is used for electricity generation on board ships, it has relatively complex operation, more components/piping and larger size than a wisely selected organic fluid based Rankine cycle (ORC).

In addition, water/steam as a working fluid is desirable for marine application due to its abundant availability and non-toxic properties. However, organic fluids are best suited for electricity generation. Especially for WHR in marine application because of its relatively better thermal match, smaller plant size, simpler plant and operability at varying engine loads. Moreover the choices of organic fluid available can be utilized to select the most suitable fluid based on the desired application. It will be understood in later chapter that an optimized ORC-WHRS for marine application also has relatively better efficiency than other WHR technologies.

1.2. Problem Description

Because of growing concern for man made climate change and the health of the environment, many recommendations are suggested and regulations enforced to reduce the carbon footprint. These rules and regulations are also applied on the maritime industry especially on sea-going ships. Recovery of waste heat energy from ships is one means to comply with these regulations. This is achieved by redirecting part of the waste heat energy back into the ship for further consumption. Such WHR methods are also economical and efficient in terms of yearly fuel consumption and system performance.

As mentioned earlier, many WHR technologies are currently being used in land-based industrial applications. Most of these may not be suitable for marine application due to flexibility, operability or safety issues in addition to other design based limiting factors such as volume or weight. Taking these challenges into account, a suitable WHRS should be considered for ship-board applications. Since on-board ships most consumers demand energy predominantly in electrical form, a system that generates electricity from waste heat source should be coupled to the engine. Under such demands and challenges, organic fluid based RC-WHRS have shown better efficiencies, simpler plant design and smaller components with respect to other WHRS in other applications outside marine for low and medium grade temperature waste heat sources.

Since the waste heat available on-board ships are of low and medium grade, an investigation needs to be carried out to understand the advantages and challenges of the usage of ORC based WHRS for marine application. Unlike other land based applications, the use of ORC-WHRS faces other additional challenges in marine application such as space constraints and operational profile of the vessel. By keeping these additional challenges in mind as well, a methodology is needed to be designed which allows for screening of fluids and plant designs to obtain the most suitable combination based on the available waste heat and selection parameter. This fluid and plant design combination should be further used to analyze off-design performance, sensitivity and dynamic analysis to understand the potential and behaviour of ORC-WHRS for application on-board ships. To carry out these screenings and analysis, a static and dynamic models are needed to be modeled which can be used for calculating overall energy efficiency of the ship in early/preliminary design phase.

1.3. Objective

The objective of this thesis is to investigate ORC technology, devise a fluid screening methodology, develop dynamic ORC plant models and analyze the application of ORC on-board ships as a WHRS for marine engines.

The sub-objectives of this thesis are described as follows. These sub-objectives were executed in the same order as well:

Fluid screening:

- Screening methodology is to be devised in order to find a suitable fluid and its associated plant layout based on the selection parameter(s).
- Influence of low temperature condenser cooling fluid on ORC plant and performance.

Dynamic model:

- Build a dynamic simple-ORC plant model by modification from an existing dynamic SRC plant model.
- Develop a dynamic recuperative-ORC plant model from the simple-ORC plant model.
- Build and implement a dynamic pump element into the ORC plant models.
- Comparison of dynamic ORC plant models to Cycle-Tempo ORC plant models for static analysis results.

Off-design performance analysis:

- Off-design performance analysis of simple and recuperative ORC-WHRS plant models to off-load conditions for systems designed at varying engine load points.

Dynamic and sensitivity analysis:

- Sensitivity analysis of ORC plant model to study the influence of model input parameters on the model output.
- Analyze the dynamic behaviour of the ORC plant model for load-drop and load-rise step functions with varying step duration for systems designed at varying engine load points.
- Analyze the dynamic behaviour of the ORC plant model for load-drop and load-rise step functions with same step duration for system designed at one engine load point.

1.4. Thesis Outline

The thesis outline and content are recorded chapter-wise. The first chapter is the introduction to this master thesis which describes the background argument, followed by the problem description, objective and the thesis outline.

The second chapter of the thesis is the literature study and review that captures the technical foundation to the topic. It shows the environmental impacts caused by burning fossil fuel at oceans by vessels for generating useful power. These impacts caused by vessels have compelled the world governing body and independent governments to impose mandatory steps and regulations on sea-going vessels in order to curb air and ocean pollution. The chapter also shows how recovery of wasted energy during fuel burning can be feasible means to comply with these regulations. Various promising and proven technologies capable of recovering waste energy are also discussed in detail.

The third chapter of the thesis lists out the reasoning on why organic Rankine cycle (ORC) may be more suitable than the others for marine application. It shows the comparison of ORC to other technologies and how ORC suits as a waste heat recovery system (WHRS) for improving the overall energy efficiency of the ship.

The fourth chapter of the thesis is regarding the screening methodology devised for ORC-WHRS in marine application. It shows the steps taken to select a suitable organic fluid and plant design based on the selection parameter. The chapter also shows how waste heat profile and the selection parameter influences the choice of organic fluids and subsequently the plant design. It also shows how low temperature cooling fluid can be used to harness the greater potential of an organic fluid to recover waste energy with better thermal efficiency. This chapter includes fluid screening, plant layouts, sizing of the heat exchangers and static analysis of ORC based WHRS.

The fifth chapter of the thesis shows the modification of an existing steam based Rankine cycle (SRC) model into an organic model in Matlab-Simulink. It shows the fundamental elements used to form this thermodynamic cycle and the reasoning to removed, add or modify certain parts within the existing SRC model in order to adapt it into a simple-ORC plant model. Further development of the simple-ORC to a recuperative-ORC plant model is also described. It also shows how a dynamic pump element is modeled to replace the original pump element.

The sixth chapter of the thesis is based on the off-design performance analysis of an ORC plant with respect to the design point of the plant and the waste heat profile. Results of the design point analysis obtained from the thermodynamic software Cycle-Tempo is used for comparison with the dynamic ORC model in Matlab-Simulink.

The seventh chapter shows the sensitivity and dynamic analysis of the ORC plant model. Sensitivity analysis of ORC plant model is performed to study the influence of model input parameters on the model output. Dynamic analysis of the ORC-WHRS when subjected to various step functions and step duration performed in this thesis are described in this chapter.

The eighth and the final chapter is about the thesis conclusions. It also includes, recommendations for further improvement to make the analysis of ORC application more accurate. It also includes recommendations for more realistic approach of ORC use on board ships.

2

Literature Study

In this chapter, the literature study carried out for this thesis is presented. The study is performed to understand the current state of man-made carbon dioxide emission related impacts on the planet, especially due to maritime activities. It also shows what measures are being taken by the maritime authorities to curb further damage due to such emissions. Moreover this study also talks about potential sources of heat energy which during normal operations on-board ships are wasted. The technologies which are capable of generating useful energy by harnessing this waste heat energy from potential sources and be directed back into the vessel are also discussed. Because these technologies can reduce the carbon dioxide emissions from ships by increasing the overall fuel efficiency.

2.1. Environmental Impact of Shipping

In the course of the most recent 650,000 years, carbon dioxide levels in the atmosphere, for the most part have ranged from 180–300 parts per million (ppm) [Solomon et al., 2007]. In any case since the Industrial Revolution, humans have far exceeded this natural range with worldwide fixation levels of carbon dioxide reaching 400.7 ppm (as on September 2016). These levels grew at an average rate of 2.17 ppm per year between the years 2006 and 2015 [Tans, 2016]. These man made carbon dioxide concentrations in the atmosphere are enhancing the natural greenhouse effect to further accelerate an unfavorable warming up of the planet. In other words, more the carbon dioxide emissions, more is the warming up of the planet. This results in an increasing global atmospheric temperature that will most certainly facilitate series of catastrophic changes across the globe. These effects not only disturb the natural conditions of the atmosphere but also the oceans and seas due to climate change. This is because considerable amounts of carbon dioxide and heat that are added to the atmosphere are absorbed by the oceans and seas. This causes significant devastating changes for many species, including humans that depend upon these water bodies [Parry et al., 2007].

Ships are an important source of carbon dioxide emissions into the fragile atmosphere, the primary contributor to climate change and ocean acidification. Because carbon dioxide emissions caused by humans are a form of pollution, identified as one of the main factors of climate change and global warming irrespective of where on Earth they occur [Friedrich et al., 2007]. Like most modes of transportation, ships mostly use fossil fuels to produce mechanical energy for propulsion and power generation. During this process it produces hot exhaust gases, a byproduct that constitutes carbon dioxide and other harmful pollutants. These gases are discharged into the environment which contributes to the problem. In addition, the fossil fuels used on-board ships are considered to be one of the dirtiest fuel on the market [Lindstad, 2015].

Over three percent of global carbon dioxide emissions can be associated with ocean-going ships [MARPOL, 2007]. These CO_2 emissions along with NO_x and SO_x are being limited and further tightened by International Maritime Organization (IMO) [Lindstad and Sandaas, 2014] in order to reduce the total exhaust gas pollutant emissions. Due to these regulations and increasing concerns, considerable attention has been given to improve the energy efficiency of ships [Yuan et al., 2016]. Because

the report by the Marine Environment Protection Committee (MEPC) of IMO indicates that there is high potential for technical developments to improve energy efficiency. Moreover, considerable efforts have been made to improve the fuel energy efficiency of ocean going ships in recent years.

The IMO has introduced regulations on maritime energy efficiency on 1st January 2013 that sets the guidelines for energy efficiency of new ship designs. In addition, it also includes a form of structure for the management of energy efficient ship operations for all new and existing ships. It is very important that energy efficiency improvements for design and operational performance also exhibit an understanding of the ship's operational profile and not just the design condition. These regulations contains the Energy Efficiency Design Index (EEDI) and Ship Energy Efficiency Management Plan (SEEMP) regulations. EEDI sets the strict guidelines for the design of new vessels within allowable EEDI value limit for a given dead-weight. EEDI calculation indicates the parameters and variables that constitute the operational profile of a ship, such as capacity, speed, main engine and auxiliary power requirements [Banks et al., 2013]. This is expressed in terms of grams of carbon dioxide per ship's capacity-mile (smaller the EEDI figure, more energy efficient is the ship design)[MARPOL, Annex VI]. These limits and regulations will become stricter in the coming years to reduce carbon dioxide emissions from ships. Hence, technological developments in the field of fuel efficiency and reduction measures has to be explored.

Energy efficiency of a ship can be increased by improving the fuel efficiency of the prime mover(s). Diesel engines are by far the most widely used prime mover for propulsion and power generation on a wide variety of vessel types. This is due to the fact that there is no other alternative prime mover to replace diesel engine which has similar power density, cost and fuel efficiency. It is also expected that diesel engines may not be replaced in a foreseeable period of time [Eyring et al., 2005]. These marine diesel engines utilizes approximately half of the fuel energy to produce useful work and the remaining is lost and dissipated to the sea and atmosphere as waste heat. There are four main sources of waste heat in a marine diesel engine namely exhaust flue gases, scavenge air cooling water, jacket cooling water and lubricating oil. The wasted heat energy of some of these waste heat sources has the potential of being recovered by means of any waste heat recovery technology. This recovery of waste heat energy from marine diesel engines will increase the overall fuel energy efficiency of ships. Moreover, the present day recovery technologies are also economically feasible to convert waste heat into mechanical or electrical power [Congress, 2016] as it reduces the ship's fuel consumption [Generation, 2014].

2.2. Waste Heat Recovery System

Waste heat recovery system (WHRS) is integrated with the diesel plant in order to increase the overall fuel efficiency of the combined plant. This increase not only reduces the fuel consumption of vessels but also reduces emissions from them. As mentioned earlier, the increase in overall fuel efficiency is achieved by utilizing heat energy from waste heat sources. The heat energy can be used to generate mechanical/electrical power or the heat energy from waste heat sources can be directly used for heating purposes. However, for any conventional vessel the available waste heat energy largely exceeds the requirement for (direct) heating purposes. This resulting in large amount of (remaining) waste heat energy that can used for producing mechanical/electrical power. This power can be redirected back into the system for propulsion and/or auxiliary services at no additional fuel consumption or carbon dioxide emissions [Singh and Pedersen, 2016].

The diesel engines used in marine application especially that of large ships run at a constant speed for a longer period of time and distance. Such an operational profile provides a more stable source of waste heat from the engines which can be recovered using suitable recovery system. Since the flow rate of these waste heat energy source are in large quantities, the potential for waste heat recovery is particularly promising. In addition to these, the availability of cooling sea water source makes WHRS appropriate for marine application [Shu et al., 2013]. The advantages of the WHRS is not only seen in the most frequent engine operating condition (i.e. design point) but also in different engine operating conditions (i.e. off-design points) [Benvenuto et al., 2016].

Heat balance of some market available engines are shown in Table 2.1 and Table 2.2 for 2-stroke and 4-stroke types respectively. It can be seen that 2-stroke types have an engine efficiency of about 50% and it is even slightly lower for 4-stroke types. The rest of the fuel energy leaves the engine in the form of heat energy. As seen in these tables, this heat energy leaves the engines in the form of exhaust gas, cooling water, lubricating oil and radiation. It can also be seen that the largest portion of these waste heat energy is in the exhaust gas followed by scavenge air cooling water and jacket cooling water. Therefore in this thesis the analysis of recovery of exhaust gas waste heat source is given the primary focus. For this analysis, it is very essential to investigate the waste heat source in terms of its quantity (energy contained) and quality (temperature). In addition, the current recovery technologies, industry practices and the limitations to heat recovery is also needed to be studied. These studies are required so as to know the amount of the recoverable heat and also how it can be used not only to improve fuel efficiency but also to reduce fuel consumption and carbon dioxide emissions.

Make	MAN B&W	Wärtsilä
Model	12K98ME/MC	12RT-flex96c
Type	2-Stroke	2-Stroke
Fuel	Diesel	Diesel
Driven	Propeller	Propeller
Shaft power	49.3%	49.3%
Exhaust gas	25.5%	25.4%
Air cooler	16.5%	14.1%
Jacket water	5.2%	6.3%
Lubricating oil	2.9%	4.3%
Heat radiation	0.6%	0.6%

Table 2.1: Heat balance of diesel engines (at 100%MCR) used in marine application for propulsion [Diesel and Turbo, 2014; Schmid, 2004].

Make	Wärtsilä	Wärtsilä
Model	6L50DF	6L50DF
Type	4-Stroke	4-Stroke
Fuel	Diesel	Gas
Driven	Generator	Generator
Shaft Power	44.6%	46.0%
Exhaust gas	24.9%	32.8%
Charge air, HT	9.9%	6.8%
Charge air, LT	4.9%	4.0%
Jacket water, HT	8.2%	5.3%
Lubricating oil, LT	6.1%	3.8%
Heat radiation	1.4%	1.3%

Table 2.2: Heat balance of diesel engines (at 100%MCR) used in marine application for power generation [Wärtsilä, 2012].

Unlike in land based applications, WHRS used for marine application are subjected to additional challenges such as regulations, limitations in space and weight, operational risk factor and operational profile. Hence, the WHRS for use on board ships should have the following features [Singh and Pedersen, 2016]:

- Efficient utilization of waste heat with high power density and small footprint.
- Ability to operate in a wide range of environmental conditions.
- Able to handle transient heat source and sink properties.
- Ability to operate and adapt to changing operational profiles of the vessel.
- Easy to integrate with other systems and highly reliable.
- Should be easy and safe to operate and maintain.

The WHRS used on a ship should be designed to benefit despite having to face distinct challenges and limitations due to its working conditions as mentioned below:

- WHRS impacts cargo capacity because ships are very sensitive to WHRS' volume.
- Dynamic loading, part loads and diverse operating profiles;
- The sink source of sea water as cooling water can have its temperature anywhere between -3 °C to +30 °C as the ship navigates around the globe [Rayner et al., 2006].

As mentioned earlier, the exhaust gas from the engine after turbocharger offers the best source of waste heat both in terms quality and quantity. While designing a WHRS for the waste heat source of engine exhaust gas, an additional limitation is also presented to the designer. This limitation is to the amount of waste heat that can be recovered from the exhaust gas is due to the acid dew point

of the pollutants. If the exhaust gas is cooled below this acid dew point due to the recovery system, the exhaust gas pollutants chemically reacts to form liquefied acid. Hence to avoid acid corrosion, the WHRS that utilizes exhaust gas should be designed in such a way that it ensures that the exhaust gas is not cooled below this acid dew point. This is the limiting factor of the waste heat recovery from the waste heat energy of exhaust gas. The usage of cleaner fuels (especially fuels of low sulphur content) in the future can reduce the risk of acid formation at lower temperatures and can increase the energy recovery potential (by eliminating this acid dew limitation) from the exhaust gas [Singh and Pedersen, 2016].

Various waste heat recovery cycles and systems that are used or being developed in land or marine applications are discussed as follows:

2.2.1. Rankine Cycle

In thermodynamics, the most efficient thermal cycle possible is considered to be the Carnot cycle that consists of four reversible, two isothermal and two adiabatic processes with no heat loses. It can also be considered as the cycle of expansion and compression of a reversible heat engine that does work with no loss of heat. Rankine cycle that uses water as working fluid is the most realistic approximation to the Carnot cycle, and it has been widely used to generate electrical power all over the world [Zhang et al., 2012].

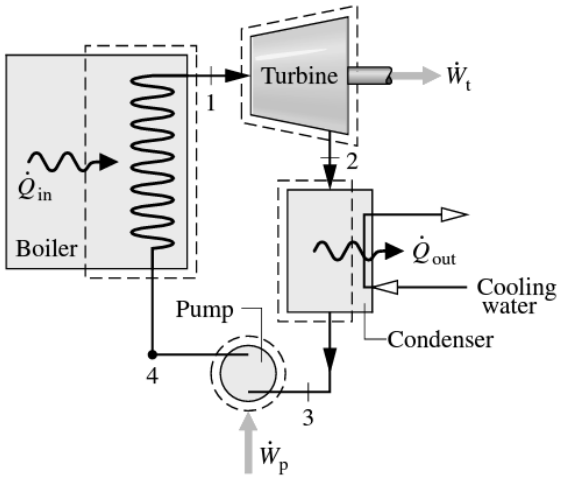

Figure 2.1: Principle work and heat transfers of Rankine cycle plant [Moran and Shapiro, 2004].

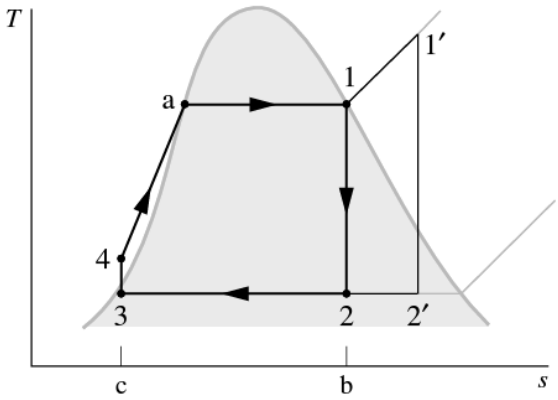

Figure 2.2: Temperature - entropy diagram of the ideal Rankine cycle [Moran and Shapiro, 2004].

The principal work and heat transfers of Rankine cycle plant are illustrated in Figure 2.1. Ideally, the working fluid (steam or organic) passes through the various components of the simple vapor power cycle. This is without irreversibilities, without frictional pressure drops in the boiler and condenser, and the working fluid passes through the boiler and condenser at constant pressure. The processes in the turbine and pump is isentropic because of the absence of irreversibilities and heat transfer with the surroundings. Such an ideal cycle is represented in the T-S diagram as shown in Figure 2.2.

As per the processes shown in Figure 2.2, we see the following series of internally reversible processes that the working fluid undergoes:
Process 1-2: Working fluid at the saturated vapour state (1 or 1') expands isentropically in the turbine to the condenser pressure (2 or 2').
Process 2-3: Heat is transferred from the working fluid to the cooling fluid, as it passes through the condenser at constant pressure to saturated liquid state (3).
Process 3-4: Isentropic compression in the pump to state 4 in the compressed liquid region.
Process 4-1: Heat is transferred to the working fluid from the heat source as it passes through the boiler at constant pressure to complete the cycle process.

The possibility of super-heating the vapor, is also included in the ideal Rankine cycle, as seen in process cycle 1'-2'-3-4-1', as shown in Figure 2.2. Considering that the ideal Rankine cycle consists of internally reversible processes, the area under the process cycle lines (as seen in Figure 2.2) can be understood as heat transfers per unit of mass flowing. Area under the process lines 1-b-c-4-a-1 represents the heat transfer to the working fluid passing through the boiler and the area under the process lines 2-b-c-3-2, is the heat transfer from the working fluid passing through the condenser, each per unit of mass flowing. The enclosed area of the process cycle 1-2-3-4-a-1 can be interpreted as the net heat input or, equivalently, the net work output, each per unit of mass flowing [Moran and Shapiro, 2004].

For a Rankine cycle, the working fluid plays a very important role. The system efficiency, operating conditions, environmental impact and economic viability primarily depends on the working fluid. It should be thermodynamically suitable for plant process such as evaporation and condensation properties. Furthermore, it must not only possess adequate chemical stability in the desired temperature range but also have the necessary thermo-physical properties that match the application. The selection considerations for the working fluid should include heat transfer properties, such as viscosity and thermal conductivity. It should also consider other non-thermodynamic properties such as global warming potential (GWP), corrosiveness, toxicity, cost etc.

The peak point of the fluid saturation line in a T-S diagram also known as the critical point proposes the proper operating temperature range for the working fluid. This critical temperature and pressure is an important data for the working fluid selection. Another important thermodynamic property for fluid selection is the freezing point of the working fluid. This point must be below the lowest operating temperature in the cycle to avoid fluid solidification. Not only for temperature, the working fluid must operate and work within an acceptable pressure range. Very high pressure or high vacuum is susceptible to impact the reliability of the cycle or increase the cost of the plant [Chen et al., 2010; Larsen et al., 2013].

Working fluids used in Rankine cycle are divided into two types, steam and organic fluids. The benefits and application of these fluids are explained as follows:

2.2.1.1 Steam Rankine Cycle

Water is used as the working fluid for steam Rankine cycle (SRC) and it is considered as the most practical working medium for thermal recovery cycles. This is due to its easy availability, no environmental impact, non-hazardous, safe and good heat transfer characteristics. These advantages makes water/steam as the most suitable working fluid for marine application. However, water as a working fluid has a few disadvantages such as high corrosiveness as a super-heated vapor and air infiltration [Bayley, 2001].

Steam based waste heat recovery systems are already in place on board ships as exhaust gas boiler (EGB) where steam produced is used for heating purposes. As mentioned earlier, the waste energy availability may exceed the heating demands, thus power generation is possible. The reasons why SRC may not be the best choice for power generation from WHR in marine application are discussed in Chapter 3.

2.2.1.2 Organic Rankine Cycle

Organic Rankine cycle (ORC) is Rankine cycle which uses a working fluid other than water in order to adapt evaporation and condensation temperatures to the available heat source [Baldi and Gabrielii, 2015]. The working principle of the ORC is the same as the steam Rankine cycle, but uses an organic working fluid with low boiling points to generate power by recovering maximum possible thermal energy from low-temperature heat sources [Chen et al., 2010]. Organic fluids also have many properties and characteristics different from water [Harrigan and Stine, 1985].

The categorization of different organic working fluids are based on their saturation vapour curve, which is the most crucial fluid characteristic. They are generalized in three categories namely dry, wet and isentropic fluids. Figure 2.3 illustrates, the Temperature – Entropy diagram of organic fluids classified as wet, dry and isentropic fluids [Bellolio et al., 2015]. An equation that approximately categorizes working fluids is discussed in a later chapter.

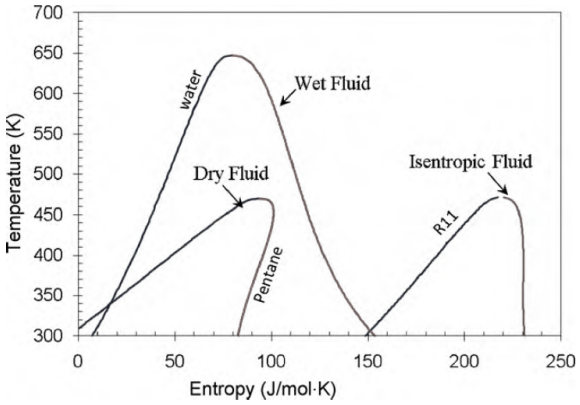

Figure 2.3: T-S diagram of fluid types: dry, isentropic and wet [Bellolio et al., 2015].

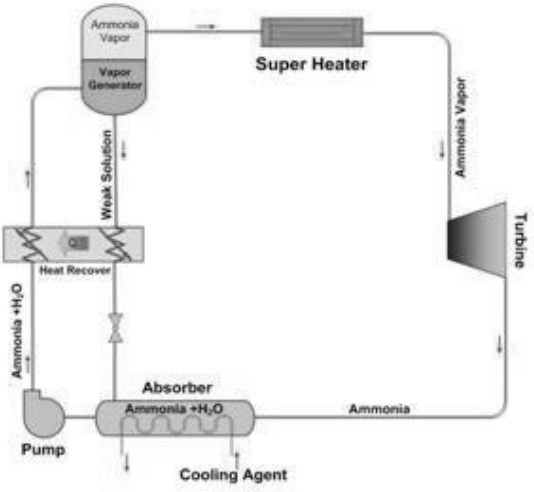

Figure 2.4: Basic configuration of Kalina cycle [Karimi et al., 2015].

2.2.2. Kalina Cycle

Kalina cycle was proposed and first developed by Dr. Alexander Kalina in the late 1970s and early 1980s. This thermodynamic power cycle uses an ammonia-water (NH_3-H_2O) mixture as the working fluid [Kalina, 1982, 1983]. He designed this power cycle to replace Rankine cycle as a bottoming cycle for a combined-cycle energy system as well as for electrical power generation using low-temperature heat sources [Kalina, 1984].

Figure 2.4 illustrates the basic configuration of ammonia – water (NH_3 — H_2O) Kalina cycle. Kalina cycle in principle is a modified Rankine cycle and is considered as a promising competitor against the ORC. This is due to its most significant improvement in thermal power plant design among various novel thermodynamic cycles. Modifications to the design of the system that exploits the advantages of ammonia-water mixture as a working fluid is necessary to complete the modification from Rankine to Kalina. This modification can be seen when comparing the basic configuration of Rankine and Kalina cycles as shown in Figure 2.1 and Figure 2.4.

2.2.3. Vapour Absorption Refrigeration System

To meet the requirements for cooling purposes such as air-conditioning or food preservation, refrigeration devices are used. Conventional vapour compression refrigeration systems use electrical energy to achieve refrigeration and meet cooling requirements. However, waste heat energy is a promising means of source to meet the cooling requirements by vapour absorption refrigeration systems (VARS). Presently, some studies are being conducted to utilize the vast amount of waste heat of diesel engines aboard ships to meet refrigeration requirements through VARS. Moreover, many studies are being conducted for the development of VARS for their application to low grade heat sources. This low grade heat source of temperatures between 50 °C to 200 °C are also economically attractive for VARS. Waste heat from ship's diesel engines can provide heat source of this temperature range to meet the vessel's refrigeration demands by waste heat driven VARS[Kececiler et al., 2000]. Especially, jacket cooling water seems to be a promising source for VARS using water-lithium bromide mixture [Shu et al., 2013].

Compression type, absorption type and injection type refrigeration technologies are currently being used in marine applications. These technologies are not only used for air-conditioning for crew comfort, but also for refrigeration for provisions storage and ice-making for fishing vessels. Compression type and injection type refrigeration technologies require additional fuel to drive them which increases the fuel consumption of the ship. Whereas, absorption type refrigeration is driven by heat energy and very little electricity. The waste heat from engines aboard vessels can be used as the heat energy source and thus increasing the fuel efficiency of the vessel. VARS are almost noise-free and nearly maintenance-free, making them highly suitable for marine applications [Wang and Wang, 2005].

The operational profile is an important consideration factor because high and constant engine load provides a steady flow of waste heat energy that can be used as the heat source for VARS. Waste heat from ship's engine by means of exhaust gas, scavenge air and jacket cooling water are all potential heat sources to drive this system. Among several fluid mixtures, ammonia-water and water-lithium bromide are the most popular working fluid mixtures used [J et al., 1998].

2.2.4. Combined Power & Cooling Cycle

This novel thermodynamic cycle that uses binary mixture to produce power and refrigeration was proposed by Dr. Yogi Goswami in 1998. It is also known as Goswami cycle. This system combines two thermodynamic cycles, the Rankine and absorption refrigeration cycles to provide power output and refrigeration with power generation as the main priority. It uses ammonia-water (NH_3-H_2O) mixture as a working fluid. This mixture is used for its advantages on heat transfer irreversibilities for low temperature finite heat sources. The cycle uses a very high concentration of (super-heated) ammonia vapour for expansion in the turbine into a very low temperature (vapour state) working fluid before condensation. This low temperature ammonia is used for providing refrigeration by condensing the ammonia in an absorption condensation process [Xu et al., 2000].

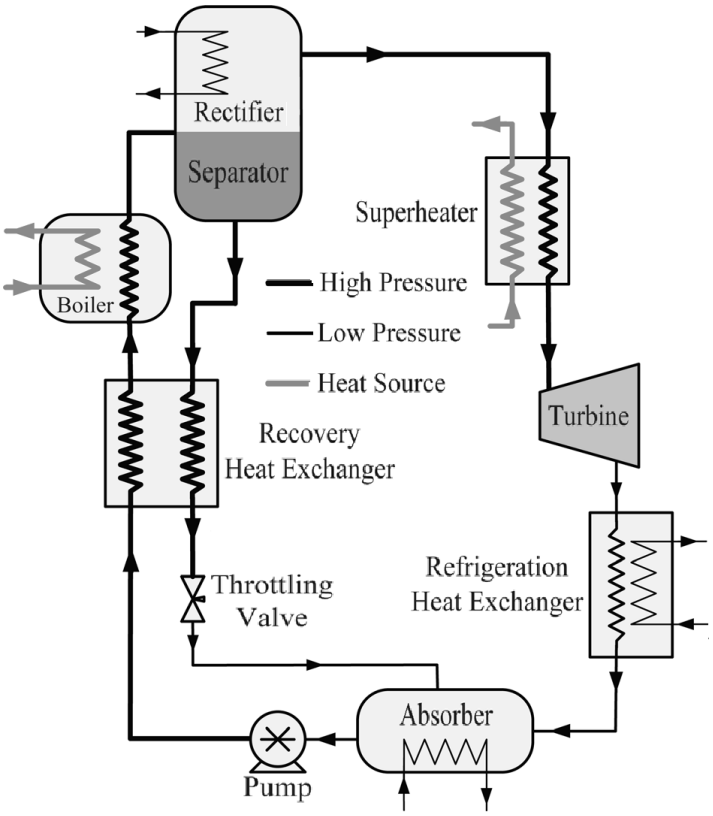

Figure 2.5: Basic configuration of combined power/cooling cycle [Demirkaya et al., 2012].

This cycle can be optimized based on the heat source and sink temperatures for low and medium temperature heat sources. The optimization can be done to provide maximum power, maximum refrigeration, combination of both or maximum thermal efficiency based on the application. The temperature of the waste heat source is the most important parameter. This is because the effective waste heat usage or efficiency of waste heat energy recovery mainly depends on the temperature difference between the source and the sink [Patel and Shukla, 2013; Xu et al., 2000]. Figure 2.5 shows the basic configuration of Goswami cycle depicting combine power and cooling schematics.

2.2.5. Thermo Electric Generator

Thermo Electric Generator (TEG) modules are solid-state devices that directly converts heat energy into electrical energy based on the process known as Seebeck effect. This is a phenomenon that causes an appearance of electrical voltage due to temperature difference across a material. TEG functions like a heat engine which is compact and has no moving parts. However, these are very expensive and less efficient. It consists of a thermo-couple composing n-type (material with excess electrons) and p-type (material deficit in electrons) elements. They are connected electrically in series and thermally in parallel. Heat transfer from one side to the other generates a voltage across the thermo-electric couple. The voltage generated by the TEG module is called Seebeck voltage, and it is directly proportional to the temperature differential between the hot and cold fluids. The block diagram of a simple TEG module is shown in Figure 2.6.

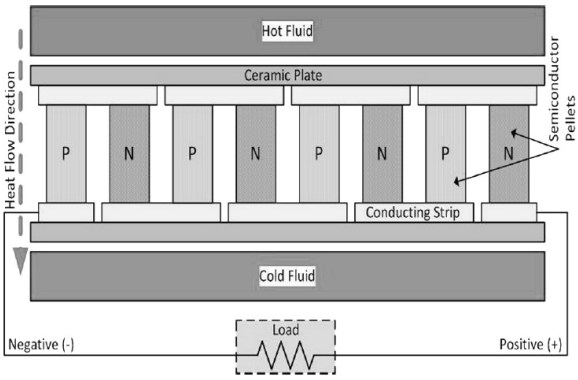

Figure 2.6: A simple TEG module block diagram [Singh and Pedersen, 2016]

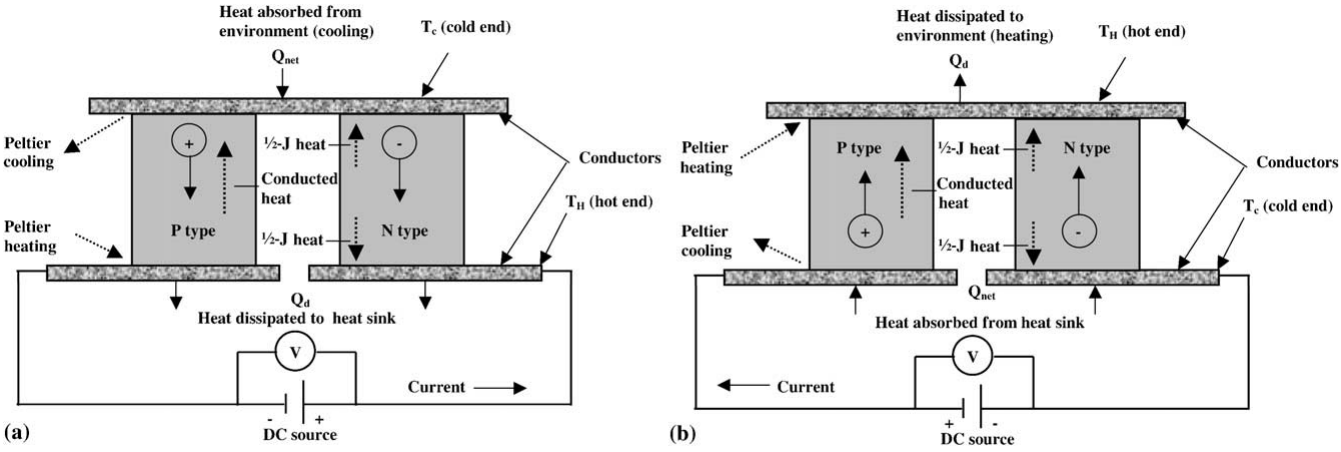

Figure 2.7: Thermoelectric module for a) cooling and b) heating [Riffat and Ma, 2003]

Performance of the TEG module depends on the thermo-electric figure-of-merit of the thermo-couple material as $ZT = S^2\sigma T/k$. Where S is the Seebeck coefficient, σ is the electrical conductivity, T is the absolute temperature and k is the thermal conductivity. Many studies on TEG modules for waste heat recovery from exhaust gas on land based applications have shown promising results. For marine applications, the working principle of TEG makes it possible to produce DC electricity. This can be achieved by applying waste heat on one side of the thermo-electric material and lower temperature sea water on the other [Shu et al., 2013].

This application is not limited to just power generation but also for refrigeration and thermal energy sensors. Thermo-electric refrigeration is based on a phenomenon called "Peltier effect". It is achieved by passing direct current through pairs of n-type and p-type semi-conducting materials. These conductors are placed between the surfaces of the source and sink. It is vice verse for thermo-electric heating. Figure 2.7 shows the schematics of thermo-electric cooling and heating [Riffat and Ma, 2003].

2.2.6. Exhaust Gas Turbine

The static pressure and the temperature at the exhaust valve outlet defines the enthalpy energy content of the exhaust gases from an internal combustion engine. This pressure and temperature in the exhaust gas receiver is higher from the ambient conditions. Hence this pressure difference can be utilized to produce work by expanding the exhaust gas in an expander. Most engines utilize part of this exhaust energy by using the turbocharger (turbine side) as the expander. The expander then runs the mechanically-coupled compressor to feed the compressed scavenge air to the engine through an intercooler.

Modern turbochargers are optimized for better design to have high efficiency, hence it is not necessary to flow all the exhaust gas through it during normal engine loads. The excess gas from the exhaust gas receiver can be passed through and expanded in a separate power turbine. This power turbine is used as a WHRS to generate mechanical or electrical power. The usage of an independent power turbine for WHR is called as turbo-compounding and such a system is called as turbo-compounding system (TCS). An additional load (e.g. generator) other than the supercharger (scavenge air compressor) can be mechanically coupled to the engine turbocharger if all the exhaust gas is used to pass through it without any bypass.

The turbocharger and the power turbine can be designed for best performance based on the optimum exhaust gas mass flow rate through each turbine in the TCS. The power generated by the turbine due to the expansion of the exhaust gas is available as rotational mechanical energy of very high rotational shaft speeds. The consumers of this energy may require slower rotational speeds or a different form of energy other than mechanical energy. Hence, this high rpm turbine shaft power needs to be converted, transformed or conditioned to suitable forms as desired by the consumers [Singh and Pedersen, 2016].

3

Research Approach of ORC-WHRS

In this chapter, ORC-WHRS is compared to other WHR technologies as discussed in Chapter 2. This comparison is specific for waste heat recovery of engine exhaust gas to generate electrical power in marine application. This chapter also discussed why organic fluid is preferred over water/steam as the working fluid in Rankine cycle for WHR in this thesis.

3.1. ORC System

Why ORC for WHR of exhaust gas in marine application?

As mentioned earlier, WHRS used on-board ships especially in cargo vessels are mostly based on SRC for expansion of steam in heating coils. These are in place to meet heating demands for fuel oil and lube oil tanks for daily consumption, pump-ability, purification and other comfort-based heating requirements of the accommodation. For this purpose ORC may not be suitable, since the chemical properties of the working fluid such as toxicity, chemical stability, chemical reactivity and flammability will be of safety and operational concern during leakage in expansion line of the heating coils.

Whereas for power generation, SRC plants are primarily used in land-based applications such as in coal powered thermal plants because the exhaust gas temperature is well above 800 °C. This is unlike the temperatures available in the waste heat of a marine diesel engine. These sources of waste heat from conventional power cycles are considered low temperature quality. Since, most energy demands on-board vessels are in electric form apart from the main propulsion demand, it can be challenging to utilize this waste heat efficiently to generate power by means of an SRC. As SRC does not allow efficient recovery of waste heat from heat sources of temperatures below 370 °C [Hung et al., 1997]. In such conditions, ORC can be used to increase the overall plant efficiency for better fuel efficiency of the system [Generation, 2014], especially for waste heat recovery from exhaust gas of internal combustion engines [Sprouse and Depcik, 2013].

Why ORC over other WHR technologies?

Even though ORC is a widely used technology for power production worldwide, it is rather new technology in the maritime industry but a very promising one. This is due to its plant simplicity and efficiency in waste heat recovery [Bellolio et al., 2015]. In addition to flexibility in choosing a suitable working fluid based on the available temperatures of the heat source and sink [Baldi and Gabrielii, 2015; Larsen et al., 2013] for better thermal match [Chen et al., 2010].

Comparison of ORC over other WHR technologies:

- ORC-WHR of exhaust gas from a marine diesel engine produced more power than SRC at design point. This leads to higher reductions in fuel consumption, CO_2 emission and EEDI. However this is achieved with the drawback of higher working fluid mass flow rate [de la Fuente et al., 2016].
- When an ORC-WHR plant is optimized for part load conditions of a marine diesel engine based on the operational profile. It can provide significant savings in yearly fuel consumption. Such a

system would be smaller in size and cheaper [Baldi et al., 2015b].
- At least for low power levels and heat sources, Kalina cycle requires a complicated plant, large heat exchanging surface and high pressure resistant & non-corrosive material for a very small gain in performance with respect to an optimized ORC [Zhang et al., 2012].
- Kalina cycle requires very high maximum pressure (for instance, 10 times more than ORC) to obtain high thermodynamic performances [Bombarda et al., 2010]. This maximum pressure of the system may be a limiting factor for marine applications. This is because the operating pressures for higher temperature of heat sources could be at 150 bar for Kalina Cycle. Such high pressures are significantly higher than the operating pressure of conventional ORC [Nguyen et al., 2014].
- For marine application the performance of Kalina cycle at best may be similar to an ORC. Based on the comparison between Kalina and ORC cycles, application of ORC cycle is superior to Kalina. This is due to its simpler plant layout, smaller heat exchangers and lower evaporating pressure to obtain the same electrical power [Bombarda et al., 2010].
- As advanced heat recovery power cycles, ORC generated more net power than SRC and Kalina cycle when used as a combined cycle for a large ship model. The same study also showed that ORC could reduce specific fuel consumption (SFC) of the engine but at the expense of increased NO_x emissions [Larsen et al., 2014].
- In terms of plant efficiency, ORC is very efficient than TEG and VARS based WHRS [Quoilin et al., 2013].
- Unlike in SRC, ORC requires only a single heat exchanger to carry out preheating, vaporization and superheating of the working fluid. Hence, making an ORC-WHRS simpler than SRC-WHRS [Quoilin et al., 2013].

Factors for fluid selection

The selection of turbine and the working fluid significantly influences the system performance [Quoilin et al., 2013; Sprouse and Depcik, 2013], system layout [Bao and Zhao, 2013] and the operational parameters [Wang et al., 2012]. For the selection of the working fluid, it has been observed that the temperature of waste heat source is a very important parameter [Larsen et al., 2013; Yu et al., 2016].

Organic fluids with low latent heat and high thermal conductivity are more suitable for low-temperature heat sources for marine applications.[Wang et al., 2011]. However, no single fluid can fully satisfy the numerous requirements of an ideal working fluid in an ORC plant process. These requirements are process simplicity, low pressure, high efficiency, low hazard and low environmental impact [Badr et al., 1985a; Chen et al., 2010; Larsen et al., 2013].

Trade-off between characteristics of various working fluids has to be made for the selection of a suitable working fluid to obtain better results. The most crucial fluid characteristic is the saturation vapour curve because it significantly determines the fluid applicability, cycle efficiency and arrangement of associated equipment in a power-generation system [Hung et al., 1997]. The cycle efficiency is also closely related to the latent heat of the fluid at low pressure. This is because a greater latent heat at low pressure yields a lower efficiency since a larger portion of the energy carried by the fluid is rejected through the condenser [Hung et al., 1997].

Organic fluids have lower latent heat than water, making it suitable for ship's low-temperature waste heat sources because such fluids require less heat to vaporize. However this low latent heat property requires the use of larger mass flow rate in comparison to steam Rankine cycle. Due to the limitations of available space on ships, selection of an optimal fluid is important since the type of fluid influences the size of the ORC plant [Badr et al., 1985b; Bellolio et al., 2015; Shu et al., 2013].

Influence of fluid type

As described earlier, organic fluids are categorized as either dry, wet or isentropic type. Unlike the other types, dry fluids have a positive slope saturated vapour curve on the T-S plot. Hence, if the fluid expansion begins as a saturated or superheated vapour, the fluid leaves the turbine in a superheated state. This is advantages because the lack of liquid formation in the turbine during expansion leads to higher efficiency. This is especially when compared to the use of wet fluids like water, where the expanding vapour leaves the turbine as wet vapour [Liu et al., 2004]. Moreover, dry fluids can begin expansion as a saturated vapour since they do not require superheating as the thermal efficiency remains almost constant despite increasing the turbine inlet temperature [Mago et al., 2008]. Whereas, SRC requires a superheater because wet fluids like water needs to be superheated to prevent turbine blade erosion. In addition, most organic fluids (dry and isentropic type) do not require to be superheated due to their operability at low temperature. Unlike SRC which usually requires multi-stage turbine, ORC requires only a single-stage turbine because dry and isentropic fluids have much lower enthalpy drops during expansion than wet fluids (e.g. water). These make ORC simpler in plant design, more economical in terms of capital and maintenance costs [Andersen and Bruno, 2005; Hung et al., 1997].

It is also advantageous for the turbine to use organic fluids for its high cycle efficiency, high internal turbine efficiency and low mechanical stress due to low blade speed. These are in addition to no blade erosion since the fluid expansion is in vapour state. The advantages also includes longer turbine life relative to steam turbines and no gearbox is required between the turbine and generator due to significant low rotational speed relative to steam turbines [Grljusic et al., 2014].

However for plant processes where the fluid expands into superheated state, it is essential to cool this superheated fluid down to its saturated state before the condensation process begins. Using a recuperative heat exchanger to preheat the liquid leaving the pump by the superheated vapour is an efficient method to de-superheat the expanded fluid before condensation [Chen et al., 2010; Hung et al., 2010]. Moreover, an ORC plant with a recuperator has higher thermodynamic efficiency and lower irreversibility than an ORC plant without[Mago et al., 2008].

Based on literature study, organic Rankine cycle (ORC) can be identified as the promising technology for WHR from ships, especially from low-grate waste heat [Larsen et al., 2013; Sprouse and Depcik, 2013], which leads to reduction in fuel consumption and emission [Bellolio et al., 2015]. Although ORC works under the same principle and have the same components as SRC, the flexibility in choosing the working fluid based on the application [Sprouse and Depcik, 2013] make it more suitable for marine application [Wang et al., 2011].

Using the arguments described in this chapter, further investigation on ORC as a WHRS of exhaust gas for engines on ships is carried out. In order to do this, firstly a suitable organic fluid and plant design should be found, based on the source-sink temperatures and selection parameters. This is done by devising a fluid screening methodology. Secondly, a dynamic simple-ORC plant will be modeled by modifying an existing SRC model. This simple-ORC plant model will be used to develop a recuperative-ORC plant. These dynamic ORC plant models will be used to analyze off-design performance of the plant based on the waste heat profile. Finally, the sensitivity and dynamic analysis of the ORC model will be performed to understand ORC application.

4

Plant Layout, Fluid Selection & Static Analysis

In this chapter, the screening methodology devised for the thesis is described. This methodology shows how suitable fluids are selected for ORC-WHRS based on the waste heat profile and selection parameters. The influence of selected fluid type on the plant layout is also covered. This chapter also covers the influence on ORC plant and performance when a low temperature cooling fluid is used for the condenser.

In marine application, the engine is the heat source for an ORC-WHRS. Due to the vessel's distinctive operational profile, the engine may be utilized for a wide operating range at varying periods. Hence, the ORC-WHRS integrated to a marine engine is subjected to varying heat source parameters due to varying engine load based on the waste heat profile. Such a recovery system should be capable of producing electricity at these varying engine loads or at least for a wide engine operating range. Therefore for an ORC-WHRS used in such an application, a screening methodology as shown in Figure 4.1 is necessary to identify the most suitable working fluid used in the system. Moreover, selection of a suitable working fluid is perhaps the most important parameter of an ORC-WHR plant in any application, since it determines the plant layout, component sizes and thermal match to heating and cooling fluids. Certain set condition based preliminary analysis has to be executed to obtain functioning fluids that perform sub-critical ORC. These functioning fluids will be further screened to obtain the most suitable fluid based on the selection parameters.

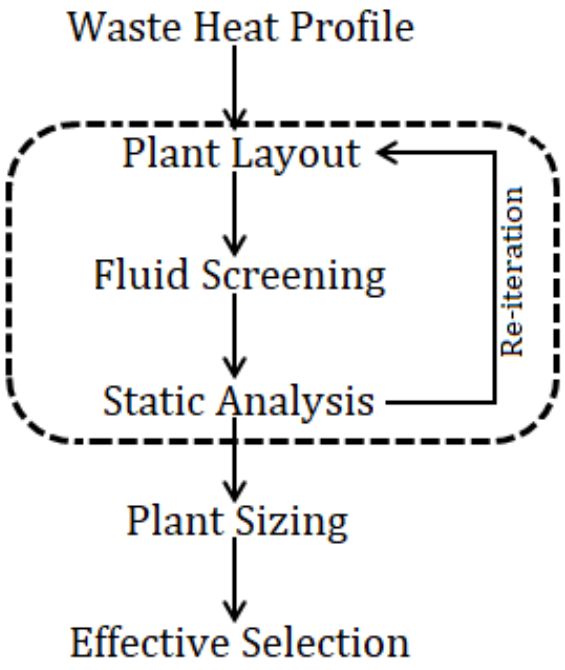

Figure 4.1: Step-wise screening and analysis flowchart

4.1. Waste Heat Profile

In order to obtain and analyze the design condition performance of different organic fluids in an ORC plant for varying engine discrete load points, the heating and cooling fluid parameters are necessary, especially the fluid temperatures. These temperatures are necessary to obtain functioning fluids that perform sub-critical thermodynamic cycle within these ranges in the ORC plant.

As mentioned earlier, the waste energy in exhaust gas of marine engines has the highest potential among other waste energy sources for power generation. Hence, the exhaust gas is considered to be the heating source of the boiler component in the ORC plant. Therefore, the initial screening of all available organic fluids are based on the temperatures of the engine exhaust gas (for boiler) and the cooling sea water (for condenser). The temperature of the cooling sea water is chosen to be fixed at 25°C. This is because, for ships the sea water is an open system and is an abundant source of cooling fluid for the condenser. This chosen sea water temperature for condenser cooling is within the annual global average sea water temperature range of the ocean surface.

The choice of cooling fluid and the temperature used are dependent on the availability of the cooling fluid and the freezing point of the organic fluid. For SRC in marine application, sea water is a feasible choice in terms of sea water availability and freezing point of water/steam working fluid. However for ORC application, condenser cooling fluid may also have lower temperatures, well below 0°C due to comparatively lower freezing points of most organic fluids than water/steam. The influence of using low temperature cooling fluid on ORC plant and performance are discussed in later part of this chapter.

For the identification of functioning working fluids, the waste heat profile of the exhaust gas of Wärtsilä 6L50DF (for power generation in gas and diesel modes) dual fuel engine has been considered. Both gas and diesel modes of the engine are considered for the analysis because the exhaust waste heat source profiles are not the same. Therefore, it may be interesting to see how the ORC-WHR plant will perform when the engine switches modes even when running at the design load point of the ORC plant.

Wärtsilä 6L50DF DE (MCR: 5700kW @ 500rpm)				
	Gas Mode		Diesel Mode	
Load	Massf.	Tempr.	Massf.	Tempr.
[%]	[kg/s]	[°C]	[kg/s]	[°C]
100	9.4	373	11.6	343
75	7.1	424	9.0	351
50	5.4	426	6.3	385

Table 4.1: Mass flow and temperature of exhaust gas at varying loads [Wärtsilä, 2012].

Table 4.1 shows the waste heat profile of the exhaust gas at different engine load points in gas and diesel modes. In order to quantify the heat energy available in any fluid, not only the mass flow and temperature but also the specific heat at constant pressure is required. The specific heat at constant pressure is not only dependent on the fluid temperature but also on the fluid constituents. The gas (fluid) constituents and its mole fraction data of the exhaust gas considered are the sample example taken from Stapersma [2010]. Unlike in reality, the gas constituents and its mole fraction data for the analysis are considered constant for all engine loads. The consequence of keeping these data constant for all engine loads for the analysis will be discussed in a later chapter.

The engine exhaust parameters are used to calculate and analyze the performance, size and layout of the ORC-WHR plant. The analysis are executed for every considered organic fluid for the exhaust gas of the engine in gas and diesel modes. In order to perform these analysis, the thermodynamic software Cycle-Tempo 5.0 and fluid property library FluidProp 2.4 are used. Apart from the exhaust gas and sea water data, input data to each component of the ORC plant in Cycle-Tempo has to be stated for the analysis to successfully complete. These input data can be stated and applied to each component of the ORC plant only after the plant layout that performs the ORC has been designed.

4.2. Initial Screening

As mentioned earlier, firstly an ORC plant has to be designed in order to perform initial screening of available organic fluids. Based on this plant design, component input data and heating & cooling fluid data, the functional fluids can be obtained and further analysis can be performed as desired.

4.2.1. Plant Layout of Simple-ORC

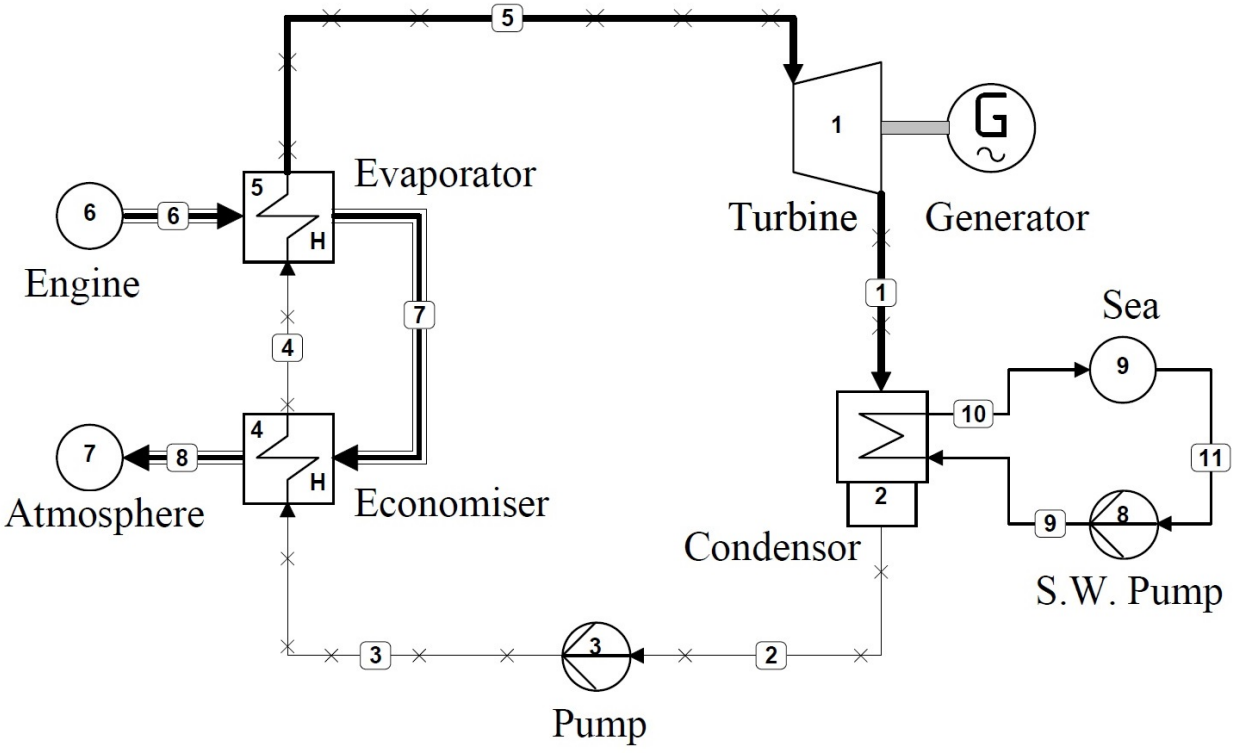

Figure 4.2: Plant layout of simple-ORC

An ORC-WHR plant is designed as a first step to screening organic fluids. Figure 4.2 shows the simplest plant layout that is considered to analyze and identify the possible functional organic working fluids. These functioning fluids will be retained for further consideration that best suits the application based on the plant size, thermal match and net power recoverability. The simple ORC plant design seen in Figure 4.2 is the same principle design of Rankine cycle seen in Figure 2.1. From the same figure comparison, it can be seen that the boiler component of the simple-ORC is split into two heat exchangers. These two heat exchangers in combination works as the single heat exchanger boiler component in principle as seen in the Rankine cycle design.

The two heat exchangers of the boiler component in the simple-ORC are the economizer and the evaporator. In the economizer, the temperature of the organic fluid is raised from condensing to evaporating temperature at constant pressure by absorbing sensible heat from the exhaust gas. The physical state of the organic fluid remains unchanged (liquid) in the economizer.

In the evaporator, the physical state of the organic fluid changes from liquid to saturated vapour at constant (evaporating) temperature and pressure along the heat exchanger length by absorbing latent heat from the exhaust gas. At design point, in both the economizer and the evaporator, the heating fluid exhaust gas remains in gas state throughout and does not change its physical state. In static analysis, the component input data ensures the desired operation and condition of the boiler and the plant for fluid screening. These input data will be discussed in the next sub-section part of this chapter.

In a real ORC plant, a single heat exchanger as the boiler component is sufficient to preheat and evaporate the organic fluid and also superheat the fluid if desired. However in this thesis approach, the boiler component is split in these two heat exchangers (i.e. economizer and evaporator) for easy equation balancing and static design calculations. To ensure the organic fluid does not superheat, the working fluid leaving the evaporator (or entering the turbine) is in saturated vapour state (i.e. dryness fraction of 1.0). This is because as mentioned earlier, the thermal efficiency remains almost constant despite increasing the fluid temperature by superheating. Hence in this thesis, a superheater block in the boiler or superheating of the working fluid are not included.

4.2.2. Fluid Screening

In addition to heating & cooling fluid data and the plant layout, component input data and initial condition of the simple-ORC plant in Cycle-Tempo has to be defined. This is required to perform the static analysis of the ORC-WHRS for all available organic fluids in Cycle-Tempo. The component input data and initial condition to perform the static analysis is shown in Appx. Section A.1.1. To analyze the performance of available fluids, the fluid is changed for every independent analysis and the initial conditions are kept unchanged. From this procedure, the organic fluids that can perform a sub-critical thermodynamic cycle can be obtained.

In order to ensure that the fluid selection and screening are performed under similar conditions to obtain a suitable working fluid, the quantity of heat input to the boiler (or the ORC) is kept constant. In addition to the engine exhaust data, the constant heat input is ensured by keeping the gas constituents & its mole fraction constant. Additionally with the design assumption that the exhaust temperature at boiler outlet is at 165°C. This temperature is chosen because it is slightly higher than the acid dew point of sulphur dioxide which could be a gas constituent depending on the type of fuel used. However this gas constituent is not included because the analysis is performed for engine in gas fuel.

To analyze the performance of different organic fluids for fluid screening, the other initial conditions that are kept constant are the evaporating pressure at 30 bar and condensing temperature at 40°C. In addition to all the above considered component input data and initial condition ensures that the fluid screening are performed under similar conditions in order to find the most suitable fluid for our application.

Functioning Fluids	
Acetone	R113
Butane	R114
1-Butene	R123
cis-2-Butene	R141B
Cyclohexane	R236ea
Cyclopentane	R245ca
Isobutane	R245fa
Ibutene	R365mfc
Ipentane	R436a
Methylcyclohexane	R436b
Neopentane	T2Butene
Pentane	Toluene
R11	–

Table 4.2: List of functioning fluids within desired temperature range

Based on the simple-ORC plant layout (Figure 4.2), heating fluid exhaust gas (Table 4.1), cooling fluid sea water and input data (Appx. Section A.1.1), all available fluids were analyzed in simple-ORC plant model in Cycle-Tempo. Based on this analysis, the organic fluids shown in Table 4.2 can complete a thermodynamic sub-critical cycle within the desired temperature range for our application.

Other fluids such as ethanol, methanol, heavy water (D_2O) and few other fluids are also functioning within the desired temperature range. However, these fluids are left out because these are wet type organic fluids with saturation vapour curves similar to water/steam. Wet type fluids are omitted from the functioning fluids list since the current simple-ORC plant layout is not the best suited design for wet fluids. This is because as mentioned earlier, the turbine expansion of such fluids in the simple-ORC plant will be in the two-phase region of the fluid. Such an expansion is highly undesirable because of induced losses in turbine efficiency. This can be avoided to accommodate wet fluids only after superheating of the working fluid in a superheater component is applied to the current simple-ORC plant model.

Among the list of functioning fluids, certain organic fluids will not or may not be used due to regulatory ban because of their detrimental effect on the environment. For example, chlorofluorocarbon (CFC) compound based fluids such as R11, R113 and R114. However, these regulatory bans/limited usage restrictions are applied to the fluid based on its application, for example of use in food refrigeration or ORC. In near future, it is highly probable that certain fluid may only be used in ORC if a leak detection system is in place.

4.2.2.1 Selection Parameter

We know that all the functioning fluids obtained may not be suitable for implementation on a ship because the fluid used also influences the plant design and size. Therefore, a selection parameter is required based on which the functioning fluids can be further screened. Volume (space available on a ship) as we know, is one of the important limiting design factors for marine application. Hence, the main decision making (selection) parameter to find a suitable organic fluid is the power density of the ORC-WHR plant. Since, the power density of a plant incorporates the power generated by the plant and the volume of the plant.

The ratio of power generation and mass flow rate is used as the screening parameter for screening the functioning fluids as listed in Table 4.2. The ratio of power generated and mass flow rate can nearly be described as power density of the plant since plant size is proportional to mass flow rate. The units of this described power density is $kW/(kg/s)$. Based on this power density equation, the functioning fluids are compared for further screening.

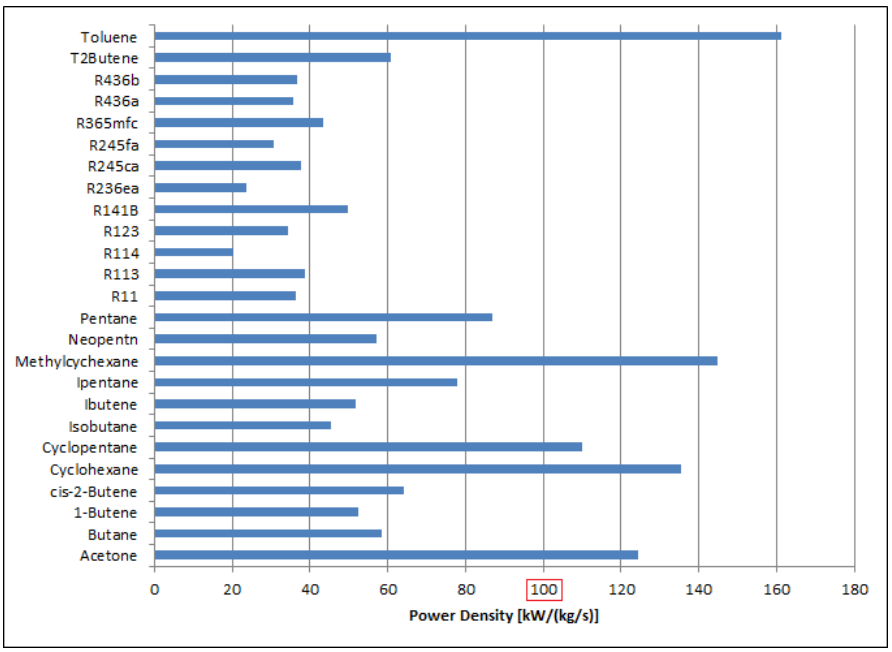

Figure 4.3: Functional fluid comparison based on power density [$kW/(kg/s)$]

Figure 4.3 shows the comparison of functional fluids based on power density and the quantitative values are given in Appx. Table A.1. It can be seen from the figure that a few organic fluids have shown larger power density than the rest. If focused on the fluids with power density larger than $100 kW/(kg/s)$, the fluids as shown in Table 4.3 are obtained and chosen for further analysis.

Fluid Name	Chemical Formula	Boiling Point [°C]	Flash Point [°C]	Specific Heat(c_p) [kJ/kg.K]	Freezing Point [°C]
Acetone	C_3H_6O	56.0	-20.0	2.14	-95.0
Methylcyclohexane	C_7H_{14}	101.0	0.38	1.89	-126.3
Cyclohexane	C_6H_{12}	80.7	-18.0	1.81	6.5
Cyclopentane	C_5H_{10}	49.3	-7.0	1.80	-93.9
Toluene	C_7H_8	110.6	4.44	1.70	-95.0

Table 4.3: Properties of promising working fluids based on selection parameter

We know that the promising organic working fluids as shown in Table 4.3 are obtained through fluid screening based on power density selection parameter only. However, this fluid screening can also be based on other design limiting factors such as weight or other operation based limiting parameters such as corrosion factor. The fluid screening may not only be based on one selection parameter as seen in this thesis, but also based on a combination of multiple selection parameters.

While selecting a suitable fluid based on selection parameter(s), other fluid characteristics also play an important selection criteria role especially in marine application. Such characteristics can be fluid properties such as toxicity or flammability, which may not be an issue during normal operation but can be of concern during unforeseen leakage. The promising fluids as seen in Table 4.3 have low flash points and are hydrocarbon based compounds which makes them flammable in ship environment. Hence, such fluid properties of the organic fluids may also be implemented into the screening methodology in order to obtain a safer fluid for marine application.

4.2.3. Static Analysis

In order to find the most suitable fluid and its most suitable plant layout, static analysis of these promising working fluids in ORC-WHRS are carried out. The power generated by these working fluids in the simple-ORC plant at the design point for discrete engine load points, fuel modes and the corresponding trends can be seen in Figure 4.4. These results are based on analysis for the waste heat profile seen in Table 4.1 under initial conditions shown in Appx. Section A.1.1. It can be seen from the figure that ORC-WHRS designed for higher engine load points generate higher power output.

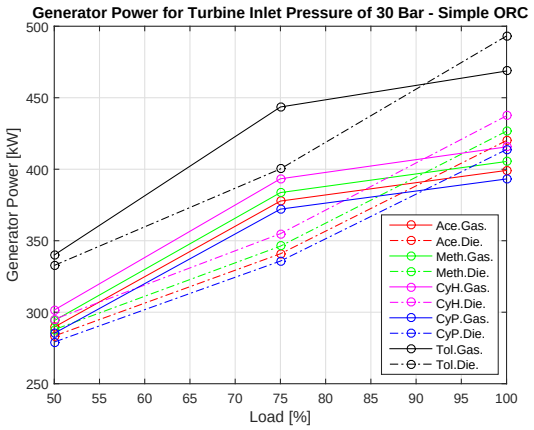

Figure 4.4: Power generated in the simple ORC plant.

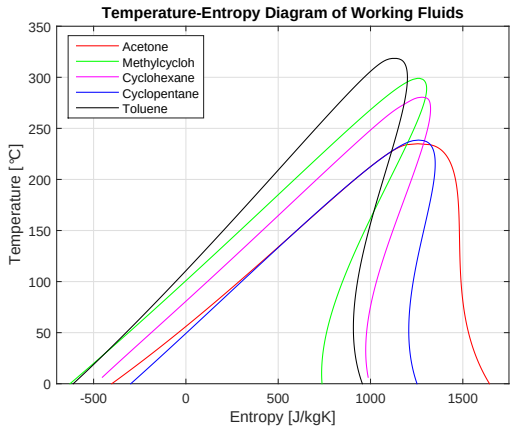

Figure 4.5: T-S diagram of the promising working fluids

However, these trends and comparisons run on a simple-ORC plant model may not be useful for fluid selection because this plant model layout is not best suited for all considered fluids. Firstly, because the T-S diagram as shown in Figure 4.5 shows that the fluids except acetone are dry type organic fluids. Secondly, because the turbine expansion is not an isentropic process (and is dependent on the turbine isentropic efficiency), therefore the working fluid after turbine expansion is in superheated state. Even though the fluid after turbine expansion is at condensing pressure, it is not at condensing temperature. Due to this, the load on the condenser is higher than desired as the condenser is required to cool down the superheated fluid down to condensing temperature. In addition to cooling water required for condensation alone, an even larger cooling water mass flow rate through the condenser is required to cool down the fluid temperature. This is because any fluid in vapour state has poor heat transfer properties in comparison to the same fluid in liquid state.

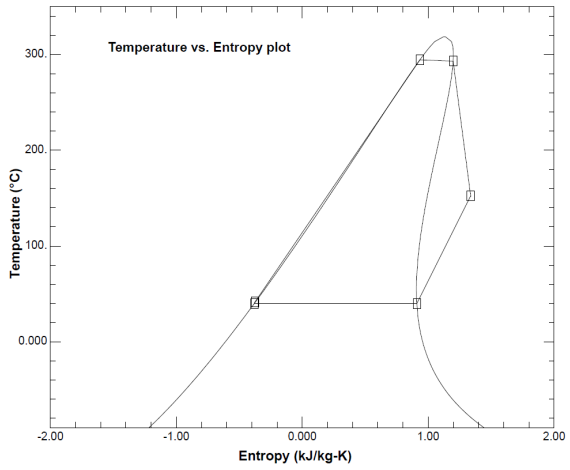

Figure 4.6: Temperature-Entropy diagram of toluene and the ORC cycle

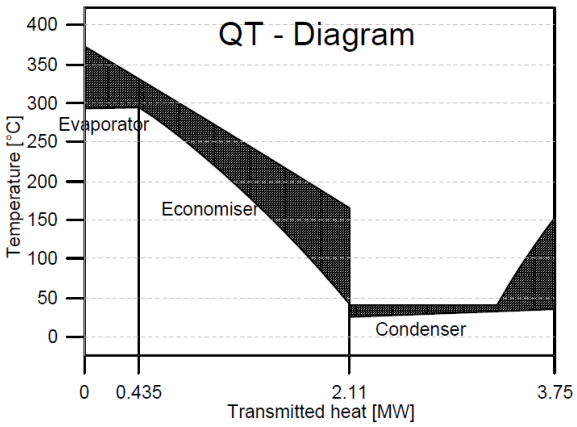

Figure 4.7: Heat tramsmitted-Temperature diagram of simple-ORC plant with toluene

To show the disadvantage of using a dry type organic fluid in a simple-ORC plant model, an example is taken from the analysis so far. As seen in Figure 4.4, we can notice that toluene has the highest power generation capability. The thermodynamic cycle of toluene in simple-ORC model representing the plant process is shown in Figure 4.6. It can be seen that the turbine expansion process leaves toluene in the superheated region clearing indicating that the fluid temperature is significantly higher than the condensing temperature.

In addition, the heat transmitted-temperature diagram of toluene in simple-ORC as shown in Figure 4.7 represents the heat transmitted to and from cooling fluid and heating fluid respectively. The load on the condenser and the loss of valuable heat energy to the cooling seawater can be seen. This load corresponds to larger cooling fluid mass flow rate and the loss corresponds to loss in plant efficiency.

Higher mass flow of cooling fluid and loss of valuable heat energy to it can be reduced and retained respectively, if changes to the plant layout can be adapted. The heat transfer of sensible heat to the cooling seawater in the condenser can be eliminated and mass flow of cooling fluid can be reduced by the introduction of a recuperator to the simple-ORC plant model. This not only increases the plant efficiency but also reduces the condenser size. Hence, a recuperator is incorporated into the simple-ORC plant to obtain a recuperative-ORC plant model. This model can be used for dry fluids to analyze and fully determine the amount of power generation and the plant size of the promising fluids in order to obtain the most suitable fluid.

4.3. Re-iteration of Initial Screening

A reiteration of the initial screening process of the screening methodology is carried out to find suitable fluids for further considerations. Hence, the steps within this process are re-executed.

4.3.1. Plant Layout of Recuperative ORC

The simple ORC plant is modified to accommodate a recuperator as shown in Figure 4.8 to have a recuperative ORC plant. As mentioned earlier, a recuperator is the heat exchanger that allows heat transfer between the working fluid after pump and the working fluid after turbine. This component reduces the cooling fluid mass flow in the condenser and subsequently reduces the amount of heat energy lost through the cooling fluid. In addition, it increases the working fluid temperature before boiler inlet which subsequently increases the plant efficiency.

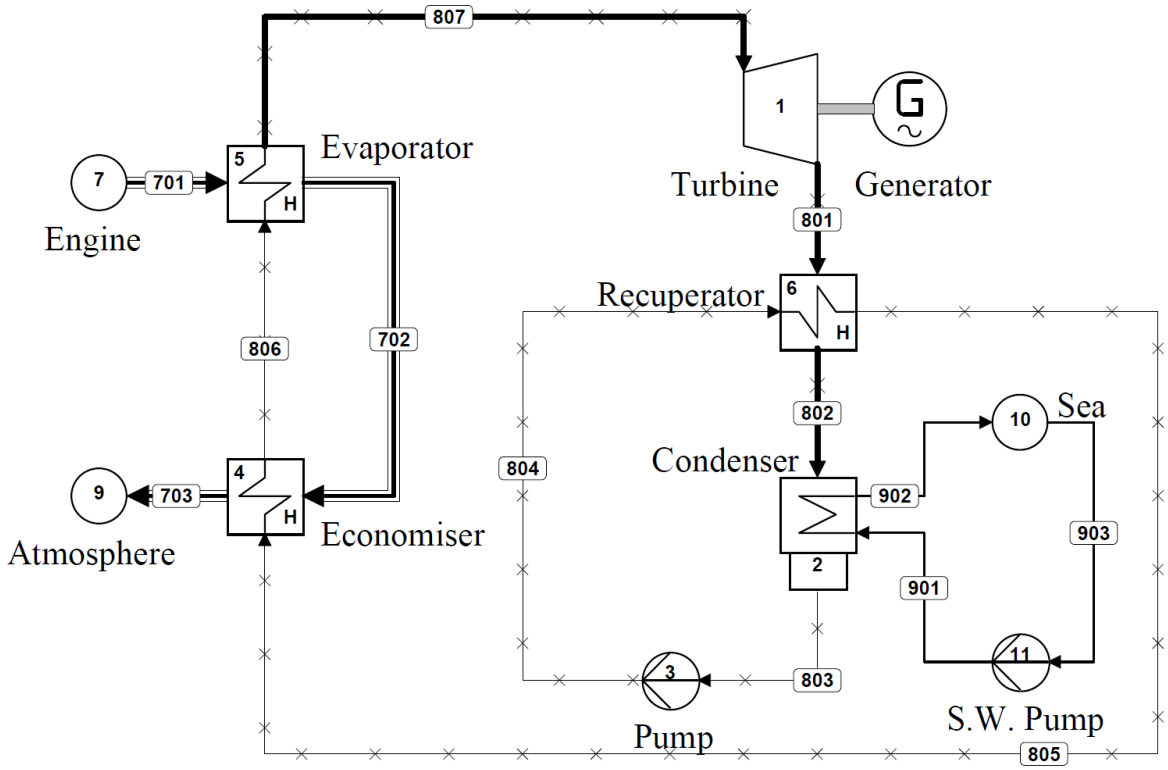

Figure 4.8: Plant layout of Recuperative ORC

4.3.2. Fluid Screening

As performed before, in addition to heating & cooling fluid data and the plant layout, component input data and initial condition of the recuperative-ORC plant in Cycle-Tempo has to be defined. This is required to perform the static analysis of the ORC-WHRS for all available organic fluids in Cycle-Tempo. The component input data and initial condition to perform the static analysis is shown in Appx. Section A.2.1. To analyze the performance of available fluids, the fluid is changed for every independent analysis and the initial conditions are kept unchanged. From this procedure, the organic fluids that can perform a sub-critical thermodynamic cycle in a recuperative-ORC plant can be obtained.

The results suggests that the fluids seen in Table 4.3 have higher power density among other functioning fluids in the desired temperature range for a recuperative-ORC plant as shown in Appx. Table A.2. This table also shows an increase in power generation in comparison to the same fluids when used in the simple-ORC plant but at relatively higher mass flow rate. The functioning fluids and promis-

ing fluids from this fluid screening are same as before with similar power densities. This is because the waste heat source temperature is the same and is the deciding factor. The selection parameter used in this screening is also the same as before as the application remains unchanged.

4.3.3. Static Analysis

The power generated by these working fluids in the recuperative-ORC plant at the design point for discrete engine load points, fuel modes and the corresponding trends can be seen in Figure 4.9. This figure captures the actual power generation potential of dry fluids in recuperative-ORC plant in comparison to the same fluids as seen in Figure 4.4 in simple-ORC plant for the same heat input. Methylcyclohexane as a working fluid has the highest potential of power generation from the exhaust gas and not toluene as seen before in the simple-ORC plant. From the same figures, we see that different fluids have different power generation potential for the same heat input to the ORC plant. However, irrespective of the fluid used, the trend of ORC-WHR performance in gas modes are similar and it is the same for diesel as well. These trends of power generation by the ORC-WHRS in gas and diesel modes are similar to the trends of heat energy input to the ORC-WHRS in gas and diesel modes respectively.

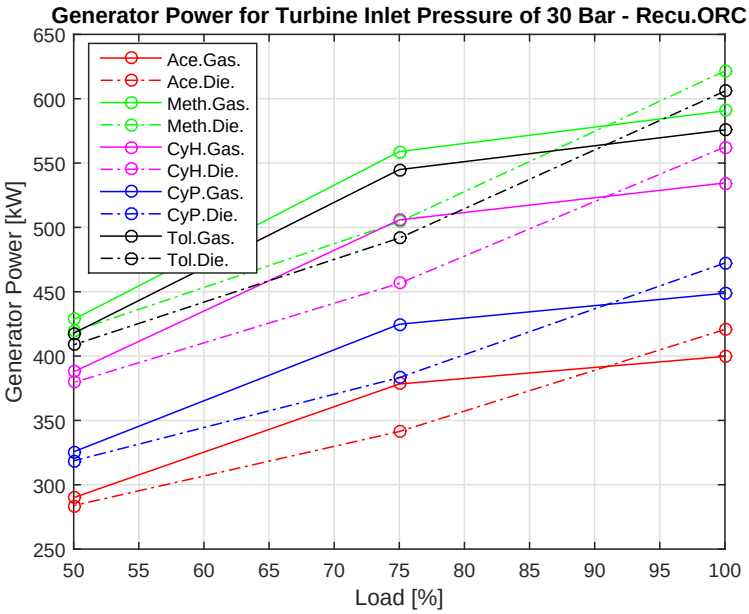

Figure 4.9: Power generated in the recuperative ORC plant with different organic fluids

For the same waste heat parameters and initial conditions, it can be seen that all the same organic fluids in recuperative-ORC plant produces more power when compared to the same organic fluid in the simple-ORC plant. As an example given before, toluene based plant cycle in recuperative-ORC is shown in Figure 4.10. This is compared to toluene based plant cycle in simple-ORC as seen in Figure 4.7 to see the increase in boiler inlet temperature (subsequently in plant efficiency). In addition, the reduction in heat energy lost to the cooling fluid in condenser can also be seen when toluene (dry fluid) is used in a recuperative-ORC plant model instead. These comparisons can also be seen in the value diagram, when the temperature term T in the Q-T diagram is replaced by $1 - \frac{T_0}{T}$ to obtain it as shown in toluene based plant cycle of recuperative-ORC in Figure 4.11.

The power generation capability is not the only criteria in our selection parameter for marine application, it is also the plant size. For selection based analysis, the power density of these fluids in both engine modes at discrete engine load points is calculated to find the most suitable design point based on the waste heat profile. However, the power density in terms of $kW/(kg/s)$ used for screening functioning fluids previously, may not enough to find the actual value or the most suitable design point.

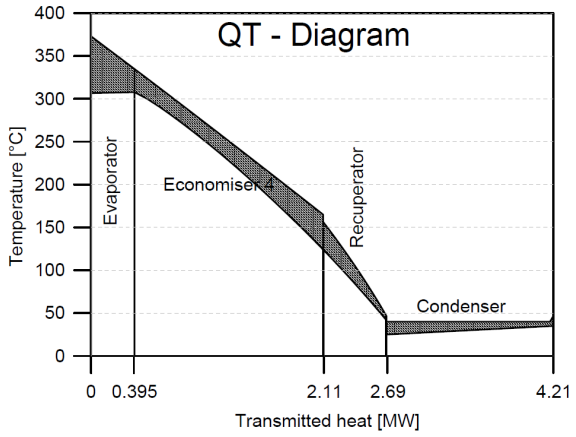

Figure 4.10: Heat transmitted-Temperature diagram of recuperative-ORC plant with toluene

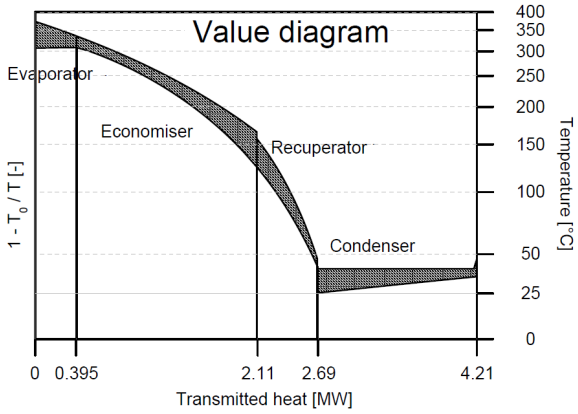

Figure 4.11: Value diagram of recuperative-ORC plant with toluene

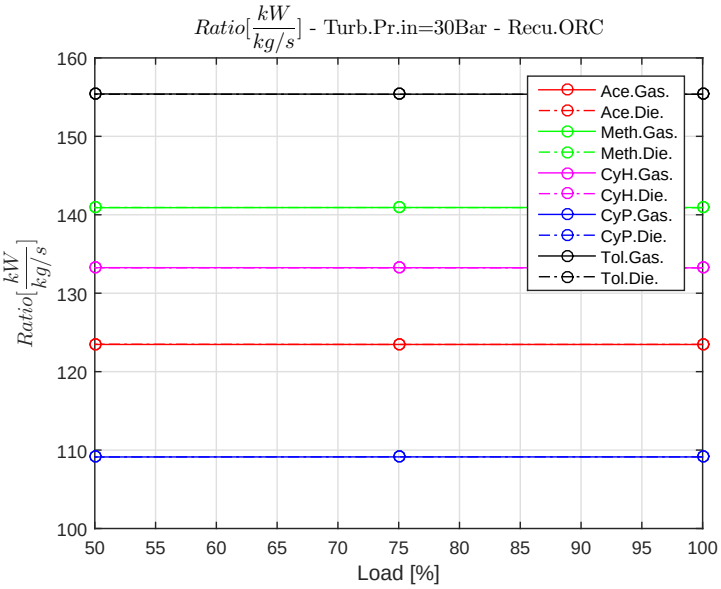

Figure 4.12: Ratio of power generation and mass flow rate of suitable fluids in recuperative-ORC

Figure 4.12 shows the power density of different organic in the recuperative-ORC plant when designed for load points across the engine load. Higher power density corresponds to higher suitability of that fluid for our application. This figure shows the fluid trends are fairly horizontal over the engine load. However, in spite of the mass flow rate being proportional to plant size, these ratios as seen in Figure 4.12 cannot be treated as decisive. This is because of the differences under same conditions in the physical properties of these fluids. Such as specific volume, thermal conductivity, Prandtl number etc., which determines the actual size of the plant components in terms of volume. Hence, the volume of the heat exchangers are calculated based on these physical properties, mass flows and heat exchanger geometry to determine the volume of the plant. The volume of the heat exchangers in an ORC plant are significantly larger than the rotating equipment such as turbines and pumps. Hence the plant size is based on the summation of the volume of the heat exchangers. Since Figure. 4.12 shows that power density in terms of $kW/(kg/s)$ is indecisive to obtain the most suitable fluid or a suitable design point region, power density in terms of kW/m^3 is calculated for different fluids in recuperative-ORC plant. After calculating the volume of recuperative-ORC plant for different fluids, the power density (kW/m^3) and the fluid trend over engine load can be obtained.

4.4. Heat Exchanger Sizing

Volume of the heat exchangers are calculated based on the Logarithmic Mean Temperature Difference (LMTD [K]). This method is used to calculate the heat transfer rate in double pipe heat exchanger. This is applicable since Cycle-Tempo uses the same method for a cross counter flow type heat exchanger. This is in order to calculate the overall heat transfer admittance ($U \cdot A$ [W/K]) of the heat exchanger, which can be used to calculate the length of the heat exchanger and subsequently the volume. The heat exchanger sizing calculations are clearly described in the thesis of Boonen [2009].

The overall heat transfer(ϕ_q[W]) across fluids is given as:

$$\phi_q = U \cdot A \cdot F \cdot \frac{\overbrace{(T_{hot\_out} - T_{cold\_in}) - (T_{hot\_in} - T_{cold\_out})}^{\text{LMTD}}}{ln\left(\frac{T_{hot\_out} - T_{cold\_in}}{T_{hot\_in} - T_{cold\_out}}\right)} \tag{4.1}$$

and the reciprocal of the overall heat transfer admittance ($U \cdot A$) equation is given as follows:

$$\frac{1}{U \cdot A} = \frac{1}{\pi \cdot L}\left(\frac{1}{D_{out} \cdot \alpha_{hot}} + \frac{ln(D_{out}/D_{in})}{2 \cdot \lambda_{wall}} + \frac{1}{D_{in} \cdot \alpha_{cold}}\right) \tag{4.2}$$

The Equation (4.1) is used to calculate the overall heat transfer admittance by substituting the values of overall heat transfer and the LMTD of that heat exchanger in Cycle-Tempo. The term $U \cdot A$ is substituted in Equation (4.2) to calculate the length L of the heat exchanger from which the heat exchanger volume is calculated. However to obtain that, the heat transfer coefficients of both hot and cold fluids should also be substituted into the equation. These terms in a heat exchanger is calculated based on the thermodynamic and transport properties of the fluids, in addition to fixed pipe dimensions.

In this application as in most applications, the heat exchangers are considered to be shell and tube type. In shell & tube type heat exchanger, the hot fluid is flowing outside the tube. This hot fluid is exhaust gas in the evaporator and economizer, and vapour form working fluid (after turbine side) in the recuperator. These fluids do not change their physical state throughout the length of the heat exchanger but only reduces its temperature by expelling sensible heat. Hence, the following convective heat transfer coefficient is used:

$$\alpha_{hot} = \frac{\overbrace{\left(0.3 + \frac{0.62 \cdot \overbrace{\left(\frac{4 \cdot \phi_m}{\pi \cdot D_{out} \cdot \mu} \cdot \frac{S_T}{S_T - D_{out}}\right)^{0.5}}^{\text{Reynolds number [-]}} \cdot Pr^{1/3}}{\left(1 + \left(\frac{0.4}{Pr}\right)^{2/3}\right)^{0.25}}\right)}^{\text{Nusselt number [-] for a single row}} \cdot \left(1 + \frac{2 \cdot D_{out}}{3 \cdot S_L}\right) \cdot k}{D_{out}}^{\text{Nusselt number [-] for pipe bundle with over 10 rows}} \tag{4.3}$$

However in the condenser, the working fluid is outside the tube and enters the heat exchanger in vapour form. The fluid then gradually changes its physical state along the length of the heat exchanger at constant temperature and exits in liquid form by expelling latent heat to the cooling water. Hence the following convective heat transfer coefficient is used:

$$\alpha_{hot} = 0.728 \cdot \left(\frac{(\rho_{liq} - \rho_{vap}) \cdot g \cdot (h_{vap} - h_{liq}) \cdot k_{liq}^3}{N_{row} \cdot v_{liq} \cdot D_{out} \cdot \left(T_{liq} - \underbrace{\left(\frac{T_{cw\_in} + T_{cw\_out}}{2} \right)}_{T_{wall}} \right)} \right)^{0.25} \tag{4.4}$$

In shell & tube type heat exchanger, the cold fluid is counter-flowed in the heat exchanger from inside the tube. This cold fluid is the liquid state working fluid in the economizer and recuperator, and cooling fluid in the condenser. The fluid does not change its physical state throughout the length of the heat exchanger but only increases its temperature by absorbing sensible heat. Hence, the following convective heat transfer coefficient is used:

$$\alpha_{cold} = \frac{\overbrace{0.023 \cdot \left(\overbrace{\frac{4 \cdot \phi_m}{\pi \cdot D_{in} \cdot \mu}}^{\text{Reynolds number [-]}} \right)^{0.8} \cdot Pr^{0.4} \cdot k}^{\text{Nusselt number [-]}}}{D_{in}} \tag{4.5}$$

However in the evaporator, the working fluid is inside the tube and enters the heat exchanger in liquid form. This fluid then gradually changes its physical state along the length of the heat exchanger at constant temperature and exits in vapour form by absorbing latent heat from the exhaust gas. Hence the following convective heat transfer coefficient is used:

$$\alpha_{cold} = \frac{\overbrace{C_1 \cdot \left(\overbrace{\frac{4 \cdot \phi_m}{\pi \cdot D_{in} \cdot \mu_{liq}}}^{\text{Reynolds number [-]}} \right) \cdot \left(\overbrace{\frac{h_{vap} - h_{liq}}{g \cdot L_{est}}}^{\text{Boiling number}} \right)^{0.5} \cdot k_{liq}}^{\text{Nusselt number [-]}}}{D_{in}} \tag{4.6}$$

4.5. Effective Selection based on Selection Parameter

After performing the necessary static calculation and sizing the plant components. The results can be used for an effective analysis to identify suitable fluid and plant design based on selection parameter.

4.5.1. Effective Analysis

Design point analysis of different working fluids (as shown in Table 4.3) at discrete engine load points in gas and diesel mode were carried out. From these analysis, parameters such as LMTD, mass flows, heat flow and overall heat transfer admittance are obtained (see Appx. Tables B.1–B.10). These parameters along with physical properties of fluids and a prescribed heat exchanger cross section geometry, the length of each heat exchanger and corresponding total volume of the plant are obtained (for an example, see Appx. Table C.1). Figure 4.13 shows the volume of the total plant for promising fluids and the trend in increase in volume of the plant with respect to corresponding increase in engine load.

After calculating the size of the heat exchangers in terms of length and volume, power density in terms of kW/m^3 of the organic fluids in the recuperative-ORC plant is obtained. Figure 4.14 shows the possible working fluid of interest and the trends. This graph is decisive in order to choose a working fluid and the plant design for further considerations. This is because, the difference seen in Figure 4.14 and Figure 4.12 shows that for power density, ratios of power generation over total volume is more realistic than with mass flow rate.

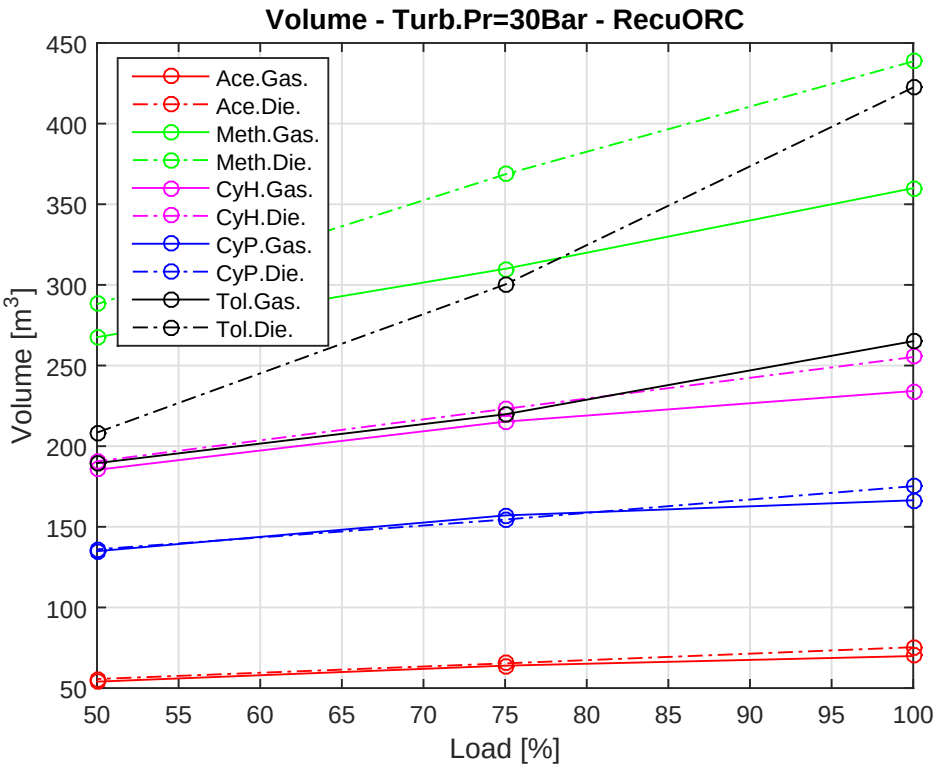

Figure 4.13: Total volume of the recuperative ORC plant with different organic fluids

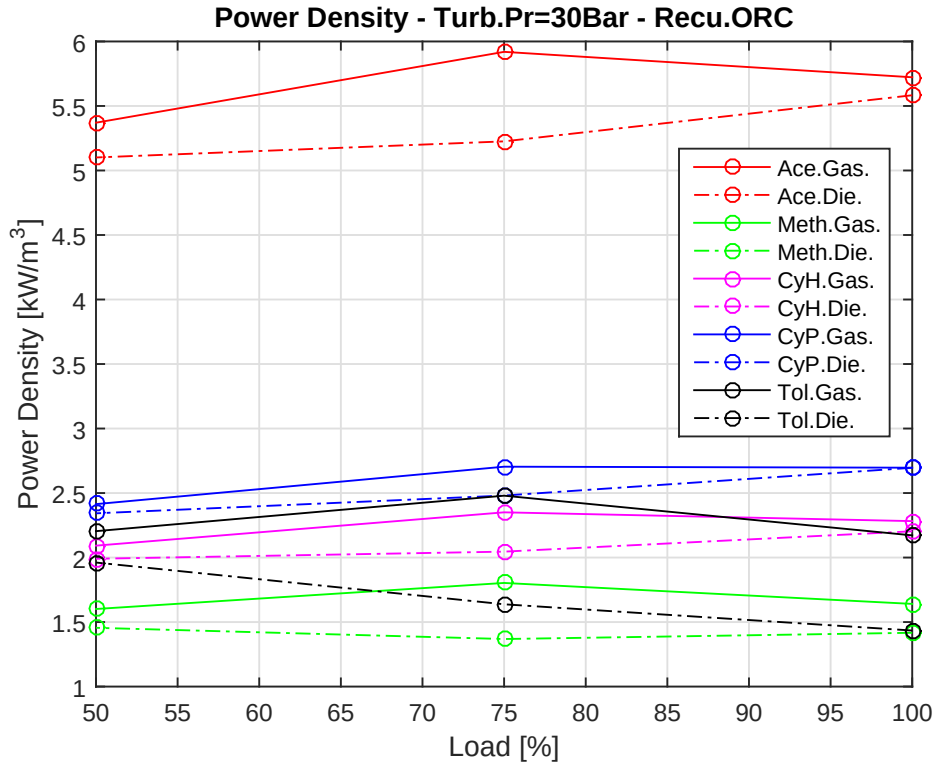

Figure 4.14: Power Density of recuperative-ORC plant with different organic fluids

From Figure 4.14, acetone as a working fluid is clearly the most suitable working fluid for the current application. The analysis of all these fluids were performed for the turbine inlet pressure of 30 bar, as mentioned earlier. When optimized for maximum cycle efficiency, acetone is still clearly the most suitable working fluid for the application as seen in Figure 4.15. This optimization function used in Cycle-Tempo finds the most optimal turbine pressure in order to obtain the highest possible cycle efficiency. The analysis data of the promising fluids in simple and recuperative-ORC plants for non-optimized and optimized calculations are shown in Appx. Table B.1 to TableB.10. The calculated component size and the power densities are shown in Table D.1 and Table D.2.

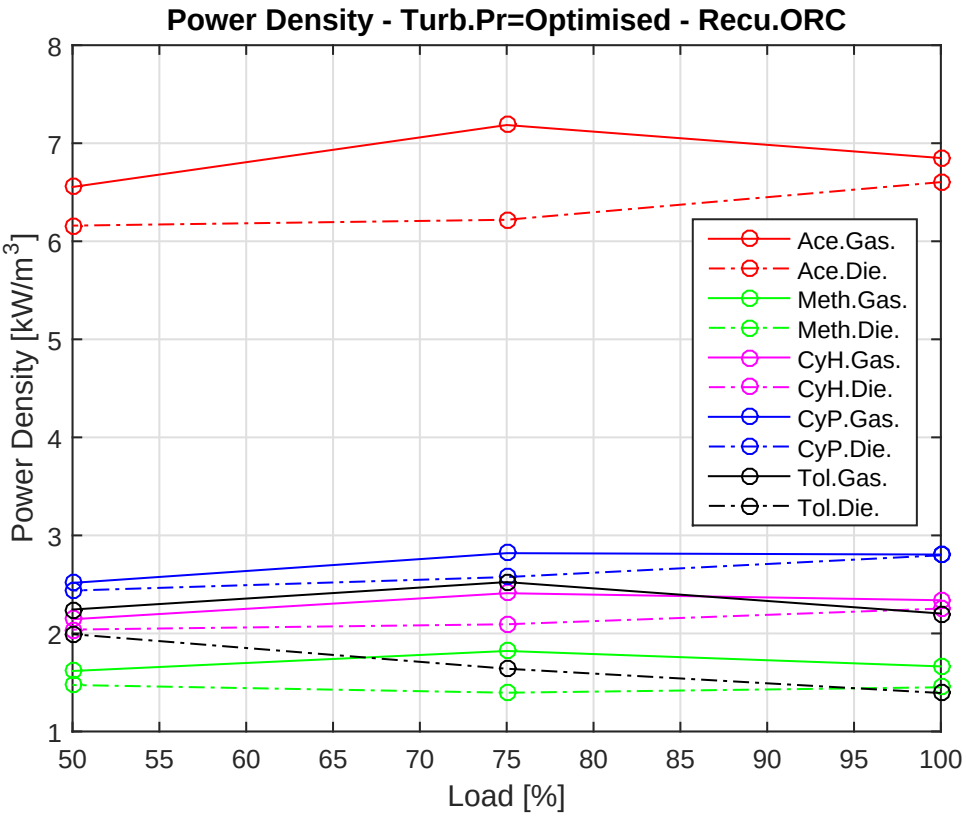

Figure 4.15: Power Density of recuperative-ORC plant with different organic fluids for optimized cycle efficiency

Acetone and cyclopentane are the two best organic fluids among the five promising fluids for our application based on power density. Cyclopentane is clearly suitable in a recuperative-ORC plant because of its dry fluid characteristics as seen in Figure 4.5. In addition, this can also be seen when comparing the same fluid in both plant designs as seen in Table A.1 and Table A.2 (also in Appx. Table B.7 and Table B.8). However from the same table comparison for acetone, the power generated is more in the simple-ORC plant than in the recuperative-ORC plant. This can be nearly understood from the T-S diagram that acetone is fairly an isentropic type organic fluid. Hence a comparison of acetone in simple and recuperative-ORC plants is necessary to fix a suitable plant design to acetone.

4.5.2. Acetone

The analysis for the recuperative ORC plant did not show any significant increase in power generation for acetone, unlike for other promising fluids, due to its isentropic saturation vapour curve characteristics. Hence a comparison of an acetone based ORC plant in a simple and recuperative-ORC plants are carried out. These analysis will determine which plant design is the most suited to acetone based on the selection parameter and the operating temperature range.

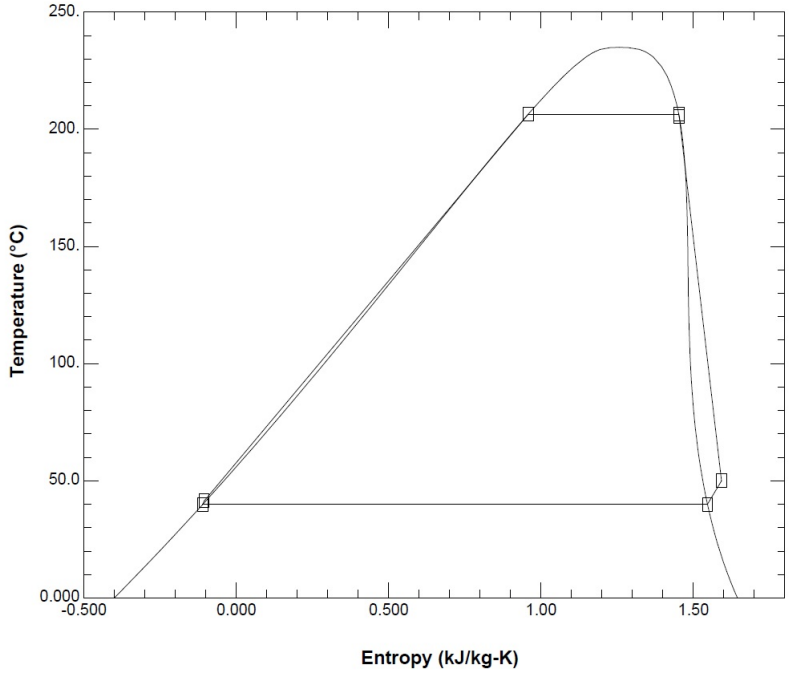

Figure 4.16: Temperature-entropy diagram of acetone and the ORC process

For the initial condition and waste heat profile, the temperature-entropy diagram of acetone and its ORC process is shown in Figure 4.16. Unlike as seen in Figure 4.6 for dry organic fluids used in simple-ORC plant, the fluid condition after turbine expansion for acetone has lower thermal load on the condenser. This means that the turbine exit temperature for acetone is significantly closer to condensing temperature when compared to the turbine exit temperature of other suitable fluids in our application. This suggests that for acetone, a recuperative-ORC plant may not bring any significant advantage over acetone when used in a simple-ORC plant.

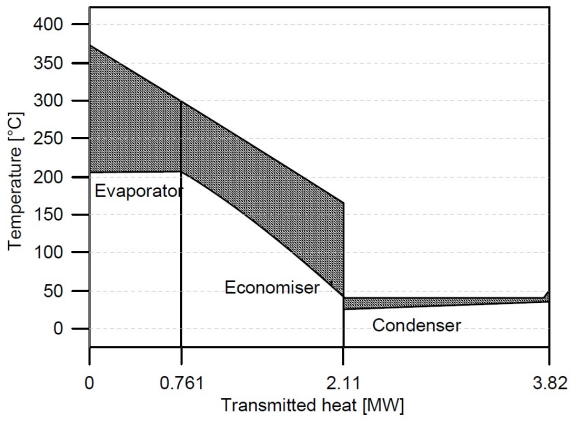

Figure 4.17: Q-T diagram of acetone in simple-ORC plant

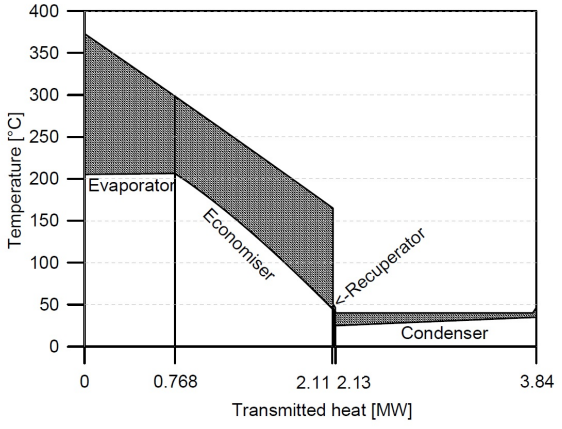

Figure 4.18: Q-T diagram of acetone in recuperative-ORC plant

Figure 4.17 and Figure 4.18 shows the heat transmitted-temperature (Q-T) diagram of acetone when used in a simple and recuperative-ORC plants respectively. It can be seen from this comparison that the heat transfer load on the condenser is almost the same and the thermal load is significantly smaller when compared to dry fluids used in a simple ORC as seen in Figure 4.6. This suggests that for acetone, simple-ORC plant is the best suited plant design. This is at least true for the temperature range in which it cycles.

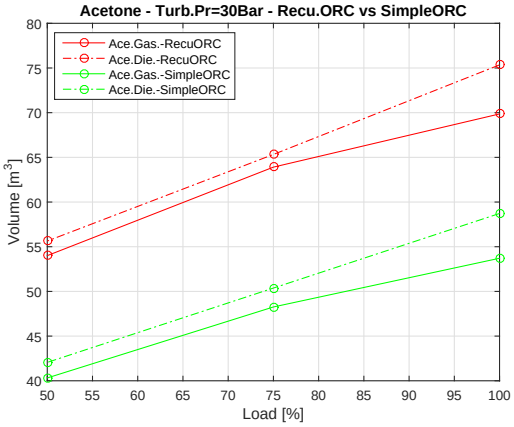

Figure 4.19: Volume of acetone for simple-ORC vs Recuperative-ORC based plant

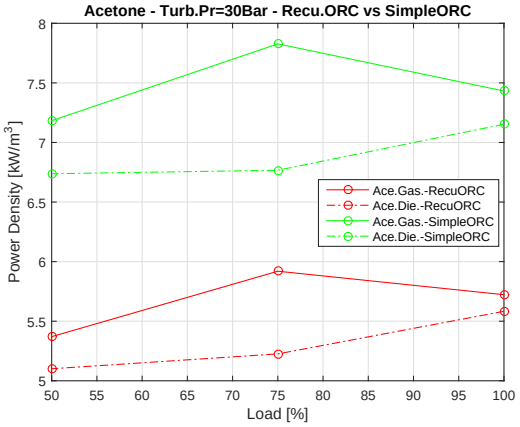

Figure 4.20: Power density of acetone for simple-ORC vs Recuperative-ORC based plant

Figure 4.19 and Figure 4.20 shows that simple-ORC plant is more suitable for acetone over recuperative-ORC plant because the plant volume is smaller and power density is higher in simple-ORC based acetone plant. The sizing of these plant components calculated are shown in Appx. Table D.3. The next most suitable fluid as per Figure 4.14 is cyclopentane used in the recuperative-ORC plant. For further analysis, acetone based simple-ORC plant and cyclopentane based recuperative -ORC plant has been considered.

4.5.3. Net Power and Plant Efficiency

The power produced by the actual ORC-plant process is the mechanical power at the turbine shaft. Since electrical power is what is desired against the waste heat, the electric power generated at the generator is the power produced by the ORC plant process. Taking auxiliary power demands of other components within the plant, net power is the actual energy recovered in electrical form from the waste heat. Electrical power required by the working fluid and cooling fluid pumps are these auxiliary demands that are met in order to run the ORC-WHRS plant.

The net power generated by the ORC plant process is given by:

$$P_{Net} = P_{Gen} - (P_{Pump} + P_{SW,Pump}) \tag{4.7}$$

where P_{Pump} and $P_{SW,Pump}$ is the electrical power required for working fluid and cooling sea water pumps respectively and P_{Gen} is the power produced by the turbo-generator.

In addition to net power, net energy and exergy efficiencies of the plant are also an important parameter to understand how efficient an ORC plant can be with respect to other WHRS systems.

The net energy efficiency of the ORC plant is given by:

$$\eta_{en} = \frac{P_{Net}}{\phi_{m,eg} \cdot C_{p,eg} \cdot (T_{eg,in} - T_0)} \tag{4.8}$$

and the net exergy efficiency of the ORC plant [Sun et al., 2017a] is given by:

$$\eta_{ex} = \frac{P_{Net}}{\phi_{m,eg} \cdot [(h_{eg,in} - h_0) - T_0 \cdot (s_{eg,in} - s_0)]} \tag{4.9}$$

4.6. Influence of Cooling Fluid on ORC Plant & Performance

For marine application, sea water is the most suitable source of cooling fluid. Besides its easy and abundant availability, it is also desirable for its surface temperature, heat transfer and thermodynamic properties. Thus making sea water a direct or indirect source of preferable cooling fluid for a condenser on board ships.

In steam Rankine cycle, the cooling fluid temperature is chosen in such a way that the water/steam working fluid in the condenser doesn't cool down below its freezing point (i.e. 0°C at 1 atm). Hence the availability and temperature of sea water makes it a suitable cooling fluid for SRC in marine application. Moreover due to the wide use of SRC in industries, (sea) water is considered as the most suitable cooling fluid. Due to this reason, it is sometimes assumed that water is the default cooling fluid even for ORC. However, this may not be true in terms of thermal efficiency, especially when organic fluids with relatively lower freezing points are used.

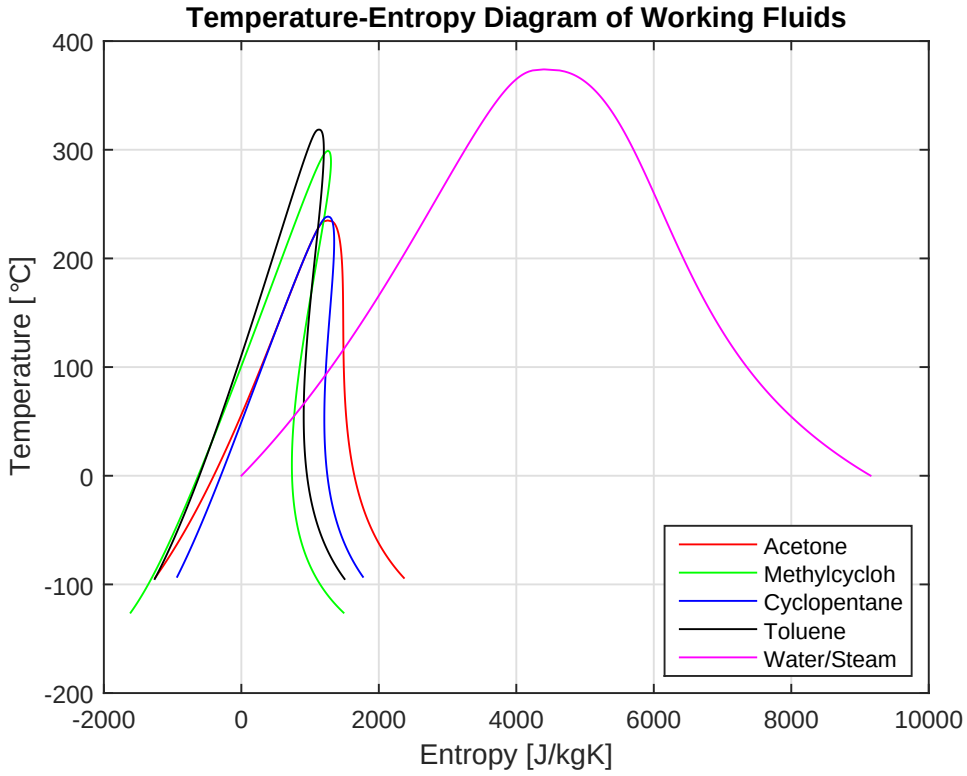

Figure 4.21: Saturation curve of working fluids in Temperature-Entropy plot

Figure 4.21 shows the saturation curves of some organic fluids and water/steam in temperature-entropy plot. It can be seen that water/steam is not fluid (solidifies) below 0°C (its freezing point). So the condensing temperature of water/steam working fluid should be well above the freezing point of water. This freezing point of water is higher than the freezing point of several organic fluids (see Table 4.3). Hence the condensing temperature of these organic working fluids in Rankine cycle process can be lower than the condensing temperature of water/steam based Rankine cycle.

It can be also be seen in Figure 4.21, that the organic fluids as seen in Table 4.3 are not only operable above 0°C but also between 0°C and its freezing point in an ORC plant. The utilization of this region is practicable only if the temperature of condenser cooling fluid is either below or around the freezing point of these organic fluids. These condenser cooling fluid temperatures will reduce the condensing temperature of the working fluid in an ORC and eventually increases the Carnot efficiency of the cycle. Higher the Carnot efficiency, higher will be the thermal efficiency of the ORC process.

The Carnot efficiency of Rankine cycle is given by:

$$\eta_{carnot} = 1 - \frac{T_{cond}}{T_{evap}} \tag{4.10}$$

and the thermal efficiency of the ORC plant process [Khennich and Galanis, 2012] is given by

$$\eta_{th} = \frac{P_{Tur} - P_{Pump}}{\phi_{m,eg} \cdot C_{p,eg} \cdot (T_{eg,in} - T_{eg,out})} \tag{4.11}$$

The highest Carnot efficiency of the ORC is possible, when the temperature of the available heating and cooling fluids are above the critical and below the freezing temperatures of the organic fluid respectively. This allows the full potential of that organic fluid in a Rankine cycle to be utilized for waste heat recovery application. For WHR of engine exhaust gas on board ships, the exhaust gas temperature are well above the critical temperature of the suitable organic fluid considered for our application. But for a condenser cooling fluid below the freezing point of the organic fluid, if available, LNG (Liquefied Natural Gas) stored in cryogenic temperature used as fuel for gas or dual fuel engine can be utilized. Lowering of the condensing temperature of an ORC by utilizing LNG as condenser cooling fluid improves the performance and the thermal efficiency of the ORC plant [Sun et al., 2017b]. This is achieved by utilizing the cold energy (i.e. cryogenic exergy) contained in LNG [Franco and Casarosa, 2014].

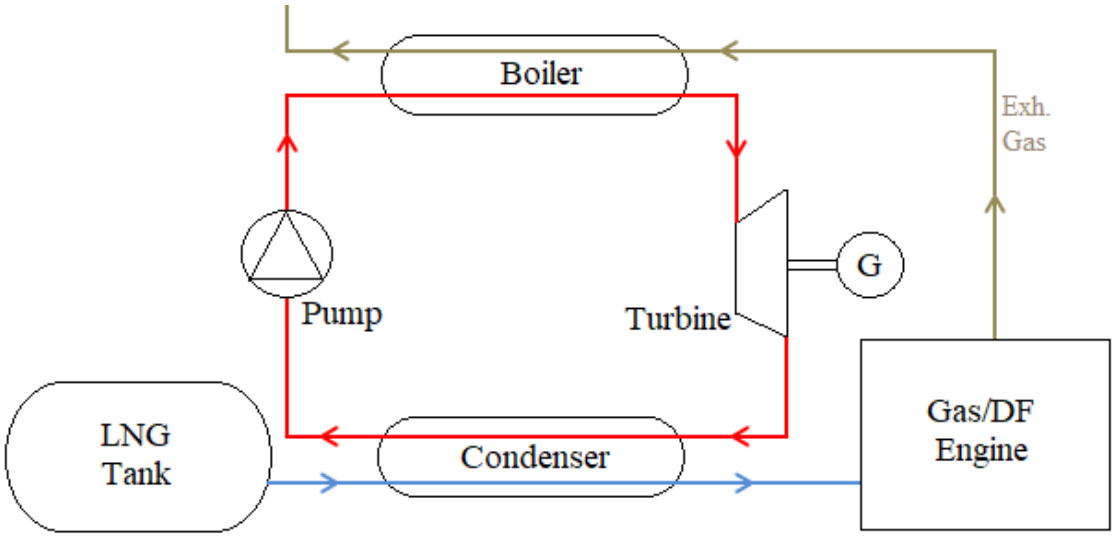

Figure 4.22: Simple schematic of ORC integrated LNG-Engine

A comparison is made between two same ORC-WHRS, but one utilizes sea water as the cooling fluid, whereas the other utilizes LNG as the cooling fluid. This captures the advantages of lowering the condensing temperature in an ORC-WHRS. For this comparison, the analysis already performed for acetone based simple-ORC is used to reflect the performance of the ORC plant with sea water as condenser cooling fluid. For the analysis of the same acetone based simple-ORC with LNG as condenser cooling fluid, an integrated plant of ORC-WHR with the dual fuel engine is designed. Figure 4.22 shows how the ORC-WHR plant is integrated to DF engine and the LNG fuel line. This system utilizes the heat energy of the exhaust gas and cold energy of LNG in the boiler and condenser of the ORC-WHRS respectively. For the analysis of this integrated design, initial conditions are kept the same as used for acetone-seawater analysis as before. However, with the changes only in the type of cooling fluid and the temperature difference of the cooling fluid in the condenser. The initial conditions for LNG based acetone in simple-ORC plant is shown in Appx. Section B.1.

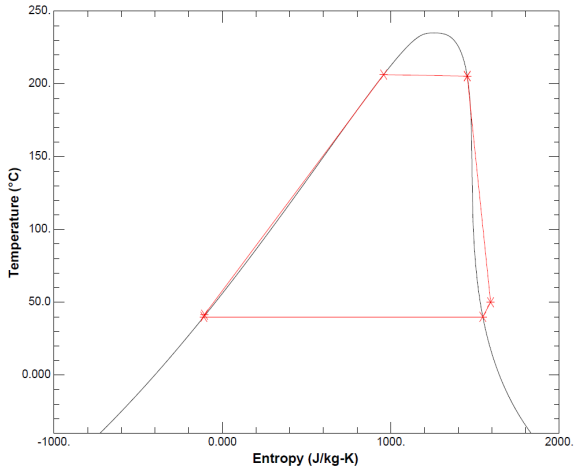

Figure 4.23: T-S diagram of ORC with water as cooling fluid

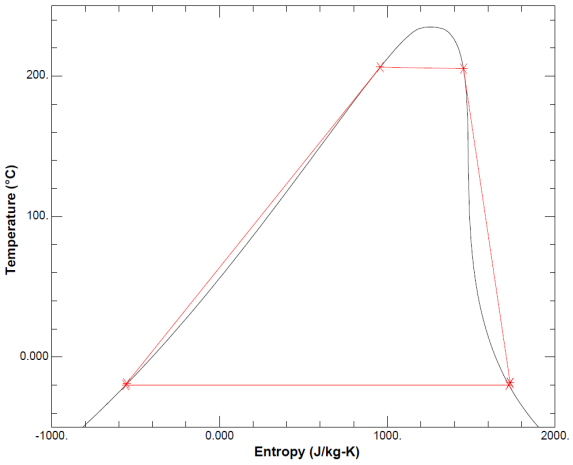

Figure 4.24: T-S diagram of ORC with LNG as cooling fluid

For the same heat input to the ORC boiler, the thermodynamic cycle of acetone based simple-ORC with sea water and LNG as cooling fluids are shown in Figure 4.23 and Figure 4.24 respectively. These figures show the temperature-entropy plot of acetone and the ORC processes. The latter figure clearly indicates comparatively a larger temperature drop in the turbine expansion process leading to higher Carnot efficiency. The temperature drop of acetone in turbine expansion process is held in such a point that the acetone exits the turbine in saturated vapour condition. This is to ensure that acetone remains in vapour state through the turbine expansion process and not in a two-phase state at any point inside the turbine. The LNG plant design and static analysis performed in Cycle-Tempo is shown in Figure B.1. Methane is used as the cooling fluid representing LNG since it contains 85 to 90% of methane in volume/volume basis.

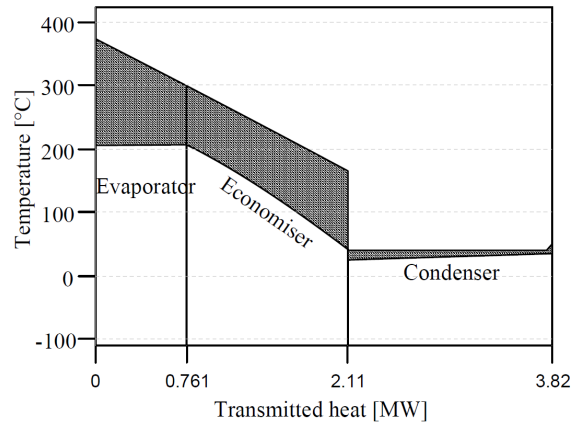

Figure 4.25: QT diagram of acetone-ORC process with sea water cooling

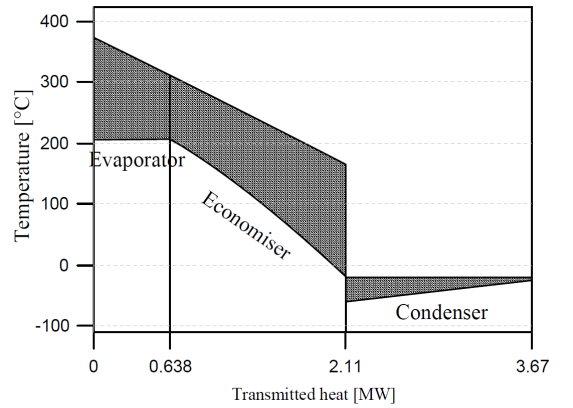

Figure 4.26: QT diagram of acetone-ORC process with LNG cooling

The performance comparison of simple-ORC plant with seawater and LNG cooling fluids are shown in Table 4.4. It can be seen that in LNG cooling process, there is significant increase in power generated due to comparatively larger temperature difference between evaporator and condenser. This increase in generator power is due to comparatively lower heat transfer in the condenser from working to cooling fluid. This can be seen in the temperature-heat transmitted (Q-T) diagrams of acetone-ORC heat exchangers with sea water and LNG cooling fluids as shown in Figure 4.25 and Figure 4.26 respectively. This increase in generator power also leads to increase in net energy and exergy efficiencies of the ORC plant process and also the power density of the plant.

Exhaust Gas IN			
Temperature	[℃]	373	373
Mass Flow	[kg/s]	9.4	9.4
Pressure	[Bar]	1.05	1.05
Cooling Fluid IN			
Fluid	[-]	Water	Methane
Temperature	[℃]	25	-60
Mass Flow	[kg/s]	40.965	20.905
Pressure	[Bar]	1.513	1.5
ORC Performance			
Generator Power	[kW]	399.17	539.65
Pump Power	[kW]	19.98	15.78
Coolng Flu. Pump Power	[kW]	3.66	0
Net Power	[kW]	375.53	523.87
Wrkng Flu. Mass flow	[kg/s]	3.207	2.688
Net Energy Efficiency	[-]	0.1036	0.1445
Net Exergy Efficiency	[-]	0.3164	0.4414
Thermal Efficiency	[-]	0.1893	0.2613
Carnot Efficiency	[-]	0.3455	0.4709
Size			
Evaporator	[m^3]	10.94	8.68
Economiser	[m^3]	24.42	20.24
Condenser	[m^3]	18.35	10.85
Total	[m^3]	53.71	39.77
Power Density	[kW/m^3]	7.43	13.57

Table 4.4: Comparison of ORC performance with water and LNG as cooling fluids

In addition to increase in efficiency of the ORC plant, using LNG as cooling fluid also leads to reduction in plant size primarily the heat exchangers. The reduction in the heat exchanger size of the boiler components are due to reduction in required working fluid mass flow rate compared to seawater cooling fluid system. This reduction is due to the relative increase in temperature difference between the working fluid inlet and outlet of the boiler. Because, we know that the heat added is proportional to the mass flow rate and enthalpy difference of the fluid in the boiler. In case of the condenser, it is also due to the reduction in mass flow of LNG cooling fluid at the considered temperatures. This reduction in plant size is an added advantage since it also contributes to the increase in power density of the ORC plant. In this analysis, the LNG cooling fluid across the condenser is in vapour state and heat transfer coefficients in general are comparatively better in liquid state (higher density). Hence, the size of the condenser could be further decreased by making changes to the pinch temperature between the working and cooling fluids and the temperature difference of the cooling fluid in the condenser.

From the analysis shown in this section, it is clear that ORC has greater potential when low temperature cooling fluid is used. The ORC-WHRS integrated to LNG fueled dual fuel/gas marine engine is an application which can certainly use this potential of organic fluids to increase the efficiency of the integrated system.

5

ORC based WHR Model

In this chapter, the development of dynamic ORC models for simple-ORC and recuperative-ORC plant layouts are discussed. These models are modified from a dynamic SRC model developed by Boonen [2009] and Ruyck [2011].

After identifying the plant layout and analyzing the potential fluids based on power density, the ORC plant is modeled in Matlab-Simulink. These models are used to analyze the off-design performance of the ORC plant based on varying engine loads. These simple and recuperative-ORC models are generic and can be used for analyzing any organic working fluid in its suitable plant model. FluidProp library and its Matlab function are used to calculate the thermodynamic and transport properties of the fluids during simulation. Hence, the type of heating fluid in the boiler and the cooling fluid in the condenser can also be changed, as desired. The simple-ORC model is also used to analyze the model sensitivity to input parameter and the dynamic behavior of the model with respect to varying step functions and duration.

5.1. Model Elements

The ORC models are based and built on the balance blocks of volume and resistance element. These elements are coupled together accordingly to form the plant models since the working principle is a closed cycle [Boonen, 2009; Grimmelius, 2005].

5.1.1. Volume Element

In these models, volume element represents components that exchange heat among fluids. Such as, the evaporator, economizer, recuperator and condenser components of the ORC plants. Volume element is used to calculate the pressure and temperature in the element with mass and energy balance. Figure 5.1 shows the causality representation of volume element.

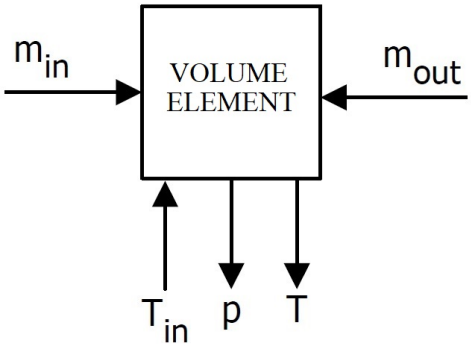

Figure 5.1: Volume Element with causality [Boonen, 2009]

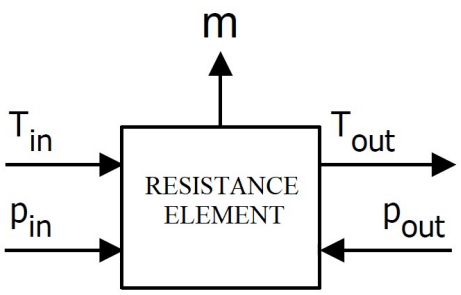

Figure 5.2: Resistance Element with causality [Boonen, 2009]

5.1.2. Resistance Element

In these models, resistance element represents components that demands or supplies work. Such as, pumps, turbo-generator and valves. This element is used to calculate the mass flow through the system and the exit temperature as a result of pressure and temperature difference with an energy balance. Figure 5.2 shows the causality representation of resistance element.

5.2. Plant Modification

Although the working principle of Rankine cycle is the same for any working fluid, be it steam or organic, the plant layout and the components are based on the type of working fluid used for the application. This makes the steam based Rankine cycle plant different from ORC plant. The existing Rankine cycle model in Matlab-Simulink is based on water/steam and the corresponding plant layout and the components can be seen in Figure 5.3 and the causality representation in Figure 5.4. To modify this plant model into ORC, removal of components such as steam drum, deaerator etc. and addition of other components such as recuperator is required.

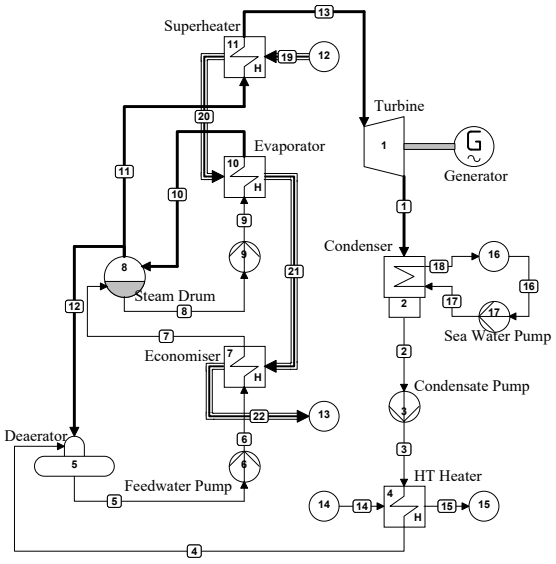

Figure 5.3: Steam Rankine cycle plant [Ruyck, 2011]

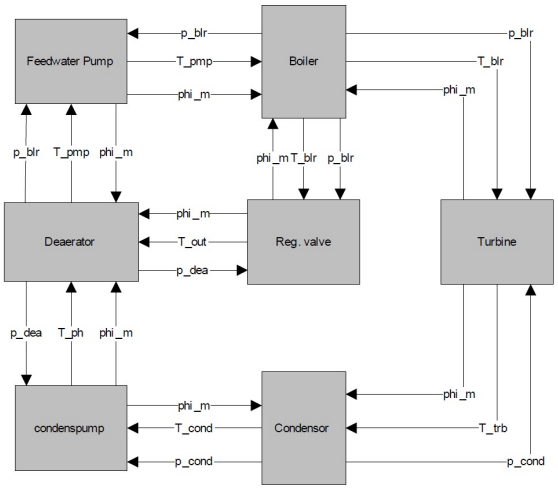

Figure 5.4: Causality representation of SCR model [Ruyck, 2011].

5.2.1. Removal of Steam Drum

A single heat exchanger can preheat, evaporate and superheat an organic fluid. Hence, a once-through boiler is used for an ORC process [Andreasen et al., 2017], which does not require a drum or re-circulation line. This is because, organic fluids have relatively smaller density difference between its vapour and liquid state than steam and water, especially for higher molecular weight organic fluids. Unlike in boilers of ORC, low vapour density in boilers of SRC can cause very different heat transfer and pressure drop characteristics between water and steam. Hence, a complete evaporation of water in a single heat exchanger is therefore avoided [Quoilin et al., 2013] and the drum (which acts as a phase separator) is used to separate the water droplets from saturated steam to avoid deposits of impurities in the superheater or to avoid carryover of water droplets by steam into an expander.

5.2.2. Removal of Deaerator

To reduce corrosion of the equipment in a steam plant, the dissolved gases like nitrogen, oxygen and carbonic acid should be removed from the water/steam line. This removal is essential for a steam process and a deaerator is used for the removal of these dissolved gases [Ruyck, 2011]. In general, air infiltration in ORC plants are low because they are often sealed. Hence, a deaerator is not necessary, however a small vacuum pump in the condenser can be used to remove any air infiltration [Algieri and

Morrone, 2012]. Moreover, working fluids as shown in Table 4.3 have their saturation pressures at condensing temperature close to the atmospheric pressure which facilitates its cycle in an ORC plant without a deaerator [Uris et al., 2014].

5.2.3. Removal of Other Components

HT heater utilizes the waste heat energy carried by the jacket cooling water from the engine to preheat the water/steam working fluid in SRC (component #4 as seen in Figure 5.3) and this heat exchanger is removed for this ORC plant model due to its relative low energy quality with respect to exhaust gas. However, this part can be implemented in an ORC system on application basis when the power density of that system is better when compared to the same system without HT heater. Superheater (comp. #11) is also removed because, as mentioned earlier, a superheater doesn't bring any significant advantage into an ORC plant in terms of thermal efficiency or expansion condition. Other additional pumps are also removed since the system is either under condenser or evaporator pressure in the heat exchangers and does not have any intermediate pressure in the system.

5.3. ORC Plant Model

In this section, ORC-WHRSs are modeled in Matlab-Simulink to use isentropic and dry type organic fluids as working fluids in simple-ORC and recuperative-ORC plant respectively. The densities, specific heat and other fluid properties changes with respect to the temperature and pressure of the fluids. The simple-ORC and recuperative-ORC plant models are discussed as follows.

5.3.1. Simple-ORC plant model

As mentioned earlier, volume and resistance elements are coupled together as a cycle to form the ORC plant model. Figure 5.5 shows the causality representation of the simple-ORC plant model based on the layout shown in Figure 4.2.

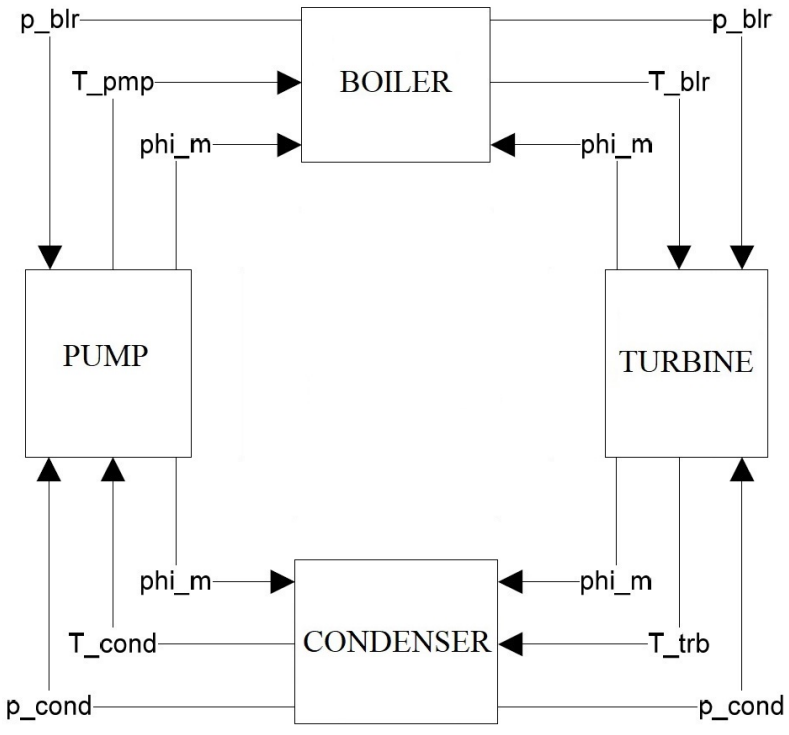

Figure 5.5: Causality representation of simple-ORC plant model (similar to SRC model in [Boonen, 2009]).

The simple ORC plant design and model are best suited for working fluids categorized as isentropic type organic fluids, such as acetone, R134a, etc. This isentropic saturated vapour curve property for acetone is at least true for the temperature range in which the application operates and performs a complete thermodynamic cycle. The categorization of a working fluid used in any application can be approximately based on the following equation:

$$\xi = \frac{ds}{dT} = \frac{C_p}{T_H} - \frac{\frac{n \cdot \frac{T_H}{T_{crit}}}{1 - \frac{T_H}{T_{crit}}} + 1}{T_H^2} \cdot \Delta h_H \tag{5.1}$$

Where the constant n is either 0.375 or 0.380, T_H is the evaporation temperature, T_{crit} is the critical temperature and Δh_H is the enthalpy of vaporization. The working fluid is considered dry fluid for $\xi >$ 0, isentropic for ξ 0 and wet fluid for $\xi <$ 0 [Jumel et al., 2012]. However other thermodynamic data or equation can be used for a more accurate categorization.

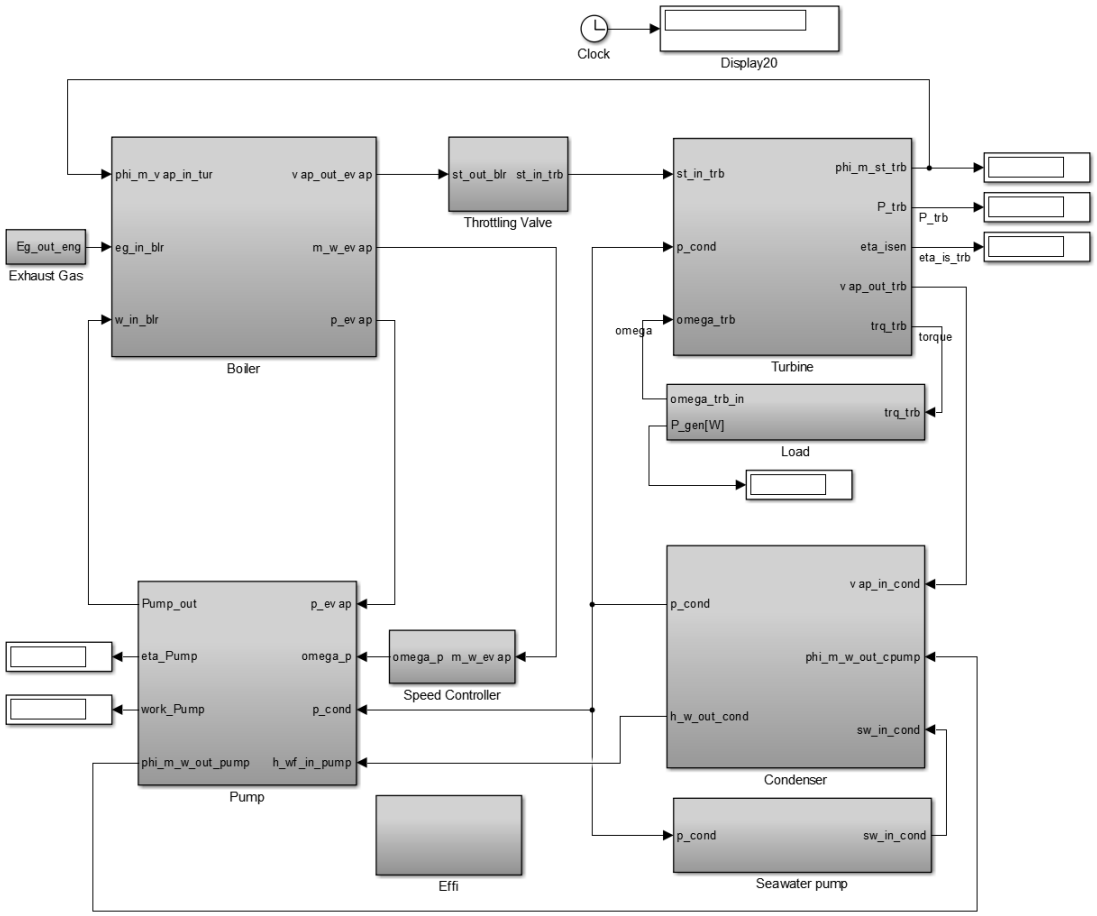

Figure 5.6: Simulink model of the simple ORC plant

System block diagram of the simple ORC plant in Simulink is shown in Figure 5.6. This is modeled based on the causality of a simple ORC plant as shown in Figure 5.5. Additional components such as sea water pump is coupled to condenser, generator load to the turbine and speed controller to the pump. These components are also necessary to obtain balance and equilibrium to the model. Each component and block are explained in detail as follows.

5.3.1.1 Boiler Model

Boiler component is modeled based on the volume element with transfer of heat energy from the waste heat source to the working fluid. As mentioned earlier, a single heat exchanger is enough to preheat and evaporate the working fluid, hence the boiler is modeled as a single heat exchanger component in Simulink. However for easy balancing and calculation as seen in Figure 4.2, the boiler component in Simulink is also split into an economizer and evaporator subsystems. Where economizer is based on only energy balance but evaporator is based on both mass and energy balance, where the actual dynamics of the boiler component is present. Figure 5.7 shows the evaporator and economizer subsystem of the boiler component.

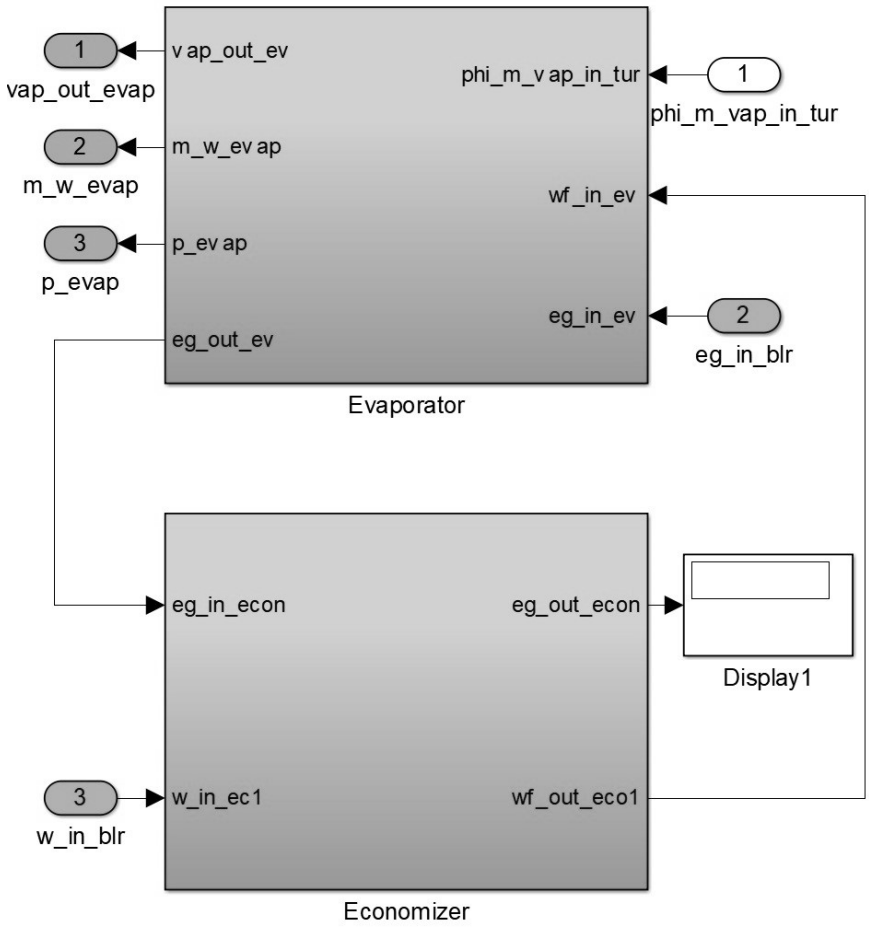

Figure 5.7: Evaporator and economizer subsystems of the boiler component

The boiler component is designed as a cross-counter flow heat exchanger. The waste heat (exhaust gas in this case) enters the evaporator element of the boiler and exits through the economizer and it is the other way around for the working fluid. Figure 5.8 shows the fluid flow and heat transfer direction inside the boiler component. The transfer of heat energy from the hot fluid to the cold fluid in all the heat exchanger of the model components such as evaporator, economizer, condenser and recuperator are given as follows:

$$\phi_q = \alpha \cdot A \cdot F \cdot \overbrace{\left(\left(\frac{T_{hot,in} + T_{hot,out}}{2}\right) - \left(\frac{T_{cold,in} + T_{cold,out}}{2}\right)\right)}^{\Delta T} \tag{5.2}$$

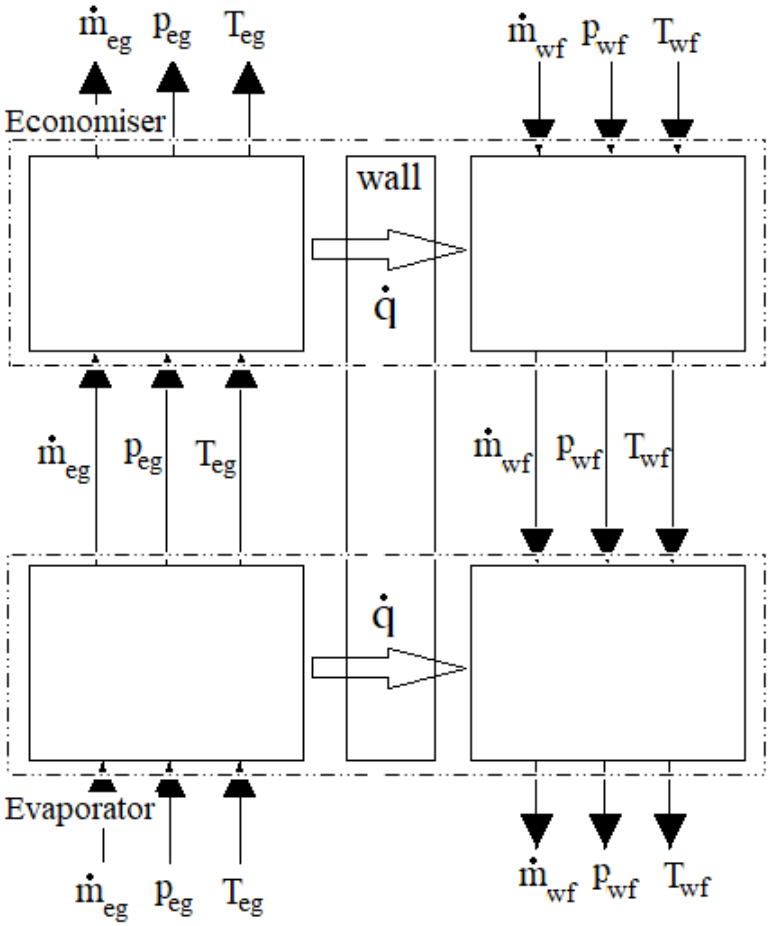

Figure 5.8: Fluid and energy flow of the boiler component

This equation captures the amount of heat transfer through convection of the hot and cold fluids. Conductive heat transfer through the wall is neglected since the thermal resistance is significantly smaller when compared to the thermal resistance due to convective heat transfer of the fluids. The amount of heat transfer is directly proportional to the mean temperature difference between the hot and cold fluids. This means that higher the temperature difference, higher is the amount of heat transferred. The amount of heat extracted or absorbed by the mass of the fluids in its control volume of the heat exchanger is based on the energy balance that is given by:

$$\phi_{q,in} - \phi_{q,out} = m \cdot C_p \cdot \frac{d\Big(\overbrace{\frac{T_{in} + T_{out}}{2}}^{T_{mean}}\Big)}{dt} = m \cdot \frac{d\Big(\overbrace{\frac{h_{in} + h_{out}}{2}}^{h_{mean}}\Big)}{dt} \tag{5.3}$$

This equation assumes linear temperature profiles of fluids inside the heat exchanger [Boonen, 2009]. All heat exchanger have the same energy balance equations for the entire length of the heat exchanger as a single element. This is used because the inlet and outlet temperatures of the hot and cold fluids of a single element heat exchanger modeled as a component do not change even when the same component is modeled as a multiple element heat exchanger to capture the actual temperature profiles. All these heat exchanger are modeled as a shell and tube type heat exchanger similar to the heat exchanger sizing calculations as seen in the previous chapter.

5.3.1.1.1 Economizer The working fluid enters the economizer in sub-cooled state due to the pump action and the heating fluid enters in gas form. As specified earlier, the economizer block is a single element block based on energy balance (see economizer part of Figure 5.8). Detailed explanation of the fundamental heat exchanger element used in the economizer is given in Section 4.2.2 of Boonen [2009].

5.3.1.1.2 Evaporator Evaporator is modeled based on mass and energy balances that captures the actual dynamics of heat exchange that makes it the main block of the boiler component . The working fluid absorbs latent and sensible heat to maintain the working fluid at turbine inlet in saturated vapour state. This means simultaneous evaporation and heating of the working fluid inside the evaporator occurs. Figure 5.9 show the evaporator element of the boiler and the fluid states. Evaporator determines the turbine inlet pressure and pump outlet pressure.

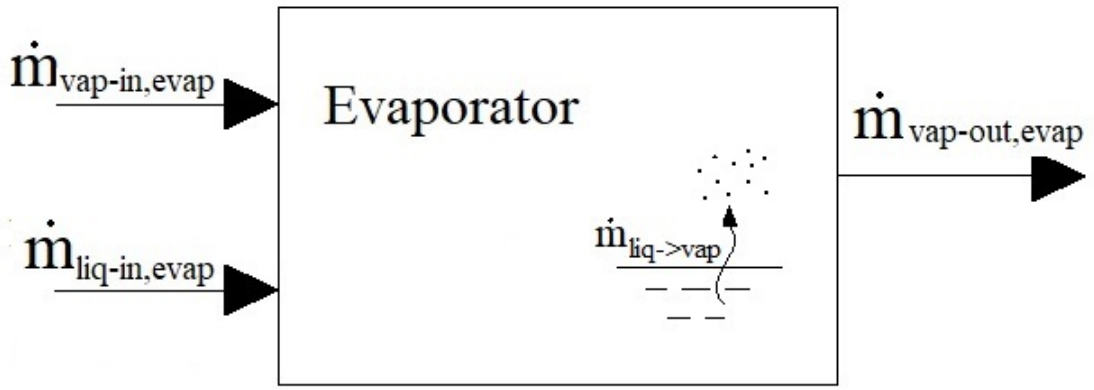

Figure 5.9: Evaporator element of the boiler component

The evaporator model is a control volume of a two-phase flow vessel since the working fluid inside the evaporator is in liquid and vapour state at any given time and length. A single element is used instead of a multiple element sub-blocks to form the complete evaporator model due to the same reasons as for the economizer. The evaporator element as seen in Figure 5.9 shows that the mass of working fluid entering the evaporator is either in liquid or liquid-vapour mixture state.

The conservation equations of the evaporator model are such that the assumptions of the working fluid are firstly, neglected height and velocity changes. This assumption has negligible deviations since the changes in internal energy due to evaporation is significantly larger when compared to the changes in internal energy due to height and volume changes. Secondly, the working fluid of liquid and vapour state is in saturated condition assuming the evaporator as an energy flow model and not a process model [Grimmelius, 2005]. Finally, the quality of outgoing working fluid is only in saturated vapour condition.

The conservation of mass in the evaporator for working fluid in liquid and vapour state is given as:

$$m_{liq} = \int \phi_{m,liq\_in} - \phi_{m,liq \rightarrow vap} \tag{5.4}$$

$$m_{vap} = \int \phi_{m,vap\_in} - \phi_{m,vap\_out} + \phi_{m,liq \rightarrow vap} \tag{5.5}$$

Based on the above mentioned assumptions and the conservation of mass equations, the following conservation of energy equation is given as follows:

$$\frac{dp_{evap}}{dt} = \left[\frac{\begin{array}{r} +\phi_{q,wall\rightarrow wf} + \phi_{m,liq\_in}(h_{liq\_in}^{p_{evap},s_{in}} - u_{liq\_in}^{p_{evap},s_{in}}) + \phi_{m,vap\_in}(h_{vap\_in}^{p_{evap},x=1} - u_{vap\_in}^{p_{evap},x=1}) \\ - \phi_{m,vap\_out}(h_{vap\_out}^{p_{evap},x=1} - u_{vap\_out}^{p_{evap},x=1}) - \phi_{m,liq\rightarrow vap}(u_{vap}^{p_{evap},x=1} - u_{liq}^{p_{evap},s_{in}}) \end{array}}{\left.\frac{du_{vap}}{dp}\right|_{sat} \cdot m_{vap} + \left.\frac{du_{liq}}{dp}\right|_{sat} \cdot m_{liq}} \right] \tag{5.6}$$

Since the volume inside the evaporator remains the same and is occupied completely by the working fluid in liquid and/or vapour state, the rate of liquid state working fluid that evaporates into saturated vapour state is given by the conservation of volume and the equation is as follows:

$$\phi_{m,liq\rightarrow vap} = \left[\frac{\begin{array}{r} (\phi_{m,vap\_out} - \phi_{m,vap\_in}) \cdot \nu_{vap}^{p_{evap},x=1} - \phi_{m,liq\_in} \cdot \nu_{liq}^{p_{evap},s_{in}} \\ - \frac{dp}{dt}\left[\left.\frac{d\nu_{vap}}{dp}\right|_{sat} \cdot m_{vap} + \left.\frac{d\nu_{liq}}{dp}\right|_{sat} \cdot m_{liq}\right] \end{array}}{\nu_{vap}^{p_{evap},x=1} - \nu_{liq}^{p_{evap},s_{in}}} \right] \tag{5.7}$$

And the heat flux or energy flow from the tube wall to the working fluid is given as:

$$\phi_{q,wall\rightarrow wf} = \alpha_{wall\rightarrow wf} \cdot A_{in,wall} \cdot F \cdot (T_{wall} - T_{mean,wf}) \tag{5.8}$$

The thermodynamic and transport properties of the heating and working fluids are a function of pressure and temperature or enthalpy.

5.3.1.2 Throttle valve

When used in operation, the throttle valve maintains the evaporator pressure at at least the nominal turbine inlet pressure. This block is similar to the one used in the SRC model to maintain steam drum pressure at a fixed magnitude during operation. The purpose of a throttle valve in an ORC plant between the boiler and turbine component is to control the pressure in the boiler and the mass flow through the turbine which in turn controls the turbine power output. Controller based throttle valve when used in a Rankine cycle plant in such an application could lead to throttle loss [Jin et al., 2017]. This loss is acceptable when the control strategy is desired for operational safety or overall energy management.

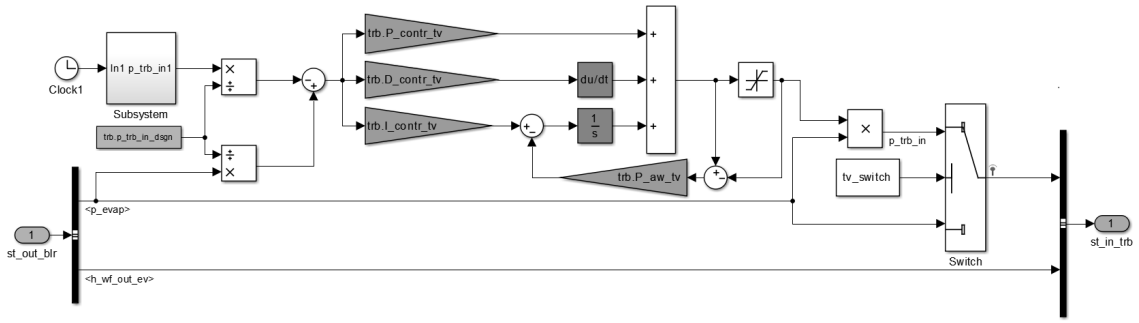

Figure 5.10: Throttle valve model in Simulink

Since the boiler and turbine model are a coupled volume and resistance element respectively, the throttle valve cannot be modeled as either a volume or resistance model based on the modeling methodology of boiler and turbine components. In general the throttle valve controls the mass flow of working fluid into the turbine and thus determines the turbine inlet pressure. But the throttle valve in this application is modeled conversely to control the turbine inlet pressure and the turbine as a resistance element calculates mass flow of the working fluid as a function of pressure difference. It is based on a controller element as shown in Figure 5.10.

5.3.1.3 Turbine and Generator Model

The turbine and the generator model are based on the modeling methodology described in van Putten and Colonna [2007] and the explanation is clearly captured in Section 3.2.3 and Section 3.2.4 of Ruyck [2011].

5.3.1.4 Condenser Model

The condenser is modeled similar to the evaporator model as a control volume of a two-phase flow vessel which determines the turbine outlet pressure and pump inlet pressure. Figure 5.11 shows the mass flow diagram of the condenser model. Since it is similar to the evaporator model, the fluid and energy flow diagram is similar to the evaporator part as seen in Figure 5.8. The only difference being is the heating fluid is now the organic fluid and the cooling fluid is sea water.

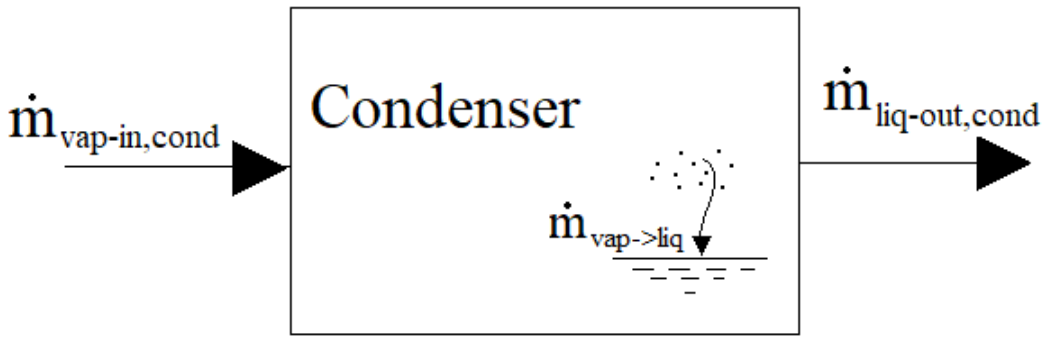

Figure 5.11: Condenser model of simple ORC

Since, the expansion of the working fluid in the turbine starts from saturated vapour point at evaporator pressure and due to the fluid type of organic fluids (which are mostly dry or isentropic fluid types), the working fluid expansion in the turbine is into the superheated region. This is also true even for an isentropic expansion process in the turbine of dry and isentropic fluid types. Hence, the working fluid inlet conditions to the condenser model of the simple-ORC plant that is suitable for isentropic fluids are in saturated vapour state at condenser pressure or slightly in superheated state based on the isentropic efficiency of the turbine.

The condenser model expels sensible heat to the cooling water from the superheated fluid until it is cooled down to condensing temperature at saturated condition. This is followed by expulsion of latent heat to the cooling water in order to condense the working fluid until the fluid is in saturated liquid state. The outlet of the condenser or inlet of the pump is always in saturated liquid state at condenser pressure. This is achieved by controlling the mass flow of cooling fluid into the condenser that in-turn determines the flow quantity of heat flux in the condenser. This is done to prevent the sub-cooling of the working fluid in the condenser, which is desirable because sub-cooling the fluid in

the condenser reduces thermal and plant efficiencies to some degree. Due to the similarities with the modeling method of the evaporator, the assumptions are also similar. Firstly, the height and velocity changes inside the condenser are neglected due to negligible internal energy changes. Secondly, the liquid and vapour form of working fluid inside the condenser is in saturated state that makes the model a result of energy flows and not a process. When these two state forms of fluid in the condenser are in saturated conditions, an equilibrium is achieved and no mass transfer among themselves would occur. Finally, the outgoing working fluid of the condenser is always in saturated liquid state at condenser pressure.

The equation for conservation of mass of liquid and vapour phase are given as:

$$m_{liq} = \int -\phi_{m,liq\_out} + \phi_{m,vap \rightarrow liq} \tag{5.9}$$

$$m_{vap} = \int \phi_{m,vap\_in} - \phi_{m,vap \rightarrow liq} \tag{5.10}$$

and the equation for conservation of energy is given as:

$$\frac{dp_{cond}}{dt} = \left[\frac{\begin{array}{c} -\phi_{q,wf \rightarrow wall} + \phi_{m,vap\_in}(h_{vap\_in}^{p_{cond},s_{in}} - u_{vap\_in}^{p_{cond},s_{in}}) \\ - \phi_{m,liq\_out}(h_{liq\_out}^{p_{cond},x=0} - u_{liq\_out}^{p_{cond},x=0}) + \phi_{m,vap \rightarrow liq}(u_{vap}^{p_{cond},s_{in}} - u_{liq}^{p_{cond},x=0}) \end{array}}{\frac{du_{vap}}{dp}\Big|_{sat} \cdot m_{vap} + \frac{du_{liq}}{dp}\Big|_{sat} \cdot m_{liq}} \right] \tag{5.11}$$

The condenser volume is constant and is occupied by the working fluid in liquid and/or vapour state at condensing pressure and the amount of condensing mass flow is given by conservation of volume and the equation is given as:

$$\phi_{m,vap \rightarrow liq} = \left[\frac{+\phi_{m,vap\_in} \cdot \nu_{vap}^{p_{cond},s_{in}} - \phi_{m,liq\_out} \cdot \nu_{liq}^{p_{cond},x=0} + \frac{dp}{dt}\left[\frac{d\nu_{vap}}{dp}\Big|_{sat} \cdot m_{vap} + \frac{d\nu_{liq}}{dp}\Big|_{sat} \cdot m_{liq} \right]}{\nu_{vap}^{p_{evap},s_{in}} - \nu_{liq}^{p_{evap},x=0}} \right] \tag{5.12}$$

The heat transferred from the working fluid to the cooling fluid through the tube wall is given as:

$$\phi_{q,wf \rightarrow wall} = \alpha_{wf \rightarrow wall} \cdot A_{out,wall} \cdot F \cdot (T_{sat} - T_{wall}) \tag{5.13}$$

5.3.1.5 Pump Model

In general, the pump is the component that creates pressure difference in the system (open or closed) and generates motion and gives direction to the fluid flow. The pump model and modification are explained as follows:

5.3.1.5.1 Original Pump Element The original pump model is modeled based on a controller. The mass quantity of working fluid in liquid state available in the boiler volume is the input signal to this controller and regulates the mass flow through the pump based on the ratio of input mass and initial mass quantities. The controller based pump element of the dynamic SRC plant model is shown in Figure 5.12. This pump element is explained in detail in Section 4.5 of Boonen [2009].

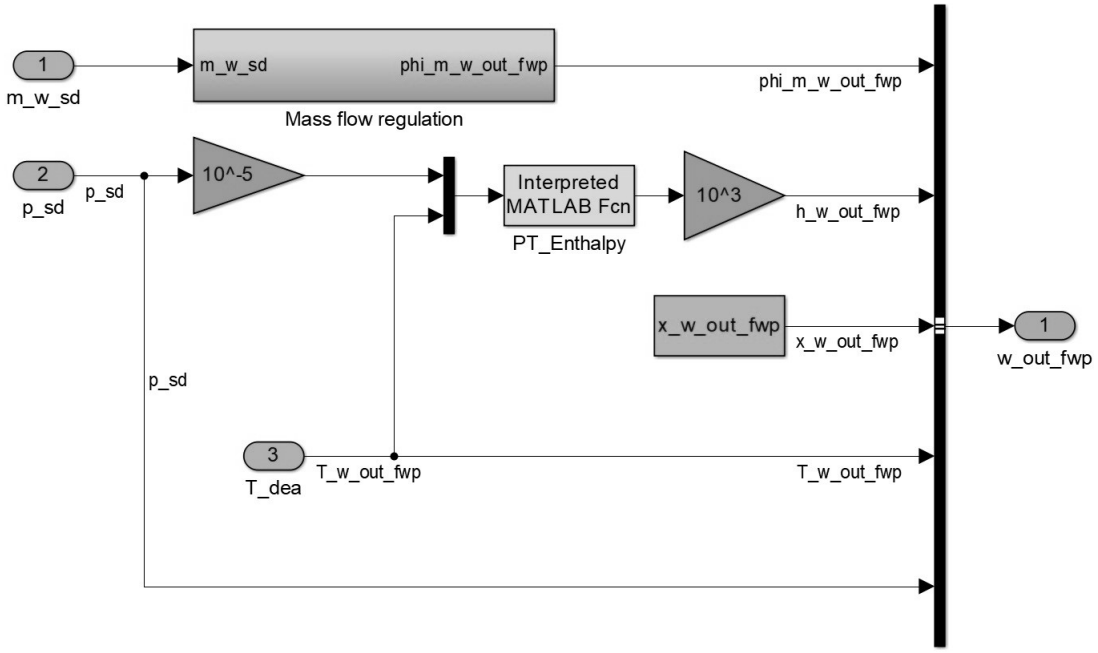

Figure 5.12: Original pump model [Boonen, 2009].

The controller based pump element is good enough to calculate the mass flow through the pump and run the Rankine cycle model to know the turbine or generator power output. However, to calculate the net power output of the complete cycle model, the electric power required by the pump has to be calculated.

The power demanded by the pump can be calculated from the mechanical work transmitted and it is given as:

$$P_{Pump} = \frac{W_{Pump}}{\eta_{m,el}} \tag{5.14}$$

where $\eta_{m,el}$ is the product of pump mechanical efficiency and the electrical efficiency of the pump motor. The mechanical work done by the pump is given as:

$$W_{Pump} = \phi_m \cdot (h_{in} - h_{out}) \tag{5.15}$$

The pump power for the original pump model will be lower than the actual value because in the original pump model the working fluid not only enters the pump in saturated liquid state but also exits in saturated liquid state. This is not an actual pump process because the working fluid exiting the pump will be in sub-cooled region depending on the pump isentropic efficiency. The pump isentropic efficiency of the original pump model is over 1.0, which is unrealistic. Therefore to calculate the pump power and subsequently the net power of the ORC plant, a modified pump model is needed. The pump isentropic efficiency is given by:

$$\eta_{Pump,isen} = \frac{h_{in} - h_{out,isen}}{h_{in} - h_{out}} \tag{5.16}$$

5.3.1.5.2 Modified Pump Element In general, the pump in an ORC plant is used to pump the condensed working fluid from the condenser to the boiler (or the recuperator, in a recuperative ORC plant). Since the ORC plant in this case has only condenser pressure and evaporator pressure, these correspond to the inlet and outlet pressures of the pump respectively. This is because the pressure losses in the system are neglected, since the economizer and the recuperator components are modeled as purely heat exchanging components based on energy balance. In addition, as mentioned before, the pressure losses in evaporator and condenser are also neglected.

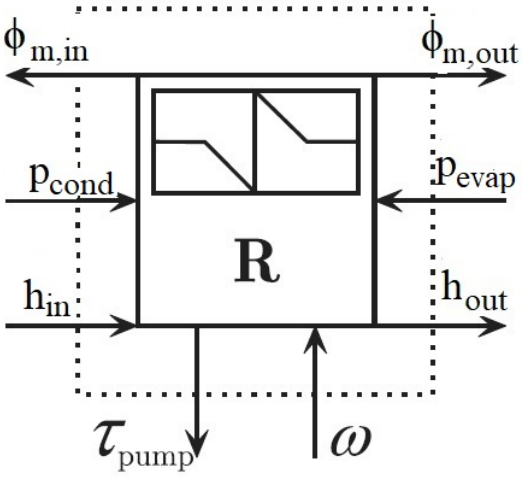

Figure 5.13: Causality representation of the pump model block [van Putten and Colonna, 2007].

As shown in Figure 5.5, the pump is modeled as a resistance element. It is modeled as a centrifugal pump neglecting momentum and the accumulation of mass powered by a variable speed electric motor. The causality representation of the pump can be seen in Figure 5.13. The pump model is based on conservation of mass and energy equation in combination with head-flow rate characteristics of the pump. As mentioned earlier, the model is a pure resistive component without the accumulation of mass. Hence the conservation of mass is given as:

$$\phi_{m,in} = \phi_{m,out} \tag{5.17}$$

and the conservation of energy equation can be written as:

$$\frac{dh_{out}}{dt} = \frac{\left[\phi_{m,in}(h_{in} - h_{mean}) - \phi_{m,out}(h_{out} - h_{mean}) + \dot{q} + W\right]}{\rho_{mean} V_{wf}} \tag{5.18}$$

The loss of heat energy from the working fluid to the pump metal casing is given by heat flux $\dot{q}$ and the energy equation for the metal casing is given as:

$$\dot{q}_M = \frac{m_M C_{p,M}}{C_{p,wf}} \cdot \frac{dh_{out}}{dt} \tag{5.19}$$

By substituting the Equation (5.19) into Equation (5.18) and accounting for the sign, we can rewrite the conservation of energy equation as:

$$\dot{q} = -\dot{q}_M \Rightarrow \frac{dh_{out}}{dt} = \frac{\left[\phi_{m,in}(h_{in} - h_{mean}) - \phi_{m,out}(h_{out} - h_{mean}) + W\right]}{\rho_{mean} V_{wf} + \frac{m_M C_{p,M}}{C_{p,wf}}} \tag{5.20}$$

The conservation of energy equation of the pump assumes that there is uniform transfer of heat from the working fluid to the pump metal casing and the temperature of the casing comes to equilibrium with the temperature of the fluid.

The mean density ρ_{mean} and mean enthalpy h_{mean} of the working fluid inside the pump are

$$\rho_{mean} = \frac{\rho_{in} + \rho_{out}}{2} \qquad h_{mean} = \frac{h_{in} + h_{out}}{2} \tag{5.21}$$

The work delivered to the fluid from the pump mechanical power is given as,

$$W = \frac{(p_{evap} - p_{cond})\phi_m}{\eta p_{mean}} \tag{5.22}$$

and the efficiency η as

$$\eta = \eta_D \left[1 - \left(1 - \frac{\dot{V}}{\dot{V}_D} \cdot \frac{n}{n_D} \right)^2 \right] \tag{5.23}$$

The volumetric flow rate $\dot{V}$ of the pump is calculated based on the pump characteristics curve which is derived from the pump design and non-dimensional parameters. The non-dimensional parabolic pump characteristics curve is given as

$$\overbrace{\left(\frac{gH}{n^2 D^2} \right)}^{H_{nd}} = a \cdot \left(\frac{\dot{V}}{nD^3} \right)^2 + b \cdot \overbrace{\left(\frac{\dot{V}}{nD^3} \right)}^{\dot{V}_{nd}} + c \tag{5.24}$$

This characteristic equation is used for a centrifugal pump with forward blade orientation. The parameters H_{nd} and $\dot{V}_{nd}$ are non-dimensional pump head and volumetric flow rate respectively. A set of equations can be solved to obtain the values for a, b and c of the non-dimensional head-volumetric flow rate characteristics curve. These equations are as follows:

$$\begin{cases} \overbrace{\left(\frac{gH_D}{n_D^2 D_D^2} \right)}^{H_{nd,D}} = a \cdot \left(\frac{\dot{V}_D}{n_D D_D^3} \right)^2 + b \cdot \overbrace{\left(\frac{\dot{V}_D}{n_D D_D^3} \right)}^{\dot{V}_{nd,D}} + c \\ 0 = a \cdot \left(\frac{\dot{V}_0}{n_D D_D^3} \right)^2 + b \cdot \underbrace{\left(\frac{\dot{V}_0}{n_D D_D^3} \right)}_{\dot{V}_{nd,0}} + c \\ \underbrace{\left(\frac{gH_0}{n_D^2 D_D^2} \right)}_{H_{nd,0}} = c \end{cases} \tag{5.25}$$

By solving Equation (5.25) and substituting the coefficients a, b and c into Equation (5.24), the actual pump head-volumetric flow rate characteristics parabolic curve can be obtained. The volumetric flow rate through the pump is obtained from this actual characteristics curve and is written as,

$$\dot{V} = \frac{-\frac{bn}{gD_D} - \sqrt{\frac{b^2 n^2}{g^2 D_D^2} + \frac{4aH}{gD_D^4} - \frac{4acn^2}{g^2 D_D^2}}}{\frac{2a}{gD_D^4}} \tag{5.26}$$

where the actual pump head H is

$$H = \frac{(p_{evap} - p_{cond})}{g\rho_{mean}} \tag{5.27}$$

The actual mass flow rate of working fluid through the pump, $\phi_{m,out}$ can be calculated from

$$\phi_{m,out} = \dot{V}_{wf} \cdot \rho_{mean} \tag{5.28}$$

As seen in Figure 5.13, the torque and the angular velocity has to be coupled to a variable rotational speed electric motor to obtain the actual rotational speed of the pump n. The rotational speed and pump torque is given as:

$$n = \frac{\omega}{2\pi} \qquad \tau = \frac{W}{\omega} \tag{5.29}$$

However the electric motor for this pump is not being modeled, instead a speed controller is used. This controller calculates the rotational speed of the pump with respect to the mass of working fluid in the evaporator. The dynamic pump element is based on the modeling method described in van Putten and Colonna [2007].

The comparison of the original pump model and dynamic model with Cycle-Tempo is made in Chapter 6. This comparison shows the difference of the two models with respect to Cycle-Tempo modeling methods.

5.3.2. Recuperative-ORC plant model

As mentioned earlier, volume and resistance elements are coupled together as a cycle to form the ORC plant model. Figure 5.14 shows the causality representation of recuperative ORC plant model based on the layout seen in Figure 4.8.

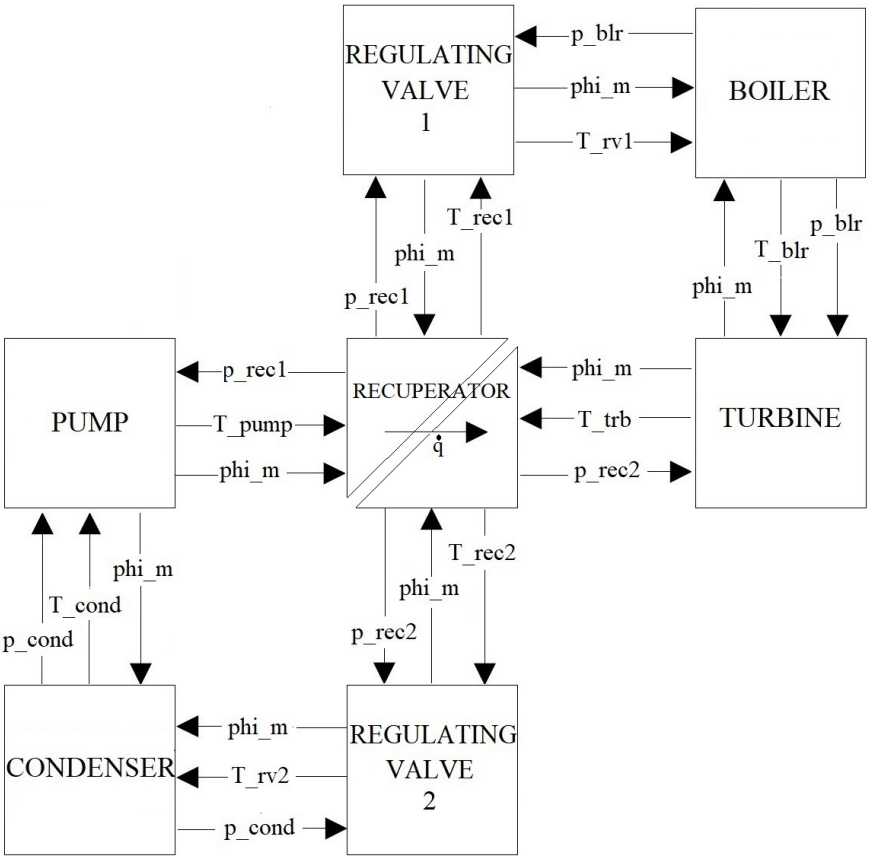

Figure 5.14: Causality representation of recuperative-ORC plant model.

This model is suitable for dry organic fluid types and the plant model and modeling method is similar to the simple-ORC plant model, although with a few additions and modifications. The overview of the Simulink model of the recuperative-ORC plant can be seen in Figure 5.15.

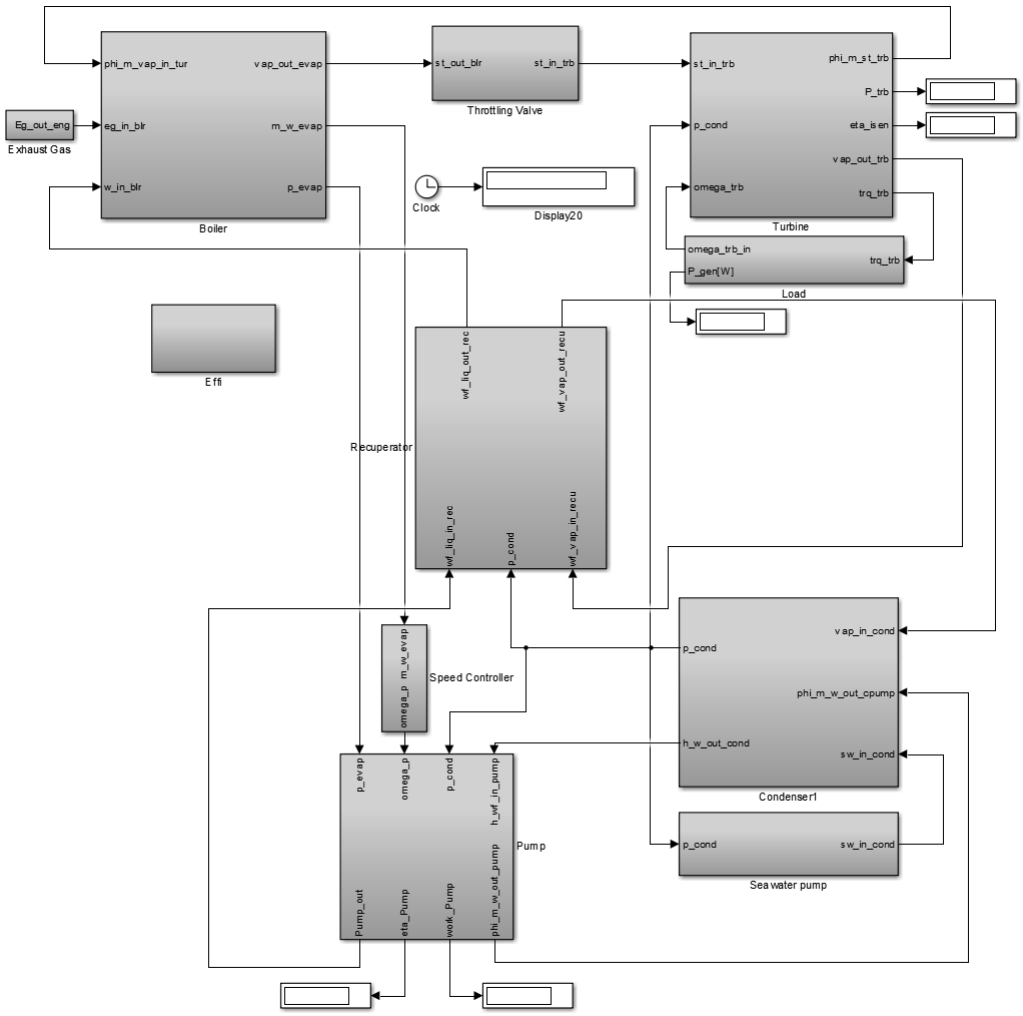

Figure 5.15: Simulink model of the recuperative-ORC plant

The recuperative-ORC plant model is built by adding a recuperator to the simple-ORC plant model with modification to the condenser. Hence, the recuperator and the condenser of the recuperative-ORC plant model is discussed since the reminder of the components are the same as seen in simple-ORC.

5.3.2.1 Recuperator

Recuperator is the heat exchanger that reduces the load on the condenser by lowering the turbine outlet temperature down to condensing temperature and increases the plant efficiency by rising the boiler inlet temperature. Recuperator model as seen in Figure 5.14 is a volume element based on mass and energy balance. Since pressure loss is neglected in the system, the recuperator volume element between turbine and condenser is subjected to condenser pressures and the recuperator volume element between pump and boiler is subjected to evaporator pressure. Hence the complete recuperator element is modeled based on energy balance only. The purpose of the recuperator is not condensation or evaporation of the working fluid in its volume but exchange of sensible heat among vapour and liquid form of the working fluid.

The recuperator block is modeled similar to the economizer block of the boiler component. The vapour side of the working fluid at condenser pressure flows outside the tubes (shell side) and the liquid side of the working fluid at evaporator pressure flows inside the tubes (tube side).

5.3.2.2 Condenser of Recuperative-ORC model

The condenser of the recuperative-ORC plant model is based on the same condenser model used in the simple-ORC plant but with an addition. Since a recuperator is placed in between the turbine and the condenser, under off-design operation the working fluid entering the condenser can also be in the two-phase region. Figure 5.16 shows the condenser model with flow qualities. The working fluid entering the condenser is in saturated vapour and/or liquid state.

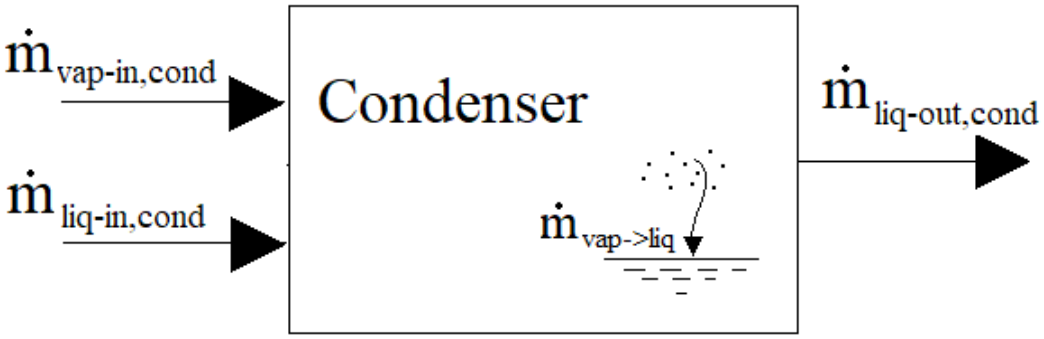

Figure 5.16: Condenser model of recuperative-ORC

The conservation of mass for liquid state is given as:

$$m_{liq} = \int \phi_{m,liq\_in} - \phi_{m,liq\_out} + \phi_{m,vap \rightarrow liq} \tag{5.30}$$

and conservation of mass in vapour state is given as:

$$m_{vap} = \int \phi_{m,vap\_in} - \phi_{m,vap \rightarrow liq} \tag{5.31}$$

The pressure in the condenser is measured as a function of incoming and outgoing mass flows and is given by the conservation of energy equation, which is as follows:

$$\frac{dp_{cond}}{dt} = \left[\frac{\begin{array}{r} -\phi_{q,wf \rightarrow wall} + \phi_{m,vap\_in}(h_{vap\_in}^{p_{cond},s_{in}} - u_{vap\_in}^{p_{cond},s_{in}}) + \phi_{m,liq\_in}(h_{liq\_in}^{p_{cond},x=0} - u_{liq\_in}^{p_{cond},x=0}) \\ - \phi_{m,liq\_out}(h_{liq\_out}^{p_{cond},x=0} - u_{liq\_out}^{p_{cond},x=0}) + \phi_{m,vap \rightarrow liq}(u_{vap}^{p_{cond},s_{in}} - u_{liq}^{p_{cond},x=0}) \end{array}}{\left.\frac{du_{vap}}{dp}\right|_{sat} \cdot m_{vap} + \left.\frac{du_{liq}}{dp}\right|_{sat} \cdot m_{liq}} \right] \tag{5.32}$$

The volume of the condenser cannot vary and the condensing mass flow is given by the conservation of volume equation and is given as follows:

$$\phi_{m,vap \rightarrow liq} = \left[\frac{\begin{array}{r} (\phi_{m,liq\_in} - \phi_{m,liq\_out}) \cdot \nu_{liq}^{p_{cond},x=0} + \phi_{m,vap\_in} \cdot \nu_{vap}^{p_{cond},s_{in}} \\ + \frac{dp}{dt}\left[\left.\frac{d\nu_{vap}}{dp}\right|_{sat} \cdot m_{vap} + \left.\frac{d\nu_{liq}}{dp}\right|_{sat} \cdot m_{liq}\right] \end{array}}{\nu_{vap}^{p_{evap},s_{in}} - \nu_{liq}^{p_{evap},x=0}} \right] \tag{5.33}$$

The transfer of heat from the working fluid to the cooling fluid through the tube wall is given in Equation (5.13).

The simple-ORC and recuperative-ORC plant models developed in Matlab-Simulink and discussed in this chapter are going to be used for off-design performance analysis in the next chapter. This is followed by sensitivity and dynamic analysis in the later chapter.

6

Design and Off- Design Performance Analysis

In this chapter, the percentage error that may be caused due to the use of sample mass fraction for analysis instead of the real values is discussed. This is followed by the comparison of the dynamic ORC plant models of Matlab-Simulink with the same ORC plant models of Cycle-Tempo. This is finally followed by the off-design performance analysis of ORC plant models designed at varying load points to off-load conditions.

In marine application, the diesel engine may be subjected to varying engine loads depending upon the operational profile of the vessel. This means that the ORC-WHRS is very likely to be subjected to varying heat source parameters depending upon the waste heat profile of the engine. Hence, the off-design performance is noteworthy to analyze for an ORC-WHRS whose design point is determined based on the engine's waste heat profile and the vessel's operational profile.

For off-design performance analysis, it is also interesting to explore the system at lower engine loads (eg. 25% to 50%). Engine exhaust data lower than 50% is not available in the product guide for the engine as seen in Table 4.1. Hence exhaust data for desired engine load points are extracted from the diesel engine B model (Version DE_B5_44_434) available from the maritime department at TU Delft. Among few engine types available in the model, an SWD engine is chosen that is closest to the engine model seen in Table 4.1 in terms to maximum power output.

6.1. Waste Heat Profile

The waste heat profile data of the SWD engine is registered for engine loads of 25, 50, 75, 85 and 100%. The load point of 85% is also interesting to investigate because ships usually operate at the nominal continuous rating which is between 85% and 90% of the maximum continuous rating of the engine primarily used for propulsion.

The waste heat profile from the engine would be distinct when the same engine is used as a prime mover for different loads, such as pumps, generators or propellers. It would be interesting to see how the ORC-WHRS would perform when the same engine has different exhaust waste heat profile when mechanically coupled as a driver to a generator load and a propeller load. The engine parameters and engine exhaust data when coupled to a generator and when coupled to a propeller are shown in Table 6.1 and Table 6.2 respectively.

As understood, the waste heat source temperature is what dictates the fluid choice which subsequently corresponds to the plant layout and the waste heat source mass flow rate dictates the size of the plant components. It can be seen in these tables that the exhaust gas values for both generator

SWD12V280 Diesel Engine of Power = 305 [kW/cyl] @ 1000 [rpm]						
For Generator as Load						
Engine Load [%]	Brake Power [kW]	Rotational Speed [rpm]	Exhaust Pressure [Pa]	Exhaust Temperature [K]	Exhaust Mass Flow [kg/s]	Mass Fraction [-]
25	915	1000	102240	754	2.4	0.437
50	1830	1000	102820	711	4.5	0.428
75	2745	1000	103700	681	6.6	0.427
85	3111	1000	104080	679	7.3	0.435
100	3660	1000	104660	688	8.2	0.455

Table 6.1: Engine and exhaust data of SWD12V280 coupled to generator

SWD12V280 Diesel Engine of Power = 305 [kW/cyl] @ 1000 [rpm]						
For Propeller as Load						
Engine Load [%]	Brake Power [kW]	Rotational Speed [rpm]	Exhaust Pressure [Pa]	Exhaust Temperature [K]	Exhaust Mass Flow [kg/s]	Mass Fraction [-]
25	407	481	102030	803	0.7	0.446
50	1325	713	102270	803	2.4	0.439
75	2560	888	103270	702	5.6	0.534
85	3090	945	103880	682	7.0	0.547
100	3775	1010	104560	748	7.2	0.493

Table 6.2: Engine and exhaust data of SWD12V280 coupled to propeller

and propeller are in the region of 680 to 800 °K and the exhaust gas mass flow rate of corresponding load points are lower in propeller load than generator load. This is because in propeller load, the rotational speeds are lower than in generator load for corresponding engine load points.

6.2. Screening & Static Analysis

As the new waste heat profile of the engine coupled to generator and propeller load are obtained, the steps in Figure 4.1 are repeated for fluid screening and suitable plant design based on the power density selection parameter. The source temperatures of this engine are higher than the source temperature of the dual fuel engine used in Chapter 4. This higher temperature increases the temperature range between the source and cooling. This could allow additional fluids to operate a complete subcritical ORC process which were outside the range during fluid screening for the dual fuel engine in Chapter 4. To investigate if any additional fluids could be added to the existing functional fluid list as seen in Table 4.2, the screening steps are repeated again.

6.2.1. Fluids

We now know that the waste heat source temperature is prime for organic fluid selection and the waste heat source mass flow corresponds to plant size proportionally. Therefore for fluid selection, the engine loads with highest and lowest exhaust temperature is used as the source temperature to analyze functional fluids. Since most organic fluids belong to dry fluid category, this functional fluid analysis is performed on the recuperative-ORC plant model in Cycle-Tempo.

Based on the waste heat profile as seen in Table 6.1 and Table 6.2 and the initial conditions as seen in Appx. Section A.2.1, the analysis for functional fluids are performed in a recuperative-ORC plant. The results as shown in Appx. Table E.1 concludes that since no additional fluids operate in the extended range, the functional fluid list seen in Table 4.2 remains the fluids of interest for the analysis of the SWD engine. The results seen in Appx. Table E.1 also indicates that the promising fluids as seen in Table 4.3 remains the highest in terms of power density for waste heat profile of SWD diesel

engine. Therefore for further analysis in the screening methodology, the suitable organic fluids seen in Table 4.3 are considered.

Since the initial conditions applied, functional and promising organic fluids obtained during fluid screening of the SWD engine are same as before as seen in the screening methodology of DF engine, the heat exchanger sizing and power density calculations will bring similar trends as seen in Figure 4.13 and Figure 4.14 respectively. Hence, acetone based simple-ORC and cyclopentane based recuperative-ORC plants are considered for off-design performance analysis for the SWD engine.

6.2.2. Plant Recoverability

Based on the values and fluid potential seen in Appx. Table E.1, it can be concluded that acetone based simple-ORC and cyclopentane based recuperative-ORC plants have the highest power densities among other promising working fluids. Therefore, the design point analysis of the two fluids in their corresponding plant design are carried out in Cycle-Tempo. This is in order to obtain values of operating parameters which are implemented into the dynamic ORC plant model for further analysis into off-design performances of both fluids with respect to the waste heat profile. The data obtained from Cycle-Tempo can be compared to the data obtained from the dynamic ORC model to understand the limitations and areas of improvements of the dynamic model as well.

6.2.2.1 Static Analysis of Design Points

The design point analysis of the acetone based simple-ORC and cyclopentane based recuperative-ORC plant are performed and the analysis is shown in Appx. Table E.3 and Appx. Table E.4 respectively. The net power generated by the two ORC systems with their corresponding fluids for the same engine under generator and propeller load are shown in Figure 6.1.

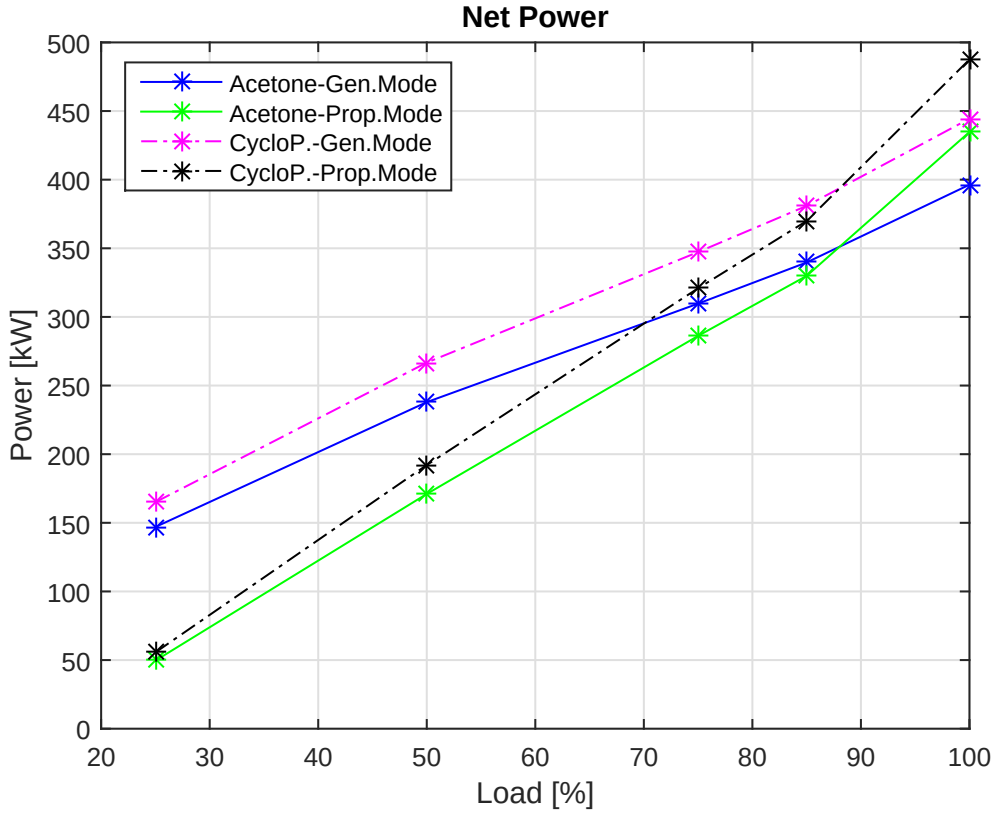

Figure 6.1: Net power generation by ORC plant for generator and propeller load

For the same heat source and under same initial conditions the net power generation of cyclopentane in recuperative-ORC plant, is higher than acetone in simple-ORC plant due to higher mass flow rate of the working fluid in the system. Comparatively, higher mass flow rate of cyclopentane in recuperative-ORC plant for the same waste heat is due to lower specific heat of cyclopentane and the temperature of cyclopentane in saturated vapour condition at 30 bar is almost the same as for acetone. And the fluid saturation curve for both these fluids are similar as seen in the T-S diagram of the organic fluids.

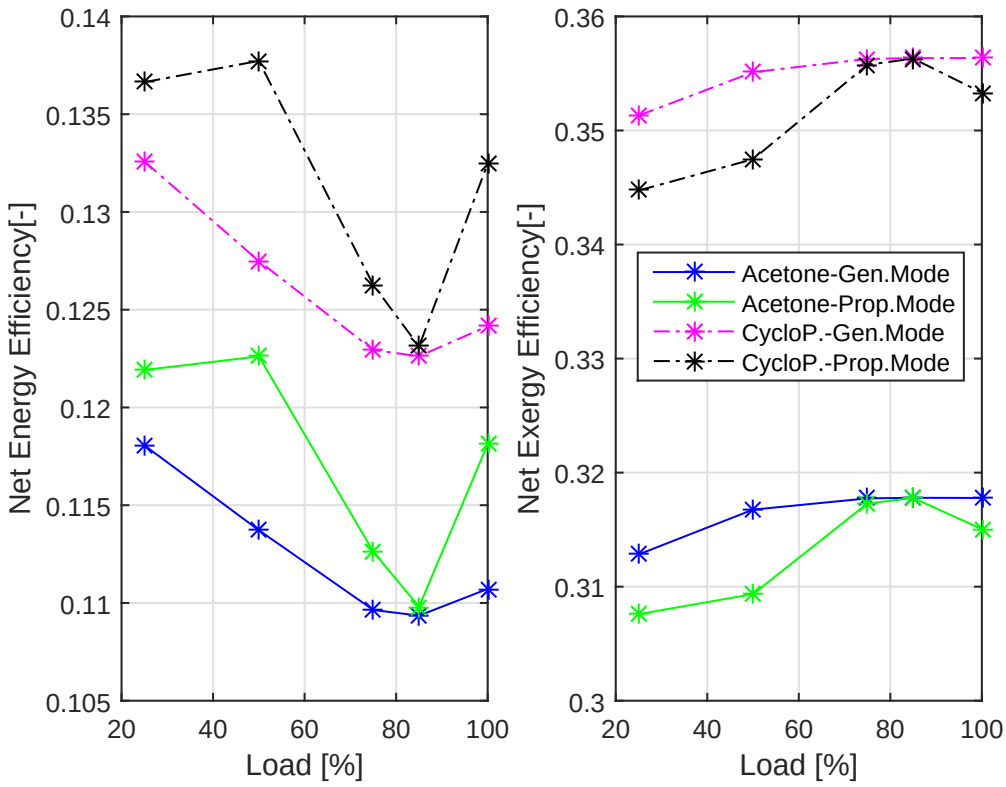

Figure 6.2: Net efficiencies of the ORC plant for generator and propeller load

The net energy are exergy efficiency of the ORC plant are shown in Figure 6.2. The net energy efficiency and the trends are proportional to the temperature profile of the waste heat source and inversely proportional for net exergy efficiency of the ORC plant. The thermal efficiency of the system will remain roughly constant and unchanged when designed for any engine load, since the initial conditions for static analysis are same.

6.2.2.2 Mass Fraction Error

Specific heat at constant pressure of a fluid depends upon the physical state, temperature and the gas composition. The waste heat profile of the engine exhaust gas has varying pressure, temperature and gas composition with respect to the engine load. The static analysis of design points for acetone based simple-ORC and cyclopentane based recuperative-ORC was carried out with the same gas composition with constant values irrespective of changing engine loads. This same gas composition with constant values is the sample values used for static analysis in Chapter 4 and the real gas compositions are given in mass fraction terms for the engine in Table 6.1 and Table 6.2.

In the analysis carried out with sample gas composition and values, there may be deviation from the actual value when real mass fraction is used instead. This deviation is studied in acetone based simple-ORC plant by comparing plant performance with sample values and real values. The real values of gas composition is converted from mass fraction as obtained from the engine model into mole fraction as needed for Cycle-Tempo plant analysis. This conversion of gas constituents from mass fraction to mole fraction of independent element of the exhaust gas constituents are shown in Appx. Table E.2.

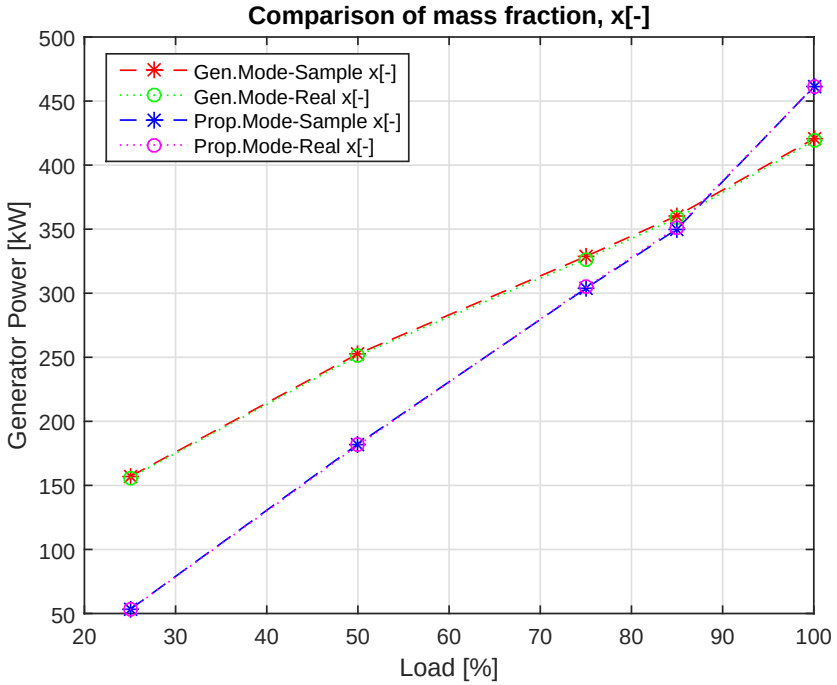

Figure 6.3: Error in generated power due to mass fraction differences for acetone based simple-ORC

Deviation due to implementation of sample values instead of real mass fraction values is shown in Figure 6.3. This figure shows the power generated by the acetone based simple-ORC plant in generator and propeller load using sample and real mass fraction values. It can be seen from this figure that the deviation is insignificant and remains as such for the entire engine load. This is because, the specific heat of the exhaust gas largely remains unchanged due to varying mass fraction of the gas compositions. The error values for this analysis is shown in Table 6.3.

Variable	Units	Generator Mode					Propeller Mode				
Engine Load	[%]	25	50	75	85	100	25	50	75	85	100
Sample x[-]	[kW]	156.8	252.7	328.7	360.5	420.5	53.1	182.2	303.7	350.1	461.2
Real x[-]	[kW]	156.0	251.2	326.7	358.5	418.9	52.9	181.3	304.5	351.3	460.9
Error	[%]	0.52	0.59	0.60	0.54	0.37	0.43	0.51	-0.25	-0.35	0.07

Table 6.3: Power generated (P_{Gen})and error for sample and real mass fraction values for acetone based simple-ORC plant analysis

Since the deviation error are small and insignificant, the sample values of the gas composition are used and kept constant for further analysis of ORC plant model. The varying mass fraction of exhaust gas with respect to engine load can be implemented into the dynamic model if necessary. However for this application it will bring no added advantage to analyze waste heat recovery potential.

6.2.3. Heat Exchanger Sizing and Power Density

For off-design performance analysis, the size of the heat exchanger components at design conditions has to be calculated. The length of a heat exchanger is calculated by using the amount of heat transferred and the overall heat transfer admittance obtained from the static analysis of design points. These lengths are then used as input for sizing the heat exchanger in the Simulink model to perform design and off-design analysis.

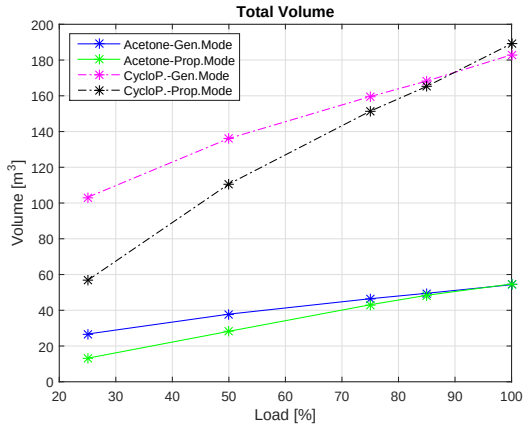

Figure 6.4: Total Volume of the ORC plant at design points and the trends

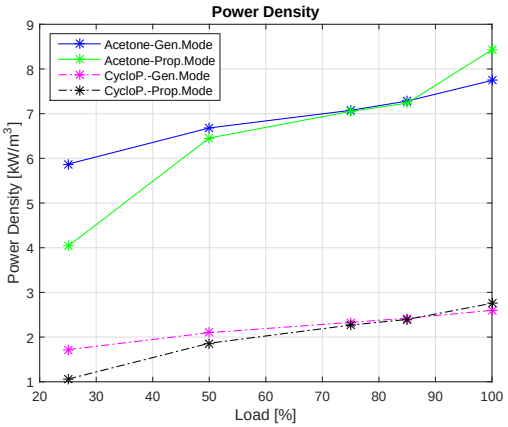

Figure 6.5: Power density of the ORC plant at design points and the trends

Based on the design point data and heat exchanger sizing formula, the total size of both the ORC plants at engine load points in both generator and propeller loads are shown in Figure 6.4. As seen before, acetone based simple-ORC plant in this analysis, requires the lowest plant volume because of its higher specific heat and simpler design due to its isentropic saturation vapour curve. Despite generating lower power than cyclopentane based recuperative-ORC plant, the power density of the plant is higher for acetone based simple-ORC plant. Figure 6.5 shows the power density of the plant at varying engine loads. As specified earlier, it can seen in this figure that despite having a lower thermal efficiency than cyclopentane based recuperative-ORC plant, acetone based simple-ORC plant has better power density. The values of volume of plant components and the plant efficiencies are shown in Appx. Table E.5 and Appx. Table E.6 for acetone and cyclopentane respectively.

6.3. Comparison with Cycle-Tempo

The current dynamic ORC plant models that can use dry or isentropic organic working fluids are based on the dynamic SRC model created and developed by Boonen [2009] and Ruyck [2011]. This Simulink model is based on the fundamental building block calculations of Cycle-Tempo. Therefore, the dynamic SRC model has been validated by comparing with Cycle-Tempo as shown in Chapter 5 of the master thesis by Boonen [2009]. The modeling of the dynamic ORC plant components especially, the heat exchangers that contributes significantly to the dynamic behaviour of the WHRS in the Simulink model are also based on the heat exchanger calculations of Cycle-Tempo. Hence, the results of the design point analysis of the dynamic ORC model in Simulink is compared with the results of the same analysis performed in Cycle-Tempo. The result comparison will give an overall viewpoint of the accuracy of the dynamic model with respect to Cycle-Tempo. Comparison of result outputs from independent components are also needed to be made to understand the degree to which these components are modeled to reality.

Turbine power and net power are the output from the process and plant respectively and since turbine power is incorporated into the net power calculations, Figure 6.6 shows the comparison of net power generated for the design point analysis of acetone based simple-ORC plant in Simulink and Cycle-Tempo. It can be seen from this figure that the net power by the dynamic simple-ORC model is slightly lower than the net power results obtained from Cycle-Tempo. This error is seen across all the design load points with an average value of less than 4%. These values and errors are shown in

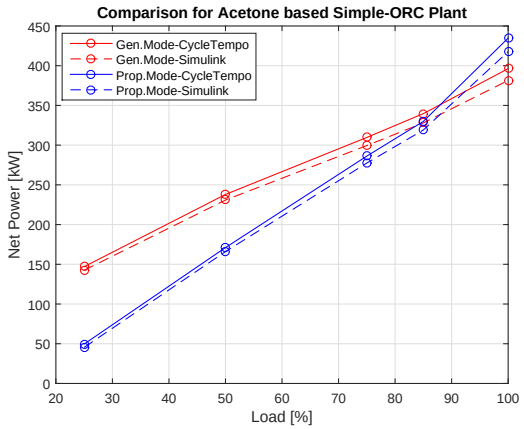

Figure 6.6: Comparison of Cycle-Tempo and Simulink model for acetone based simple-ORC plant

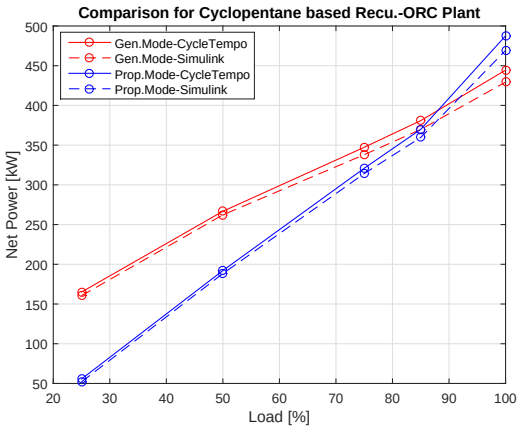

Figure 6.7: Comparison of Cycle-Tempo and Simulink model for cyclopentane based recuperative-ORC plant

Table 6.4. This error is caused because the analysis in Cycle-Tempo model is performed with turbine isentropic efficiency of 75% and the same analysis in Simulink is calculation the isentropic efficiency of the dynamic turbine element at 73%. This is the primary factor that contributes to the error seen here. This error can be minimized when the turbine isentropic efficiency are almost constant in Cycle-Tempo and Simulink model. This can be achieved by using better parametric values in Simulink in the dynamic turbine-generator element that can be obtained from measurements of a real ORC turbine-generator.

The net power obtained from the dynamic simple-ORC model has a negligible error when compared to the results obtained from the Cycle-Tempo analysis. Hence, this ORC model in Matlab-Simulink can be used for off-design performance analysis. This model can also be used to understand the dynamic and sensitivity analysis of simple-ORC WHRS model for waste heat source profile of a marine engine.

Acetone based Simple-ORC										
Load Type	Generator					Propeller				
Load [%]	25	50	75	85	100	25	50	75	85	100
Cycle-Tem	146.98	237.92	309.70	339.69	396.34	49.60	171.03	286.19	329.90	434.75
Mat-Sim	142.54	230.91	299.49	328.01	381.46	45.37	165.98	277.48	319.05	417.75
Error [%]	-3.02	-2.95	-3.30	-3.44	-3.75	-8.53	-2.95	-3.04	-3.29	-3.91

Table 6.4: Net power output comparison of simple-ORC model in Simulink and Cycle-Tempo

Cyclopentane based Recuperative ORC										
Load Type	Generator					Propeller				
Load [%]	25	50	75	85	100	25	50	75	85	100
Cycle-Tem	165.06	266.73	347.26	380.90	444.45	55.59	192.11	320.88	369.90	487.55
Mat-Sim	160.50	262.22	338.00	369.78	429.37	52.03	188.32	314.18	359.67	469.20
Error [%]	-2.76	-1.69	-2.67	-2.92	-3.39	-6.40	-1.97	-2.09	-2.77	-3.76

Table 6.5: Net power output comparison of recuperative-ORC model in Simulink and Cycle-Tempo

The same can be said about the recuperative-ORC model as shown in Figure 6.7, as this model is a modified version of the dynamic simple-ORC plant model. Similar to the comparison for simple-ORC, the results obtained from the recuperative model in Simulink is slightly lower than the results from Cycle-Tempo. This error is seen across all design load points with an average value of slightly over 3%. These values and errors are also shown in Table 6.5 for reasons as same as before. The net power obtained from the recuperative-ORC model has a negligible error when compared to the results from Cycle-Tempo. Hence, this recuperative-ORC plant model can be used for off-design analysis.

Acetone Based Simple ORC Plant Gen Mode										
Design Point		100%			75%			25%		
Comparison		C-Tem	M-Sim	Error [%]	C-Tem	M-Sim	Error [%]	C-Tem	M-Sim	Error [%]
P_{Gen}	[kW]	420.5	404.5	-3.80	328.7	317.5	-3.41	156.8	151.1	-3.64
P_{Pump}	[kW]	20.35	20.30	-0.25	15.98	15.86	-0.76	8.09	7.61	-6.00
$P_{SW,Pump}$	[kW]	3.84	2.77	-27.8	3.04	2.15	-29.2	1.76	1.03	-41.5
$\phi_{m,wf}$	[kg/s]	3.38	3.37	-0.32	2.64	2.63	-0.36	1.26	1.26	-0.08
$\phi_{m,sw}$	[kg/s]	43.16	43.02	-0.33	33.74	33.48	-0.74	16.10	15.96	-0.87
p_{evap}	[bar]	30.00	29.92	-0.26	30.00	29.91	-0.29	30.00	29.98	-0.06
p_{cond}	[bar]	0.57	0.57	0.00	0.57	0.57	0.00	0.57	0.57	0.00
$T_{eg-out,evap}$	[℃]	325.4	325.6	0.08	320.8	321.1	0.09	368.3	368.1	-0.05
$T_{eg-out,econ}$	[℃]	165.0	165.8	0.50	165.0	165.8	0.54	165.0	165.1	0.06

Table 6.6: Comparison of acetone based simple-ORC plant model analysis with Cycle-Tempo analysis

Apart from the comparison of the power output from the plant models, a comparison of the main model parameters for design point analysis in Cycle-Tempo are made to understand the error within the Simulink model and the components. This comparison can be used to understand the degree to which these Simulink models resemble the actual process and the area that could be improved for better accuracy. This comparison is made for the ORC system designed for the engine loads of 25, 75 and 100% of SWD engine in generator load. Table 6.6 shows the comparison of acetone based ORC model designed for different load points. It can be seen from this table that most parameters have negligible error between the Simulink and Cycle-tempo model analysis of less than 1%.

In acetone based simple-ORC model, the highest inaccuracy is seen in the sea water pump component across all loads. This component as explained earlier is a controller based model. The difference in the values in kW terms is about 1 kW which is significantly smaller when compared to generator power output of the ORC plant, thus making it negligible while calculating other performance parameters such as net power, net efficiencies and net power densities.

Cyclopentane Based Recuperative ORC Plant Gen Mode										
Design Point		100%			75%			25%		
Comparison		C-Tem	M-Sim	Error [%]	C-Tem	M-Sim	Error [%]	C-Tem	M-Sim	Error [%]
P_{Gen}	[kW]	475.4	459.9	-3.26	371.6	361.8	-2.64	177.3	171.5	-3.23
P_{Pump}	[kW]	27.22	27.82	2.20	21.41	21.70	1.34	10.52	10.27	-2.37
$P_{SW,Pump}$	[kW]	3.74	2.73	-27.0	2.95	2.12	-28.1	1.72	0.79	-53.8
$\phi_{m,wf}$	[kg/s]	4.33	4.35	0.61	3.38	3.40	0.50	1.61	1.61	0.07
$\phi_{m,sw}$	[kg/s]	41.92	42.42	1.19	32.77	32.96	0.60	15.63	12.34	-21.06
p_{evap}	[bar]	30.00	30.15	0.49	30.00	30.12	0.40	30.00	30.02	0.06
p_{cond}	[bar]	0.74	0.74	0.00	0.74	0.74	0.00	0.74	0.74	0.00
$T_{eg-out,evap}$	[℃]	328.2	328.0	-0.05	323.6	323.4	-0.05	371.9	370.0	-0.49
$T_{eg-out,econ}$	[℃]	165.0	166.2	0.78	165.0	166.5	0.96	165.0	168.5	2.14

Table 6.7: Comparison of cyclopentane based recuperative-ORC plant model analysis with Cycle-Tempo analysis

Similar model parameter comparison is also made for cyclopentane based recuperative-ORC model. This comparison is made for the ORC system designed for the engine loads of 25, 75 and 100% of SWD engine in generator load. Table 6.7 shows the comparison of cyclopentane based recuperative-ORC model designed for different load points in Simulink and Cycle-Tempo. Similar to the comparison seen for acetone based simple-ORC, this model comparison also shows that most parameters have negligible error between the Simulink and Cycle-tempo model analysis of less than 1%.

Although there is room for improvement, the dynamic ORC model designed for dry and isentropic organic fluids can be used for off-design performance analysis. This is because the model results obtained from design point analysis are comparable to the results obtained from Cycle-Tempo calculations.

In the case of pump component in the model, the original pump was based on a controller element and not a resistance element. Despite this fact, the original model was capable of bringing equilibrium to the dynamic model by calculating the mass flow rate through the system based on the mass of liquid fluid in the boiler element. This calculated mass flow rate is comparable to the results obtained from the Cycle-Tempo model. Since net power is what is required to analyze the system performance, this pump model cannot be used to obtain pump work because the fluid enters and leaves the pump in saturated liquid state. This is untrue, because the actual pump process in Rankine cycle is based on the isentropic efficiency of the pump. Due to the pump isentropic efficiency, the actual pumping action leaves the fluid in subcooled phase and not in saturated liquid phase. Hence the original pump has an isentropic efficiency of over 1.0. Hence, the modification of the pump element from controller element into resistance element is made to capture the actual work required within the pump element between the shaft power and the working fluid. This dynamic pump element and the original pump element are compared with Cycle-Tempo pump model.

Acetone-Simple-ORC designed at 100% of SWD Engine in Generator Load						
Model		Cycle-Tempo	Original Model		Dynamic Model	
Variable	Units	Value	Value	Error [%]	Value	Error [%]
P_{Pump}	[kW]	20.35	8.17	-59.86	20.30	-0.23
W_{pump}	[kW]	17.23	6.92	-59.83	17.15	-0.45
η_{Pump}	[-]	0.75	1.86	147.87	0.75	0.00
$T_{wf,in}$	[℃]	40.00	40.00	0.01	40.00	0.01
$T_{wf,out}$	[℃]	41.40	40.00	-3.37	41.40	0.00
$h_{wf,in}$	[kJ/kg]	-35.47	-35.47	0.00	-35.47	0.00
$h_{wf,out}$	[kJ/kg]	-30.37	-33.41	10.02	-30.38	0.03
$\phi_{m,wf}$	[kg/s]	3.38	3.36	-0.52	3.37	-0.32
Acetone-Simple-ORC designed at 75% of SWD Engine in Generator Load						
Model		Cycle-Tempo	Original Model		Dynamic Model	
Variable	Units	Value	Value	Error [%]	Value	Error [%]
P_{Pump}	[kW]	15.98	6.41	-59.86	15.86	-0.76
W_{pump}	[kW]	13.47	5.41	-59.83	13.40	-0.53
η_{Pump}	[-]	0.75	1.86	147.87	0.75	0.00
$T_{wf,in}$	[℃]	40.00	40.00	0.01	40.00	0.01
$T_{wf,out}$	[℃]	41.40	40.00	-3.37	41.40	0.00
$h_{wf,in}$	[kJ/kg]	-35.47	-35.47	0.00	-35.47	0.00
$h_{wf,out}$	[kJ/kg]	-30.37	-33.41	10.02	-30.38	0.03
$\phi_{m,wf}$	[kg/s]	2.64	2.63	-0.51	2.63	-0.36
Acetone-Simple-ORC designed at 25% of SWD Engine in Generator Load						
Model		Cycle-Tempo	Original Model		Dynamic Model	
Variable	Units	Value	Value	Error [%]	Value	Error [%]
P_{Pump}	[kW]	8.09	3.24	-59.89	7.60	-6.00
W_{pump}	[kW]	6.43	2.58	-59.84	6.42	-0.02
η_{Pump}	[-]	0.75	1.86	147.87	0.75	0.00
$T_{wf,in}$	[℃]	40.00	40.00	0.01	40.00	0.01
$T_{wf,out}$	[℃]	41.40	40.00	-3.37	41.40	0.01
$h_{wf,in}$	[kJ/kg]	-35.47	-35.47	0.00	-35.47	0.00
$h_{wf,out}$	[kJ/kg]	-30.37	-33.41	10.02	-30.37	-0.01
$\phi_{m,wf}$	[kg/s]	1.26	1.25	-0.53	1.26	-0.08

Table 6.8: Comparison of Cycle-Tempo analysis with original and dynamic pump model for acetone based simple-ORC model

Even though the pump power is approximately 5% of the generated power, the dynamic model is necessary. This is not only to calculate the actual pump power but also the actual expansion process which gives the actual pump exit values of the working fluid. This is important since, the exit values of the working fluid variables from the pump are the input to the boiler element which has significant influence on the dynamics of the ORC model. Since the dynamic pump element modeled for the ORC model is same for simple and recuperative plant models, the comparison of the original model and dynamic model with cycle-tempo is carried out for acetone based ORC model. The same comparison results are also comparable for cyclopentane based recuperative-ORC model as well.

The comparison is performed for SWD engine connected to generator load for engine loads of 25, 75 and 100%. The pump model comparison for the acetone based ORC model are shown in Table 6.8. It can be seen from this table that the error in the original pump element with respect to Cycle-Tempo is greater than acceptable, especially the isentropic efficiency of the pump. This error is seen across all design points of the engine load because the inlet and outlet condition of the working fluid in the original pump element are a constant value that are unchanged during off-design or transient loading. In the same table, the comparison of dynamic pump element with Cycle-Tempo is also seen. In this table, the error seen in the values between the dynamic model and the Cycle-Tempo model are acceptable due to negligible error values especially the pump isentropic efficiency and the condition of the working fluid exiting the pump. These comparison results also show that the dynamic model is acceptable because of negligible error when the ORC-WHRS is designed for any engine load since it approximately captures the actual pump process.

6.4. Off-design Performance Analysis

The off-design performance analysis carried out in the dynamic models are described in this part of the thesis. Before performing this analysis, it is necessary to understand the influence of throttle valve in an ORC plant. As mentioned earlier, the throttle valve is usually used in an SRC plant to protect the turbine at high loads. This is because of very high rotational speeds and it is also used to maintain the steam drum pressure at a desired value irrespective of the load. Such a throttle valve may not be necessary for ORC plant because the turbine has comparatively lower rotational speeds and a steam drum is not required in an ORC plant.

The throttle valve model used in the SRC is a controller based model which holds the steam drum pressure at desired value. When used in the ORC, it maintains the pressure of the evaporator (boiler component as a whole) at a desired value. This usage of throttle valve is not desired in this model because by holding the evaporator pressure constant and since the condenser pressure is already held constant by regulating the mass flow of cooling sea water, the pressure difference across the pump is also held constant irrespective of varying load. This pressure difference is required to calculate the mass flow rate through the system because the pump model is a dynamic resistance model. Hence a varying pressure difference in accordance with varying waste heat load profile is necessary to calculate the actual mass flow rate through the system. However, the effect of throttle valve is needed to analyze to see the difference in performance of an ORC plant with and without a throttle valve.

6.4.1. Throttle Valve

As mentioned in previous chapter, the throttle valve design is a controller based model which is used between the boiler element and the turbine element. The performance of the dynamic ORC plant model with throttle valve switched On and Off is compared to see the influence of throttling effect in the turbine. The throttling valve ensures that the boiler pressure is maintained at at-least the nominal design pressure in off-design and transient conditions.

Figure 6.8 shows the comparison of throttling effect for acetone based simple-ORC at 100% design point. It can be seen that at lower load points, the turbine power generated when throttling valve switch On is lower than the same off-design performance analysis without throttling. This is because for highest design point, in throttling mode, the pressure in the boiler is maintained at nominal design value throughout the waste heat profile. This maintains the pressure difference across the pump at a

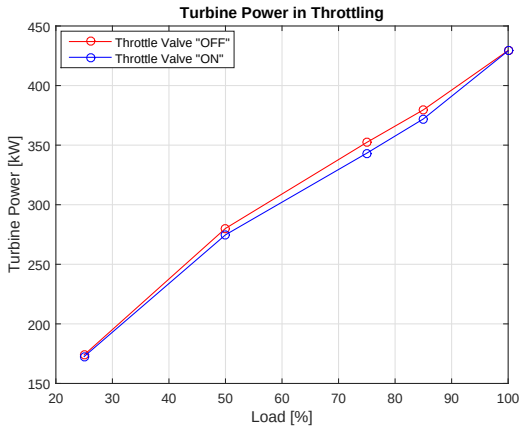

Figure 6.8: Throttling effect comparison for turbine power of acetone based simple-ORC at 100% design point of generator mode.

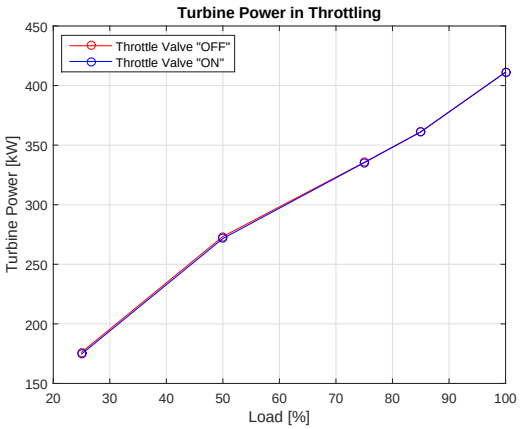

Figure 6.9: Throttling effect comparison for turbine power of acetone based simple-ORC at 75% design point of generator mode.

constant value. Hence in throttling mode, the mass flow through the system is lower in low load conditions due to lower pump rotational speeds caused by increase in liquid level in the boiler due to the throttling effect. This makes such a throttle value unnecessary for an ORC system designed for higher engine load points. It is also because the turbine at that design point is capable of safely functioning at higher mass flow rates.

Figure 6.9 shows the comparison of throttling effect for acetone based simple-ORC at 75% design point. It can be seen that at higher load points, the turbine power generated when throttling valve switch On is equal to the same off-design performance analysis without throttling. This is because during throttling in higher loads, the turbine pressure is equal to the boiler pressure. This is due to higher mass flow rate through the pump to ensure maintaining the liquid fluid level in the evaporator to replace the rapidly evaporating fluid due to higher waste heat flow through the boiler.

In lower load conditions, the effect in the plant at this design point is the same as before and the difference in turbine power is even lower. Moreover, the maximum saturation limit of the throttle valve block is the evaporator pressure because the turbine inlet pressure cannot be higher than the evaporator pressure. It can be seen that such a throttle valve model doesn't bring any added value in at least the off-design performance analysis. Hence the off-design analysis of the ORC plant models are carried out without the use of the throttle valve block. This means that the turbine model and the boiler model are coupled directly and turbine inlet pressure and evaporator pressure are equal to each other.

6.4.2. Off-Design of ORC-WHRS of Engine with Generator Load

The off-design performance analysis are carried out at five engine load points of the engine coupled to a generator load as seen in Table 6.1. To perform this analysis, the static design analysis is performed independently to obtain the values as seen in $GeneratorMode$ column of Appx. Table E.3 and Appx. Table E.4 for acetone based simple-ORC and cyclopentane based recuperative-ORC plant model respectively. Based on these parametric values, the Simulink model is set up to the desired set design point and the waste heat profile is run through the Simulink model to obtain the off-design performance of the ORC-WHRS with respect to the engine load.

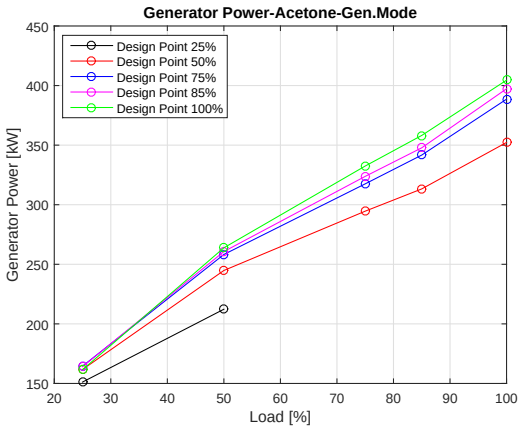

Figure 6.10: Generator power by acetone based simple-ORC in generator mode

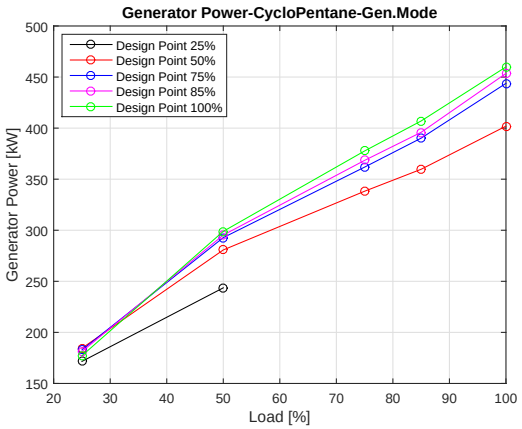

Figure 6.11: Generator power by cyclopentane based recuperative-ORC in generator mode

Figure 6.10 and Figure 6.11 shows the electrical power generated at the generator end by acetone and cyclopentane respectively in their associated plant. It can be seen that the flexibility of the usage of both the fluids in such a waste heat profile are similar in trends because as seen earlier acetone and cyclopentane have almost similar temperature limits. This can be seen in Figure 4.5 and Figure 4.21 which clearly shows the saturation curve characteristics of the two organic fluids. Comparatively, cyclopentane based recuperative-ORC plant generates more power than acetone based simple-ORC plant for the same temperature drop in the turbine due to higher mass flow rate of cyclopentane in the plant because of its lower specific heat.

It can also be seen in the Figure 6.10 and Figure 6.11 that the waste heat profile is such that it allows a complete subcritical ORC plant operation when the design point is anywhere between 50% and 100%. This means that in off-design conditions, the waste heat doesn't heat up the organic fluid in the evaporator beyond the critical temperature into super-critical region. However for the same system when designed for engine loads below 50%, the working fluid in the evaporator could be pushed beyond the critical temperature during off-design conditions because the temperature and mass flow rate of the waste heat is such that the evaporation mass flow rate of the organic fluid in the boiler is higher than the pump capacity. This meaning that the pump is incapable of compensating the boiler with liquid organic fluid for the evaporating fluid to maintain liquid content in the evaporator to handle higher off-design conditions for a subcritical ORC process in the system. Because of slow condensation process of the working fluid.

For loads between 50 and 100, it can be seen that the system designed at higher load points produced higher generator power than systems designed for lower load points. This is because the length of the heat exchangers for systems of higher design points are larger than the systems of lower design points, hence the heat transfer area is also larger. This allows for larger transfer (heat input) of energy from the waste heat to the working fluid in the boiler for a system of higher design point than a system of lower design point for the same waste heat load input.

In lower load region, the system designed at lower design points shows comparatively better power generation than systems of higher design points. This is due to higher mass flow rate of systems designed for low load than systems of higher design points. This higher mass flow rate is due to better pump efficiency of systems designed for low load than systems of higher design points.

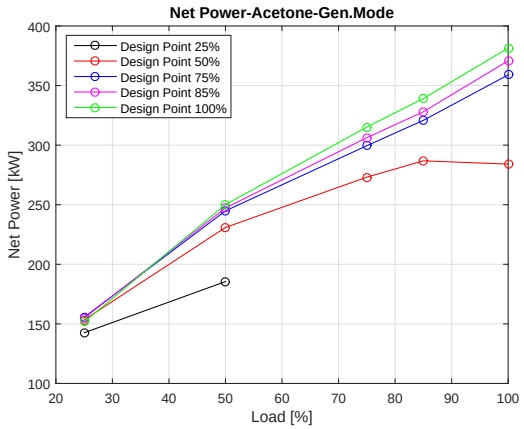

Figure 6.12: Net power by acetone based simple-ORC in generator mode

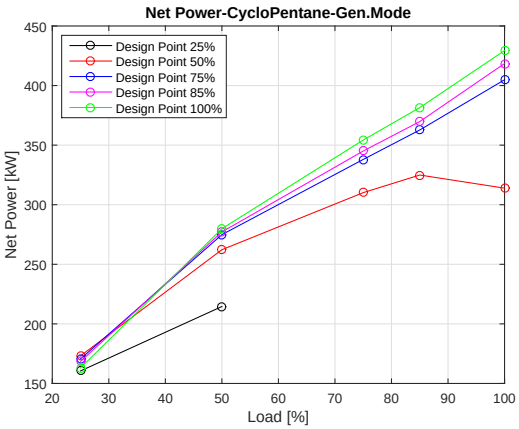

Figure 6.13: Net power by cyclopentane based recuperative-ORC in generator mode

As per the thermodynamic cycle process, ORC plant not only generated power but also required electrical power to drive the working fluid and cooling fluid pumps. When taken into consideration, the net power generated by the complete ORC system is what contributes to the overall efficiency of the engine and WHRS combined. Figure 6.12 and Figure 6.13 shows the net power generated by the ORC plant with respect to the load profile. When comparing net power and generator power, it can be seen that the system designed for 50% load point shows a gradual drop in net power when the system is subjected to an off-design condition higher than 85%. This is due to higher power demand by the working fluid pump to compensate higher evaporation rate of the fluid in the boiler with liquid organic fluid to sustain the ORC process within subcritical region. Such high off-design condition demand higher pump power due to higher mass flow rate and larger pressure difference across the pump than nominal. This is also true for the sea water pump. Moreover, the sea water cooling system of the condenser unit is an open system with a maximum flow rate twice the nominal value since most low pressure cooling systems have identical pumps connected in parallel for higher combined capacity for redundancy and off-design condition. This serves as a limit to the cooling fluid line of the condenser unit that dictates the rate of heat transfer and subsequently the condenser temperature.

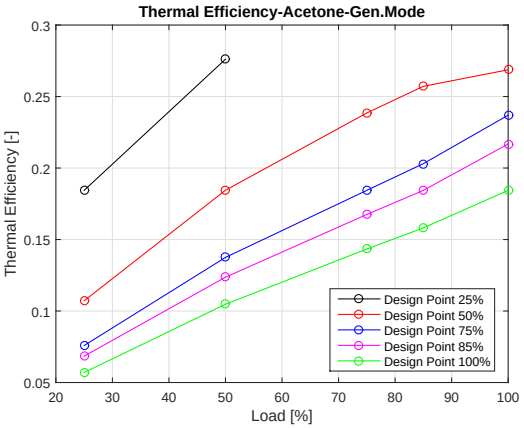

Figure 6.14: Thermal efficiency of acetone based simple-ORC in generator mode

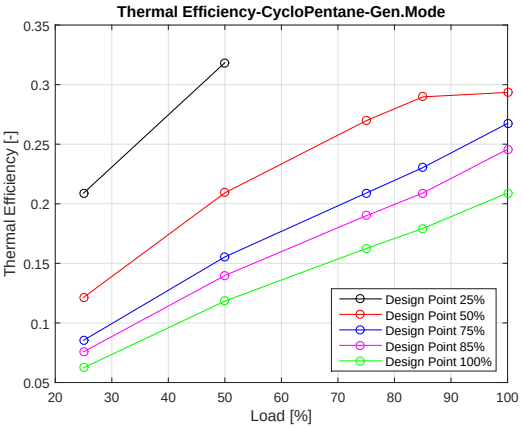

Figure 6.15: Thermal efficiency of cyclopentane based recuperative-ORC in generator mode

Since the design condition of the ORC plant for any engine load has the same initial condition, the thermal efficiency of the system at any design point is roughly the same. Hence the system has better thermal efficiency at higher off-design loads and lower thermal efficiency at lower off-design loads. This is shown in Figure 6.14 and Figure 6.15 for acetone based simple-ORC plant and cyclopentane based recuperative-ORC plant respectively. Based on the waste heat profile of this engine in generator

load, the highest possible thermal efficiencies for the ORC-WHRS flexible of working across all engine loads is seen for the system designed for 50% engine load condition.

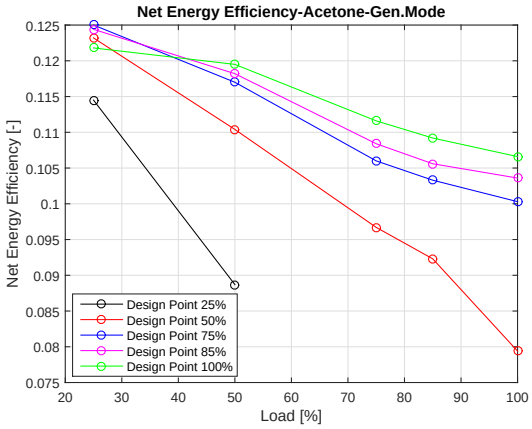

Figure 6.16: Net energy efficiency of acetone based simple-ORC in generator mode

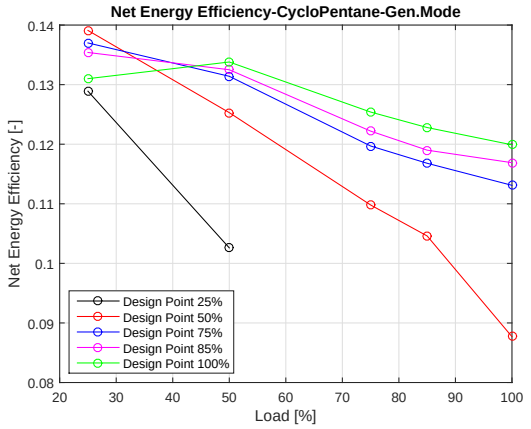

Figure 6.17: Net energy efficiency of cyclopentane based recuperative-ORC in generator mode

Unlike thermal efficiency, the net energy efficiency is higher at low load points and lower at high engine load points. Figure 6.16 and Figure 6.17 shows the net energy efficiency of acetone based simple-ORC and cyclopentane based recuperative-ORC respectively. By following the design points of the figures, it can be seen that the net energy efficiency is higher at low load points and gradually decreases along the increasing load points. In off design performances, it can be seen that the ORC plants designed for higher design points have better net energy efficiency even in off design conditions than ORC system designed for lower design points. This is true for the engine load between ≈45% and 100%. Changes are seen for lower engine loads with the system designed at 75% showing highest net efficiency at 25% engine load as seen in Figure 6.16. Moreover, by looking at the trends at lower engine load points, it can be speculated that the systems designed at lower load points have better net energy efficiency at low off-design condition than systems designed at higher load points, if projected beyond 25% and below. This can be seen in Figure 6.17, where the system designed at 50% showing highest net energy efficiency at 25% engine load.

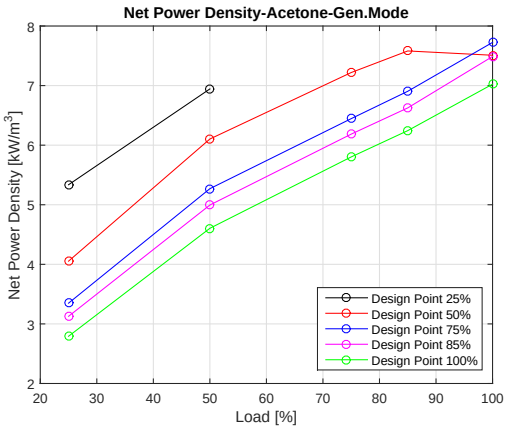

Figure 6.18: Net power density of acetone based simple-ORC in generator mode

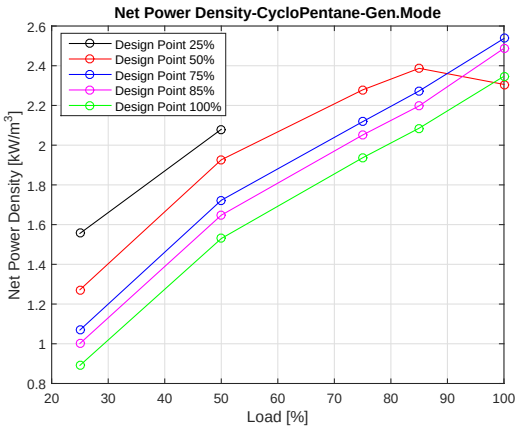

Figure 6.19: Net power density of cyclopentane based recuperative-ORC in generator mode

The net power obtained is used to analyze the net power density of the system. Figure 6.18 and Figure 6.19 shows the net power density of acetone based simple-ORC and cyclopentane based recuperative-ORC respectively. Despite generated lower net power, systems designed for lower load points show better net power density than systems designed for higher load points. Except at higher

engine load point region, it can be see that the system designed for 50% load point has the highest net power density followed by system designed for 75% across the engine profile.

6.4.3. Off-Design of ORC-WHRS of Engine with Propeller Load

As mentioned earlier, the waste heat profile is what dictates the performance of the ORC-WHRS and the waste heat profile of the engine varies based on the load that it is coupled to. It is interesting to analyze the off design performance of the ORC-WHRS for system designed for different engine load points. The SWD engine coupled to a propeller load is further investigated to analyze the performance and see the difference in performances with ORC-WHRS of the same engine when coupled to the generator as before.

The off-design performance analysis are carried out at five engine load points of the engine coupled to a propeller load as seen in Table 6.2. To perform this analysis, the static design analysis is performed independently to obtain the values as seen in $PropellerMode$ column of Appx. Table E.3 and Appx. Table E.4 for acetone based simple-ORC and cyclopentane based recuperative-ORC plant model respectively. Based on these parametric values, the Simulink model is set up to the desired set design point and the waste heat profile is run through the Simulink model to obtain the off-design performance of the ORC-WHRS with respect to the engine load.

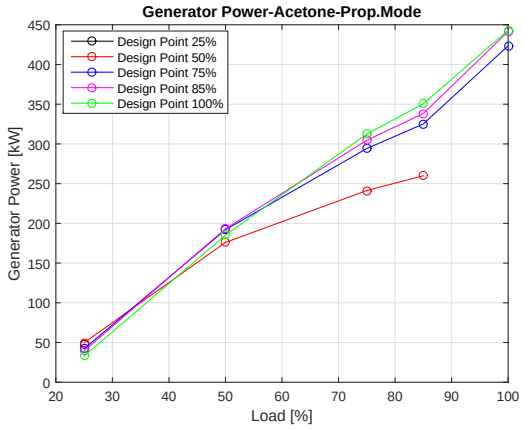

Figure 6.20: Generator power by acetone based simple-ORC in propeller mode

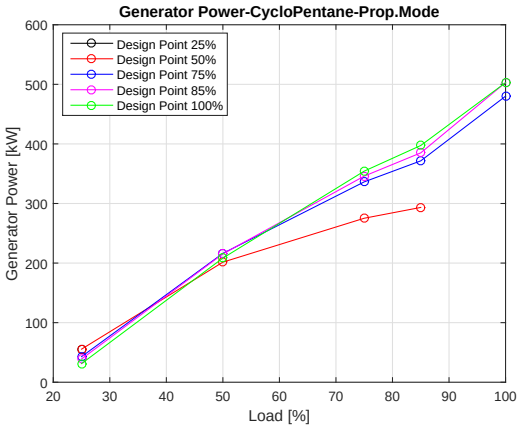

Figure 6.21: Generator power by cyclopentane based recuperative-ORC in propeller mode

Figure 6.20 and Figure 6.21 shows the generator power for acetone based simple-ORC and cyclopentane based recuperative-ORC respectively. It can be seen that the system designed for low loads do not have a wider operating flexibility as seen before for the same engine when used in generator load. This is true for both acetone and cyclopentane.

As seen for in generator load, the system designed for lower load points produce higher generator power however this flip over occurs in the region at $\approx$ 60% and below whereas for in generator mode it was in the region of $\approx$ 40% and below. However the generator power shows a growing trend as the engine load increases irrespective of the design point of the ORC-WHRS. Hence, net power produced is to be considered since, it is what contributes to the overall efficiency of the ship.

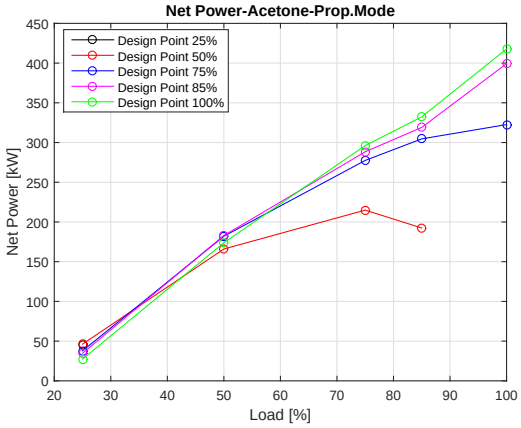

Figure 6.22: Net power by acetone based simple-ORC in propellerr mode

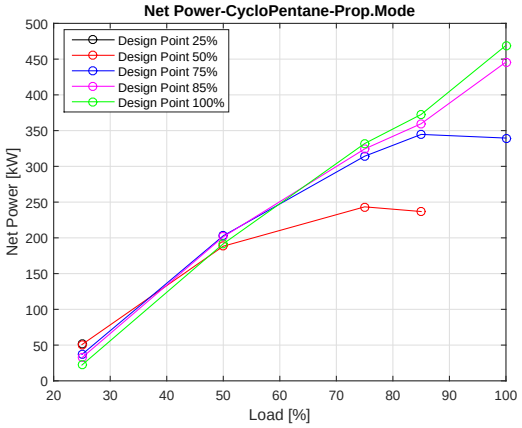

Figure 6.23: Net power by cyclopentane based recuperative-ORC in propeller mode

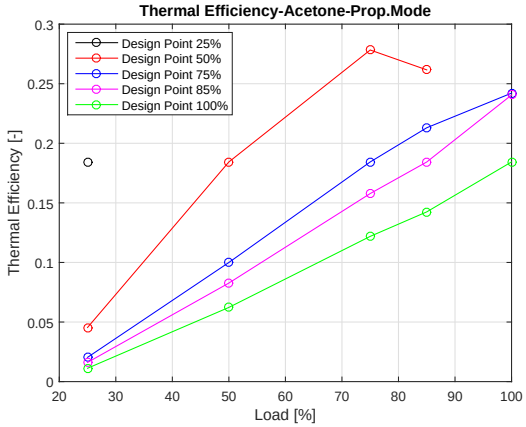

Figure 6.24: Thermal efficiency of acetone based simple-ORC in propeller mode

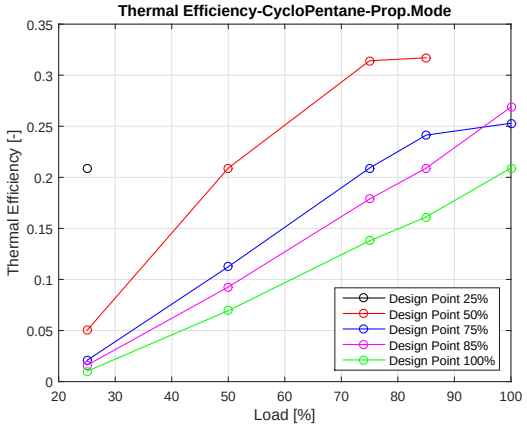

Figure 6.25: Thermal efficiency of cyclopentane based recuperative-ORC in propeller mode

Figure 6.22 and Figure 6.23 shows the net power produced by acetone based simple-ORC and cyclopentane based recuperative-ORC respectively for the engine couple to a propeller. Since the waste heat profile of the same engine is now different, the systems designed at lower and middle load point are showing reduction in net power generation during higher off-design conditions. This is seen for the system designed between 50% and 75% engine load point in propeller load compared to the the system designed for 50% engine load in generator load. This reduction is primarily due to the power demand by the pump. Such reductions are reflected in the thermal efficiency of the system which was not seen in the analysis of the generator load. Figure 6.24 and Figure 6.25 shows the thermal efficiency of acetone based simple-ORC and cyclopentane based recuperative-ORC respectively. By comparing the thermal efficiency data of acetone and cyclopentane for generator and propeller, it can be seen that in thermal efficiency trends are not similar but decreasing for certain design points. Unlike as seen in generator load, especially for 100% engine load, the system designed for 85% is better than systems designed for either higher or lower engine load points.

As seen for in generator load, acetone and cyclopentane based ORC-WHRS showed highest net energy efficiencies at lower engine load points when designed at any load point. This is changed for the same systems when used for an engine with propeller load. Figure 6.26 and Figure 6.27 shows net energy efficiency of acetone based simple-ORC and cyclopentane based recuperative-ORC respectively. It can be seen that the systems shows highest net efficiencies at 50% engine load when the system are designed at any load point over 50%. As seen in generator load, systems designed at higher load point showed higher net energy efficiencies at high load and vice-versa for low loads.

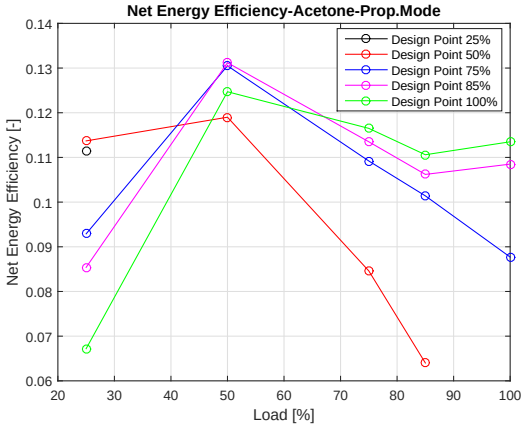

Figure 6.26: Net energy efficiency of acetone based simple-ORC in propeller mode

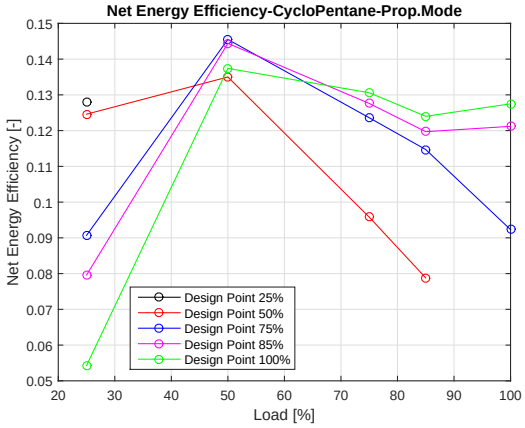

Figure 6.27: Net energy efficiency of cyclopentane based recuperative-ORC in propeller mode

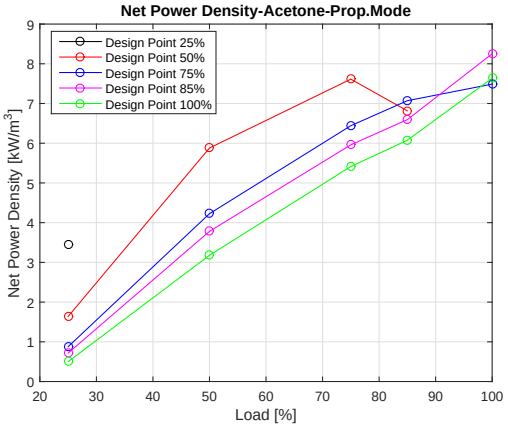

Figure 6.28: Net power density of acetone based simple-ORC in propeller mode

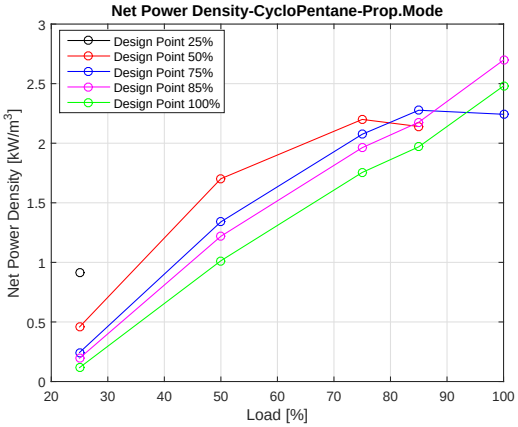

Figure 6.29: Net power density of cyclopentane based recuperative-ORC in propeller mode

Figure 6.28 and Figure 6.29 shows net power density of acetone based simple-ORC and cyclopentane based recuperative-ORC respectively. It can be seen that system designed for 85% has the highest power density at 100% engine load.

The off-design performance data are shown in Appx. Tables F.1 to F.8.

The nominal operating point of the engine (point at which the engine runs the most) is based on the operational profile of the vessel. Therefore the ORC-WHRS may be designed for that nominal operating point of the engine. These off-design performance analysis can be used to understand the potential of the ORC-WHRS based on the waste heat profile of the engine for its designed point. When operational profile of the vessel is incorporated into the analysis, the net power density of ORC system designed at different load points can be plotted over time period. This is in order to obtain net energy density to understand which design point could be most beneficial in terms of energy density. Not just the net energy density but with the specific fuel consumption of the engine and the operational profile, the net power can be used to calculate how much waste energy is recovered in mass of fuel terms which is used to understand the extent of yearly fuel savings and subsequently the reduction in carbon dioxide emissions.

7

Dynamic and Sensitivity Analysis

This chapter focuses on the sensitivity and dynamic analysis of the dynamic ORC model. Firstly, sensitivity analysis is performed to observe which model input parameter or set of parameters are sensitive and significant to ORC performance based on the model output. Secondly, dynamic analysis is performed to understand the dynamic behaviour of the ORC plant model process when subjected to load step functions of waste heat input parameters. This analysis shows the model stabilization time with respect to step duration and load variations of the model input parameters.

7.1. Sensitivity Analysis

In general, the analysis of how a variability in the model input source parameter(s) can be apportioned to variability in the model output is termed as sensitivity analysis [Saltelli, 2002]. This model can be a mathematical model or represent a system and in our case, the model is an ORC based WHR system. Sensitivity analysis of ORC-WHRS model is performed to analyze the sensitivity of ORC performance and model parameters with respect to changes to the model input. Since the ORC plant model in our case is used for waste heat recovery of exhaust gas from a marine diesel engines, the model input parameters of this ORC system are the engine exhaust parameters namely exhaust pressure, temperature and mass flow.

To analyze the influence of each input parameter on the model output, other input parameters are to be kept constant. This analysis is performed on acetone based simple-ORC plant model only, since the obtaining results will be similar for cyclopentane based recuperative-ORC plant model. This is because, as mentioned in earlier chapters that the recuperative plant model is similar to and based on simple plant model. Cyclopentane as a working fluid is also similar to acetone especially the saturation liquid curve, critical point and freezing point. This is shown in the T-S diagram of these fluids in Figure 4.21.

We know that the model input parameters are the pressure, temperature and mass flow of the waste heat source fluid into the boiler component of the ORC model. In our application, this waste heat source fluid is the exhaust gas from a marine diesel engine. The diesel engine chosen is the same SWD12V280 used in Chapter 6 for off-design performance analysis. The sensitivity analysis is carried out for ORC plant model sized to the design point for exhaust gas heat profile of 100% in generator mode as seen in Table 6.1.

7.1.1. Varying Pressure

Exhaust gas pressure is an input to the ORC model and to understand the effect of uncertainty in the exhaust pressure input on the ORC model performance output, the engine exhaust pressure is varied as other input parameters are kept constant. This analysis is carried out for varying discrete pressure points from 0.5 bar to 1.05 bar.

p_{eg}	P_{Gen}	P_{Net}	η_{Net}	$\phi_{m,wf}$	$\phi_{m,sw}$	$\phi_{q,cond}$	$\phi_{q,econ}$	$\phi_{q,evap}$	p_{evap}	p_{cond}
[bar]	[kW]	[kW]	[%]	[kg/s]	[kg/s]	[MW]	[MW]	[MW]	[bar]	[bar]
1.05	404.53	381.46	10.66	3.37	43.02	1.81	1.41	0.81	29.92	0.57
1.0466	404.53	381.46	10.66	3.37	43.02	1.81	1.41	0.81	29.92	0.57
1.037	404.53	381.46	10.66	3.37	43.02	1.81	1.41	0.81	29.92	0.57
1.03	404.53	381.46	10.66	3.37	43.02	1.81	1.41	0.81	29.92	0.57
1.0224	404.53	381.46	10.66	3.37	43.02	1.81	1.41	0.81	29.92	0.57
1.02	404.53	381.46	10.66	3.37	43.02	1.81	1.41	0.81	29.92	0.57
0.5	404.53	381.46	10.66	3.37	43.02	1.81	1.41	0.81	29.92	0.57

Table 7.1: Sensitivity analysis of simple-ORC plant model for varying exhaust pressure

Table 7.1 shows the model output parametric results for varying exhaust pressure in the ORC-WHRS. It can be seen from the results that uncertainties in the exhaust pressure model input has no influence on the model output. The influence is not exactly null, but too small to be considered significant. The exhaust pressure is used to assist in calculating the specific heat, thermal conductivity, density and viscosity of the exhaust gas in the exhaust side of the boiler component of the model. These thermodynamic and transport properties of the exhaust gas vary insignificantly with respect to varying pressures or at least for range of exhaust pressure considered for this analysis. This insignificance is because the exhaust gas is in gas state and the changes in thermodynamic and transport properties of any fluid in gas form for varying pressure is significantly smaller to the changes seen for the same fluid but in liquid form. In addition to this, the range of the varying pressure used for this analysis may be small to capture any significant change to the model output. However the pressure range used is a realistic range for a marine diesel engine .

7.1.2. Varying Temperature

Exhaust gas temperature is another input parameter to the ORC model and the sensitivity of this model to exhaust temperature is performed and described in this section. To understand the effect of uncertainty in the exhaust temperature input on the ORC model performance output, the engine exhaust temperature is varied as other input parameters are kept constant. This analysis is carried out for varying discrete temperature points from 350°C to 500°C.

$T_{eg,in}$	P_{Gen}	P_{Net}	η_{Net}	$\phi_{m,wf}$	$\phi_{m,sw}$	$\phi_{q,cond}$	$\phi_{q,econ}$	$\phi_{q,evap}$	p_{evap}	p_{cond}
[C]	[kW]	[kW]	[%]	[kg/s]	[kg/s]	[MW]	[MW]	[MW]	[bar]	[bar]
500	535.71	469.35	10.54	4.61	86.31	2.42	1.82	1.13	37.88	0.63
481	511.09	465.48	10.94	4.30	86.31	2.27	1.73	1.05	36.07	0.60
450	464.17	432.38	10.99	3.84	74.10	2.05	1.58	0.94	33.17	0.57
415	404.53	381.46	10.66	3.37	43.02	1.81	1.41	0.81	29.92	0.57
408	394.92	372.81	10.62	3.29	39.99	1.77	1.38	0.79	29.39	0.57
400	383.83	362.74	10.58	3.21	36.89	1.73	1.34	0.76	28.78	0.57
350	312.19	296.04	10.08	2.68	23.12	1.45	1.10	0.58	24.72	0.57

Table 7.2: Sensitivity analysis of simple-ORC plant model for varying exhaust temperature

Table 7.2 shows the model output parametric results for varying exhaust temperature in the ORC-WHRS. It can be seen from the results that uncertainties in the exhaust temperature model input has significant influence on the model output, unlike as seen for in varying pressure. It can be seen from the table that the heat transmitted in the heat exchanger, mass flow of the working fluid and the evaporator pressure has an increasing trend as the exhaust temperature increases. However, the power produced by the ORC-WHRS and plant efficiency are the model outputs that are the most important to analyze the sensitivity of the WHR system output with respect to uncertainties in varying model input. These output parameters are largely focused on, because the power produced and plant efficiency captures the actual ORC model output performance as a WHRS of a diesel engine.

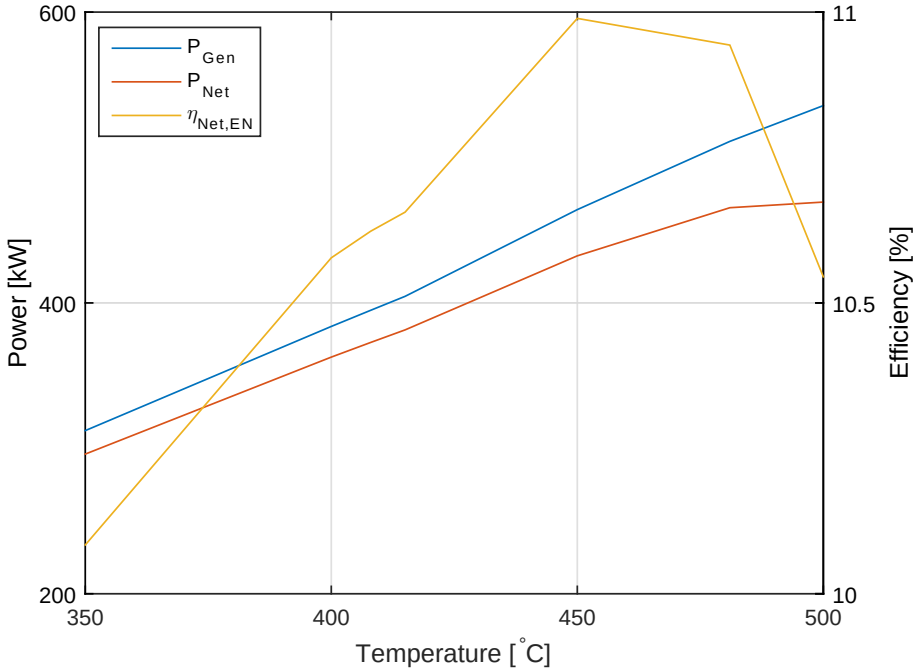

Figure 7.1: Sensitivity analysis of simple-ORC plant model for varying exhaust temperature on power produced and plant efficiency

Figure 7.1 shows the changing power and efficiency of the ORC-WHRS with respect to changing exhaust temperature. It can be seen from this figure that the power output of the ORC generator increases to increasing temperature. Since net power is the actual recoverability of the ORC system, it can be seen from the same figure that the net power of the system increases to increasing exhaust temperature until around 450°C. Beyond this exhaust temperature, the rate of increase in net power gradually reduces for increasing exhaust temperature and becomes almost constant especially between 480°C and 500°C. This is mainly due to two factors that affects the turbine power and pump power.

Firstly, for the factor that affects the turbine power is the increase in condensing pressure and condensing temperature with respect to increasing exhaust temperature. This is due to the limits on the mass flow rate of the cooling fluid to the condenser. This mass flow rate limit of the cooling fluid is twice the mass flow rate at design point. This corresponds to a meaning that there are two identical cooling fluid pumps connected in parallel to each other. These are placed for redundancy or to cope up with increasing condenser load or increasing cooling fluid inlet temperature (This limit is also seen and discussed in Chapter 6 during off-design performance analysis). This cooling fluid mass flow rate limit is capable of maintaining the desired condenser pressure and temperature as the load on the condenser increases as exhaust temperature increases, but only until the limit. Beyond a certain exhaust temperature (450°C and above in this case), the condensing pressure and temperature also increases. This affects the turbine expansion process by decreasing it from the evaporation temperature to increasing condenser temperature. This results in shorter turbine expansion thus leading to reduction in turbine power generation of the ORC-WHRS.

Finally, for the factor that effects the pump power is the increase in pump power due to rapid increase in evaporator pressure due to increasing exhaust temperature. This rapid increase results in increase in the pressure difference ($\Delta p = p_{evap} - p_{cond}$) across the pump. This increase leads to increase in pump power necessary to perform the ORC plant process in the plant model for WHR. This increase in pump power leads to reduction in the net power output of the system. The reduction in net power output is reflected onto the net energy efficiency curve as seen in Figure 7.1. It shows that the net energy efficiency increases and is the highest for this system under these exhaust conditions at

around 450°C. Any further increase in exhaust temperature will result in decrease in the net energy efficiency of the plant. Based on the decreasing trend of the net energy efficiency curve as seen for exhaust temperatures between 450 and 500, it can be understood that any increase in exhaust temperature beyond 500 will also have reduction in the net energy efficiency and this will also reflect in the gradual reduction in the net power output as well.

7.1.3. Varying Mass-Flow Rate

Exhaust gas mass flow rate is the third and final input parameter of the ORC plant model that is analyzed for model sensitivity. To understand the effect of uncertainty in the exhaust mass flow input on the ORC model performance output, the engine exhaust mass flow is varied as other input parameters are kept constant. This analysis is carried out for varying discrete mass flow rate points from 2 kg/s to 9 kg/s.

$\phi_{m,eg}$	P_{Gen}	P_{Net}	η_{Net}	$\phi_{m,wf}$	$\phi_{m,sw}$	$\phi_{q,cond}$	$\phi_{q,econ}$	$\phi_{q,evap}$	p_{evap}	p_{cond}
[kg/s]	[kW]	[kW]	[%]	[kg/s]	[kg/s]	[MW]	[MW]	[MW]	[bar]	[bar]
9	435.83	408.99	10.41	3.61	55.88	1.93	1.53	0.84	31.64	0.57
8.2	404.53	381.46	10.66	3.37	43.02	1.81	1.41	0.81	29.92	0.57
8	396.98	374.67	10.73	3.31	40.61	1.78	1.38	0.80	29.51	0.57
7	357.46	338.46	11.08	3.01	30.78	1.62	1.22	0.76	27.30	0.57
6.6	340.77	322.92	11.21	2.89	27.62	1.56	1.15	0.74	26.36	0.57
6	314.75	298.46	11.39	2.70	23.49	1.46	1.05	0.70	24.87	0.57
5	268.49	254.51	11.66	2.36	17.82	1.28	0.88	0.65	22.15	0.57
4	218.16	206.26	11.81	2.00	13.24	1.08	0.70	0.58	19.08	0.57
3	163.10	153.18	11.70	1.61	9.39	0.87	0.51	0.50	15.55	0.57
2.4	127.49	118.76	11.34	1.34	7.33	0.72	0.39	0.45	13.15	0.57
2	102.58	94.71	10.85	1.16	6.03	0.62	0.31	0.41	11.39	0.57

Table 7.3: Sensitivity analysis of simple-ORC plant model for varying exhaust massflow

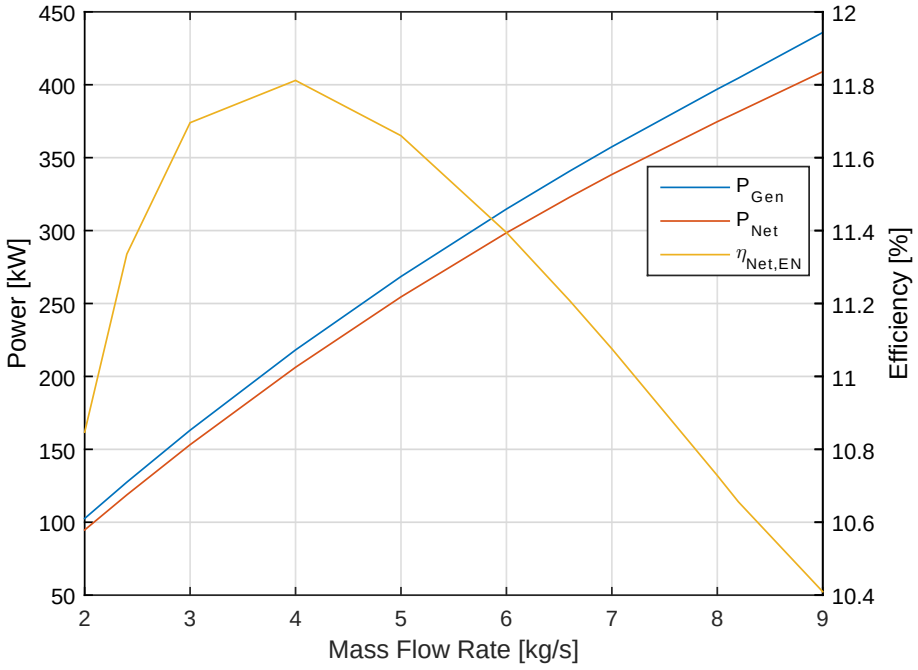

Figure 7.2: Sensitivity analysis of simple-ORC plant model for varying exhaust mass flow rate on power produced and plant efficiency

Table 7.2 shows the model output parametric results for varying exhaust mass flow rate in the ORC-WHRS. It can be seen from this table that the generator power and the net power is increasing for increasing exhaust gas mass flow rate. However, this increase is not reflected in the net energy efficiency of the plant and these trend curves are shown in Figure 7.2. Based on this figure, it can be seen that the maximum net plant efficiency is seen around 4 kg/s and starts to decrease as the exhaust mass flow rate increases. When following this decreasing trend, it can be understood that any further increase in exhaust flow rate beyond the calculated 9 kg/s will result in further decrease in net plant efficiency. Such a trend will be reflected onto the generated power and net power output eventually resulting in gradual decrease due to the factor that effects the turbine power.

The factor that effects the turbine power in this sensitivity analysis is the same as the first factor explained in the varying temperature sensitivity analysis. This is because the sea water mass flow rate has a gradual exponential increasing trend for increasing exhaust mass flow rate as shown in Figure 7.3. From the trend seen in this figure, it can be understood that any small further increase in exhaust mass flow rate beyond 9kg/s will quickly result in the plant system reaching the cooling fluid mass flow rate limit. Hence, the factor effecting the turbine power occurs.

Regarding the factor that effects the pump power as seen in varying temperature sensitivity analysis will also eventually occur but that may not appear as quickly in varying exhaust mass flow rate sensitivity analysis. This is because the rate of increase in evaporator pressure in varying exhaust mass flow rate is smaller when compared to the same in varying exhaust temperature analysis.

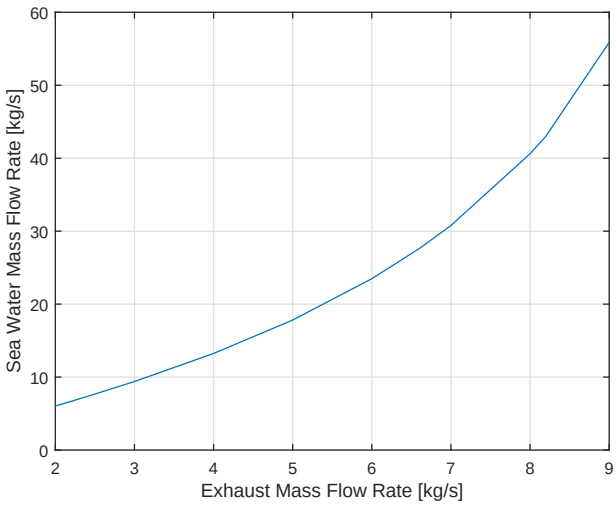

Figure 7.3: Sensitivity analysis of simple-ORC plant model for varying exhaust mass flow rate on sea water mass flow rate

For the sensitivity analysis seen above, the model input parameters of waste heat to the boiler component of the ORC plant model was carried out. The sensitivity of the ORC plant model can also be extended to varying cooling fluid (CF) parameters of model input to condenser component. As mentioned earlier, we know that the CF pump is modeled based on a controller element that regulates CF mass flow in order to maintain working fluid (WF) condensing temperature. In addition, since sea water (SW) open system is the CF used in this thesis, the only realistic parameter that can vary is the SW temperature.

The sensitivity of the ORC plant model to varying SW temperature can be understood from the model element and analysis performed so far. For decreasing SW temperature, the SW mass flow rate will also decrease according in order to maintain WF condensing temperature. This decrease will subsequently lead to decrease in CF pump power. However, this will have insignificant effect on the net power and the net efficiency. This is because as mentioned earlier, the CF pump power is less than 1% of the generated power. For increasing SW temperature, the SW mass flow rate will also increase according in order to maintain WF condensing temperature. This also has the same effect as seen before for decreasing SW temperature. However for increasing SW temperature higher than a certain degree, the CF mass flow limit is reached and gradual increase in WF condensing temperature is seen. This leads to the same effects as seen before for increasing WF condensing temperature.

7.2. Dynamic Analysis

In general, dynamic analysis of a model is performed to study the behaviour of the model response to transient or dynamic loads. This analysis can be used to understand the dynamics of an actual plant as the model closely represents it.

In this section, dynamic analysis of the ORC plant model is covered. As seen before in the sensitivity analysis section of this chapter, the dynamic analysis of the ORC-WHRS is carried out for acetone based simple-ORC plant model. In the analysis, the ORC plant model is subjected to step functions in its model input parameters. These step functions input parameters are the engine exhaust data from the SWD engine as seen in Table 6.1. The model output response to these step functions are recorded and represented in terms of time to stabilization with respect to step duration and load variations. The stabilization time of the ORC model is considered and recorded for the generator power parameter. The generator power of the model output is considered as the parameter to analyze the dynamic behaviour of the ORC plant model. This is because it is the actual desired output of a WHRS and the last parameter to stabilize to equilibrium in response to any step or transient input function. The time to stabilization of the model output (i.e. P_{Gen}) is also taken at points of 5% and 1% to equilibrium. These two additional points will show the dynamic behaviour of the model in responds to step functions while advancing towards equilibrium state.

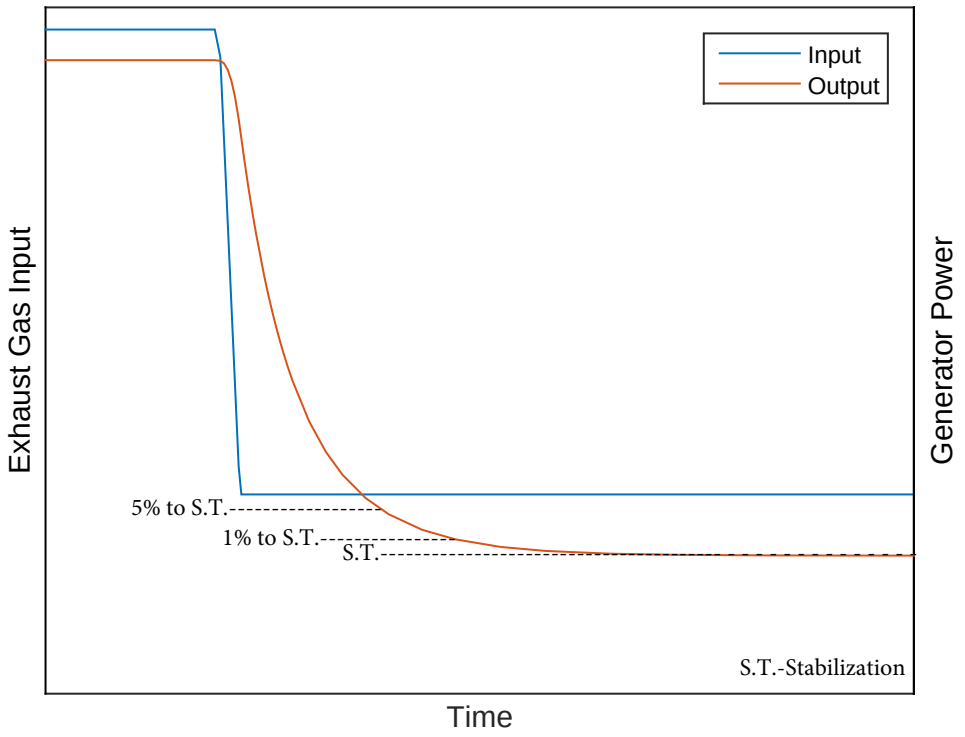

Figure 7.4: Graphical representation of the stabilization points for analysis of the dynamic behaviour of the ORC model.

The additional points and the equilibrium of the model output during step function response of the model input is shown in Figure 7.4 and it shows load drop step function model input as an example. It also shows hows the points of stabilization and the time of stabilization are considered for this analysis. The input legend of this figure represents the step load function engine input parameters to the ORC model, which translates to step load input function of the exhaust mass flow, temperature and pressure to the boiler component of the ORC plant model. The output legend of the same graph represents the generated power of the ORC model output.

The step functions used to analyze the dynamic behaviour of the ORC plant model is given as a load-drop and load-rise input step functions. Such inputs will show how the ORC plant model designed for a specific operating point of the engine responds when subjected to increasing or decreasing engine loads.

7.2.1. Load-Drop Step Function

In this sub-section the load-drop step function as the model input to analyze the dynamic behaviour of the ORC plant model in response to decrease in load is discussed. In this analysis, the responses of the ORC-WHR plant model designed for different engine load points when subjected to the same engine load-drop are studied. As mentioned earlier, these responses are captured in terms of stabilization time and the load-drop dynamic response example is seen in Figure 7.4.

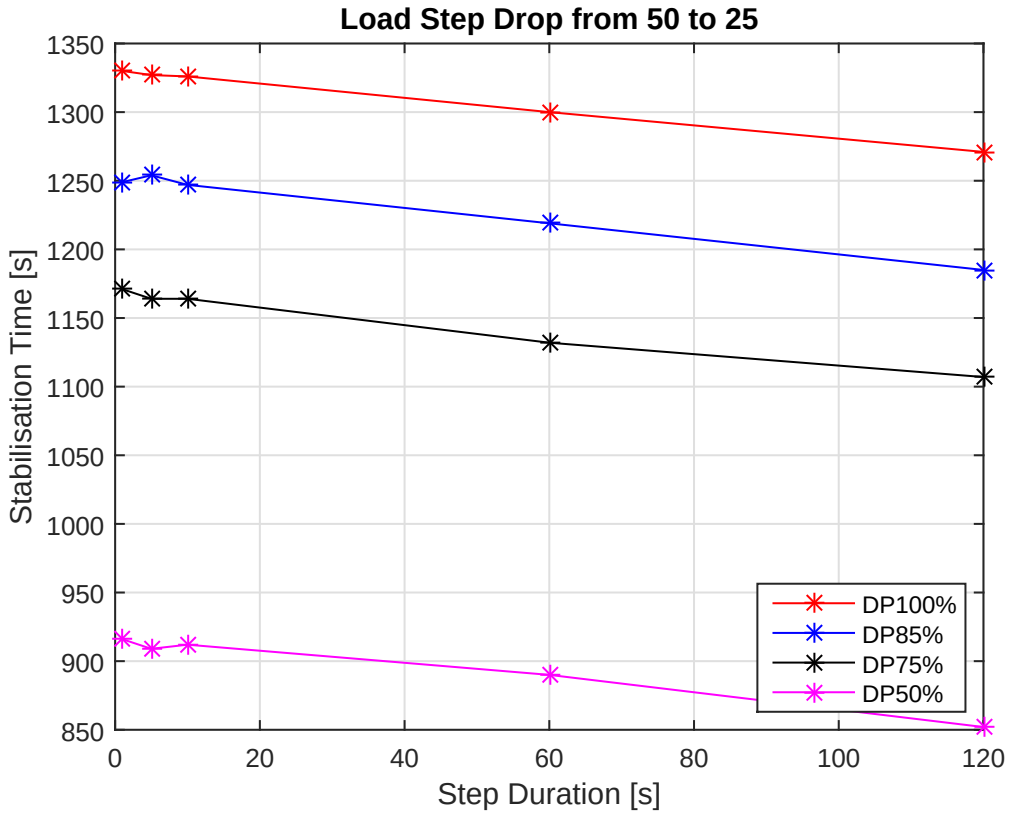

Figure 7.5: Stabilization time vs Step duration of the model for load-drop from 50 to 25% of the engine load

For the analysis, the ORC plant model is subjected to a load drop in engine exhaust input from 50% to 25% engine load. Figure 7.5 shows the model output response (of 5% to stabilization) to this load drop of the ORC model when designed for different engine load points. Two noticeable trends can be seen in this figure. Firstly, the response of the ORC model output of the same design point becomes faster as the duration of the step load function increases. This is because when the step duration is the shortest, the load drop is almost instantaneous in the ORC model and when the load drop is complete, the ORC model has shown negligible or no response to it at all. Whereas in longer step duration (longer than what is considered instantaneous), the load drop is gradual in the ORC model and by the time the load drop is complete, the ORC model has already shown non-negligible response to it. This model response comes closer and closer to equilibrium as the step duration of load-drop increase. This means that when the step duration of the load-drop to the model input is the longest possible, the model output response to equilibrium is instantaneous (time to stabilization is ~ 0 sec) by the time the load drop is complete.

Secondly, the response of the ORC model for the same step duration becomes longer as the design point of the ORC plant increases. This means that an ORC plant designed at a lower engine load point has a faster response than an ORC plant designed at a relatively higher engine load point when subjected to the same load drop and step duration. An ORC-WHRS designed at different engine load points have the same thermodynamic cycle processes (same fluid properties after each independent process within the cycle), however with the difference in the fluid mass flow rate. This difference in mass flow rate quantities with respect to different design points for the same cycle influences the size of the components of the ORC plant especially the heat exchangers. In this relation, as mentioned in the earlier chapters, higher the ORC design point (i.e. higher engine exhaust gas mass flow rate) higher is the fluid mass flow rate which leads to larger heat exchangers. Larger heat exchangers takes longer time to reach thermal equilibrium in comparison to smaller heat exchangers when subjected to the same load variations. Hence the ORC plant designed at a lower engine load point has a faster response than an ORC plant designed at a relatively higher engine load point when subjected to the same load drop and step duration.

To confirm if these two noticeable trends are true in nature, other load-drop step functions with the same analytic conditions as used seen in here has to be carried out.

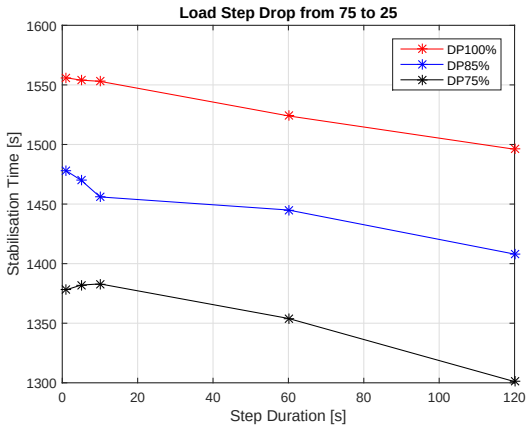

Figure 7.6: Stabilization time vs Step duration of the model for load-drop from 75 to 25% of the engine load

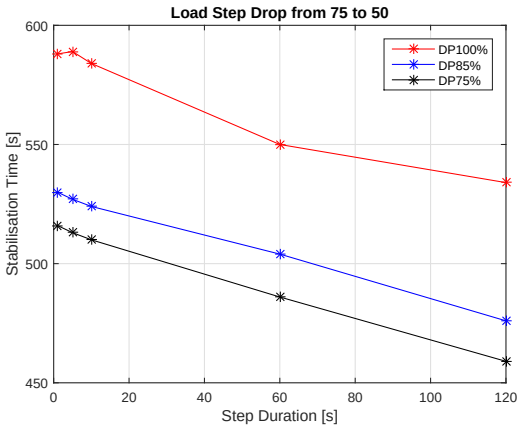

Figure 7.7: Stabilization time vs Step duration of the model for load-drop from 75 to 50% of the engine load

To further understand the dynamic behaviour of the ORC plant model to load-drop step function, the same analysis as seen before is carried out for load drop in engine exhaust input from 75% to 25% and 75% to 50% engine load. The analysis to these step functions are shown in Figure 7.6 and Figure 7.7 respectively. In these two figures it can be noticed that the trends seen in them are similar to the ones seen in Figure 7.5. Since the noticeable trends seen as these figures are the same, it can be understood that these trends are due to the reasons mentioned above. If this is so, then these reasons should hold true for not only the current load-drop step function analysis but also for load-rise step function.

The complete analysis tables comprising the stabilization time for load-drop analysis is shown from Appx. Table G.1 - Appx. Table G.4.

7.2.2. Load-Rise Step Function

In this sub-section the load-rise step function as the model input to analyze the dynamic behaviour of the ORC plant model in response to increase in load is discussed. In this analysis, the responses of the ORC-WHR plant model designed for different engine load points when subjected to the same engine load-rise are studied. As mentioned earlier, these responses are captured in terms of stabilization time and the load-rise dynamic response example is the graphical inverse of the load-drop example seen in Figure 7.4.

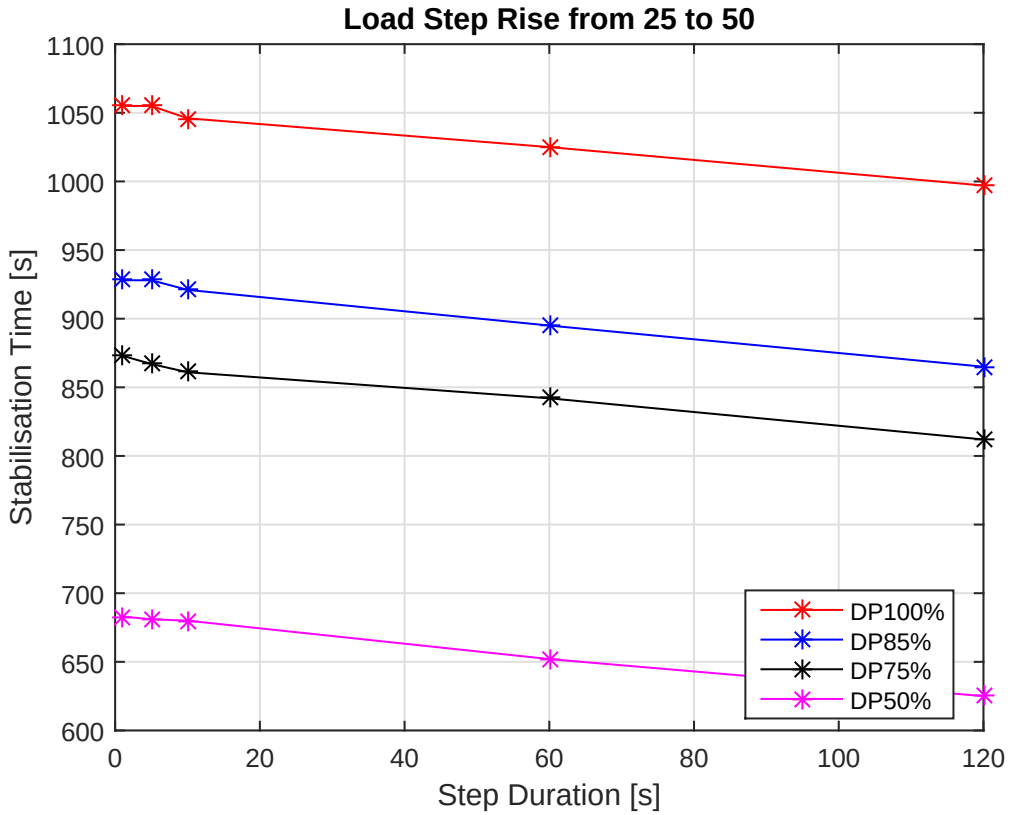

Figure 7.8: Stabilization time vs Step duration of the model for load-rise from 25 to 50% of the engine load

For the analysis, the ORC plant model is subjected to a load rise in engine exhaust input from 25% to 50% engine load. Figure 7.8 shows the model output response (of 5% to stabilization) to this load rise of the ORC model when designed for different engine load points. Two noticeable trends can be seen in this figure and these trends are similar to those appeared in the load-drop step function analysis. It can be understood that these trends have the same reasons as well. Such trends and similarities to other load steps can be analyzed across different design points.

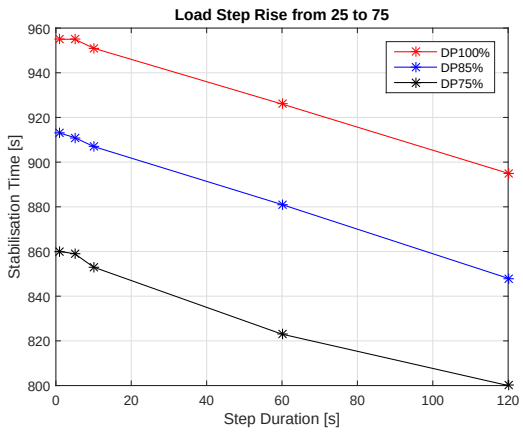

Figure 7.9: Stabilization time vs Step duration of the model for load-rise from 25 to 75% of the engine load

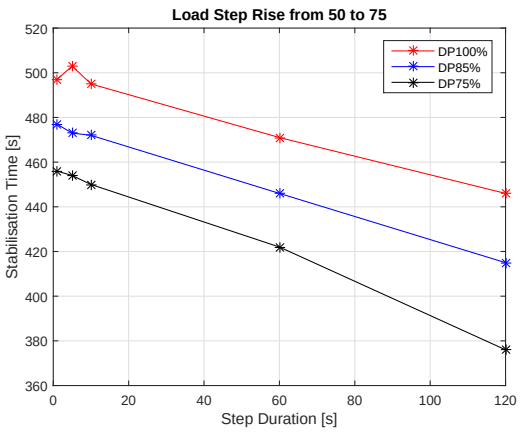

Figure 7.10: Stabilization time vs Step duration of the model for load-rise from 50 to 75% of the engine load

As performed before, to further understand the dynamic behaviour of the ORC plant model to load-rise step function, the same analysis as seen before is carried out for load rise in engine exhaust input from 25% to 75% and 50% to 75% engine load. The analysis to these step functions are shown in Figure 7.9 and Figure 7.10 respectively. By analyzing the trends seen in these figures, it can be understood that these trends are similar to the ones seen during load-rise analysis from 25% to 50%. Moreover, these dynamic behaviour of the model to load-rise step functions are similar to the dynamic behaviour of the model to load-drop step functions.

The complete analysis tables comprising the stabilization time for load-drop analysis is shown from Appx. Table G.5 - Appx. Table G.8.

7.2.3. Same Design Point

In this sub-section, the analysis of the dynamic behaviour of the model when subjected to different step functions for an ORC-WHR plant designed at the same point is carried out. This analysis is unlike the ones seen before, where the analysis of the dynamic behaviour of the model subjected to the same step function across various design points were carried out. When comparing these analysis of the same step functions seen in sub-sections of load-drop and load-rise, it can noticed that the ORC model under same conditions takes longer time to drop from A→B than the time needed to rise from B→A.

As an example when considering only the load step between 25% and 50% for the ORC plant designed for 100% engine load, it can be seen in Figure 7.5 that the load drop from 50% to 25% takes longer time for the model to stabilize than the time needed to stabilize when the load is raised from 25% back to 50% as seen in Figure 7.8. This pattern can also be observed for other load steps and design points from the same load-drop and load-rise analysis sub-sections.

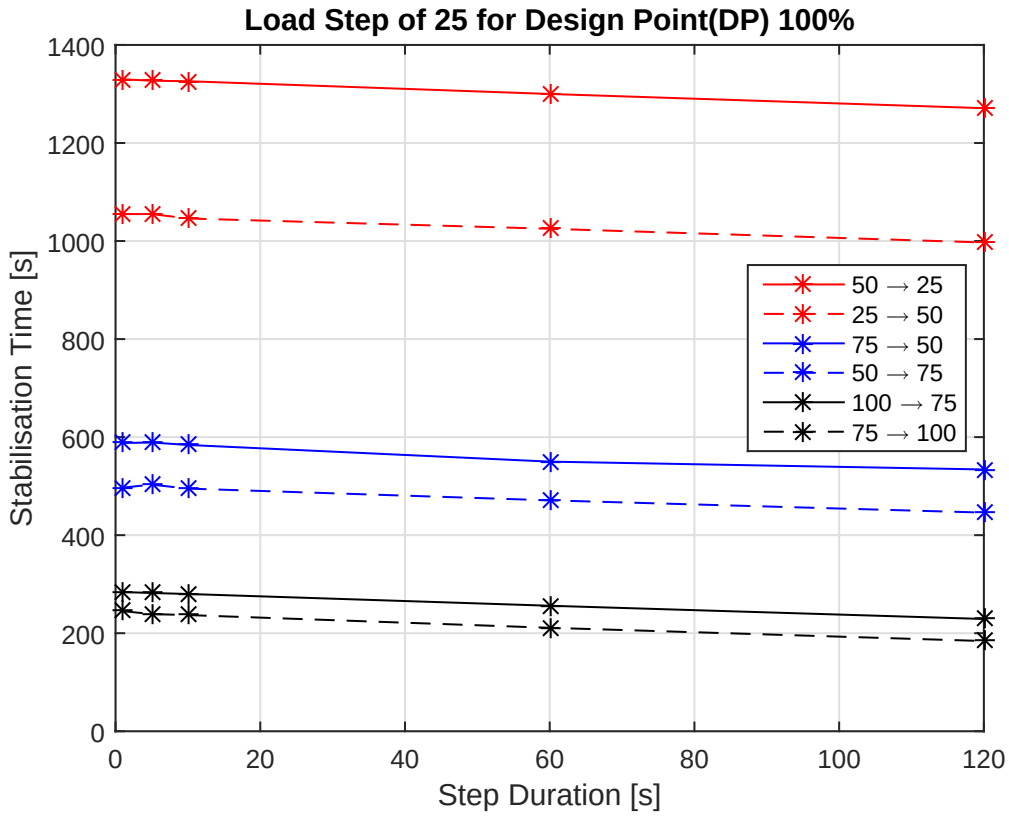

Figure 7.11: Stabilization time vs Step duration for step function of the model designed at 100% of the engine load

When observing such a pattern for the same design point, it can also be noticed that the time difference is different for different starting points even though the step difference is the same and this pattern is shown in Figure 7.11. From this figure it can be seen that for the same step difference of 25% used in this analysis, the time difference between the time needed for the model to go from points A→B and the time needed to return from B→A increases as the load points A and B gets smaller. Moreover, the ratios of time difference between them also slightly increases as the load points get smaller.

In all the analysis performed, it can be seen that the model response time to step rise is faster than to step down for the same load difference across all step duration. This is not only true for the ORC plant model design point of 100% as seen in Figure 7.11 but also true for other design points as well. It also appears from the same analysis data seen in Appx. Table G.1 - Appx. Table G.8 that the load drop is moving away from the design point, thus slower and the load rise is moving towards the design point of the ORC model, thus faster . However this is not the reason as in the case seen in the high off-load analysis for the system designed at 75% shown in Appx. Table G.12. In this analysis table, it can be seen that the higher off-load analysis are the step load functions of 85→100 and 100→85. In these two analysis results, it can be seen that the time to stabilization is still faster for the load rise of 85→100 despite moving away from the plant design point than the time to stabilization for the load drop of 100→85 despite moving towards the design point. This means that load rise are faster than load drop for the same load difference across all step duration irrespective of the plant design point.

So far the analysis of the dynamic behaviour of the ORC model was carried out to understand the time to stabilization with respect to step duration and this time to stabilization are analyzed at 5% before model stabilization. The same analysis are further looked into time to stabilization with respect to load difference, this will provide a better understanding of the dynamic response behaviour of the model.

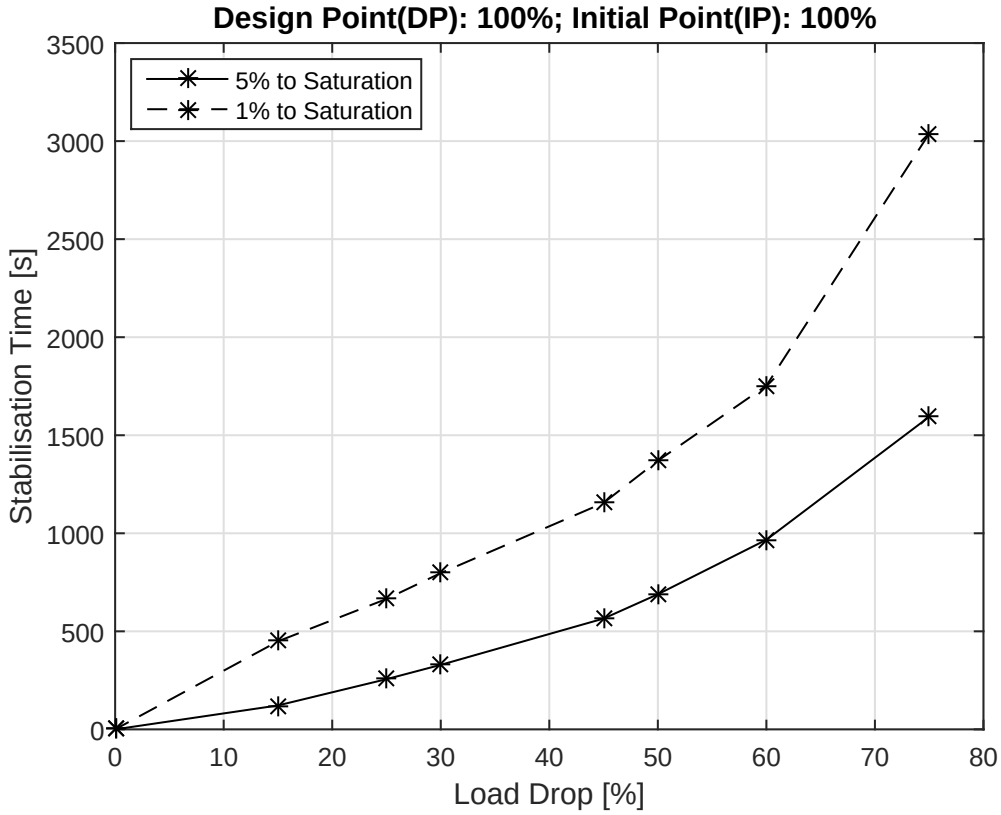

Figure 7.12: Stabilisation time vs Step duration of 60s duration for 100% initial point of the model designed at 100% of the engine load

The analysis of time to stabilization with respect to load difference (Initial point-Load drop) of step duration of 60 sec is shown in Figure 7.12. This analysis is performed for the ORC plant designed for 100% engine load and the initial load of this analysis is 100% and the load is dropped consequently lower at constant step duration. It can be seen from this analysis, that there are more load points than seen in the analysis performed previously. These new load points are taken at the engine loads of 40,55 and 70% in generator load as shown in Appx. Table G.9. With these new load points along with the previously considered points, the analysis of load drop from the initial load point of 100% as seen in Figure 7.12 shows that the time to stabilization increases as the load drop increases. This analysis has the initial load point of 100% and load drops lower from 100→85 and gradually drops until the load drops from 100→25. From the same figure, it can also be seen that the time required to reach from 5% to 1% of stabilization time also increases as the load drop increases. Such a trend is also the same for the time required to reach from 1% of stabilization time to model equilibrium, thus meaning that the total time to equilibrium is longer for larger load drop. This trend and behaviour is not only true for the analysis performed for constant step duration of 60 sec as seen here but also true for analysis of load drop of constant slope as shown in Appx. Table G.11. This analysis as mentioned before is performed for the initial load pf 100% and the step load is dropped. The same analysis shall be performed for load rise as it necessary to understand the total dynamic behaviour, hence the analysis initial load of 25% and the step load of rise is carried out.

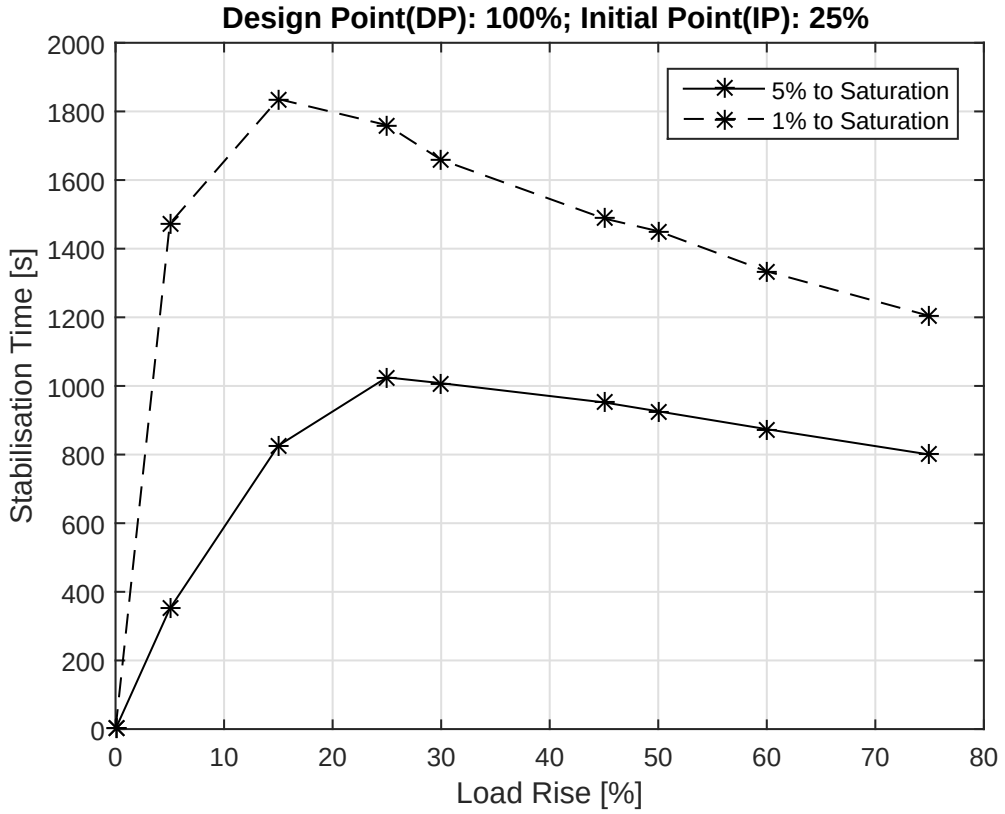

Figure 7.13: Stabilisation time vs Step duration of 60s duration for 25% initial point of the model designed at 100% of the engine load

Figure 7.13 shows the analysis for load rise from initial load of 25% for the plant design point at 100% of step duration of 60 sec. This analysis has a very peculiar trend comparatively to the same analysis for initial load point of 100%. Hence an additional engine load point of 30% is also introduced in this analysis as seen in Appx. Table G.9 and the analysis results as shown in Appx. Table G.10. This analysis has the initial load point of 25% and load rises higher from 25→30 and gradually rises until the load rise from 25→100. From this figure, it can be seen that the system has the similar trend (not gradual exponential increase) until the load rise of up to 25% compared to the same analysis for initial load point of 100%. However, this trend leads to a peak unlike seen previously around 25% as

the load rise increases. Moreover, as the load rise is increased beyond 25%, the time to stabilization decreases. This shows that the system takes longer to stabilize when the load rises from 25→50 than the time required to stabilize for load rise from 25→100. This trend could probably be due to the temperature difference profile of the exhaust gas input between the initial load and the final load or due to the fluid properties. However, additional analysis or investigation is required to justify this trend.

Not just the analysis of the dynamic behaviour of the model from the perspective of initial load condition, but analysis of the dynamic behaviour of the model when the system end point is constant is necessary. The same analysis is used to understand the dynamic behaviour for the system of varying initial load points to end points of 100 and 25%.

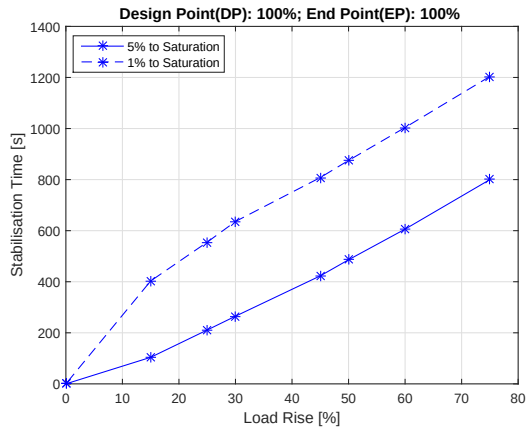

Figure 7.14: Stabilization time vs Step duration of 60s duration for 100% final point of the model designed at 100% of the engine load

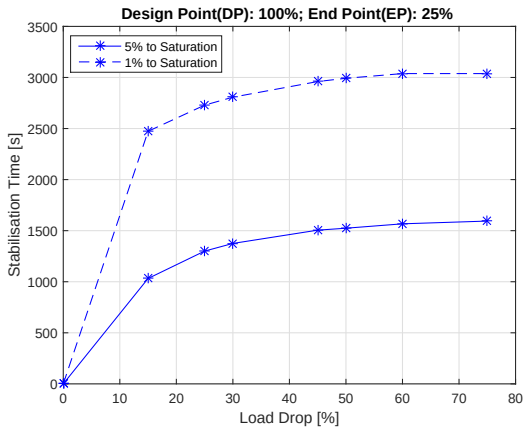

Figure 7.15: Stabilization time vs Step duration of 60s duration for 25% final point of the model designed at 100% of the engine load

Figure 7.14 and Figure 7.15 shows the time to stabilization for 5% and 1% to equilibrium for the end points of 100 and 25% respectively. As performed before, these analysis are compared for the model designed at 100% engine load. It can be seen for the end point of 100%, the time to stabilization increases as the initial load is lowered (load rise increases) and the time difference between 5% and 1% to stabilization remains almost constant across all the load difference between the initial and end point. This is also seen for the analysis of 25% end point where the time difference between 5% and 1% to stabilization remains almost constant across all the load difference. However unlike seen in the analysis of 100% end point, the rate of increase of stabilization time as the load drop increases slows down as the load drop difference becomes larger.

8

Conclusions and Recommendations

In this chapter, the conclusions and recommendation of this thesis are discussed.

8.1. Conclusions

In this section, the conclusions that can be taken away from this thesis are discussed and these conclusions may required additional investigation for further confirmation.

Review and Early Analysis

In this subsection, conclusions that can be derived from chapters 2 to 4 are discussed here.

- From literature (as discussed in Chapters 2 & 3), it can be understood that ORC-WHRS has promising advantages in marine application over other considered systems in terms of flexibility and simplicity.
- ORC-WHRS application is capable of meeting EEDI and SEEMP benchmarks or at least contribute significantly in meeting them by assisting other systems or measures.
- For ORC-WHRS, a suitable organic fluid is necessary to be found based on the application. This search begins with early analysis of ORC plant designs based on the waste heat source and cooling fluid profiles.
- It is understood from a number of static analysis that waste heat profile is perhaps the most important parameter necessary to find suitable organic fluids for any desired application.
- A screening methodology is devised in this thesis that is based on the waste heat source profile and selection parameters to find functioning and most suitable fluids.
- From numerous analysis performed during screening methodology, it is understood that it is waste heat temperature that influences the choice of functioning fluids and waste heat mass flow influences the volume size of ORC components and subsequently the plant size.
- Due to limitations in choice flexibility that occurs in the maritime industry, all the functioning fluids found in the early analysis may not be suitable for the desired application.
- Selection parameters such as power density, etc. are necessary in screening methodology in order to screen functioning fluids to find most suitable working fluids.
- In this thesis, power density is the only selection parameter considered, since it is probably the most or one of the most important parameter, as volume is unarguably an important limiting factor that needs to be considered for any addition installation on-board vessels.
- For the application of ORC-WHR of engine exhaust gas and with the current screening methodology of power density selection parameter, it may be possible that acetone is perhaps the most suitable fluid for marine application in a simple-ORC plant. This is because, as concluded before, the waste heat temperature influences the fluid choice and the exhaust gas temperature range of most marine engines are similar. The only difference will be seen in the plant size which corresponds to the exhaust gas mass flow rate.
- According to the above reasoning, cyclopentane is the second most suitable fluid for marine application in a recuperative-ORC plant.

- Acetone based simple-ORC plant has a net plant energy efficiency of slightly over 10.3%. This corresponds to fuel's energy recovery of about 3.0%. This fuel energy recovery may slightly increase at lower engine loads.
- Cyclopentane based recuperative-ORC plant has a net plant energy efficiency of slightly over 11.5%. This corresponds to fuel's energy recovery of about 3.2%. Both these results are obtained for engine in gas mode and these values slightly vary for the same engine when in diesel mode.
- It shall be noted that both these fluids have a low critical temperature than the result of the fluids as seen in Table 4.3. It is possible that ORC plants using fluids of low critical temperature may have better power density than plants using fluids of relatively higher critical temperature. This, however requires more analysis to confirm.
- If working fluid is chosen based on net power and not power density, Methylcyclohexane based recuperative-ORC plant will be the most suitable plant. The net plant energy efficiency of this system is as high as 15.4% with corresponding fuel's energy recovery of about 4.3%. However, this system will require significantly larger volume relative to ORC system using acetone or cyclopentane.
- Many organic fluids are fluidic well below 0°C, unlike water/steam working fluid which becomes ice (freezing point). This unexplored region of organic fluids can be utilized to exploit the full potential to improve the thermal efficiency of the ORC plant.
- Low temperature cooling fluids like LNG can be used as the cooling agent instead of the commonly used sea water for the ORC plant condenser. The brief analysis of this system carried out in this thesis, did show significant improvement to the ORC performance and also reduction in plant size.
- Comparison analysis of sea water and LNG as cooling fluids for the acetone based simple-ORC plant showed that by using LNG, the plant efficiency increased from 10.3 to 14.4%. This corresponds to fuel savings from 3.0 to 4.1%.
- In addition to the above mentioned advantage, using low temperature LNG also increased the power density of the plant from 7.4 to 13.35 kW/m^3.

Dynamic Model

The dynamic models presented in this thesis were modified and developed from SRC into ORC. These models include a system for a simple-ORC plant design and the other for a recuperative-ORC plant design.

In this subsection, conclusions that can be derived from chapters 5 are discussed here.

- The simple-ORC model is most suited to study isentropic organic fluids and the recuperative-ORC model is for dry fluids. Isentropic and dry type fluids cover most of the organic fluids used for Rankine cycle. Hence these two models have the flexibility to be used to study most of the organic fluids for use in the ORC for WHR application.
- Just as the flexibility in the choice of working fluid in the dynamic model, the waste heat source and the cooling fluid can also has the same flexibility.
- The dynamic behaviour of the ORC model is predominantly influenced by the dynamics of the heat exchangers and this is due to the type of modeling method used. This is because in reality, the dynamics of other components such as a pump and turbine in comparison to heat exchangers are insignificant.
- Since the response time of turbine or pump components are in fraction of seconds or in very few seconds (fast response), this makes the response comparatively insignificant to the response time of heat exchangers which are in minutes (very slow response). Hence the response of pump and turbine with respect to the rest of the plant (momentum is instantaneous) is not modeled and the dynamic response is with respect to heat loss to its own body. Such a modeling strategy is acceptable according to several literature studies where they model the resistance components as a static model.

Off-Design Analysis

In this subsection, conclusions that can be derived from chapters 6 are discussed here.

- This mass fraction comparison shows that the results from sample values deviated about 0.07% to 0.6% from the real value results. Hence, the inputs to the ORC model for analysis can exclude mass fraction data obtained from the engine exhaust and sample values of gas constituents can be used instead.
- The dynamic ORC models of Matlab-Simulink are compared to the ORC models of Cycle-Tempo, since the thermodynamic structure of the dynamic models are based on the same in Cycle-Tempo.
- The comparison of static analysis results of the same design point and input conditions of simple and recuperative-ORC plant models in Matlab-Simulink and Cycle-Tempo were performed. These comparison results showed that the dynamic ORC model in Matlab-Simulink very closely represents the thermodynamic model of the same in Cycle-Tempo as the error deviations are within acceptable range.
- The error deviations seen in the electrical power required for the seawater cooling pump is negligible, as it does not change the net power calculated significantly because the power required by the sea water cooling pump is less than 1% of the generated power.
- The original pump block used in the SRC model was replaced by a dynamic pump block for the ORC model. The difference in results of these two blocks were compared to the Cycle-Tempo results. The comparison results showed that the new dynamic pump block is more realistic than the original block. This block can be modified to be used also for cooling water fluid pump for the ORC condenser.
- In the model, a controller based throttle valve block is used between the boiler and the turbine block of the ORC models. To capture the effect of the throttle valve, a model simulation results with and without the throttle valve was carried out. The results showed that this throttle valve block didn't bring any significant change to the model output and this block can be removed (ORC plant may not require a throttle valve for most applications).
- Off-design performance analysis was carried out for the same engine of two different exhaust waste heat profiles (generator and propeller load). These two profiles were analyzed for acetone based simple and cyclopentane based recuperative-ORC plant models designed at discrete engine load points.
- The analysis results showed how much the flexibility of the ORC plant performance is influenced by the waste heat profile. The results also showed that the plant designed at higher loads have a broader flexibility across the complete engine profile than the plants designed at lower engine loads points.
- From off-design performance analysis, it is understood that plants designed at lower engine loads points has limited flexibility across the engine profile due to the low critical points of organic fluids compared to water/steam and limitations due to cooling fluid mass flow rate limit factor. These two factors either push the working fluid into the super-critical region or the net power output decreases as the off-load condition increases.

Dynamic and Sensitivity Analysis

In this subsection, conclusions that can be derived from chapters 7 are discussed here.

- In the sensitivity analysis, it was seen that the uncertainties of exhaust pressure input to the model performance output has almost no influence.
- From sensitivity analysis, the influence of uncertainties in the exhaust temperature and mass flow inputs are present to a noticeable extent. It shows that the rate of change of model performance output to the rate of change of exhaust mass flow is higher than for exhaust temperature.
- The uncertainties of the model output in the generated power is greatly influenced by uncertainties of the waste heat mass flow rate followed by uncertainties of the waste heat temperature.
- In dynamic analysis, it is seen that the load rise is faster that load drop of the same load difference for any step duration for the system designed at any load point.
- In dynamic analysis, it is seen that the time difference between the load drop and load rise increases as the initial point decreases for same step difference, this is true at least for systems designed at higher load points.

- For the ORC systems designed at higher load points, the responses are slower compared to systems designed at lower load points for the analysis of same changes of step load and step duration.
- For the analysis of same design and same initial load point, the response time is longer as the load drop increases. However for load rise step functions, the response time increases to a certain load rise increment and then reduces as the load rise increases beyond the peak response time.

8.2. Recommendations

In this section, the recommendations on how to further continue this topic and pathway are discussed here. It can be understood from this thesis that the application of ORC as WHRS for marine application has a promising scope. A further deep investigation and study of ORC-WHRS when introduced to marine related technical and economical complexity has to be carried out to fully understand the advantages and/or challenges of such an application. Hence the recommendations to further continue this thesis are briefly described.

Screening Methodology

As seen in Chapter 4 of this thesis, the screening methodology to find the most suitable fluid with respect to the available waste heat profile and selection parameter are given. This screening methodology can be improvised to accommodate the influence of cooling fluid profile and/or other selection parameter(s) in order to find the most suitable fluid on application basis for use in the maritime industry.

In this subsection, recommendations that can be given for chapter 4 are discussed here.

- The cooling fluid profile of closed systems (e.g. LNG) should also be incorporated into the fluid screening methodology to find the most suitable fluid on application basis to fully exploit the advantages of an organic fluid.
- To further understand the advantages in using low-temperature cooling fluids, the example application of using LNG as cooling fluid and its complete plant system described in Chapter 4 should be thoroughly investigated.
- If other additional limiting factors are also considered significant, then those parameters can be used along with power density as a set of selection parameters in the screening methodology.
- Weight of a plant is one such additional limiting factor that can be used and the weight limiting factor can be considered in terms of specific power (kW/kg) to form a selection parameter.
- Selection parameters like power density and specific power are based on design oriented limiting factors, but other limiting factors that are operability oriented such as corrosion-factor, etc. can also be used as a selection parameter.

Dynamic Model

In this subsection, recommendations that can be given for chapter 5 are discussed here.

- The current cooling water pump is a controller based model which serves the purpose for an open system. However, when the cooling fluid is part of a closed system then the cooling water pump should be replaced by a dynamic pump and such a pump is described in Chapter 5 used as the working fluid pump model.
- If throttling effect is interesting to study, a dynamic throttle valve can be modeled. However such a block could change the causality structure of the model, therefore a pre-analysis of the benefits of using such a valve should be assessed before implementation.
- Pressure loss of fluids in the components or pipes are not calculated in the ORC model. This pressure loss can be implemented into the model if necessary, however it should be kept in mind that the loss in pressure in the system would be very small. This is because the density of organic fluids are lower than water/steam and the pressure loss in the vapour part of the ORC plant will be even smaller because of its lower density.
- If pressure drop in the system is required to be calculated, then the recuperator heat exchanger model used in the recuperative-ORC plant model should also be re-modeled as necessary.

- The current dynamic ORC model is based on the Cycle-Tempo model and the comparison seen in Chapter 6 shows that the results from the dynamic model very closely relates to the results from the Cycle-Tempo. However, these results can only be compared for static analysis. The results of the dynamic response behaviour shall be compared to experimental or real plant data to fully understand the extent to which the dynamic model represents the actual plant dynamics.

Off-Design Analysis

In this subsection, recommendations that can be given for chapter 6 are discussed here.

- It will be interesting to see the influence of a closed system cooling fluid (by making use of the LNG application as explained before) on the results of the off-design performance analysis. This is especially on how varying temperatures (evaporating and condensing) during off-load conditions across the engine load will effect the ORC performance.
- The off-design performance analysis should be extended into the operational profile of the vessel in terms of power/energy with respect to time. Such an extension will give the ship designer a better understanding of the ORC-WHRS in marine application in terms energy recovery, fuel savings and carbon-dioxide emission reductions.
- The design and off-design analysis are performed for the system with a fixed design evaporating pressure of 30 bar across the engine load. The same analysis shall be performed for varying design evaporating pressure across the engine load. For example, take the evaporating pressure of the ORC plant at 10 bar designed for 25% engine load and increase the evaporating pressure as the design point increases with respect to the engine load. This analysis may give a different picture of the system flexibility during off-design performance analysis especially for systems subjected to higher off-load conditions.

Other

In this subsection, recommendations that can be given in general are discussed here.

- Screening methodology, analysis and other study should be performed by using model input data and initial conditions other than the ones used here.
- Economical aspects such as the capex and opex of the system can be estimated based on the static analysis performed in this thesis, especially the capex. However, to thoroughly investigate the opex of the system the operational profile of the vessel may be necessary.
- This current analysis can be extended by incorporating a pre-heater before the boiler component whose waste heat source is the jacket water from the same engine. This is because jacket water is the next best source of waste heat from marine diesel engines after exhaust gas. This waste heat from jacket water can be utilized within the exhaust gas based ORC-WHRS to improve the efficiency of the overall plant.

Within the scope of this thesis, the ORC-WHRS is producing energy in electrical form. When the operational profile of the vessel is incorporated into the early (preliminary) design phase study, the auxiliary and hotel load requirements of the vessel shall also be considered. These requirements will give the designer an understanding on when the electricity supply and demand rates vary from each other and at what amount. This will give a better picture to see whether an incorporation of a WHRS with an energy storage device will be beneficial for the total energy management of the vessel. Hence an investigation of incorporating an energy storage device with ORC-WHRS for better fuel efficiency of the vessel should be carried out. A brief literature study into this direction has been carried out and is shown in Appendix H.

A

Fluid Selection Analysis and Initial Condition Data

A.1. Simple-ORC Plant Data

A.1.1. Input Data and Initial conditions of simple ORC

System data: NAPP=9, NLIN=11, NCYCLE=3, NPRODF=1, EPS=1.0e-06,MINITM=5, NPRINT=4
Apparatus: NO=1, TYPE= 3, APNAME='Turbine', TUCODE=0, GDCODE= 1, PIN= 30, ETHAI=0.75
Apparatus: NO=2, TYPE= 4, APNAME='Condenser', EEQCOD= 1, DELP1=0.5, DELT1= 10, DELP2=0, DELTH= 5, SATCOD=0
Apparatus: NO=3, TYPE= 8, APNAME='Pump', ETHAI=0.75
Apparatus: NO=4, TYPE= 6, APNAME='Economiser', DELP1=0.5, DELP2=0.02
Apparatus: NO=5, TYPE=12, APNAME='Evaporator', DELP1=0.5, DELP2=0.02
Apparatus: NO=6, TYPE=10, APNAME='Engine', POUT= 1.05, TOUT= 373, DELM= 9.4
Apparatus: NO=7, TYPE=10, APNAME='Atmosphere', TIN= 165
Apparatus: NO=8, TYPE= 8, APNAME='S.W. Pump', ETHAI=0.75
Apparatus: NO=9, TYPE=10, APNAME='Sea', POUT= 1.013, DELP=0, TOUT= 25
Generator: NO=1, IGAPP=1, ETAGEN=0.95
Medium: Pipe No = 5, Library = RefProp, Fluid = BENZENE.FLD
Medium: Pipe No = 6, Type = 'GASMIX'
Specie = AR, CO2, H2O, N2, O2.
Mole % = 0.95, 5.72, 6.42, 74.85, 12.06.
Medium: Pipe No = 9, Type = 'WATERSTM'
Pipe:NO=2, XINL = 0
Pipe:NO=4, XINL = 0
Pipe:NO=5, XINL = 1
Production Func.: Apparatus numbers:4,5, Power=0
Environment: User defined environment
Environment pressure: 1.01325 bar
Environment temperature: 15 °C
Heating values calculated at 1 atm, 25 °C
State functions for water/steam calculation: IAPWS Industrial Formulation 1997 (IAPWS-IF97)
Cycle-Tempo 5.0 (Build 484)

Name	Power Output	Mass Flow	Ratio
[-]	[kW]	[kg/s]	[kW/kg/s]
Acetone	399.17	3.207	124.46
Butane	278.03	4.755	58.47
1Butene	268.32	5.109	52.51
Methylcyclohe.	405.42	2.799	144.84
Cyclohexane	415.64	3.07	135.38
Cyclopentane	393.2	3.578	109.89
C2Butene	294.09	4.591	64.05
Isobutan	251.19	5.519	45.51
Ibutene	264.05	5.09	51.87
Ipentane	323.11	4.141	78.02
Neopentn	286.68	5.011	57.21
Pentane	336.29	3.867	86.96
R11	350.64	9.615	36.46
R113	363.57	9.409	38.64
R114	272.00	13.492	20.16
R123	331.49	9.64	34.38
R141b	359.02	7.193	49.91
R236EA	256.75	10.931	23.48
R245CA	303.16	8.023	37.78
R245FA	280.29	9.094	30.82
R365MFC	318.7	7.317	43.55
R436A	204.69	5.713	35.82
R436B	208.34	5.668	36.75
Toluene	468.69	2.91	161.06
T2Butene	284.91	4.696	60.67

Table A.1: Functioning fluids for simple ORC plant based on 100% engine load in gas mode as per Table 4.1 and Figure 4.2

A.2. Recuperative-ORC Plant Data

A.2.1. Initial conditions of Recuperative ORC

System data: NAPP=10, NLIN=13, NCYCLE=3, NPRODF=1, EPS=1.0e-06, MINITM=5, NPRINT=4
Apparatus: NO=1, TYPE=3, APNAME='Turbine', TUCODE=0, GDCODE= 1, PIN= 30, ETHAI=0.75
Apparatus: NO=2, TYPE=4, APNAME='Condenser', EEQCOD= 1, DELP1=0.5, DELT1= 10, DELP2=0, DELTH= 5, SATCOD=0
Apparatus: NO=3, TYPE=8, APNAME='Pump', ETHAI=0.75
Apparatus: NO=4, TYPE=6, APNAME='Economiser', DELP1=0.5, DELP2=0.02
Apparatus: NO=5, TYPE=12, APNAME='Evaporator', DELP1=0.5, DELP2=0.02
Apparatus: NO=6, TYPE=6, APNAME='Recuperator', DELP1=0.5, DELP2=0.02, DELTL= 5
Apparatus: NO=7, TYPE=10, APNAME='Engine', POUT= 1.05, TOUT= 373, DELM= 9.4
Apparatus: NO=9, TYPE=10, APNAME='Atmosphere', TIN= 165
Apparatus: NO=10, TYPE=10, APNAME='Sea', POUT= 1.013, DELP=0, TOUT= 25
Apparatus: NO=11, TYPE=8, APNAME='SW Pump', ETHAI=0.75
Generator: NO=1, IGAPP=1, ETAGEN=0.95
Medium: Pipe No = 701, Type = 'GASMIX'
Specie = AR, CO2, H2O, N2, O2.
Mole % = 0.95, 5.72, 6.42, 74.85, 12.06.
Medium: Pipe No = 807, Library = RefProp, Fluid = BENZENE.FLD
Medium: Pipe No = 901, Type = 'WATERSTM'
Pipe: NO=806, XINL = 0
Pipe: NO=807, XINL = 1
Production Func.: Apparatus numbers:4,5,6, Power=0
Environment: User defined environment
Environment pressure: 1.01325 bar

Name	Power Output	Mass Flow	Ratio
[-]	[kW]	[kg/s]	[kW/kg/s]
Acetone	399.77	3.238	123.46
Butane	298.02	5.11	58.32
1 Butene	273.68	5.224	52.38
Methylcyclohe.	590.62	4.191	140.92
Cyclohexane	534.53	4.012	133.23
Cyclopentane	448.84	4.113	109.12
C2Butene	300.99	4.711	63.89
Isobutan	261.81	5.766	45.40
Ibutene	271.62	5.249	51.74
Ipentane	389.85	5.02	77.65
Neopentn	337.61	5.921	57.01
Pentane	405.31	4.687	86.47
R11	356.99	9.828	36.32
R113	428.92	11.18	38.36
R114	291.5	14.503	20.09
R123	356.18	10.405	34.23
R141B	384.04	7.73	49.68
R236EA	281.87	12.036	23.41
R245CA	337.29	8.965	37.62
R245FA	298.88	9.731	30.71
R365MFC	385.38	8.903	43.28
R436A	206.93	5.787	35.75
R436B	211.72	5.771	36.68
Toluene	575.81	3.706	155.37
T2Butene	294.07	4.86	60.50

Table A.2: Functioning fluids for Recuperative ORC plant based on 100% engine load in gas mode as per Table 4.1 and Figure 4.8

Environment temperature: 15 °C
Heating values calculated at 1 atm, 25 °C
State functions for water/steam calculation: IAPWS Industrial Formulation 1997 (IAPWS-IF97)
Cycle-Tempo 5.0 (Build 484)

B

Static Analysis Data of Promising Working Fluids - Wärtsilä

B.1. Initial Condition for LNG as Cooling Fluid

System data: NAPP=10, NLIN=11, NCYCLE=3, NPRODF=1, EPS=1.0e-06,MINITM=5, NPRINT=4
Apparatus: NO=1, TYPE=3, APNAME='Turbine', TUCODE=0, GDCODE= 1,PIN= 30, ETHAI=0.75
Apparatus: NO=2, TYPE=4, APNAME='Condenser', EEQCOD= 1, DELP1=0,DELT1= 35, DELP2=0, DELTH= 5, SATCOD=0
Apparatus: NO=3, TYPE=8, APNAME='Pump', ETHAI=0.75
Apparatus: NO=4, TYPE=6, APNAME='Economiser', DELP1=0.5, DELP2=0.02
Apparatus: NO=5, TYPE=12, APNAME='Evaporator', DELP1=0.5, DELP2=0.02
Apparatus: NO=6, TYPE=10, APNAME='Engine', POUT= 1.05, TOUT= 373,DELM= 9.4
Apparatus: NO=7, TYPE=10, APNAME='Uptake', TIN= 165
Apparatus: NO=8, TYPE=10, APNAME='LNG Tank', POUT= 1.5,TOUT= -60
Apparatus: NO=9, TYPE=10, APNAME='Engine'
Apparatus: NO=10, TYPE=10, APNAME='Sink/Source', DELP=0, DELH=0
Generator: NO=1, IGAPP=1, ETAGEN=0.95
Medium: Pipe No = 5, Library = RefProp, Fluid = ACETONE.FLD
Medium: Pipe No = 601, Type = 'GASMIX'
Specie = AR, CO2, H2O, N2, O2.
Mole % = 0.95, 5.72, 6.42, 74.85, 12.06.
Medium: Pipe No = 901, Library = RefProp, Fluid = METHANE.FLD
Pipe: NO=2, XINL =0
Pipe: NO=4, XINL =0
Pipe: NO=5, XINL = 1
Production Func.: Apparatus numbers:4,5, Power=0
Environment: User defined environment
Environment pressure: 1.01325 bar
Environment temperature: 15 °C
Heating values calculated at 1 atm, 25 °C
State functions for water/steam calculation:
IAPWS Industrial Formulation 1997 (IAPWS-IF97)

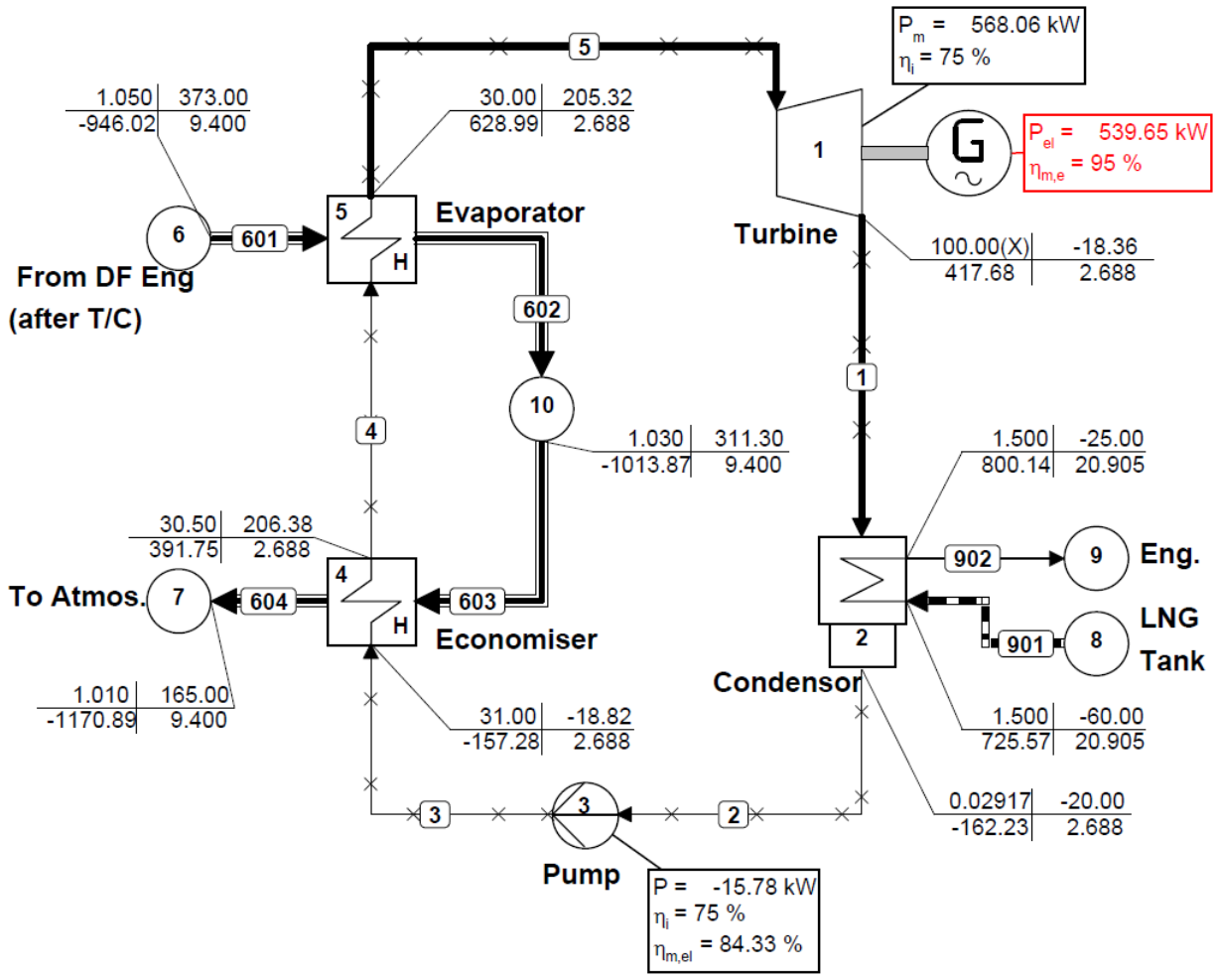

Figure B.1: Acetone based ORC process with LNG as cooling fluid

Table B.1: Acetone in gas mode in simple and recuperative ORC

Acetone												
Wartsila 6L50DF DE IMO Tier 2 Gas Mode												
	WITHOUT Recuperator						WITH Recuperator					
	NOT Optimised			Optimised for Efficiency			NOT Optimised			Optimised for Efficiency		
Load (%)	100.00	75.00	50.00	100.00	75.00	50.00	100.00	75.00	50.00	100.00	75.00	50.00
Generator (kW)	399.17	377.74	289.58	411.95	389.82	298.82	399.77	378.30	290.02	404.33	382.61	293.31
Ref Pump (kW)	19.98	18.93	14.58	26.39	25.00	19.25	20.50	19.42	14.95	23.19	21.97	16.92
SW Pump (kW)	3.66	3.47	2.69	3.64	3.45	2.68	3.66	3.47	2.69	3.65	3.46	2.69
Turb Press IN (bar)	30.00	30.00	30.00	39.29	39.28	39.23	30.00	30.00	30.00	34.25	34.24	34.22
Turb Temp IN (°C)	205.32	205.32	205.32	222.99	222.96	222.87	205.32	205.32	205.32	213.88	213.87	213.82
Massfl of Ref (kg/s)	3.21	3.03	2.33	3.27	3.09	2.37	3.24	3.06	2.35	3.23	3.06	2.34
Massfl of CW (kg/s)	40.97	38.77	29.72	40.78	38.59	29.58	40.96	38.76	29.72	40.90	38.71	29.67
Net Power (kW)	375.53	355.34	272.32	381.92	361.37	276.89	375.62	355.42	272.37	377.48	357.18	273.70
Absorbable Energy (kW)	3972.13	3403.94	2601.03	3972.13	3403.94	2601.03	3972.13	3403.94	2601.03	3972.13	3403.94	2601.03
Net Sys Energy Effi (%)	9.45	10.44	10.47	9.61	10.62	10.65	9.46	10.44	10.47	9.50	10.49	10.52
Absorbable Exergy (kW)	1197.76	1129.12	865.71	1197.76	1129.12	865.71	1197.76	1129.12	865.71	1197.76	1129.12	865.71
Net Sys Exergy Effi (%)	31.35	31.47	31.46	31.89	32.00	31.98	31.36	31.48	31.46	31.52	31.63	31.62
Recov energy effici (%)	0.07	0.08	0.10	0.07	0.08	0.10	0.07	0.08	0.10	0.07	0.08	0.10
Heat trans in Condr (kW)	1710.49	1618.66	1240.90	1702.61	1611.20	1235.19	1710.31	1618.48	1240.77	1707.85	1616.16	1238.99
OHTA. in Condr. [U*A] (kW/K)	187.92	177.83	136.33	187.05	177.01	135.70	187.90	177.81	136.31	187.63	177.55	136.12
Heat trans in Econr (kW)	1353.02	1280.38	981.57	1580.86	1495.53	1145.45	1345.64	1273.40	976.22	1448.90	1370.96	1050.54
OHTA. in Econo. [U*A] (kW/K)	12.59	10.25	7.82	14.38	11.54	8.79	12.72	10.36	7.90	13.48	10.89	8.30
Heat trans in Recupr(kW)	-	-	-	-	-	-	20.21	19.12	14.66	5.81	5.53	4.32
OHTA. in Recup. [U*A] (kW/K)	-	-	-	-	-	-	3.52	3.33	2.56	1.10	1.05	0.82
Heat trans in Evapr (kW)	760.73	719.89	551.88	532.88	504.74	388.00	768.10	726.87	557.23	664.84	629.31	482.91
OHTA. in Evap. [U*A] (kW/K)	6.01	4.28	3.25	4.37	3.03	2.30	6.09	4.33	3.29	5.38	3.78	2.87
Power Density [kW/(kg/s)]	124.47	124.50	124.50	126.06	126.07	126.08	123.46	123.47	123.47	125.14	125.12	125.13

Acetone												
Wartsila 6L50DF DE IMO Tier 2 Diesel Mode												
	WITHOUT Recuperator						WITH Recuperator					
	NOT Optimised			Optimised for Efficiency			NOT Optimised			Optimised for Efficiency		
Load (%)	100.00	75.00	50.00	100.00	75.00	50.00	100.00	75.00	50.00	100.00	75.00	50.00
Generator (kW)	420.05	340.87	283.37	433.50	351.76	292.40	420.68	341.38	283.79	425.48	345.26	287.01
Ref Pump (kW)	21.00	17.11	14.27	27.74	22.60	18.84	21.54	17.55	14.64	24.38	19.86	16.56
SW Pump (kW)	3.84	3.14	2.66	3.82	3.13	2.65	3.84	3.14	2.66	3.83	3.14	2.65
Turb Press IN (bar)	30.00	30.00	30.00	39.30	39.26	39.22	30.00	30.00	30.00	34.25	34.23	34.21
Turb Temp IN (°C)	205.32	205.32	205.32	222.99	222.92	222.86	205.32	205.32	205.32	213.90	213.85	213.81
Massfl of Ref (kg/s)	3.37	2.74	2.28	3.44	2.79	2.32	3.41	2.77	2.30	3.40	2.76	2.29
Massfl of CW (kg/s)	43.11	34.98	29.08	42.91	34.82	28.95	43.10	34.98	29.08	43.04	34.93	29.04
Net Power (kW)	395.21	320.62	266.44	401.94	326.03	270.91	395.30	320.69	266.49	397.27	322.26	267.80
Absorbable Energy (kW)	4517.63	3584.33	2746.06	4517.63	3584.33	2746.06	4517.63	3584.33	2746.06	4517.63	3584.33	2746.06
Net Sys Energy Effi (%)	8.75	8.95	9.70	8.90	9.10	9.87	8.75	8.95	9.70	8.79	8.99	9.75
Absorbable Exergy (kW)	1275.44	1030.72	848.29	1275.44	1030.72	848.29	1275.44	1030.72	848.29	1275.44	1030.72	848.29
Net Sys Exergy Effi (%)	30.99	31.11	31.41	31.51	31.63	31.94	30.99	31.11	31.41	31.15	31.27	31.57
Recovenergy effi (%)	0.07	0.07	0.09	0.07	0.08	0.10	0.07	0.08	0.09	0.07	0.08	0.09
Heat trans in Condr (kW)	1799.96	1460.66	1214.27	1791.66	1453.94	1208.69	1799.76	1460.50	1214.14	1797.17	1458.41	1212.40
OHTA. in Condr. [U*A] (kW/K)	197.75	160.47	133.40	196.83	159.73	132.79	197.72	160.45	133.39	197.44	160.22	133.20
Heat trans in Econr (kW)	1423.78	1155.40	960.50	1663.61	1349.02	1120.72	1416.02	1149.10	955.27	1524.85	1236.91	1027.88
OHTA. in Econo. [U*A] (kW/K)	14.78	11.63	8.59	17.14	13.41	9.77	14.95	11.76	8.69	15.95	12.51	9.18
Heat trans in Recupr(kW)	-	-	-	-	-	-	21.27	17.26	14.35	6.09	5.03	4.24
OHTA. in Recup. [U*A] (kW/K)	-	-	-	-	-	-	3.71	3.01	2.50	1.15	0.95	0.80
Heat trans in Evapr (kW)	800.52	649.62	540.04	560.70	456.00	379.82	808.28	655.92	545.28	699.45	568.11	472.66
OHTA. in Evap. [U*A] (kW/K)	7.83	5.98	3.96	5.86	4.44	2.87	7.94	6.06	4.01	7.11	5.40	3.53
Power Density [kW/(kg/s)]	124.50	124.50	124.50	126.05	126.08	126.09	123.48	123.46	123.49	125.14	125.14	125.11

Table B.2: Acetone in diesel mode in simple and recuperative ORC

Methylcyclohexane (C1CC6)												
Wartsila 6L50DF DE IMO Tier 2 Gas Mode 1/2014												
	WITHOUT Recuperator						With Recuperator					
	Not Optimized			Optimised for Efficiency			Not Optimized			Optimized For Efficiency		
Load (%)	100.00	75.00	50.00	100.00	75.00	50.00	100.00	75.00	50.00	100.00	75.00	50.00
Generator (kW)	405.42	383.66	294.12	x	x	x	590.62	558.91	428.48	593.36	561.50	430.45
Ref Pump (kW)	18.10	17.14	13.20	x	x	x	27.28	25.86	19.94	28.86	27.35	21.09
SW Pump (kW)	3.64	3.45	2.68	x	x	x	3.26	3.09	2.49	3.25	3.08	2.49
Turb Press IN (bar)	30.00	30.00	30.00	x	x	x	30.00	30.00	30.00	31.91	31.91	31.90
Turb Temp IN (°C)	286.82	286.82	286.82	x	x	x	286.82	286.82	286.82	291.72	291.71	291.69
Massfl of Ref (kg/s)	2.80	2.65	2.03	x	x	x	4.19	3.97	3.04	4.19	3.96	3.04
Massfl of CW (kg/s)	40.77	38.58	29.58	x	x	x	36.29	34.34	26.33	36.26	34.31	26.30
Net Power (kW)	383.68	363.06	278.24	x	x	x	560.08	529.97	406.04	561.25	531.07	406.87
Absorbable Energy Power (kW)	3972.13	3403.94	2601.03	x	x	x	3972.13	3403.94	2601.03	3972.13	3403.94	2601.03
Net Sys Energy Effi (%)	9.66	10.67	10.70	x	x	x	14.10	15.57	15.61	14.13	15.60	15.64
Absorbable Exergy (kW)	1197.76	1129.12	865.71	x	x	x	1197.76	1129.12	865.71	1197.76	1129.12	865.71
Net Sys Exergy Effi (%)	32.03	32.15	32.14	x	x	x	46.76	46.94	46.90	46.86	47.03	47.00
Recov energy effi (%)	0.07	0.08	0.10	x	x	x	0.10	0.12	0.14	0.10	0.12	0.14
Heat trans in Condr (kW)	1702.29	1610.90	1234.95	x	x	x	1515.32	1433.97	1099.31	1513.82	1432.55	1098.22
OHTA. [U*A] (kW/K)	187.02	176.98	135.67	x	x	x	166.48	157.54	120.77	166.31	157.38	120.65
Heat trans in Econr (kW)	1851.60	1752.19	1343.27	x	x	x	1721.17	1628.77	1248.65	1813.10	1715.69	1314.82
OHTA. in Econo. [U*A] (kW/K)	21.10	15.40	11.71	x	x	x	68.97	43.41	32.88	69.13	43.80	33.18
Heat trans in Recupr(kW)	-	-	-	x	x	x	1051.24	994.80	762.64	1049.36	993.03	761.31
OHTA. in Recup. [U*A] (kW/K)	-	-	-	x	x	x	76.36	72.26	55.40	76.29	72.20	55.35
Heat trans in Evapr (kW)	262.15	248.08	190.18	x	x	x	392.57	371.50	284.80	300.65	284.57	218.63
OHTA. in Evap. [U*A] (kW/K)	3.64	2.06	1.56	x	x	x	6.08	3.34	2.52	4.62	2.52	1.91
Power Density[kW/(kg/s)]	144.84	144.83	144.89	x	x	x	140.93	140.93	140.90	141.75	141.76	141.74

Table B.3: Methylcyclohexane in gas mode in simple and recuperative ORC

Methylcyclohexane (C1CC6)												
Wartsila 6L50DF DE IMO Tier 2 Diesel Mode												
WITHOUT Recuperator							WITH Recuperator					
	NOT Optimised			Optimised for Efficiency			NOT Optimized			Optimized for Efficiency		
Load (%)	100.00	75.00	50.00	100.00	75.00	50.00	100.00	75.00	50.00	100.00	75.00	50.00
Generator (kW)	426.63	346.21	287.81	x	x	x	621.51	504.36	419.28	624.40	506.70	421.23
Ref Pump (kW)	19.03	15.50	12.92	x	x	x	28.67	23.39	19.52	30.33	24.75	20.66
SW Pump (kW)	3.82	3.13	2.65	x	x	x	3.42	2.80	2.46	3.42	2.79	2.46
Turb Press IN (bar)	30.00	30.00	30.00	x	x	x	30.00	30.00	30.00	31.92	31.92	31.92
Turb Temp IN (°C)	286.82	286.82	286.82	x	x	x	286.82	286.82	286.82	291.75	291.75	291.75
Massfl of Ref (kg/s)	2.95	2.39	1.99	x	x	x	4.41	3.58	2.98	4.41	3.57	2.97
Massfl of CW (kg/s)	42.90	34.81	28.94	x	x	x	38.19	30.99	25.76	38.15	30.96	25.74
Net Power (kW)	403.78	327.58	272.24	x	x	x	589.42	478.17	397.30	590.65	479.16	398.11
Absorbable Energy Power (kW)	4517.63	3584.33	2746.06	x	x	x	4517.63	3584.33	2746.06	4517.63	3584.33	2746.06
Net Sys Energy Effi (%)	8.94	9.14	9.91	x	x	x	13.05	13.34	14.47	13.07	13.37	14.50
Absorbable Exergy (kW)	1275.44	1030.72	848.29	x	x	x	1275.44	1030.72	848.29	1275.44	1030.72	848.29
Net Sys Exergy Effi (%)	31.66	31.78	32.09	x	x	x	46.21	46.39	46.84	46.31	46.49	46.93
Recov energy effi (%)	0.07	0.08	0.10	x	x	x	0.10	0.11	0.14	0.10	0.11	0.14
Heat trans in Condr (kW)	1791.32	1453.65	1208.45	x	x	x	1594.58	1294.00	1075.72	1593.00	1292.71	1074.66
OHTA. [U*A] (kW/K)	196.80	159.70	132.76	x	x	x	175.18	142.16	118.18	175.01	142.02	118.06
Heat trans in Econr (kW)	1948.44	1581.16	1314.44	x	x	x	1811.20	1469.78	1221.86	1908.66	1548.84	1287.58
OHTA. in Econo. [U*A] (kW/K)	28.34	21.29	13.93	x	x	x	112.23	78.69	43.48	110.79	78.18	43.68
Heat trans in Recupr(kW)	-	-	-	-	x	x	1106.22	897.70	746.27	1104.19	896.05	744.90
OHTA. in Recup. [U*A] (kW/K)	-	-	-	-	x	x	80.35	65.21	54.21	80.28	65.15	54.16
Heat trans in Evapr (kW)	275.86	223.86	186.10	x	x	x	413.11	335.24	278.69	315.64	256.18	212.96
OHTA. in Evap. [U*A] (kW/K)	6.32	4.37	2.23	x	x	x	11.25	7.58	3.68	8.60	5.78	2.79
Power Density[kW/(kg/s)]	144.87	144.86	144.85	x	x	x	140.90	140.92	140.93	141.75	141.77	141.78

Table B.4: Methylcyclohexane in diesel mode in simple and recuperative ORC

Cyclohexane												
Wartsila 6L50DF DE IMO Tier 2 Gas Mode 1/2014												
	WITHOUT Recuperator						WITH Recuperator					
	NOT Optimised			Optimised for Efficiency			NOT Optimized			Optimized for Efficiency		
Load (%)	100.00	75.00	50.00	100.00	75.00	50.00	100.00	75.00	50.00	100.00	75.00	50.00
Generator (kW)	415.64	393.32	301.53	x	x	x	534.53	505.83	387.78	548.22	518.78	397.69
Ref Pump (kW)	19.55	18.52	14.26	x	x	x	25.80	24.45	18.85	31.38	29.74	22.94
SW Pump (kW)	3.62	3.43	2.67	x	x	x	3.37	3.20	2.55	3.35	3.18	2.54
Turb Press IN (bar)	30.00	30.00	30.00	x	x	x	30.00	30.00	30.00	37.27	37.26	37.24
Turb Temp IN (°C)	256.28	256.28	256.28	x	x	x	256.28	256.28	256.28	273.35	273.33	273.27
Massfl of Ref (kg/s)	3.07	2.91	2.23	x	x	x	4.01	3.80	2.91	3.98	3.77	2.89
Massfl of CW (kg/s)	40.54	38.36	29.41	x	x	x	37.67	35.65	27.33	37.45	35.44	27.17
Net Power (kW)	392.47	371.37	284.60	x	x	x	505.36	478.19	366.38	513.48	485.86	372.21
Absorbable Energy Power (kW)	3972.13	3403.94	2601.03	x	x	x	3972.13	3403.94	2601.03	3972.13	3403.94	2601.03
Net Sys Energy Effi (%)	9.88	10.91	10.94	x	x	x	12.72	14.05	14.09	12.93	14.27	14.31
Absorbable Exergy (kW)	1197.76	1129.12	865.71	x	x	x	1197.76	1129.12	865.71	1197.76	1129.12	865.71
Net Sys Exergy Effi (%)	32.77	32.89	32.87	x	x	x	42.19	42.35	42.32	42.87	43.03	42.99
Recov energy effi (%)	0.07	0.09	0.10	x	x	x	0.09	0.11	0.13	0.09	0.11	0.13
Heat trans in Condr (kW)	1692.78	1601.90	1228.05	x	x	x	1573.06	1488.61	1141.20	1563.56	1479.62	1134.31
OHTA. [U*A] (kW/K)	185.97	175.99	134.92	x	x	x	172.82	163.54	125.37	171.78	162.55	124.62
Heat trans in Econr (kW)	1693.88	1602.94	1228.85	x	x	x	1565.11	1481.08	1135.43	1822.99	1724.68	1321.31
OHTA. in Econo. [U*A] (kW/K)	17.43	13.38	10.19	x	x	x	28.63	20.90	15.89	31.85	22.98	17.47
Heat trans in Recupr(kW)	-	-	-	x	x	x	647.94	613.15	470.05	657.29	622.03	476.91
OHTA. in Recup. [U*A] (kW/K)	-	-	-	x	x	x	48.57	45.96	35.24	48.99	46.36	35.54
Heat trans in Evapr (kW)	419.87	397.33	304.60	x	x	x	548.64	519.19	398.02	290.76	275.59	212.14
OHTA. in Evap. [U*A] (kW/K)	4.45	2.83	2.14	x	x	x	6.32	3.95	2.99	3.45	2.09	1.59
Power Density[kW/(kg/s)]	135.39	135.39	135.40	x	x	x	133.23	133.25	133.26	137.64	137.64	137.66

Table B.5: Cyclohexane in gas mode in simple and recuperative ORC

Cyclohexane												
Wartsila 6L50DF DE IMO Tier 2 Diesel Mode												
	WITHOUT Recuperator						WITH Recuperator					
	NOT Optimised			Optimised for Efficiency			NOT optimized			Optimized for Efficiency		
Load (%)	100.00	75.00	50.00	100.00	75.00	50.00	100.00	75.00	50.00	100.00	75.00	50.00
Generator (kW)	437.38	354.93	295.06	x	x	x	562.49	456.46	379.46	576.89	468.13	389.16
Ref Pump (kW)	20.55	16.74	13.96	x	x	x	27.11	22.11	18.45	32.97	26.91	22.46
SW Pump (kW)	3.80	3.11	2.64	x	x	x	3.54	2.90	2.52	3.52	2.88	2.51
Turb Press IN (bar)	30.00	30.00	30.00	x	x	x	30.00	30.00	30.00	37.28	37.25	37.23
Turb Temp IN (°C)	256.28	256.28	256.28	x	x	x	256.28	256.28	256.28	273.35	273.31	273.27
Massfl of Ref (kg/s)	3.23	2.62	2.18	x	x	x	4.22	3.43	2.85	4.19	3.40	2.83
Massfl of CW (kg/s)	42.66	34.62	28.78	x	x	x	39.64	32.17	26.74	39.40	31.98	26.58
Net Power (kW)	413.03	335.08	278.46	x	x	x	531.84	431.45	358.49	540.40	438.34	364.19
Absorbable Energy Power (kW)	4517.63	3584.33	2746.06	x	x	x	4517.63	3584.33	2746.06	4517.63	3584.33	2746.06
Net Sys Energy Effi (%)	9.14	9.35	10.14	x	x	x	11.77	12.04	13.05	11.96	12.23	13.26
Absorbable Exergy (kW)	1275.44	1030.72	848.29	x	x	x	1275.44	1030.72	848.29	1275.44	1030.72	848.29
Net Sys Exergy Effi (%)	32.38	32.51	32.83	x	x	x	41.70	41.86	42.26	42.37	42.53	42.93
Recov energy effi (%)	0.07	0.08	0.10	x	x	x	0.09	0.10	0.13	0.09	0.10	0.13
Heat trans in Condr (kW)	1781.32	1445.54	1201.70	x	x	x	1655.34	1343.30	1116.71	1645.34	1335.19	1109.97
OHTA. [U*A] (kW/K)	195.70	158.81	132.02	x	x	x	181.86	147.58	122.68	180.76	146.69	121.94
Heat trans in Econr (kW)	1782.47	1446.47	1202.48	x	x	x	1646.97	1336.51	1111.06	1918.42	1555.97	1292.85
OHTA. in Econo. [U*A] (kW/K)	21.81	16.80	11.69	x	x	x	37.73	28.59	18.93	42.53	32.08	20.98
Heat trans in Recupr(kW)	-	-	-	-	x	x	681.82	553.30	459.97	691.67	561.33	466.68
OHTA. in Recup. [U*A] (kW/K)	-	-	-	-	x	x	51.11	41.48	34.48	51.55	41.84	34.78
Heat trans in Evapr (kW)	441.83	358.54	298.06	x	x	x	577.34	468.51	389.48	305.88	249.05	207.69
OHTA. in Evap. [U*A] (kW/K)	6.59	4.82	2.83	x	x	x	9.57	6.95	4.00	5.45	3.91	2.18
Power Density[kW/(kg/s)]	135.37	135.37	135.35	x	x	x	133.23	133.23	133.24	137.65	137.64	137.66

Table B.6: Cyclohexane in diesel mode in simple andrecuperative ORC

Table B.7: Cyclopentane in gas mode in simple and recuperative ORC

Cyclopetane												
Wartsila 6L50DF DE IMO Tier 2 Gas Mode 1/2014												
	WITHOUT Recuperator						WITH Recuperator					
	NOT Optimised			Optimised for Efficiency			NOT Optimized			Optimized for Efficiency		
Load (%)	100.00	75.00	50.00	100.00	75.00	50.00	100.00	75.00	50.00	100.00	75.00	50.00
Generator (kW)	393.20	372.09	285.25	411.55	389.45	x	448.84	424.74	325.62	465.18	440.20	337.44
Ref Pump (kW)	23.38	22.15	17.07	32.00	30.33	x	27.21	25.79	19.89	34.13	32.35	24.96
SW Pump (kW)	3.67	3.49	2.70	3.65	3.46	x	3.56	3.38	2.65	3.54	3.36	2.64
Turb Press IN (bar)	30.00	30.00	30.00	41.49	41.49	x	30.00	30.00	30.00	38.44	38.42	38.38
Turb Temp IN (°C)	208.23	208.23	208.23	232.00	231.99	x	208.23	208.23	208.23	226.20	226.18	226.10
Massfl of Ref (kg/s)	3.58	3.39	2.60	3.58	3.39	x	4.11	3.89	2.98	4.08	3.86	2.96
Massfl of CW (kg/s)	41.19	38.98	29.88	40.90	38.71	x	39.86	37.72	28.92	39.60	37.47	28.73
Net Power (kW)	366.15	346.46	265.48	375.90	355.66	x	418.07	395.58	303.08	427.51	404.49	309.84
Absorbable Energy Power (kW)	3972.13	3403.94	2601.03	3972.13	3403.94	x	3972.13	3403.94	2601.03	3972.13	3403.94	2601.03
Net Sys Energy Effi (%)	9.22	10.18	10.21	9.46	10.45	x	10.53	11.62	11.65	10.76	11.88	11.91
Absorbable Exergy (kW)	1197.76	1129.12	865.71	1197.76	1129.12	x	1197.76	1129.12	865.71	1197.76	1129.12	865.71
Net Sys Exergy Effi (%)	30.57	30.68	30.67	31.38	31.50	x	34.90	35.03	35.01	35.69	35.82	35.79
Recov energy effi (%)	0.06	0.08	0.09	0.07	0.08	x	0.07	0.09	0.11	0.08	0.09	0.11
Heat trans in Condr (kW)	1719.72	1627.39	1247.59	1707.97	1616.28	x	1664.50	1575.14	1207.54	1653.41	1564.64	1199.50
OHTA. [U*A] (kW/K)	188.93	178.79	137.06	187.64	177.57	x	182.86	173.05	132.66	181.65	171.89	131.78
Heat trans in Econr (kW)	1476.16	1396.91	1070.90	1806.88	1709.58	x	1380.84	1306.70	1001.75	1638.79	1550.34	1187.51
OHTA. in Econo. [U*A] (kW/K)	13.15	10.70	8.16	15.51	12.39	x	15.60	12.55	9.57	17.84	14.13	10.76
Heat trans in Recupr(kW)	-	-	-	-	-	x	315.65	298.71	228.99	311.38	294.71	226.04
OHTA. in Recup. [U*A] (kW/K)	-	-	-	-	-	x	29.56	27.97	21.45	29.30	27.73	21.27
Heat trans in Evapr (kW)	637.58	603.35	462.55	306.86	290.69	x	732.91	693.56	531.70	474.96	449.93	345.94
OHTA. in Evap. [U*A] (kW/K)	4.87	3.47	2.63	2.45	1.68	x	5.85	4.15	3.15	3.90	2.69	2.05
Power Density[kW/(kg/s)]	109.89	109.89	109.88	114.86	114.88	x	109.13	109.13	109.12	114.04	114.04	114.04

Cyclopentane												
Wartsila 6L50DF DE IMO Tier 2 Diesel Mode												
	WITHOUT Recuperator						WITH Recuperator					
	NOT Optimised			Optimised for Efficiency			NOT Optimized			Optimized for Efficiency		
Load (%)	100.00	75.00	50.00	100.00	75.00	50.00	100.00	75.00	50.00	100.00	75.00	50.00
Generator (kW)	413.77	335.77	279.13	433.09	351.42	292.13	472.31	383.28	318.63	489.52	397.22	330.19
Ref Pump (kW)	24.57	20.03	16.71	33.63	27.43	22.90	28.59	23.33	19.47	35.85	29.27	24.43
SW Pump (kW)	3.86	3.16	2.66	3.83	3.14	2.65	3.74	3.06	2.61	3.72	3.04	2.60
Turb Press IN (bar)	30.00	30.00	30.00	41.51	41.47	41.44	30.00	30.00	30.00	38.44	38.41	38.37
Turb Temp IN (°C)	208.23	208.23	208.23	232.03	231.95	231.91	208.23	208.23	208.23	226.21	226.15	226.08
Massfl of Ref (kg/s)	3.77	3.06	2.54	3.77	3.06	2.54	4.33	3.51	2.92	4.29	3.48	2.90
Massfl of CW (kg/s)	43.34	35.17	29.24	43.04	34.93	29.04	41.95	34.04	28.30	41.67	33.81	28.11
Net Power (kW)	385.34	312.58	259.76	395.63	320.85	266.58	439.98	356.89	296.55	449.95	364.91	303.16
Absorbable Energy Power (kW)	4517.63	3584.33	2746.06	4517.63	3584.33	2746.06	4517.63	3584.33	2746.06	4517.63	3584.33	2746.06
Net Sys Energy Effi (%)	8.53	8.72	9.46	8.76	8.95	9.71	9.74	9.96	10.80	9.96	10.18	11.04
Absorbable Exergy (kW)	1275.44	1030.72	848.29	1275.44	1030.72	848.29	1275.44	1030.72	848.29	1275.44	1030.72	848.29
Net Sys Exergy Effi (%)	30.21	30.33	30.62	31.02	31.13	31.43	34.50	34.63	34.96	35.28	35.40	35.74
Recov energy effi (%)	0.07	0.07	0.09	0.07	0.08	0.09	0.08	0.08	0.10	0.08	0.09	0.11
Heat trans in Condr (kW)	1809.66	1468.54	1220.82	1797.30	1458.51	1212.49	1751.56	1421.39	1181.62	1739.89	1411.92	1173.76
OHTA. [U*A] (kW/K)	198.81	161.34	134.12	197.45	160.23	133.21	192.43	156.16	129.82	191.15	155.12	128.95
Heat trans in Econr (kW)	1553.37	1260.56	1047.92	1901.96	1542.05	1281.27	1453.06	1179.15	980.25	1724.67	1398.63	1161.74
OHTA. in Econo. [U*A] (kW/K)	15.46	12.15	8.98	18.55	14.50	10.53	18.52	14.52	10.62	21.48	16.76	12.08
Heat trans in Recupr(kW)	-	-	-	-	-	-	332.16	269.55	224.08	327.66	265.99	221.22
OHTA. in Recup. [U*A] (kW/K)	-	-	-	-	-	-	31.11	25.24	20.99	30.84	25.03	20.81
Heat trans in Evapr (kW)	670.93	544.46	452.62	322.34	262.97	219.28	771.24	625.86	520.29	499.64	406.39	338.81
OHTA. in Evap. [U*A] (kW/K)	6.36	4.85	3.21	3.31	2.51	1.61	7.67	5.84	3.85	5.25	3.97	2.56
Power Density[kW/(kg/s)]	109.90	109.91	109.89	114.88	114.88	114.88	109.13	109.13	109.12	114.05	114.05	114.02

Table B.8: Cyclopentane in diesel mode in simple and recuperative ORC

Table B.9: Toluene in gas mode in simple and recuperative ORC

Toluene												
Wartsila 6L50DF DE IMO Tier 2 Gas Mode 1/2014												
	WITHOUT Recuperator						WITH Recuperator					
	NOT Optimised			Optimised for Efficiency			NOT Optimized			Optimized for Efficiency		
Load (%)	100.00	75.00	50.00	100.00	75.00	50.00	100.00	75.00	50.00	100.00	75.00	50.00
Generator (kW)	468.69	443.53	340.02	478.14	452.47	346.86	575.81	544.90	417.73	584.22	552.86	423.82
Ref Pump (kW)	16.74	15.86	12.20	21.50	20.36	15.67	21.55	20.42	15.73	25.20	23.88	18.40
SW Pump (kW)	3.50	3.32	2.62	3.49	3.31	2.61	3.28	3.11	2.50	3.27	3.10	2.50
Turb Press IN (bar)	30.00	30.00	30.00	38.83	38.83	38.80	30.00	30.00	30.00	35.62	35.62	35.60
Turb Temp IN (°C)	293.07	293.07	293.07	313.67	313.66	313.61	293.07	293.07	293.07	306.70	306.69	306.65
Massfl of Ref (kg/s)	2.91	2.75	2.11	2.92	2.77	2.12	3.71	3.51	2.69	3.69	3.49	2.68
Massfl of CW (kg/s)	39.15	37.04	28.40	39.01	36.91	28.30	36.54	34.58	26.51	36.41	34.45	26.41
Net Power (kW)	448.45	424.35	325.20	453.15	428.79	328.57	550.98	521.37	399.50	555.76	525.88	402.93
Absorbable Energy Power (kW)	3972.13	3403.94	2601.03	3972.13	3403.94	2601.03	3972.13	3403.94	2601.03	3972.13	3403.94	2601.03
Net Sys Energy Effi (%)	11.29	12.47	12.50	11.41	12.60	12.63	13.87	15.32	15.36	13.99	15.45	15.49
Absorbable Exergy (kW)	1197.76	1129.12	865.71	1197.76	1129.12	865.71	1197.76	1129.12	865.71	1197.76	1129.12	865.71
Net Sys Exergy Effi (%)	37.44	37.58	37.56	37.83	37.98	37.95	46.00	46.17	46.15	46.40	46.57	46.54
Recov energy effi (%)	0.08	0.10	0.11	0.08	0.10	0.12	0.10	0.12	0.14	0.10	0.12	0.14
Heat trans in Condr (kW)	1634.52	1546.77	1185.79	1628.68	1541.24	1181.55	1525.91	1443.99	1106.99	1520.23	1438.61	1102.87
OHTA. [U*A] (kW/K)	179.57	169.93	130.27	178.93	169.32	129.81	167.64	158.64	121.62	167.01	158.05	121.16
Heat trans in Econr (kW)	1678.27	1588.17	1217.52	1902.97	1800.50	1379.64	1559.22	1475.51	1131.16	1718.70	1626.37	1246.33
OHTA. in Econo. [U*A] (kW/K)	23.48	16.08	12.21	26.27	17.58	13.34	48.00	28.67	21.70	51.33	30.30	22.93
Heat trans in Recupr(kW)	-	-	-	-	-	-	577.55	546.54	418.99	576.26	545.33	418.10
OHTA. in Recup. [U*A] (kW/K)	-	-	-	-	-	-	39.48	37.36	28.64	39.41	37.29	28.59
Heat trans in Evapr (kW)	435.48	412.10	315.93	210.78	199.76	153.81	554.53	524.76	402.29	395.05	373.90	287.12
OHTA. in Evap. [U*A] (kW/K)	7.85	4.04	3.05	4.40	2.07	1.56	11.73	5.64	4.25	9.02	4.11	3.09
Power Density[kW/(kg/s)]	161.06	161.05	161.07	163.63	163.64	163.61	155.37	155.37	155.41	158.37	158.37	158.38

Toluene												
Wartsila 6L50DF DE IMO Tier 2 Diesel Mode												
	WITHOUT Recuperator						WITH Recuperator					
	NOT Optimised			Optimised for Efficiency			NOT Optimized			Optimized for Efficiency		
Load (%)	100.00	75.00	50.00	100.00	75.00	50.00	100.00	75.00	50.00	100.00	75.00	50.00
Generator (kW)	493.20	400.23	332.72	x	x	x	605.93	491.71	408.77	614.78	498.88	414.73
Ref Pump (kW)	17.60	14.33	11.94	x	x	x	22.66	18.46	15.40	26.48	21.59	18.01
SW Pump (kW)	3.68	3.01	2.58	x	x	x	3.44	2.82	2.47	3.43	2.81	2.46
Turb Press IN (bar)	30.00	30.00	30.00	x	x	x	30.00	30.00	30.00	35.62	35.61	35.60
Turb Temp IN (°C)	293.07	293.07	293.07	x	x	x	293.07	293.07	293.07	306.70	306.66	306.65
Massfl of Ref (kg/s)	3.06	2.49	2.07	x	x	x	3.90	3.17	2.63	3.88	3.15	2.62
Massfl of CW (kg/s)	41.19	33.43	27.79	x	x	x	38.46	31.21	25.94	38.31	31.09	25.85
Net Power (kW)	471.92	382.89	318.20	x	x	x	579.83	470.43	390.90	584.87	474.48	394.26
Absorbable Energy Power (kW)	4517.63	3584.33	2746.06	x	x	x	4517.63	3584.33	2746.06	4517.63	3584.33	2746.06
Net Sys Energy Effi (%)	10.45	10.68	11.59	x	x	x	12.83	13.12	14.23	12.95	13.24	14.36
Absorbable Exergy (kW)	1275.44	1030.72	848.29	x	x	x	1275.44	1030.72	848.29	1275.44	1030.72	848.29
Net Sys Exergy Effi (%)	37.00	37.15	37.51	x	x	x	45.46	45.64	46.08	45.86	46.03	46.48
Recov energy effi (%)	0.08	0.09	0.11	x	x	x	0.10	0.11	0.14	0.10	0.11	0.14
Heat trans in Condr (kW)	1720.01	1395.79	1160.34	x	x	x	1605.72	1303.04	1083.24	1599.74	1298.19	1079.21
OHTA. [U*A] (kW/K)	188.96	153.34	127.48	x	x	x	176.41	143.15	119.01	175.75	142.62	118.56
Heat trans in Econr (kW)	1766.05	1433.14	1191.40	x	x	x	1640.77	1331.48	1106.89	1808.63	1467.23	1219.59
OHTA. in Econo. [U*A] (kW/K)	36.37	25.67	15.14	x	x	x	116.74	63.89	29.50	132.28	69.66	31.41
Heat trans in Recupr(kW)	-	-	-	x	x	x	607.76	493.20	410.00	606.40	492.13	409.13
OHTA. in Recup. [U*A] (kW/K)	-	-	-	x	x	x	41.54	33.71	28.02	41.47	33.65	27.98
Heat trans in Evapr (kW)	458.26	371.87	309.15	x	x	x	583.53	473.54	393.66	415.67	337.79	280.95
OHTA. in Evap. [U*A] (kW/K)	16.92	10.66	4.65	x	x	x	36.27	18.30	6.76	33.03	15.23	5.10
Power Density[kW/(kg/s)]	161.02	161.06	161.05	x	x	x	155.37	155.36	155.37	158.37	158.37	158.35

Table B.10: Toluene in diesel mode in simple and recuperative ORC

C

Heat Exchanger Sizing Calculation Sheet-Example

Table C.1: Heat exchanger calculation for acetone (1/3)

Acetone						
Wartsila 6L50DF DE IMO Tier 2 Gas Mode 1/2014						
	WITHOUT Recuperator			WITH Recuperator		
	Optimised for Efficiency			NOT Optimised		
Load (%)	100	75	50	100	75	50
Generator (kW)	411.95	389.82	298.82	399.77	378.30	290.02
Ref Pump (kW)	26.39	25.00	19.25	20.50	19.42	14.95
SW Pump (kW)	3.64	3.45	2.68	3.66	3.47	2.69
Turb Press IN (bar)	39.29	39.28	39.23	30.00	30.00	30.00
Turb Temp IN (°C)	222.99	222.96	222.87	205.32	205.32	205.32
Massfl of Ref (kg/s)	3.27	3.09	2.37	3.24	3.06	2.35
Massfl of CW (kg/s)	40.78	38.59	29.58	40.96	38.76	29.72
Net Power (kW)	381.92	361.37	276.89	375.62	355.42	272.37
Absorbable Energy Power (kW)	3972.13	3403.94	2601.03	3972.13	3403.94	2601.03
Net Sys Energy Effi (%)	9.61	10.62	10.65	9.46	10.44	10.47
Absorbable Exergy (kW)	1197.76	1129.12	865.71	1197.76	1129.12	865.71
Net Sys Exergy Effi (%)	31.89	32.00	31.98	31.36	31.48	31.46
Recov energy effi (%)	0.07	0.08	0.10	0.07	0.08	0.10
Heat trans in Condr (kW)	1702.61	1611.20	1235.19	1710.31	1618.48	1240.77
OHTA. [U*A] (kW/K)	187.05	177.01	135.70	187.90	177.81	136.31
Heat trans in Econr (kW)	1580.86	1495.53	1145.45	1345.64	1273.40	976.22
OHTA. in Econo. [U*A] (kW/K)	14.38	11.54	8.79	12.72	10.36	7.90
Heat trans in Recupr(kW)	-	-	-	20.21	19.12	14.66
OHTA. in Recup. [U*A] (kW/K)	-	-	-	3.52	3.33	2.56
Heat trans in Evapr (kW)	532.88	504.74	388.00	768.10	726.87	557.23
OHTA. in Evap. [U*A] (kW/K)	4.37	3.03	2.30	6.09	4.33	3.29
Mass Flow of Exhaust Gas	9.4	7.1	5.4	9.4	7.1	5.4
Exhaust Gas	GasMix, AR, CO2, H2O, N2, O2, .0095, .0572, .0642, .7485, .1206					
Working Fluid	RefProp, acetone					
C.W.	IF97					
Evaporator						
LMTD [K]	121.98	166.60	168.33	126.20	167.70	169.32
E.G. Pres. IN (bar)	1.05	1.05	1.05	1.05	1.05	1.05
E.G. Temp. IN (°C)	373	424	426	373	424	426
Enthalpy of E.G. IN [J/kg]	-946001.76	-889145.41	-886901.17	-946001.76	-889145.41	-886901.17
Density of E.G. IN [kg/m³]	0.56	0.52	0.52	0.56	0.52	0.52
Thermal Cond of EG IN [W/mK]	0.04	0.05	0.05	0.04	0.05	0.05
Kine Visco of EG IN [m²/s]	5.337E-05	6.064E-05	6.093E-05	5.337E-05	6.064E-05	6.093E-05
Prandtl No. of E.G. IN [-]	0.751335	0.753728	0.753821	0.751335	0.753728	0.753821
Exhaust Gas Press OUT (bar)	1.03	1.03	1.03	1.03	1.03	1.03
Exhaust Gas Temp OUT (°C)	321.51	360.14	361.48	298.58	331.71	333.01
Enthalpy of E.G. OUT [J/kg]	-1002686.62	-960226.17	-958746.09	-1027703.05	-991513.99	-990088.04
Density of E.G. OUT	0.60	0.56	0.56	0.63	0.59	0.59
V_0 [m/s]	2.66	2.17	1.66	2.66	2.17	1.66
V_mean [m/s]	4.39	3.58	2.73	4.39	3.58	2.73
Re_D [-]	4110.52	2948.27	2237.99	4110.52	2948.27	2237.99
Nu[1] [-]	32.15	27.31	23.83	32.15	27.31	23.83
No. of rows [-]	24	24	24	24	24	24
Phi_stagg [-]	1.33	1.33	1.33	1.33	1.33	1.33
Nu (stack) (10-) [-]	42.42	36.03	31.45	42.42	36.03	31.45
Nu (stack) (10+) [-]	42.87	36.41	31.78	42.87	36.41	31.78
alpha_E.G. [W/m²K]	38.08	34.39	30.08	38.08	34.39	30.08
D_in [m]	0.04	0.04	0.04	0.04	0.04	0.04
D_out [m]	0.05	0.05	0.05	0.05	0.05	0.05
S_T [m]	0.1	0.1	0.1	0.1	0.1	0.1
S_L [m]	0.1	0.1	0.1	0.1	0.1	0.1
Breadth of HE [m]	2.5	2.5	2.5	2.5	2.5	2.5
Height of HE [m]	2.5	2.5	2.5	2.5	2.5	2.5
Area of C/S of HE [m²]	6.25	6.25	6.25	6.25	6.25	6.25
W.F. Press IN (bar)	39.79	39.78	39.73	30.5	30.5	30.5
W.F. Temp IN (°C)	223.83	223.81	223.72	206.38	206.38	206.38
Enthalpy of WF IN [J/kg]	455181.00	455111.17	454762.20	391753.33	391753.33	391753.33
Density of WF IN [kg/m³]	432.41	432.49	432.91	497.54	497.54	497.54
Thermal Cond of WF IN [W/mK]	0.08	0.08	0.08	0.09	0.09	0.09
Kinem.Visco. of W.F. IN [m²/s]	1.80E-07	1.80E-07	1.80E-07	1.80E-07	1.80E-07	1.80E-07
Prandtl No. of W.F. IN [-]	4.93	4.93	4.91	3.58	3.58	3.58
W.F. Pressure OUT (bar)	39.29	39.28	39.23	30.00	30.00	30.00
W.F. Temperature OUT (°C)	222.99	222.96	222.87	205.32	205.32	205.32
Enthalpy of W.F. OUT [J/kg]	618302.88	618327.17	618448.02	628990.76	628990.76	628990.76
V_0 [m/s]	6.01	5.69	4.36	5.18	4.90	3.76
V_mean [m/s]	6.01	5.69	4.36	5.18	4.90	3.76
Re_D [-]	1335454.26	1263309.89	967468.11	1149081.34	1087333.30	833598.54
C_1	0.000935	0.000935	0.000935	0.000935	0.000935	0.000935

Table C.2: Heat exchanger calculation for acetone (2/3)

L_evap_estimat [m]	733	562	489	1021	805	699
g [m/s²]	9.81	9.81	9.81	9.81	9.81	9.81
Boiling Number [-]	22.69	29.60	34.12	23.69	30.04	34.60
Nu [-]	5947.17	6426.88	5284.03	5228.86	5572.29	4584.45
alpha_W.F. [W/m²K]	12553.40	13566.59	11156.66	11717.92	12487.55	10273.79
L_evap [m]	733.06	562.69	489.50	1021.60	805.24	699.08
L_HE [m]	1.27	0.98	0.85	1.77	1.40	1.21
m^3	7.95	6.11	5.31	11.09	8.74	7.59
Economiser						
LMTD [K]	109.91	129.61	130.30	105.79	122.98	123.62
Exhaust Gas Pressure IN	1.03	1.03	1.03	1.03	1.03	1.03
Exhaust Gas Temperature IN	321.51	360.14	361.48	298.58	331.71	333.01
Enthalpy of E.G. IN [J/kg]	-1002686.62	-960226.17	-958746.09	-1027703.05	-991513.99	-990088.04
Density of E.G. IN [kg/m³]	0.60	0.56	0.56	0.63	0.59	0.59
Therm.Cond. of E.G. IN [W/mK]	0.04	0.04	0.04	0.04	0.04	0.04
Kinem.Visco. of E.G. IN [m²/s]	4.73E-05	5.26E-05	5.28E-05	4.43E-05	4.87E-05	4.89E-05
Prandtl No. of E.G. IN [-]	0.75	0.75	0.75	0.75	0.75	0.75
Exhaust Gas Pressure OUT	1.01	1.01	1.01	1.01	1.01	1.01
Exhaust Gas Temperature OUT	165	165	165	165	165	165
Enthalpy of E.G. OUT [J/kg]	-1170843.54	-1170843.54	-1170843.54	-1170843.54	-1170843.54	-1170843.54
V_0 [m/s]	2.50	2.01	1.53	2.40	1.92	1.46
V_mean [m/s]	4.12	3.31	2.52	3.96	3.16	2.41
Re_D [-]	4350.83	3147.66	2390.54	4470.00	3248.16	2466.80
Nu¹ [-]	33.03	28.16	24.58	33.45	28.58	24.95
No. of rows [-]	24	24	24	24	24	24
Phi_stagg [-]	1.33	1.33	1.33	1.33	1.33	1.33
Nu (stack) (10-) [-]	43.58	37.16	32.44	44.14	37.72	32.92
Nu (stack) (10+) [-]	44.04	37.55	32.78	44.60	38.11	33.27
alpha_E.G. [W/m²K]	36.62	32.83	28.70	35.95	32.12	28.09
D_in [m]	0.04	0.04	0.04	0.04	0.04	0.04
D_out [m]	0.05	0.05	0.05	0.05	0.05	0.05
S_T [m]	0.1	0.1	0.1	0.1	0.1	0.1
S_L [m]	0.1	0.1	0.1	0.1	0.1	0.1
Breadth of HE [m]	2.5	2.5	2.5	2.5	2.5	2.5
Height of HE [m]	2.5	2.5	2.5	2.5	2.5	2.5
Area of C/S of HE [m²]	6.25	6.25	6.25	6.25	6.25	6.25
W.F. Pressure IN	40.29	40.28	40.23	31	31	31
W.F. Temperature IN	41.89	41.89	41.89	44.35	44.35	44.35
Enthalpy of W.F. IN [J/kg]	-28583.37	-28584.08	-28587.61	-23870.00	-23870.00	-23870.00
Density of W.F. IN [kg/m³]	770.01	770.01	770.01	766.21	766.21	766.21
Therm.Cond. of W.F. IN [W/mK]	0.15	0.15	0.15	0.15	0.15	0.15
Kinem.Visco. of W.F. IN [m²/s]	3.50E-07	3.50E-07	3.50E-07	3.42E-07	3.42E-07	3.42E-07
Prandtl No. of W.F. IN [-]	3.91	3.91	3.91	3.86	3.86	3.86
W.F. Pressure OUT	39.79	39.78	39.73	30.5	30.5	30.5
W.F. Temperature OUT	223.83	223.81	223.72	206.38	206.38	206.38
Enthalpy of W.F. OUT [J/kg]	455181.00	455111.17	454762.20	391753.33	391753.33	391753.33
V_0 [m/s]	3.38	3.20	2.45	3.36	3.18	2.44
V_mean [m/s]	3.38	3.20	2.45	3.36	3.18	2.44
Re_D [-]	385772.24	364998.64	279778.48	392844.74	371734.49	284988.35
Nu [-]	1168.59	1117.97	903.74	1179.10	1128.13	912.09
alpha_W.F. [W/m²K]	4384.19	4194.27	3390.52	4382.96	4193.50	3390.41
L_eco [m]	2526.91	2259.59	1970.44	2275.42	2071.90	1808.62
L_HE [m]	4.39	3.92	3.42	3.95	3.60	3.14
m^3	27.42	24.52	21.38	24.69	22.48	19.62
Recuperator						
W.F. Pressure HOT IN				0.5859	0.5859	0.5859
W.F. Temperature HOT IN				50.89	50.89	50.89
Enthalpy of WF HOT IN [J/kg]				499015.27	499015.27	499015.27
Density of WF HOT IN [kg/m³]				1.30	1.30	1.30
Therm.Cond. of WF HOT IN [W/mK]				0.016	0.016	0.016
Kinem.Visco. of WF HOT IN [m²/s]				6.69E-06	6.69E-06	6.69E-06
Prandtl No. of WF HOT IN [-]				0.79	0.79	0.79
W.F. Pressure HOT OUT				0.57	0.57	0.57
W.F. Temperature HOT OUT				46.48	46.48	46.48
Enthalpy of WF HOT OUT [J/kg]				492784.948	492784.948	492784.948
V_0 [m/s]				0.40	0.38	0.29
V_mean [m/s]				0.65	0.62	0.47
Re_D [-]				4885.42	4622.89	3544.12
Nu¹ [-]				35.74	34.77	30.48
No. of rows [-]				24	24	24
Phi_stagg [-]				1.33	1.33	1.33
Nu (stack) (10-) [-]				47.15	45.88	40.22
Nu (stack) (10+) [-]				47.65	46.36	40.64
alpha_wf Vap. [W/m²K]				15.54	15.12	13.25

Table C.3: Heat exchanger calculation for acetone (3/3)

D_in [m]				0.04	0.04	0.04
D_out [m]				0.05	0.05	0.05
S_T [m]				0.1	0.1	0.1
S_L [m]				0.1	0.1	0.1
Breadth of HE [m]				2.5	2.5	2.5
Height of HE [m]				2.5	2.5	2.5
Area of C/S of HE [m²]				6.25	6.25	6.25
W.F. Pressure COLD IN				31.5	31.5	31.5
W.F. Temperature COLD IN				41.48	41.48	41.48
Enthalpy of W.F. IN [J/kg]				-30095.18	-30095.18	-30095.18
Density of W.F. IN [kg/m³]				769.50	769.50	769.50
Therm.Cond. of W.F. IN [W/mK]				0.15	0.15	0.15
Kinem.Visco. of W.F. IN [m²/s]				3.50E-07	3.50E-07	3.50E-07
Prandtl No. of W.F. IN [-]				3.91	3.91	3.91
W.F. Pressure COLD OUT				31	31	31
W.F. Temperature COLD OUT				44.35	44.35	44.35
Enthalpy of W.F. OUT [J/kg]				-23870	-23870	-23870
V_0 [m/s]				3.35	3.17	2.43
V_mean [m/s]				3.35	3.17	2.43
Re_D [-]				383067.59	362482.73	277895.54
Nu [-]				1161.98	1111.75	898.84
alpha_wFluid liq.[W/m²K]				4352.97	4164.81	3367.21
L_recup [m]				1450.04	1410.39	1233.83
L_HE [m]				2.52	2.45	2.14
m^3				15.73	15.30	13.39
Condenser						
LMTD [K]	10.22	10.24	10.29	13.16	13.16	13.16
W.F. Pressure IN	0.5659	0.5659	0.5659	0.5659	0.5659	0.5659
W.F. Temperature IN	41.59	41.61	41.69	46.48	46.48	46.48
Enthalpy of W.F. IN [J/kg]	485588.64	485618.09	485735.88	492784.95	492784.95	492784.95
Density of W.F. IN [kg/m³]	1.30	1.30	1.30	1.28	1.28	1.28
W.F. Pressure OUT	0.5659	0.5659	0.5659	0.5659	0.5659	0.5659
W.F. Temperature OUT	40	40	40	40	40	40
Enthalpy of W.F. OUT [J/kg]	-35471.58	-35471.58	-35471.58	-35471.58	-35471.58	-35471.58
Density of W.F. OUT [kg/m³]	767.66	767.66	767.66	767.66	767.66	767.66
Therm.Cond. of W.F. OUT [W/mK]	0.15	0.15	0.15	0.15	0.15	0.15
Kinem.Visco. of W.F. OUT [m²/s]	3.48E-07	3.48E-07	3.48E-07	3.48E-07	3.48E-07	3.48E-07
Density of WF at Sat. Vap.	1.31	1.31	1.31	1.31	1.31	1.31
Enthlpy of WF at Sat. Vap.	483252.59	483252.59	483252.59	483252.59	483252.59	483252.59
g [m/s²]	9.81	9.81	9.81	9.81	9.81	9.81
alpha_Work. Flu. [W/m²K]	1201.81	1201.81	1201.81	1201.81	1201.81	1201.81
N_rows [-]	10	10	10	10	10	10
D_in [m]	0.04	0.04	0.04	0.04	0.04	0.04
D_out [m]	0.05	0.05	0.05	0.05	0.05	0.05
S_T [m]	0.1	0.1	0.1	0.1	0.1	0.1
S_L [m]	0.1	0.1	0.1	0.1	0.1	0.1
Breadth of HE [m]	1.2	1.2	1.2	1.2	1.2	1.2
Height of HE [m]	1.5	1.5	1.5	1.5	1.5	1.5
Area of C/S of HE [m²]	1.8	1.8	1.8	1.8	1.8	1.8
C.W. Pressure IN	1.513	1.513	1.513	1.513	1.513	1.513
C.W. Temperature IN	25	25	25	25	25	25
Enthalpy of C.W. IN [J/kg]	104975.58	104975.58	104975.58	104975.58	104975.58	104975.58
Density of C.W. IN [kg/m³]	997.07	997.07	997.07	997.07	997.07	997.07
Therm.Cond. of C.W. IN [W/mK]	0.607	0.607	0.607	0.607	0.607	0.607
Kinem.Visco. of C.W. IN [m²/s]	8.93E-07	8.93E-07	8.93E-07	8.93E-07	8.93E-07	8.93E-07
Prandtl No. of C.W. IN [-]	6.130	6.130	6.130	6.130	6.130	6.130
C.W. Pressure OUT	1.013	1.013	1.013	1.013	1.013	1.013
C.W. Temperature OUT	35	35	35	35	35	35
Enthalpy of C.W. OUT [J/kg]	146730.81	146730.81	146730.81	146730.81	146730.81	146730.81
V_0 [m/s]	32.54	30.80	23.61	32.69	30.94	23.72
V_mean [m/s]	32.54	30.80	23.61	32.69	30.94	23.72
Re_D [-]	1458244.58	1379960.85	1057921.11	1464824.85	1386183.49	1062677.50
Nu [-]	4052.91	3877.90	3135.20	4067.54	3891.88	3146.47
alpha_CW [W/m²K]	61525.05	58868.24	47593.79	61747.05	59080.51	47764.90
L_cond [m]	1015.03	961.57	741.52	1019.53	965.83	744.78
L_HE [m]	10.15	9.62	7.42	10.20	9.66	7.45
m^3	18.27	17.31	13.35	18.35	17.39	13.41
Total [m^3]	53.64	47.93	40.04	69.86	63.91	54.00
kW/m^3	7.68	8.13	7.46	5.72	5.92	5.37

D

Component Sizes of ORC plant of Suitable Fluids - Wärtsilä

Plant Volume and Density-Wärtsilä 6L50DF DE-Gas Mode							
Fluid Name	[-]	Acetone					
Plant Type	[-]	Recuperator-Not Optimized			Recuperator-Optimized		
Load	[%]	100	75	50	100	75	50
Evaporator	[m³]	11.085029	8.7374	7.585514	9.794884	7.61776	6.617141
Economisee	[m³]	24.689873	22.4815	19.62481	25.94935	23.41688	20.43136
Recuperator	[m³]	15.733954	15.3037	13.38797	4.964381	4.850592	4.318398
Condenser	[m³]	18.35158	17.385	13.406	18.32571	17.36047	13.38728
Total Volume	[m³]	69.860436	63.9077	54.00429	59.03433	53.24571	44.75418
Power Density	[kW/m³]	5.7224092	5.91948	5.370314	6.849066	7.185744	6.553801
Fluid Name	[-]	Methylcyclohexane					
Plant Type	[-]	Recuperator-Not Optimized			Recuperator-Optimized		
Load	[%]	100	75	50	100	75	50
Evaporator	[m³]	11.050101	6.71718	5.792645	8.406199	5.080394	4.39031
Economisee	[m³]	130.05112	91.0708	78.92961	129.4733	91.14385	79.01291
Recuperator	[m³]	190.45198	185.263	162.1627	190.3905	185.2038	162.1195
Condenser	[m³]	28.412475	26.9052	20.70265	28.38465	26.87888	20.6824
Total Volume	[m³]	359.96567	309.956	267.5876	356.6547	308.3069	266.2051
Power Density	[kW/m³]	1.6407676	1.80319	1.60127	1.663682	1.821237	1.616986
Fluid Name	[-]	Cyclohexane					
Plant Type	[-]	Recuperator-Not Optimized			Recuperator-Optimized		
Load	[%]	100	75	50	100	75	50
Evaporator	[m³]	11.513642	7.96145	6.887087	6.273185	4.203461	3.648483
Economisee	[m³]	54.669171	44.4914	38.71313	59.66798	47.83451	41.60002
Recuperator	[m³]	140.92269	137.091	119.9963	141.5494	137.6957	120.5353
Condenser	[m³]	27.093713	25.6573	19.74654	26.93211	25.5045	19.62925
Total Volume	[m³]	234.19921	215.201	185.343	234.4226	215.2381	185.413
Power Density	[kW/m³]	2.2823732	2.3505	2.092229	2.338597	2.410261	2.144887
Fluid Name	[-]	Cyclopentane					
Plant Type	[-]	Recuperator-Not Optimized			Recuperator-Optimized		
Load	[%]	100	75	50	100	75	50
Evaporator	[m³]	10.643398	8.35095	7.248499	7.082488	5.413883	4.709686
Economisee	[m³]	30.190089	27.145	23.68548	33.84673	29.85517	26.02725
Recuperator	[m³]	101.25008	98.4855	86.17285	100.7216	97.97448	85.74783
Condenser	[m³]	24.371787	23.0819	17.77289	24.21176	22.9304	17.65675
Total Volume	[m³]	166.45536	157.063	134.8797	165.8626	156.1739	134.1415
Power Density	[kW/m³]	2.6964587	2.70426	2.414151	2.804611	2.818652	2.515552
Fluid Name	[-]	Toluene					
Plant Type	[-]	Recuperator-Not Optimized			Recuperator-Optimized		
Load	[%]	100	75	50	100	75	50
Evaporator	[m³]	21.38323	11.3776	9.787784	16.4378	8.279378	7.126118
Economisee	[m³]	91.724542	61.0805	52.92467	96.92334	63.64217	55.12627
Recuperator	[m³]	130.50693	126.942	111.0928	130.4193	126.856	111.0144
Condenser	[m³]	21.489537	20.354	15.68044	21.41081	20.27958	15.62323
Total Volume	[m³]	265.10424	219.754	189.4857	265.1912	219.0571	188.89
Power Density	[kW/m³]	2.1720136	2.47959	2.204546	2.203014	2.523817	2.24374

Table D.1: Plant Volume and power density of suitable fluids in recuperative-ORC plant in Gas Mode

Plant Volume and Density-Wärtsilä 6L50DF DE-Diesel Mode							
Fluid Name	[-]	Acetone					
Plant Type	[-]	Recuperator-Not Optimized			Recuperator-Optimized		
Load	[%]	100	75	50	100	75	50
Evaporator	[m³]	13.33354	11.4639	8.826879	11.93931	10.23	7.7789286
Economisee	[m³]	26.57888	23.60923	20.43994	28.15804	24.945	21.421295
Recuperator	[m³]	16.14333	14.5329	13.24426	5.07134	4.6403	4.2892143
Condenser	[m³]	19.29313	15.72136	13.12532	19.26593	15.699	13.107
Total Volume	[m³]	75.34888	65.32739	55.6364	64.43462	55.515	46.596438
Power Density	[kW/m³]	5.583096	5.225679	5.100797	6.603283	6.2193	6.1594837
Fluid Name	[-]	Methylcyclohexane					
Plant Type	[-]	Recuperator-Not Optimized			Recuperator-Optimized		
Load	[%]	100	75	50	100	75	50
Evaporator	[m³]	18.88332	14.33022	8.09622	14.42051	10.926	6.132905
Economisee	[m³]	194.4812	153.9136	99.28301	190.8368	151.97	99.032025
Recuperator	[m³]	195.357	175.9737	160.4302	195.3051	175.93	160.38649
Condenser	[m³]	29.88062	24.31153	20.26516	29.85145	24.288	20.245415
Total Volume	[m³]	438.6022	368.5291	288.0746	430.4139	363.11	285.79683
Power Density	[kW/m³]	1.417024	1.368576	1.455456	1.450697	1.3954	1.4738792
Fluid Name	[-]	Cyclohexane					
Plant Type	[-]	Recuperator-Not Optimized			Recuperator-Optimized		
Load	[%]	100	75	50	100	75	50
Evaporator	[m³]	16.06815	13.15474	8.808301	9.132908	7.3928	4.7789188
Economisee	[m³]	66.12167	56.57052	43.79212	73.27959	62.383	47.586021
Recuperator	[m³]	144.5653	130.2034	118.6891	145.2159	130.79	119.23239
Condenser	[m³]	28.49277	23.18567	19.3296	28.32268	23.048	19.214933
Total Volume	[m³]	255.2479	223.1144	190.6191	255.9511	223.62	190.81226
Power Density	[kW/m³]	2.203701	2.045857	1.990671	2.253907	2.0935	2.0394916
Fluid Name	[-]	Cyclopentane					
Plant Type	[-]	Recuperator-Not Optimized			Recuperator-Optimized		
Load	[%]	100	75	50	100	75	50
Evaporator	[m³]	12.86033	11.04068	8.463002	8.79293	7.5004	5.6138549
Economisee	[m³]	32.83037	29.07501	24.9083	37.43142	32.971	27.762445
Recuperator	[m³]	103.8765	93.53531	85.23805	103.3341	93.06	84.817541
Condenser	[m³]	25.62823	20.8619	17.39856	25.45982	20.725	17.284923
Total Volume	[m³]	175.1954	154.5129	136.0079	175.0183	154.26	135.47876
Power Density	[kW/m³]	2.695904	2.48057	2.342731	2.796965	2.5751	2.4372085
Fluid Name	[-]	Toluene					
Plant Type	[-]	Recuperator-Not Optimized			Recuperator-Optimized		
Load	[%]	100	75	50	100	75	50
Evaporator	[m³]	61.19759	34.75203	14.88875	55.71097	28.904	11.236127
Economisee	[m³]	204.7307	126.5174	68.29735	229.5561	136.46	71.825281
Recuperator	[m³]	133.8862	120.5559	109.8747	133.798	120.49	109.80232
Condenser	[m³]	22.59559	18.39978	15.35077	22.51285	18.333	15.294814
Total Volume	[m³]	422.4101	300.2251	208.4115	441.5779	304.18	208.15855
Power Density	[kW/m³]	1.434459	1.637804	1.96136	1.392235	1.6401	1.9923756

Table D.2: Plant Volume and power density of suitable fluids in recuperative-ORC plant in Diesel Mode

Plant Volume and Density-Wärtsilä 6L50DF DE-Gas Mode							
Fluid Name	[-]	Acetone based Simple-ORC					
Plant Type	[-]	Not Optimized			Optimized		
Load	[%]	100	75	50	100	75	50
Evaporator	[m³]	10.940255	8.62565	7.488545	7.954161	6.105585	5.311362
Economisee	[m³]	24.417249	22.2469	19.42061	27.41875	24.51808	21.38059
Condenser	[m³]	18.353588	17.3868	13.40744	18.27062	17.30834	13.34727
Total Volume	[m³]	53.711093	48.2594	40.31659	53.64352	47.932	40.03923
Power Density	[kW/m³]	7.4317982	7.82728	7.182651	7.679399	8.132771	7.463181
Fluid Name	[-]	Acetone based Recuperative-ORC					
Plant Type	[-]	Not Optimized			Optimized		
Load	[%]	100	75	50	100	75	50
Evaporator	[m³]	11.085029	8.7374	7.585514	9.794884	7.61776	6.617141
Economisee	[m³]	24.689873	22.4815	19.62481	25.94935	23.41688	20.43136
Recuperator	[m³]	15.733954	15.3037	13.38797	4.964381	4.850592	4.318398
Condenser	[m³]	18.35158	17.385	13.406	18.32571	17.36047	13.38728
Total Volume	[m³]	69.860436	63.9077	54.00429	59.03433	53.24571	44.75418
Power Density	[kW/m³]	5.7224092	5.91948	5.370314	6.849066	7.185744	6.553801
Plant Volume and Density-Wärtsilä 6L50DF DE-Diesel Mode							
Fluid Name	[-]	Acetone based Simple-ORC					
Plant Type	[-]	Not Optimized			Optimized		
Load	[%]	100	75	50	100	75	50
Evaporator	[m³]	13.155874	11.3121	8.712339	9.833005	8.39889	6.308174
Economisee	[m³]	26.271449	23.3401	20.21801	29.98702	26.4967	22.56867
Condenser	[m³]	19.295149	15.723	13.12677	19.20788	15.65215	13.06785
Total Volume	[m³]	58.722472	50.3752	42.05711	59.0279	50.54774	41.9447
Power Density	[kW/m³]	7.1531389	6.76663	6.737742	7.343985	6.958966	6.971084
Fluid Name	[-]	Acetone based Recuperative-ORC					
Plant Type	[-]	Not Optimized			Optimized		
Load	[%]	100	75	50	100	75	50
Evaporator	[m³]	13.333543	11.4639	8.826879	11.93931	10.2296	7.778929
Economisee	[m³]	26.578875	23.6092	20.43994	28.15804	24.94542	21.4213
Recuperator	[m³]	16.143325	14.5329	13.24426	5.07134	4.64033	4.289214
Condenser	[m³]	19.293133	15.7214	13.12532	19.26593	15.69921	13.107
Total Volume	[m³]	75.348877	65.3274	55.6364	64.43462	55.51456	46.59644
Power Density	[kW/m³]	5.5830958	5.22568	5.100797	6.603283	6.21927	6.159484

Table D.3: Comparison of acetone in simple and recuperative-ORC for gas and deisel mode

E

Static Analysis and Component Size Data - SWD Engine

Mode @ Load	Propeller Mode @ 25%			Generator Mode @ 85%		
Parameter	Power Output	Mass Flow	Ratio	Power Output	Mass Flow	Ratio
Units	[kW]	[kg/s]	[kW/(kg/s)]	[kW]	[kg/s]	[kW/(kg/s)]
Acetone	53.25	0.431	123.55	361.14	2.925	123.47
Butane	39.69	0.681	58.28	269.23	4.617	58.31
1 Butene	36.45	0.696	52.37	247.23	4.719	52.39
Methylcyc	78.67	0.558	140.99	533.56	3.786	140.93
Cyclohexane	71.2	0.534	133.33	482.88	3.624	133.25
Cyclopentane	59.78	0.548	109.09	405.47	3.715	109.14
C2Butene	40.09	0.628	63.84	271.91	4.256	63.89
Isobutan	34.87	0.768	45.40	236.51	5.209	45.40
Ibutene	36.18	0.699	51.76	245.38	4.742	51.75
Ipentane	51.93	0.669	77.62	352.19	4.535	77.66
Neopentn	44.97	0.789	57.00	304.99	5.349	57.02
Pentane	53.99	0.624	86.52	366.15	4.234	86.48
R11	47.55	1.309	36.33	322.5	8.878	36.33
R113	57.13	1.489	38.37	387.48	10.1	38.36
R114	38.83	1.932	20.10	263.33	13.102	20.10
R123	47.44	1.386	34.23	321.77	9.399	34.23
R141B	51.15	1.03	49.66	346.93	6.983	49.68
R236EA	37.54	1.603	23.42	254.63	10.873	23.42
R245CA	44.92	1.194	37.62	304.7	8.098	37.63
R245FA	39.81	1.296	30.72	270	8.79	30.72
R365MFC	51.33	1.186	43.28	348.15	8.043	43.29
R436A	27.56	0.771	35.75	186.94	5.228	35.76
R436B	28.2	0.769	36.67	191.27	5.214	36.68
Toluene	76.69	0.494	155.24	520.18	3.348	155.37
T2Butene	39.17	0.647	60.54	265.65	4.391	60.50

Table E.1: Functional fluids based on exhaust gas data of SWD diesel engine

Mode	Load [%]	x [-]	N_2 [%]	Ar [%]	CO_2 [%]	H_2O [%]	O_2 [%]
Generator	25	0.437	76.05	0.90	5.87	5.37	11.85
	50	0.428	76.09	0.90	5.75	5.26	12.04
	75	0.427	76.09	0.90	5.74	5.25	12.06
	85	0.435	76.06	0.90	5.85	5.34	11.89
	100	0.455	75.96	0.90	6.11	5.59	11.48
Propeller	25	0.446	76.00	0.90	5.99	5.48	11.66
	50	0.439	76.04	0.90	5.90	5.39	11.81
	75	0.534	75.58	0.90	7.18	6.57	9.82
	85	0.547	75.52	0.90	7.35	6.73	9.55
	100	0.493	75.78	0.90	6.62	6.06	10.68

Table E.2: Real mole fraction data of gas constituents

Table E.3: Acetone based simple-ORC plant data for generator and propeller mode

ACETONE											
Parameter	Units	Generator Mode					Propeller Mode				
Engine Load	[%]	25	50	75	85	100	25	50	75	85	100
Generator Power	[kW]	156.83	252.72	328.72	360.51	420.53	53.15	182.24	303.79	350.12	461.22
Turbine Power	[kW]	165.08	266.02	346.02	379.48	442.66	55.95	191.83	319.78	368.55	485.49
Ref Pump	[kW]	8.09	12.33	15.98	17.50	20.35	2.94	9.24	14.79	17.00	22.28
CW Pump	[kW]	1.76	2.47	3.04	3.32	3.84	0.61	1.97	2.81	3.22	4.19
Net Power	[kW]	146.98	237.92	309.70	339.69	396.34	49.60	171.03	286.19	329.90	434.75
Recovered Power	[%]	16.06	13.00	11.28	10.92	10.83	12.19	12.91	11.18	10.68	11.52
Massflow_WF	[kg/s]	1.26	2.03	2.64	2.90	3.38	0.43	1.46	2.44	2.81	3.71
Massflow_CW	[kg/s]	16.10	25.94	33.74	37.00	43.16	5.46	18.70	31.18	35.93	47.33
Exh_Evap-Econ	[°C]	368.38	340.37	320.89	319.59	325.43	400.43	400.43	334.52	321.54	364.47
Tur-Cond	[bar]	0.57	0.57	0.57	0.57	0.57	0.57	0.57	0.57	0.57	0.57
Tur-Cond	[°C]	49.99	49.99	49.99	49.99	49.99	49.99	49.99	49.99	49.99	49.99
Tur-Cond	[kJ/kg]	497.95	497.95	497.95	497.95	497.95	497.95	497.95	497.95	497.95	497.95
Cond-Pump	[bar]	0.57	0.57	0.57	0.57	0.57	0.57	0.57	0.57	0.57	0.57
Cond-Pump	[°C]	40.00	40.00	40.00	40.00	40.00	40.00	40.00	40.00	40.00	40.00
Cond-Pump	[kJ/kg]	-35.48	-35.48	-35.48	-35.48	-35.48	-35.48	-35.48	-35.48	-35.48	-35.48
Pump-Econ	[bar]	30.00	30.00	30.00	30.00	30.00	30.00	30.00	30.00	30.00	30.00
Pump-Econ	[°C]	41.40	41.40	41.40	41.40	41.40	41.40	41.40	41.40	41.40	41.40
Pump-Econ	[kJ/kg]	-30.37	-30.37	-30.37	-30.37	-30.37	-30.37	-30.37	-30.37	-30.37	-30.37
Econ-Evap	[bar]	30.00	30.00	30.00	30.00	30.00	30.00	30.00	30.00	30.00	30.00
Econ-Evap	[°C]	205.32	205.32	205.32	205.32	205.32	205.32	205.32	205.32	205.32	205.32
Econ-Evap	[kJ/kg]	388.26	388.26	388.26	388.26	388.26	388.26	388.26	388.26	388.26	388.26
Evap-Tur	[bar]	30.00	30.00	30.00	30.00	30.00	30.00	30.00	30.00	30.00	30.00
Evap-Tur	[°C]	205.32	205.32	205.32	205.32	205.32	205.32	205.32	205.32	205.32	205.32
Evap-Tur	[kJ/kg]	628.99	628.99	628.99	628.99	628.99	628.99	628.99	628.99	628.99	628.99
Heat_trans_Cond	[kW]	672.05	1082.92	1408.62	1544.82	1802.04	227.77	780.91	1301.79	1500.32	1976.41
Heat_trans_Econ	[kW]	527.41	849.86	1105.46	1212.35	1414.22	178.75	612.85	1021.62	1177.43	1551.06
Heat_trans_Evap	[kW]	303.29	488.71	635.70	697.16	813.25	102.79	352.42	587.48	677.08	891.94
UA_Cond	[kW/K]	73.83	118.97	154.75	169.72	197.97	25.02	85.79	143.02	164.83	217.13
UA_Econ	[kW/K]	3.70	6.58	9.25	10.20	11.61	1.14	3.91	8.08	9.82	11.03
UA_Evap.	[kW/K]	1.41	2.72	4.10	4.54	5.06	0.40	1.39	3.41	4.34	4.26

CYCLOPENTANE											
Parameter	Units	Generator Mode					Propeller Mode				
Engine Load	[%]	25	50	75	85	100	25	50	75	85	100
Generator Power	[kW]	177.30	285.69	371.62	407.55	475.41	60.09	206.02	343.43	395.81	521.41
Turbine Power	[kW]	186.63	300.73	391.18	429.00	500.43	63.25	216.86	361.51	416.64	548.85
Ref Pump	[kW]	10.52	16.54	21.41	23.43	27.22	3.91	11.98	19.82	22.77	29.78
CW Pump	[kW]	1.72	2.42	2.95	3.22	3.74	0.59	1.93	2.73	3.14	4.08
Net Power	[kW]	165.06	266.73	347.26	380.90	444.45	55.59	192.11	320.88	369.90	487.55
Recovered Power	[%]	18.04	14.58	12.65	12.24	12.14	13.66	14.50	12.53	11.97	12.92
Massflow_WF	[kg/s]	1.61	2.60	3.38	3.71	4.33	0.55	1.88	3.13	3.60	4.74
Massflow_CW	[kg/s]	15.63	25.19	32.77	35.93	41.92	5.30	18.17	30.28	34.90	45.97
Exh_Evap-Econ	[°C]	371.91	343.42	323.61	322.29	328.23	404.49	404.49	337.47	324.27	367.93
Tur-Recu	[bar]	0.74	0.74	0.74	0.74	0.74	0.74	0.74	0.74	0.74	0.74
Tur-Recu	[°C]	99.50	99.50	99.50	99.50	99.50	99.50	99.50	99.50	99.50	99.50
Tur-Recu	[kJ/kg]	463.05	463.05	463.05	463.05	463.05	463.05	463.05	463.05	463.05	463.05
Recu-Cond	[bar]	0.74	0.74	0.74	0.74	0.74	0.74	0.74	0.74	0.74	0.74
Recu-Cond	[°C]	46.65	46.65	46.65	46.65	46.65	46.65	46.65	46.65	46.65	46.65
Recu-Cond	[kJ/kg]	386.99	386.99	386.99	386.99	386.99	386.99	386.99	386.99	386.99	386.99
Cond-Pump	[bar]	0.74	0.74	0.74	0.74	0.74	0.74	0.74	0.74	0.74	0.74
Cond-Pump	[°C]	40.00	40.00	40.00	40.00	40.00	40.00	40.00	40.00	40.00	40.00
Cond-Pump	[kJ/kg]	-17.63	-17.63	-17.63	-17.63	-17.63	-17.63	-17.63	-17.63	-17.63	-17.63
Pump-Recu	[bar]	30.00	30.00	30.00	30.00	30.00	30.00	30.00	30.00	30.00	30.00
Pump-Recu	[°C]	41.65	41.65	41.65	41.65	41.65	41.65	41.65	41.65	41.65	41.65
Pump-Recu	[kJ/kg]	-12.24	-12.24	-12.24	-12.24	-12.24	-12.24	-12.24	-12.24	-12.24	-12.24
Recu-Econ	[bar]	30.00	30.00	30.00	30.00	30.00	30.00	30.00	30.00	30.00	30.00
Recu-Econ	[°C]	80.04	80.04	80.04	80.04	80.04	80.04	80.04	80.04	80.04	80.04
Recu-Econ	[kJ/kg]	63.80	63.80	63.80	63.80	63.80	63.80	63.80	63.80	63.80	63.80
Econ-Evap	[bar]	30.00	30.00	30.00	30.00	30.00	30.00	30.00	30.00	30.00	30.00
Econ-Evap	[°C]	208.23	208.23	208.23	208.23	208.23	208.23	208.23	208.23	208.23	208.23
Econ-Evap	[kJ/kg]	396.54	396.54	396.54	396.54	396.54	396.54	396.54	396.54	396.54	396.54
Evap-Tur	[bar]	30.00	30.00	30.00	30.00	30.00	30.00	30.00	30.00	30.00	30.00
Evap-Tur	[°C]	208.23	208.23	208.23	208.23	208.23	208.23	208.23	208.23	208.23	208.23
Evap-Tur	[kJ/kg]	578.73	578.73	578.73	578.73	578.73	578.73	578.73	578.73	578.73	578.73
Heat_trans_Cond	[kW]	652.74	1051.81	1368.14	1500.43	1750.26	221.22	758.48	1264.38	1457.21	1919.62
Heat_trans_Econ	[kW]	536.79	864.97	1125.11	1233.90	1439.35	181.93	623.74	1039.78	1198.36	1578.62
Heat_trans_Recu	[kW]	122.69	197.70	257.16	282.03	328.99	41.58	142.57	237.66	273.91	360.82
Heat_trans_Evap	[kW]	293.91	473.61	616.05	675.62	788.11	99.61	341.53	569.33	656.16	864.37
UA_Cond	[kW/K]	71.71	115.55	150.31	164.84	192.29	24.30	83.33	138.91	160.09	210.89
UA_Econ	[kW/K]	4.47	8.00	11.32	12.49	14.19	1.37	4.69	9.85	12.02	13.33
UA_Recu	[kW/K]	11.53	18.58	24.17	26.51	30.93	3.91	13.40	22.34	25.75	33.92
UA_Evap.	[kW/K]	1.38	2.66	4.01	4.44	4.94	0.39	1.35	3.33	4.25	4.14

Table E.4: Cyclopentane based recuperative-ORC plant data for generator and propeller mode

Acetone based Simple-ORC						
Generator Load						
Load	[%]	25	50	75	85	100
Evaporator	[m³]	4.8633377	7.050984	8.948193406	9.44614074	9.872239371
Economiser	[m³]	14.46654	19.05963	22.36281422	23.4704777	25.14001407
Condenser	[m³]	7.3837444	11.72252	15.15492878	16.5892871	19.29660532
Total	[m³]	26.713622	37.83314	46.46593641	49.5059056	54.30885876
Power Density	[kW/m³]	5.8707875	6.679858	7.074429687	7.28216151	7.74330394
Net Energy Efficiency	[-]	0.118062	0.113722	0.109641798	0.10935195	0.110718074
Net Exergy Efficiency	[-]	0.3128269	0.316755	0.317742008	0.3177923	0.317779107
Thermal Efficiency	[-]	0.1890086	0.189542	0.189572672	0.18958882	0.189614126
Propeller Load						
Load	[%]	25	50	75	85	100
Evaporator	[m³]	2.4635256	4.630276	7.975016847	9.20279465	8.540278499
Economiser	[m³]	8.0492068	15.06633	21.07640481	23.060537	25.03628837
Condenser	[m³]	2.6625973	8.534757	14.02957086	16.1207191	21.1310836
Total	[m³]	13.17533	28.23136	43.08099252	48.3840507	54.70765047
Power Density	[kW/m³]	4.0340547	6.455232	7.051601698	7.23626887	8.430630744
Net Energy Efficiency	[-]	0.1219154	0.122613	0.112620864	0.10980541	0.118127852
Net Exergy Efficiency	[-]	0.3075905	0.30935	0.317296839	0.31777267	0.315054873
Thermal Efficiency	[-]	0.1882956	0.189178	0.189558876	0.18958389	0.189628318

Table E.5: Volume, density and efficiency calculations for acetone based simple-ORC

Cyclopentane based Recuperative-ORC						
Generator Load						
Load	[%]	25	50	75	85	100
Evaporator	[m³]	4.7208725	6.8614	8.727956208	9.21549904	9.624202894
Economiser	[m³]	17.426812	23.13524	27.32017835	28.6872552	30.66550687
Condenser	[m³]	9.7300108	15.50431	20.07463697	21.9847531	25.59088153
Recuperator	[m³]	71.286677	90.6252	103.447739	108.356796	117.0631202
Total	[m³]	103.16437	136.1261	159.5705105	168.244304	182.9437115
Power Density	[kW/m³]	1.7186166	2.098715	2.328876424	2.42237028	2.59866817
Net Energy Efficiency	[-]	0.1325848	0.127492	0.122939008	0.12261814	0.124157662
Net Exergy Efficiency	[-]	0.3513078	0.355111	0.356277332	0.35634575	0.35635294
Thermal Efficiency	[-]	0.2120245	0.212327	0.212392025	0.21241683	0.212466977
Propeller Load						
Load	[%]	25	50	75	85	100
Evaporator	[m³]	2.386058	4.486377	7.765696427	8.97563495	8.294698977
Economiser	[m³]	9.6261676	18.02475	25.63036379	28.1663355	30.1956553
Condenser	[m³]	3.4568705	11.26135	18.57602317	21.3607684	28.03463451
Recuperator	[m³]	41.242443	76.87324	99.42061832	106.76519	122.6272822
Total	[m³]	56.711539	110.6457	151.3927017	165.267929	189.152271
Power Density	[kW/m³]	1.0595727	1.861979	2.268471307	2.39495953	2.756562198
Net Energy Efficiency	[-]	0.1366386	0.137725	0.126271997	0.12311919	0.132474375
Net Exergy Efficiency	[-]	0.3447371	0.347479	0.355757398	0.35630225	0.353318007
Thermal Efficiency	[-]	0.2108	0.212274	0.212366628	0.21240894	0.212495118

Table E.6: Volume, density and efficiency calculations for cyclopentane based recuperative-ORC

F

Off-design Performance Analysis Data

Acetone-SimpleORC-Generator Load					
Net Power [kW]					
	Design Point [-]				
Load [%]	25	50	75	85	100
25	142.5	153.4	155.6	154.8	151.7
50	185.5	230.9	244.9	247.3	250.1
75		273.1	299.5	306.2	315.1
85		286.8	320.8	328.0	339.1
100		284.1	359.0	370.7	381.5
Net Energy Efficiency [-]					
Load [%]	25	50	75	85	100
25	0.115	0.123	0.125	0.124	0.122
50	0.089	0.110	0.117	0.118	0.120
75		0.097	0.106	0.108	0.112
85		0.092	0.103	0.106	0.109
100		0.079	0.100	0.104	0.107
Net Exergy Efficiency [-]					
Load [%]	25	50	75	85	100
25	0.302	0.325	0.330	0.328	0.322
50	0.245	0.305	0.324	0.327	0.330
75		0.277	0.303	0.310	0.319
85		0.264	0.296	0.302	0.312
100		0.224	0.283	0.292	0.300
Turbine Power [kW]					
Load [%]	25	50	75	85	100
25	160.6	172.4	174.1	176.0	174.0
50	223.7	258.5	273.3	276.2	280.1
75		310.6	335.5	342.5	352.3
85		330.3	361.1	367.9	379.6
100		371.6	411.3	421.0	429.4

Table F.1: Off design performance data for acetone based simple-ORC in generator load 1/2

Acetone-SimpleORC-Generator Load					
Pump Power					
	Design Point				
Load [%]	25	50	75	85	100
25	7.61	7.64	8.32	8.63	9.28
50	24.72	12.24	12.08	12.19	12.65
75		18.12	15.86	15.62	15.64
85		23.10	18.08	17.39	17.05
100		64.83	25.28	22.65	20.30
Net Power Density					
Load [%]	25	50	75	85	100
25	5.336	4.053	3.348	3.127	2.793
50	6.944	6.103	5.270	4.995	4.605
75		7.219	6.445	6.186	5.803
85		7.581	6.905	6.626	6.244
100		7.509	7.725	7.489	7.024
Thermal Efficiency					
Load [%]	25	50	75	85	100
25	0.184	0.107	0.076	0.068	0.057
50	0.276	0.184	0.137	0.124	0.105
75		0.239	0.184	0.168	0.143
85		0.257	0.203	0.184	0.158
100		0.269	0.237	0.217	0.184
Generator Power					
Load [%]	25	50	75	85	100
25	151.17	161.69	164.53	164.07	161.54
50	212.29	244.81	258.24	260.71	263.85
75		294.59	317.51	323.79	332.46
85		313.27	341.67	347.77	358.16
100		352.26	388.59	397.32	404.53

Table F.2: Off design performance data for acetone based simple-ORC in generator load 2/2

Table F.3: Off design performance data for acetone based simple-ORC in propeller load 1/2

Acetone-SimpleORC-Propeller Load					
Net Power [kW]					
	Design Point				
Load [%]	25	50	75	85	100
25	45.4	46.2	37.8	34.7	27.3
50		166.0	182.1	183.0	173.9
75		214.9	277.5	288.4	296.2
85		192.4	304.6	319.1	332.4
100			322.6	399.3	417.8
Net Energy Efficiency [-]					
Load [%]	25	50	75	85	100
25	0.112	0.114	0.093	0.085	0.067
50		0.119	0.131	0.131	0.125
75		0.085	0.109	0.114	0.117
85		0.064	0.101	0.106	0.111
100			0.088	0.109	0.114
Net Exergy Efficiency [-]					
Load [%]	25	50	75	85	100
25	0.281	0.286	0.234	0.215	0.169
50		0.299	0.328	0.330	0.313
75		0.236	0.305	0.317	0.325
85		0.183	0.289	0.303	0.316
100			0.231	0.285	0.299
Turbine Power [kW]					
Load [%]	25	50	75	85	100
25	54.4	57.2	50.8	48.5	43.1
50		186.4	204.2	206.0	198.7
75		254.2	310.7	322.2	331.5
85		273.5	343.4	357.7	372.0
100			448.8	469.1	472.0

Table F.4: Off design performance data for acetone based simple-ORC in propeller load 2/2

Acetone-SimpleORC-Propeller Load					
Pump Power [kW]					
	Design Point				
Load [%]	25	50	75	85	100
25	2.57	3.33	4.23	4.58	5.45
50		8.82	9.10	9.49	10.55
75		24.02	14.71	14.53	14.86
85		65.10	17.71	16.92	16.53
100			96.85	37.64	22.35
Net Power Density [kW/m^3]					
Load [%]	25	50	75	85	100
25	3.444	1.638	0.877	0.717	0.500
50		5.879	4.226	3.781	3.179
75		7.613	6.441	5.960	5.414
85		6.815	7.071	6.594	6.075
100			7.488	8.252	7.636
Thermal Efficiency [-]					
Load [%]	25	50	75	85	100
25	0.184	0.045	0.020	0.016	0.011
50		0.184	0.100	0.083	0.062
75		0.278	0.184	0.158	0.122
85		0.262	0.213	0.184	0.142
100			0.242	0.241	0.184
Generator Power [kW]					
Load [%]	25	50	75	85	100
25	48.28	49.77	42.21	39.51	32.98
50		175.99	191.99	193.22	185.13
75		241.34	294.19	304.64	312.42
85		259.92	325.17	338.28	350.59
100			423.46	441.56	443.17

Cyclopentane-RecuperativeORC-Generator Load					
Net Power [kW]					
	Design Point [-]				
Load [%]	25	50	75	85	100
25	160.5	173.2	170.6	168.5	163.1
50	214.6	262.2	274.9	277.2	279.9
75		310.1	338.0	345.1	354.3
85		324.9	362.7	369.8	381.5
100		313.9	404.9	418.5	429.4
Net Energy Efficiency [-]					
Load [%]	25	50	75	85	100
25	0.129	0.139	0.137	0.135	0.131
50	0.103	0.125	0.131	0.133	0.134
75		0.110	0.120	0.122	0.125
85		0.105	0.117	0.119	0.123
100		0.088	0.113	0.117	0.120
Net Exergy Efficiency [-]					
Load [%]	25	50	75	85	100
25	0.340	0.367	0.362	0.357	0.346
50	0.284	0.347	0.363	0.366	0.370
75		0.314	0.342	0.349	0.359
85		0.299	0.334	0.341	0.351
100		0.247	0.319	0.330	0.338
Turbine Power [kW]					
Load [%]	25	50	75	85	100
25	181.8	196.3	195.5	194.2	190.7
50	256.5	296.4	309.9	312.9	317.5
75		357.0	383.0	390.4	401.0
85		379.9	413.4	420.0	432.7
100		425.2	471.8	482.9	490.7

Table F.5: Off design performance data for cyclopentane based recuperative-ORC in generator load 1/2

Cyclopentane-RecuperativeORC-Generator Load					
Pump Power [kW]					
	Design Point				
Load [%]	25	50	75	85	100
25	10.27	10.64	11.62	12.18	13.57
50	27.05	16.85	16.66	16.94	17.96
75		24.83	21.70	21.45	21.73
85		31.56	24.72	23.79	23.54
100		84.76	34.73	31.01	27.82
Net Power Density [kW/m^3]					
Load [%]	25	50	75	85	100
25	1.556	1.272	1.069	1.002	0.891
50	2.080	1.926	1.723	1.647	1.530
75		2.278	2.118	2.051	1.936
85		2.387	2.273	2.198	2.085
100		2.306	2.537	2.488	2.347
Thermal Efficiency [-]					
Load [%]	25	50	75	85	100
25	0.209	0.121	0.085	0.076	0.062
50	0.318	0.209	0.155	0.140	0.118
75		0.270	0.209	0.190	0.162
85		0.290	0.230	0.209	0.179
100		0.293	0.267	0.246	0.209
Generator Power [kW]					
Load [%]	25	50	75	85	100
25	171.6	184.5	182.9	181.3	177.2
50	243.6	280.7	292.8	295.3	298.9
75		338.2	361.8	368.4	377.6
85		359.7	390.2	395.9	407.0
100		401.9	443.8	453.5	459.9

Table F.6: Off design performance data for cyclopentane based recuperative-ORC in generater load 2/2

Table F.7: Off design performance data for cyclopentane based recuperative-ORC in propeller load 1/2

Cyclopentane-RecuperativeORC-Propeller Load					
Net Power [kW]					
	Design Point [-]				
Load [%]	25	50	75	85	100
25	52.0	50.7	36.9	32.4	22.1
50		188.3	202.9	201.5	191.7
75		243.4	314.2	324.4	331.9
85		236.8	344.7	359.7	372.6
100			339.6	445.9	469.2
Net Energy Efficiency [-]					
Load [%]	25	50	75	85	100
25	0.128	0.125	0.091	0.080	0.054
50		0.135	0.146	0.144	0.137
75		0.096	0.124	0.128	0.131
85		0.079	0.115	0.120	0.124
100			0.092	0.121	0.128
Net Exergy Efficiency [-]					
Load [%]	25	50	75	85	100
25	0.322	0.314	0.228	0.200	0.137
50		0.339	0.366	0.363	0.346
75		0.267	0.345	0.356	0.364
85		0.225	0.327	0.342	0.354
100			0.243	0.319	0.335
Turbine Power [kW]					
Load [%]	25	50	75	85	100
25	62.2	63.3	52.0	48.5	41.9
50		213.1	229.8	229.5	223.4
75		289.8	355.6	366.4	376.6
85		308.9	393.2	408.1	422.7
100			512.1	539.1	540.2

Table F.8: Off design performance data for cyclopentane based recuperative-ORC in propeller load 2/2

Cyclopentane-RecuperativeORC-Generator Load					
Pump Power [kW]					
	Design Point				
Load [%]	25	50	75	85	100
25	3.53	4.59	5.88	6.49	8.94
50		12.09	12.61	13.27	15.96
75		29.54	20.19	19.95	21.09
85		54.23	24.14	23.12	23.10
100			136.63	52.65	30.69
Net Power Density [kW/m^3]					
Load [%]	25	50	75	85	100
25	0.917	0.458	0.244	0.196	0.117
50		1.702	1.340	1.219	1.014
75		2.200	2.075	1.963	1.755
85		2.140	2.277	2.176	1.970
100			2.243	2.698	2.481
Thermal Efficiency [-]					
Load [%]	25	50	75	85	100
25	0.209	0.050	0.021	0.016	0.010
50		0.209	0.112	0.093	0.069
75		0.314	0.209	0.179	0.138
85		0.317	0.241	0.209	0.161
100			0.253	0.269	0.209
Generator Power [kW]					
Load [%]	25	50	75	85	100
25	55.9	55.5	43.0	39.0	31.2
50		201.6	216.3	215.5	208.3
75		275.3	336.3	345.9	354.3
85		293.4	371.6	385.0	397.4
100			480.1	503.0	502.8

G

Dynamic Analysis Data

Load-Drop DP:100%							
100→25				75→50			
[kW]	169.6	163.1	161.5		277	266.4	263.8
[s]	5%	1%	0.10%	[s]	5%	1%	0.10%
1	1632	3079	7703	1	588	1247	5078
5	1627	3048	7840	5	589	1248	5069
10	1624	3085	7663	10	584	1255	5106
60	1594	3038	7707	60	550	1223	4823
120	1575	3005	7621	120	534	1199	4597
100→50				50→25			
[kW]	277	266.4	263.8		169.6	163.1	161.5
[s]	5%	1%	0.10%		5%	1%	0.10%
1	718	1397	5468		1330	2769	7369
5	717	1396	5402		1327	2788	7445
10	714	1399	5334		1326	2797	7554
60	689	1370	5436		1300	2729	7529
120	665	1340	5503		1271	2700	7400
100→75				75→25			
[kW]	349.1	335.9	332.5		169.6	163.1	161.5
[s]	5%	1%	0.10%		5%	1%	0.10%
1	284	695	2074		1556	3006	7666
5	282	695	2421		1554	3033	7490
10	280	694	2384		1553	2978	7897
60	256	665	2195		1524	2992	7659
120	229	638	2381		1496	2928	7752
100→85				85→25			
[kW]	376.1	361.8	358.2		169.6	163.1	161.5
[s]	5%	1%	0.10%		5%	1%	0.10%
1	150	477	1748		1590	3017	7861
5	149	472	1891		1588	3057	7796
10	146	475	1780		1577	3042	7827
60	122	449	1897		1567	3038	7838
120	95	420	1624		1527	2991	7499
85→75				85→50			
[kW]	349.1	335.9	332.5		277	266.4	263.8
[s]	5%	1%	0.10%	[s]	5%	1%	0.10%
1	102	508	1804	1	665	1333	5055
5	96	502	1895	5	658	1329	5098
10	78	491	1689	10	656	1325	5176
60	53	463	1898	60	629	1310	4884
120	33	436	1759	120	605	1275	5231

Table G.1: Load-drop analysis data for design point of 100%

Load Drop Design Point:85%							
85→25				75→50			
[kW]	172.3	165.7	164.1	[kW]	273.7	263.3	260.7
[s]	5%	1%	0.10%	[s]	5%	1%	0.10%
1	1504	2822	5498	1	530	1141	3514
5	1506	2833	5772	5	527	1161	3336
10	1495	2846	5623	10	524	1125	3430
60	1473	2809	5533	60	504	1150	3356
120	1431	2733	5636	120	476	1099	3224
85→50				50→25			
[kW]	273.7	263.3	260.7		172.3	165.7	164.1
[s]	5%	1%	0.10%		5%	1%	0.10%
1	600	1219	3395		1249	2567	5180
5	597	1261	3278		1254	2579	5399
10	593	1212	3490		1247	2566	5446
60	571	1202	3351		1219	2521	5248
120	541	1158	3525		1185	2506	5395
85→75				75→25			
[kW]	340	327	323.8		172.3	165.7	164.1
[s]	5%	1%	0.10%		5%	1%	0.10%
1	86	482	1769		1478	2785	5472
5	85	474	1811		1470	2804	5724
10	82	474	1878		1456	2761	5561
60	59	453	1712		1445	2756	5662
120	31	415	1806		1408	2704	5635

Table G.2: Load-drop analysis data for design point of 85%

Load Drop Design Point:75%						
	75→25					
kW	172.7	166.1	164.5			
[s]	5%	1%	0.10%			
1	1378	2653	8280			
5	1382	2634	8417			
10	1383	2637	8284			
60	1354	2625	8255			
120	1301	2539	8187			
	75→50			50→25		
kW	271.1	260.8	258.2	172.7	166.1	164.5
[s]	5%	1%	0.10%	5%	1%	0.10%
1	516	1092	2976	1171	2408	8335
5	513	1101	2836	1164	2434	8114
10	510	1065	2764	1164	2413	8052
60	486	1063	2792	1132	2403	8003
120	459	1020	2583	1107	2344	8071

Table G.3: Load-drop analysis data for design point of 75%

Load Drop Design Point:50%			
	50→25		
kW	169.8	163.3	161.7
[s]	5%	1%	0.10%
1	916	1669	3940
5	909	1703	3848
10	912	1670	3873
60	890	1642	3908
120	852	1636	3635

Table G.4: Load-drop analysis data for design point of 50%

Load Rise Design Point:100%						
	25→50			50→75		
kW	250.6	261.2	263.9	315.9	329.2	332.5
[s]	5%	1%	0.10%	5%	1%	0.10%
1	1055	1795	3502	497	987	3804
5	1055	1790	3482	503	1003	3671
10	1046	1769	3806	495	1006	4019
60	1025	1760	3229	471	951	3974
120	997	1735	3481	446	931	3982
	25→75			75→85		
kW	315.9	329.2	332.5	340.3	354.6	358.2
[s]	5%	1%	0.10%	5%	1%	0.10%
1	955	1474	4499	27	431	3665
5	955	1465	4794	81	481	3420
10	951	1462	4831	80	484	3614
60	926	1451	4623	52	455	3510
120	895	1412	4416	26	432	3408
	25→85			85→100		
kW	340.3	354.6	358.2	384.3	400.5	404.5
[s]	5%	1%	0.10%	5%	1%	0.10%
1	909	1370	5668	150	452	1919
5	907	1365	5912	130	436	1761
10	903	1367	5886	127	430	1736
60	874	1334	5612	104	403	1743
120	846	1302	5787	76	377	1663
	25→100			50→100		
kW	384.3	400.5	404.5	384.3	400.5	404.5
[s]	5%	1%	0.10%	5%	1%	0.10%
1	830	1240	3230	516	908	3015
5	830	1238	3333	512	901	2817
10	825	1230	3212	511	905	3049
60	800	1204	3174	486	875	2953
120	771	1178	3138	456	849	2886
	50→85			75→100		
kW	340.3	354.6	358.2	384.3	400.5	404.5
[s]	5%	1%	0.10%	5%	1%	0.10%
1	531	984	4861	245	582	2350
5	527	981	4813	239	589	2130
10	526	986	5065	237	583	2121
60	499	961	4815	211	555	2059
120	471	924	4775	184	532	2045

Table G.5: Load-rise analysis data for design point of 100%

Load Rise Design Point:85%						
	25→50			50→75		
kW	247.7	258.1	260.7	307.6	320.6	323.8
[s]	5%	1%	0.10%	5%	1%	0.10%
1	928	1693	3630	477	947	3089
5	928	1705	3953	473	943	2838
10	921	1684	3905	472	935	2810
60	895	1647	3497	446	914	2836
120	865	1617	3857	415	889	2743
	25→75			75→85		
kW	307.6	320.6	323.8	330.4	344.3	347.8
[s]	5%	1%	0.10%	5%	1%	0.10%
1	913	1392	3741	74	455	2693
5	911	1394	3701	115	492	2857
10	907	1381	4033	52	432	2788
60	881	1326	3605	43	425	2737
120	848	1335	3941	17	392	2742
	25→85			50→85		
kW	330.4	344.3	347.8	330.4	344.3	347.8
[s]	5%	1%	0.10%	5%	1%	0.10%
1	865	1297	4855	503	928	3935
5	865	1296	4727	501	910	3942
10	863	1302	4842	497	919	3802
60	837	1279	4657	472	896	3935
120	806	1240	4521	442	860	3842

Table G.6: Load-rise analysis data for design point of 85%

Load Rise Design Point:75%						
	25→50			50→75		
kW	245.4	255.7	258.3	301.6	314.3	317.5
[s]	5%	1%	0.10%	5%	1%	0.10%
1	873	1572	4166	456	909	2978
5	867	1561	4125	454	890	2731
10	861	1571	3836	450	891	2690
60	842	1541	3801	422	866	2737
120	812	1491	3899	376	818	2934
	25-75					
kW	301.6	314.3	317.5			
[s]	5%	1%	0.10%			
1	860	1276	3594			
5	859	1310	3775			
10	853	1303	3637			
60	823	1273	3769			
120	800	1250	3502			

Table G.7: Load-rise analysis data for design point of 75%

Load Rise Design Point:50%			
	25→50		
kW	232.6	242.4	244.8
[s]	5%	1%	0.10%
1	683	1148	3014
5	681	1141	3098
10	680	1157	2803
60	652	1137	2837
120	625	1097	2795

Table G.8: Load-rise analysis data for design point of 50%

Diesel Mode (SWD12V280) P_cyl = 305kW; Generator Load						
Load [%]	P_B [kW]	Speed [rpm]	p_eg [Pa]	T_eg [K]	m_eg [kg/s]	x [-]
25	915	1000	102240	754	2.4	0.437
30	1098	1000	102325	748	2.8	0.4374
40	1464	1000	102547	731	3.6	0.4337
50	1830	1000	102820	711	4.5	0.428
55	2013	1000	102985	702	5	0.4251
70	2562	1000	103510	684	6.2	0.4247
75	2745	1000	103700	681	6.6	0.427
85	3111	1000	104080	679	7.3	0.435
100	3660	1000	104660	688	8.2	0.455

Table G.9: Engine and exhaust data of SWD12V280 coupled to generator with additional load points

Design Point: 100%			
	25→30		
[kW]	177.6	185	186.9
[s]	5%	1%	0.10%
60	351	1473	4601
	25→40		
[kW]	216.1	225.2	227.5
[s]	5%	1%	0.10%
60	833	1853	4750
	25→75		
[kW]	315.9	329.2	332.5
[s]	5%	1%	0.10%
60	927	1441	4509
	25→100		
[kW]	384.3	400.5	404.5
[s]	5%	1%	0.10%
60	804	1202	3186

Table G.10: Load-drop and Load-rise analysis data for design point of 100% with additional load points including 30%

Design Point :100%											
	25→40				40→25				40→55		
[kW]	216.1	225.2	227.5	[kW]	169.6	163.1	161.5	[kW]	267.7	279	281.8
[s]	5%	1%	0.10%	[s]	5%	1%	0.10%	[s]	5%	1%	0.10%
15	894	1850	4764		1060	2500	7432	15	575	1230	3269
60	826	1836	4758		1032	2473	7374	60	548	1208	2981
	25→55				55→25				40→70		
[kW]	267.7	279	281.8	[kW]	169.6	163.1	161.5	[kW]	303.1	315.8	319
[s]	5%	1%	0.10%	[s]	5%	1%	0.10%	[s]	5%	1%	0.10%
30	1024	1698	3482		1399	2865	7425	30	670	1205	2647
60	1008	1659	3908		1375	2807	7567	60	652	1163	2542
	25→70				70→25				40→85		
[kW]	303.1	315.8	319	[kW]	169.6	163.1	161.5	[kW]	340.3	354.6	358.2
[s]	5%	1%	0.10%	[s]	5%	1%	0.10%	[s]	5%	1%	0.10%
45	959	11542	13237		1504	2964	7902	45	658	1111	5364
60	952	1488	2941		1505	2960	7718	60	649	1099	5504
	25→85				85→25				40→100		
[kW]	340.3	354.6	358.2	[kW]	169.6	163.1	161.5	[kW]	384.3	400.5	404.5
[s]	5%	1%	0.10%	[s]	5%	1%	0.10%	[s]	5%	1%	0.10%
60	874	1334	5612		1567	3038	7838	60	606	1004	2901
	25→100				100→25				55→70		
[kW]	384.3	400.5	404.5	[kW]	169.6	163.1	161.5	[kW]	303.1	315.8	319
[s]	5%	1%	0.10%	[s]	5%	1%	0.10%	[s]	5%	1%	0.10%
75	795	1200	3423		1583	3020	7838	15	336	864	2209
60	800	1204	3174		1594	3038	7707	60	234	762	2233
	55→40				55→85				85→55		
[kW]	238.9	229.8	227.5	[kW]	340.3	354.6	358.2	[kW]	295.9	284.6	281.8
[s]	5%	1%	0.10%	[s]	5%	1%	0.10%	[s]	5%	1%	0.10%
15	652	1417	3565	30	428	883	4607		504	1091	2862
60	629	1410	3679	60	416	862	4522		496	1092	3293
	70→40				55→100				100→55		
[kW]	238.9	229.8	227.5	[kW]	384.3	400.5	404.5	[kW]	295.9	284.6	281.8
[s]	5%	1%	0.10%	[s]	5%	1%	0.10%	[s]	5%	1%	0.10%
30	849	1600	3820	45	431	816	2722		575	1167	3246
60	828	1596	3950	60	423	808	2851		565	1155	3073
	85→40				70→85				85→70		
[kW]	238.9	229.8	227.5	[kW]	340.3	354.6	358.2	[kW]	335	322.2	319
[s]	5%	1%	0.10%	[s]	5%	1%	0.10%	[s]	5%	1%	0.10%
45	931	1693	4148	15	189	614	3911		209	671	2678
60	922	1684	4110	60	166	591	4250		189	660	3140
	100→40				70→100				100→70		
[kW]	238.9	229.8	227.5	[kW]	384.3	400.5	404.5	[kW]	335	322.2	319
[s]	5%	1%	0.10%	[s]	5%	1%	0.10%	[s]	5%	1%	0.10%
				30	283	652	2536		344	809	3893
60	967	1753	3957	60	265	636	2542		329	797	3855
	70→55				85→100				100→85		
[kW]	295.9	284.6	281.8	[kW]	384.3	400.5	404.5	[kW]	376.1	361.8	358.2
[s]	5%	1%	0.10%	[s]	5%	1%	0.10%	[s]	5%	1%	0.10%
15	339	920	2622	15	124	10444	11930		143	472	1796
60	319	921	2683	60	104	403	1743		122	449	1897

Table G.11: Load-drop and Load-rise analysis data for design point of 100% with additional load points

Design Point:75%											
	25→40				40→25				40→55		
[kW]	215.6	224.6	226.9	[kW]	172.7	166.1	164.5	[kW]	259.9	270.9	273.6
[s]	5%	1%	0.10%	[s]	5%	1%	0.10%	[s]	5%	1%	0.10%
15	751	1598	4726		916	2088	7698	15	500	1113	2488
60	733	1581	5037		838	2096	8078	60	472	1087	2487
	25→55				55→25				40→70		
[kW]	259.9	270.9	273.6	[kW]	172.7	166.1	164.5	[kW]	290.3	302.5	305.6
[s]	5%	1%	0.10%	[s]	5%	1%	0.10%	[s]	5%	1%	0.10%
30	867	1500	3092		1235	2500	8273	30	615	1082	2750
60	858	1475	3083		1216	2444	8186	60	600	1069	2643
	25→70				70→25				40→85		
[kW]	290.3	302.5	305.6	[kW]	172.7	166.1	164.5	[kW]	324.6	338.3	341.7
[s]	5%	1%	0.10%	[s]	5%	1%	0.10%	[s]	5%	1%	0.10%
45	856	1313	3324		1340	2580	8323	45	601	998	2800
60	853	1322	3466		1330	2617	8303	60	593	989	2791
	25→85				85→25				40→100		
[kW]	324.6	338.3	341.7	[kW]	172.7	166.1	164.5	[kW]	369.2	384.7	388.6
[s]	5%	1%	0.10%	[s]	5%	1%	0.10%	[s]	5%	1%	0.10%
60	786	1193	3213		1380	2603	8571	60	516	786	1376
	25→100				100→25				55→70		
[kW]	369.2	384.7	388.6	[kW]	172.7	166.1	164.5	[kW]	290.3	302.5	305.6
[s]	5%	1%	0.10%	[s]	5%	1%	0.10%	[s]	5%	1%	0.10%
75	669	957	2049		1344	2607	8295	15	274	746	2137
60	680	964	2090		1359	2634	8382	60	247	722	2152
	55→40				55→85				85→55		
[kW]	238.2	229.2	226.9	[kW]	324.6	338.3	341.7	[kW]	287.3	276.3	273.6
[s]	5%	1%	0.10%	[s]	5%	1%	0.10%	[s]	5%	1%	0.10%
15	552	1295	3194	30	391	771	2300		444	962	4028
60	534	1237	3349	60	376	756	2281		438	920	3907
	70→40				55→100				100→55		
[kW]	238.2	229.2	226.9	[kW]	369.2	384.7	388.6	[kW]	287.3	276.3	273.6
[s]	5%	1%	0.10%	[s]	5%	1%	0.10%	[s]	5%	1%	0.10%
30	731	1474	3576	45	363	598	1380		452	853	3701
60	706	1446	3207	60	360	590	1410		448	833	3768
	85→40				70→85				85→70		
[kW]	238.2	229.2	226.9	[kW]	324.6	338.3	341.7	[kW]	320.9	308.7	305.6
[s]	5%	1%	0.10%	[s]	5%	1%	0.10%	[s]	5%	1%	0.10%
45	782	1506	3648	15	180	528	1490		188	533	2475
60	775	1497	3584	60	158	506	1315		172	513	2529
	100→40				70→100				100→70		
[kW]	238.2	229.2	226.9	[kW]	369.2	384.7	388.6	[kW]	320.9	308.7	305.6
[s]	5%	1%	0.10%	[s]	5%	1%	0.10%	[s]	5%	1%	0.10%
				30	248	441	1487		289	515	1319
60	762	1433	3264	60	235	426	1470		253	481	1211
	70→55				85→100				100→85		
[kW]	287.3	276.3	273.6	[kW]	369.2	384.7	388.6	[kW]	358.8	345.1	341.7
[s]	5%	1%	0.10%	[s]	5%	1%	0.10%	[s]	5%	1%	0.10%
15	302	848	3236	15	130	301	1597		146	330	1920
60	274	821	3133	60	111	286	1533		125	313	1632

Table G.12: Load-drop and Load-rise analysis data for design point of 75% with additional load points

H

Literature Study on Energy Storage

This appendix contains a brief literature study on energy storage devices currently used in various industries. A direction towards which device may be suited for marine application in terms of technology development and flexibility is tried to be captured.

H.1. Energy Storage System (ESS)

Reduction of air emissions from electricity generation is a potentially important incidental benefit of energy storage (ER) use. Energy Storage refers to a process of converting electrical energy from a power network into a form that can be stored for converting back to electrical energy when needed.

ESS have many advantages, such as: capable of meeting short-term, random fluctuations in demand; Eliminates voltage sags and surges; Eliminates the necessity of having part-loaded main plant which is held in readiness to meet sudden and unforeseen demands; Eliminates the need of having redundant power generating units on standby for power emergencies which arise from the failure of generating units and/or transmission lines; Capable of storing surplus electrical energy generated; Capable of meeting peak electrical load demands; Provides time varying energy management; Capable of improving power quality and reliability; Capable of assisting with the management of distributed and standby power generation system [Kousksou et al., 2014; Luo et al., 2015].

Through various energy storage system applications, it is also considered to be multi-beneficial to both the utilities and their customers since the application improves operational efficiency of the system, reduces the primary fuel consumption by conserving energy, provides certainty of energy supply and decreases environmental impacts.

Energy storage systems in a power system can be defined as any installation or method which is usually subject to an independent control. With the assistance of energy storage systems, it is possible to convert and store electrical energy generated by the power system in any appropriate form and reconvert back to electrical energy when necessary. Basically, energy storage is used in the power system in three different modes: charging, storing and discharging. During each of these modes, a balance between power and energy in the power system has to be maintained so that the energy storage system has to have the appropriate rated power and energy capacity. For the need to satisfy different applications, different energy storage technologies are available based on their characteristics unique to specific applications.

Generally, energy storage systems can be classified as either electrical energy storage systems or thermal energy storage systems. Electrical energy storage (EES) system includes a wide range of technologies, which provides electrical energy storage either directly or indirectly through an electrical input and output. Storage of that energy can be in other forms and those principle technologies are: mechanical storage, such as flywheel energy storage, pumped hydroelectric storage and compressed air energy storage; electrochemical storage, such as battery and flow battery; electrical storage, such

as capacitor, super-capacitor and superconducting magnetic; chemical storage, such as hydrogen [Kousksou et al., 2014]. Storage of electricity can be achieved effectively, however, it is often transformed into another form of storable energy and reconverted back into electricity whenever required for immediate consumption [Ibrahim et al., 2008]. Thermal energy storage systems are used to provide heating or cooling resources by utilizing either the thermochemical reactions, sensible or latent heat latent heat capacity of materials, which can be replenished as required [Kousksou et al., 2014].

H.1.1. Electrical Energy Storage System

Electricity is the most preferred form of energy for most applications as it is the most versatile, because, it can be readily transmitted over long distances and it can be distributed to consumers by cables, however there is often the issue of matching the supply to meet the demand. The frequently encountered issue of mismatch has lead to the development and application of systems for the efficient storage of electricity. Electric energy storage is the capability of storing energy in any form and reconvert into electricity for use during other periods when the use or cost is more beneficial.

H.1.1.1 Battery Energy Storage

Batteries are an electrochemical devices that has the ability to deliver the energy in electrical form from the chemical energy generated by electrochemical reactions. When a load is connected to the cell's terminals, these reactions are triggered inside a basic cell, between between two electrodes plunged into an electrolyte. These reactions are the transfer of electrons from one electrode to the other through an external electric circuit. Generally, a battery consists of a single cell or multiple cells that may be connected in series or parallel or both to each other, depending on the desired voltage output and capacity. A basic battery cell consists of an anode, cathode, electrolyte and separator. The anode is the negative electrode which provides electrons to the load connected and is oxidized during the electrochemical reaction. The cathode is the positive electrode which accepts the electrons and is reduced during the reaction. The electrolyte provides the medium for transfer of electrons between the anode and the cathode. The separator is used for electrical insulation between the positive and negative electrodes.

During discharging mode, a flow of electrons through an external circuit is generated due to electrochemical reactions at the two electrodes. In charging mode, the electrochemical reactions are reversed through the application of external voltage across the electrodes. Materials used as electrodes and electrolyte are the main difference between different battery systems and also determine the specific characteristics o the batteries. Lead acid battery, nickel based battery, sodium sulfur battery and lithium based battery are those battery systems that are either in use and/or potentially suitable for utility scale battery energy storage applications.

H.1.1.2 Flywheel Energy Storage (FES)

The core of the system contains a mass rotating about its axis on two magnetic bearings in order to decrease friction at high speeds and is mechanically coupled with an electric machine. This core structure is entirely placed in a vacuum chamber to reduce wind shear, Figure H.1 depicts the basic features of a flywheel storage system. Principally, the energy is transferred to the flywheel and stored as kinetic energy when the electric machine works as a motor, thus charging this storage device. When necessary, the FES discharges this kinetic energy back into the electric machine which then operates as a generator. The Kinetic energy stored in the flywheel during charging, is proportional to the mass and the square of its rotating speed. The tensile strength of the flywheel material ultimately limits the maximum storability of the energy storage system and the energy density of the flywheel energy storage depends on the product of a shape factor, considering the inertia of the rotating disk and the permissible tangential strength of the disk which depends on its material. The maximum specific energy of the FES is defined by the ratio of the energy density and the density of the material of the rotating disk [Kousksou et al., 2014].

Basic FES system consists of a flywheel (also known as a rotor), an electric machine (that works as a motor as well as a generator), rotor bearings and power electronic interface. Currently, this system is applied to various applications. However, the ship network is very different from land-based grid system, because the ship operates in a wide variety of operating conditions and these conditions vary from ship to ship. Moreover, the ship power network quality changes frequently in a wide range. Mostly, a critical problem of a fully electric ship is the voltage fall that is induced by the high power pulse electrical equipment. To resolve this critical issue, an energy storage technology is a promising solution [G et al., 2017].

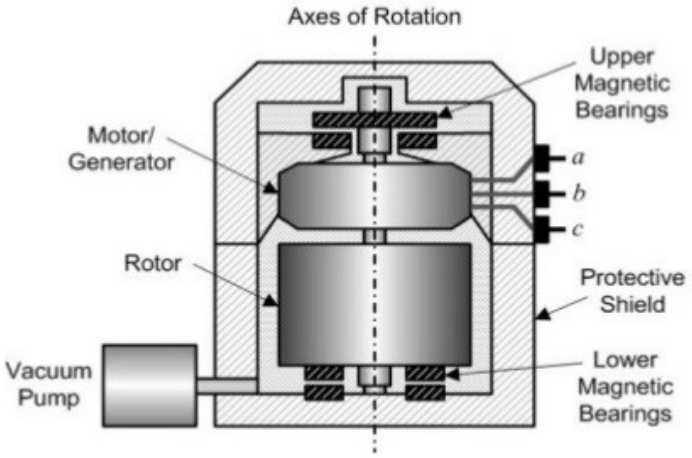

Figure H.1: The flywheel storage system [Molina, 2010]

FES has very high number of charge/discharge cycles and is independent of the temperature and the depth of the discharge. Therefore, the lifetime of FES system is more than 20 years and the disposal does not have any environmental concerns. Monitoring the state of charge of an FES system is simple and reliable since only the rotational speed of the flywheel is needed to know. The disadvantages of an FES systems are its relatively poor energy density and large standby losses. Moreover, the self-discharge rates for the complete system is about 20% of the stored capacity per hour. These are the primary factors for not considering FES system as an adequate devices for long-term energy storage. This FES technology may be used based on the application, for example in formula racing. The main limitation to widespread use of FES systems is the high costs due to profound precision engineering involved. As of now, the research focuses on improving the materials and the manufacturing processes to achieve a long-term mechanical stability of the system, decrease the losses to the rotor bearings and the cost reductions. Moreover, the safety aspects and containment of these systems for mobile applications are research challenges.

H.1.1.3 Compressed Air Energy Storage (CAES)

This type of storage system works by storing energy in compressed air form in an air reservoir, by means of a compressor powered by off-peak/low-cost electric energy. This system requires a unique clutch to allow the turbine/generator to operate in both directions, where rotation is one direction is while charging and the other is for discharging the energy.

Figure H.2 depicts a schematic of a basic compressed air storage system. In charging mode, the generator operates as a motor to provide mechanical power to operate the compressor, which compresses atmospheric air into the air reservoir. During discharging mode, the plant uses the compressed air from the air reservoir to operate its combustion turbine. Fuel, such as natural gas is burned during the plant discharge, in the same manner as gas generation in a conventional combustion turbine plant. As the turbine is mechanically coupled to the generator, it generates electricity. Presently, the application of compressed air storage system is not widespread, and there are currently two land based plants; one in Germany of 290 MW and the other in the USA of 110MW [Kousksou et al., 2014]. CAES systems have high initial capital costs, slow response, and limitations in terms of location [Ferreira et al., 2013].

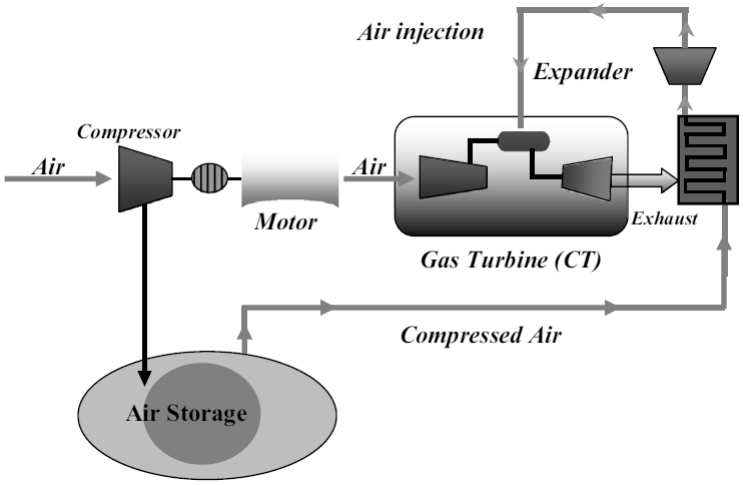

Figure H.2: A basic compressed air storage system [Kousksou et al., 2014]

H.1.1.4 Pumped Hydroelectric Energy Storage (PHES/PHS)

This type of energy storage system uses a method of storing and producing electricity to supply high peak demands by pumping water from a lower reservoir to an upper reservoir. A typical pumped hydroelectric system plant uses two water reservoirs that are separated vertically to use potential energy to operate a turbine to generate electricity, as shown in Figure H.3. The water is pumped from the lower reservoir to the upper reservoir during off-peak electricity demand hours and during high peak hours, the water from the upper reservoir is released back into the lower reservoir through a turbine-generator set that converts the potential energy into electrical energy. The quantity of energy stored depends on the height difference between the two reservoirs and the total volume of water stored.

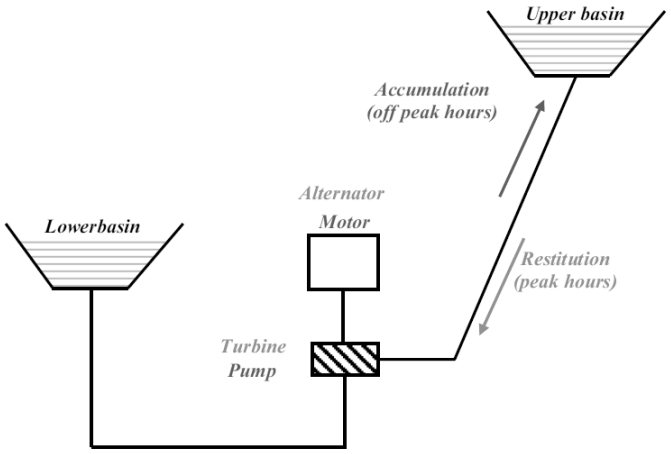

Figure H.3: The pumped hydro storage system [Kousksou et al., 2014]

Water pressure, flow rate through the turbines and rated power of the pump/turbine and generator/motor units determines the rated power of the pumped hydroelectric plant. During charging and discharging, the pumping and generation respectively can be accomplished either by using a single-unit, reversible pump-turbines or by separate pumps and turbines. Based on the installed equipment(s), the switching between pumping and generating can occur within minutes. Due to its relatively low energy density, the pumped hydroelectric plant requires either a very large volume of water or a large difference in height between the two reservoirs.

H.1.1.5 Hydrogen Storage Systems (with fuel-cells)

One of the most efficient, cleanest and lightest fuels is hydrogen, however it must be produced from other primary energy sources since it is not found naturally. Despite this fact, it is expected to play a significant role in the future energy systems. Hydrogen, like electricity, must be produced and transported. One main advantage of hydrogen is it's storage application, unlike electricity, which must be consumed as it is produced or it can be stored if converted to another energy form. Hydrogen on the other hand, can be produced and stored for direct usage in fuel cells, or can be transported to other consumers to produce electricity. Figure H.4 represent the basic feature of a simple hydrogen fuel cell that uses hydrogen fuel and oxygen to produce electricity and water in generation mode and a reversible hydrogen fuel cell uses electricity to split water molecules to produce hydrogen and oxygen, and this hydrogen produced is stored for later consumption.

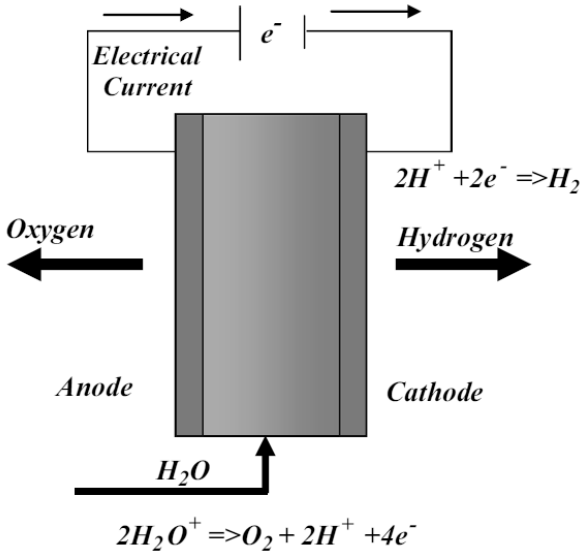

Figure H.4: Hydrogen fuel cell [Kousksou et al., 2014]

The essential parts of a hydrogen fuel cell consists of an electrolyzer unit, used to convert the electrical energy input to split water into hydrogen and oxygen, the hydrogen storage system itself and a hydrogen energy conversion, used to reconvert the stored chemical energy in the hydrogen back into electrical energy. By means of these elements, the water molecules are electrolytically decomposed into hydrogen and oxygen. There are other concepts of hydrogen fuel cells, and the main technologies include Proton Exchange Membrane Fuel Cells (PEM-FCs), Alkaline Fuel Cells (AFCs), Phosphoric Acid Fuel Cells (PAFCs) and Regenerative Fuel Cells (RFCs). This technology of energy storage in chemical form possess many advantages, such as high energy density, applicability at small and large scale and simple modular use. The lifetime and cycle life of this system is estimated at more than 15 years and 20,000 charge and discharge cycles respectively. However, these systems are currently expensive and have a very low round trip efficiency (20-50%). Hence, it is a major R&D challenge to reduce the cost of a hydrogen fuel cell [Kousksou et al., 2014].

H.1.1.6 Capacitor and Super-capacitor

These systems are used to store electricity in electrical energy form. Capacitors are used to store energy as electric charge in between two metal or conductive plates that are separated by a dielectric membrane that acts as an insulating material, when a voltage differential is applied across the plates. One of the two plates will have induced in a charge of the opposite sign, when the other plate is charged with electricity from a direct current source. The size of the plates, the separation of the plates, and the type of material used for the dielectric are factors that determine the capacitance of a capacitor.

The amount of energy stored in a capacitor is directly proportional to their capacity and the square of the voltage between the terminals of the electrochemical cell. The capacity if proportional to the distance between the electrodes. Capacitors are widely being used in many utility power control applications. Long cycle life and immediate recharge capability are some of the notable advantages if a capacitor used for small energy storage and short discharge use. However, the most significant disadvantage of a capacitor is the low energy density. The usage of large capacitors is uneconomical and often inconvenient because for large capacity, a very large dielectric is required.

A super-capacitor works on the same principle as a capacitor except for the fact that the insulating material is replaced by electrolyte ionic conductor. In an electrolyte ionic conductor, the movement of

the ions are made along a conducting electrode with a very large specific surface providing higher energy density to the system. Super-capacitor as an energy storage device have very high power output and the current energy storage systems under trial reach approximately 50–100 kW. The energy stored will supply the load only for a few seconds to minutes for most applications. Compared to battery storage systems, the in-out efficiency of super-capacitors are very high, however the self-discharge rate is considerable high. But the primary disadvantage in using super-capacitors as energy storage is is high costs, estimated at 5 times more than that of cost of lead acid batteries [Kousksou et al., 2014] and super-capacitors have a low energy density [Ferreira et al., 2013].

H.1.1.7 Superconducting Magnetic Energy Storage (SMES)

The working principle of a superconducting magnetic energy storage system (SMES), when used as an energy storage device is that it stores electrical energy in a magnet field without conversion to chemical or mechanical forms. It is succeeded by inducing DC current into coil made of superconducting cables of nearly zero resistance. It is generally made of niobiumtitane (NbTi) filaments that operate at very low temperatures of around -270°C. The current increases and decreased during charging and discharging processes respectively and has to be converted for AC or DC voltage application.

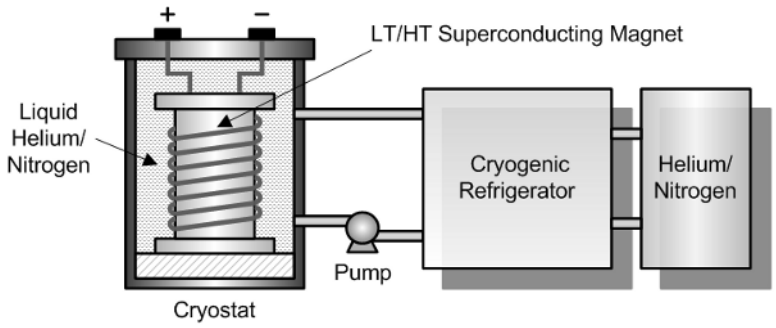

Figure H.5: Superconducting magnetic energy storage [Molina, 2010]

The basic schematic of a SMES system is shown in Figure H.5 and it is clear that considerable energy is required for refrigeration for the total system. There is relatively, significant resistive loses because the current flows through the non-superconducting components and solid-state switches. Despite these loses, the overall efficiency in commercial applications in the range of the MW is very high. Similar to batteries, the SMES system provides rapid response for either charge or discharge. However, the amount of energy available is independent of the discharge rating. Despite the mechanical stress in the components leading to material fatigue, the lifetime of the superconducting coil and the number of charge and discharge are significantly high and most likely exceed all other energy storage technologies [Nielsen and Molinas, 2010]. In spite of these features, there are very few SMES systems in use because of the high costs and the effects of the magnetic field.

H.1.2. Thermal Energy Storage (TES) System

Thermal energy storage (TES) systems are extensively identified as a technique to integrate renewable energies into the electricity production mix on the generation side, however its application on the demand side is also feasible. TES systems have established the capability to shift electrical loads from high-peak to off- peak hours. Hence, they have the ability to become a strong instrument in demand-side management programs. Thermal storage technology guarantees energy security, efficiency and environmental quality. It can also be established as a temporary storage of thermal energy at high or low temperatures. TES systems also have the capability of effectively increase the usage of thermal energy equipment and of facilitating large- scale switching. These systems are generally used for applications to correct the mismatch between supply and demand energy [Kousksou et al., 2014]. Figure H.6 represents the TES plant layout of their design.

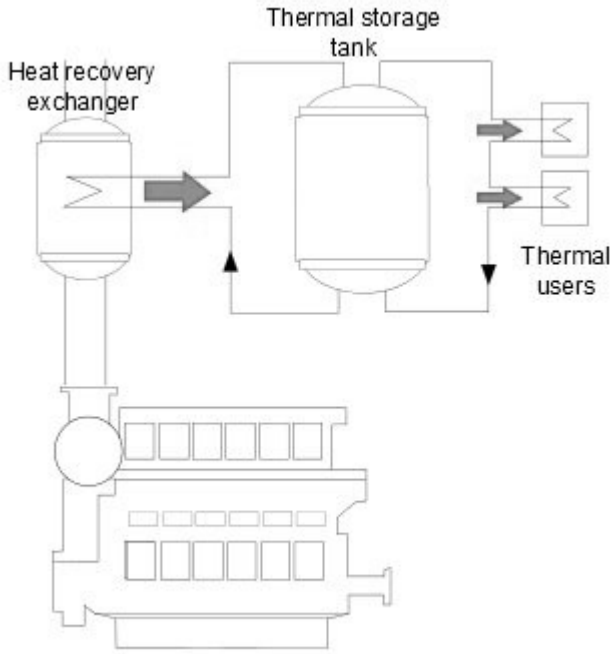

Figure H.6: TES plant layout [Baldi et al., 2015a]

H.1.2.1 Sensible Heat Storage

In a sensible heat storage system, the energy is stored by changing the temperature of the storage method. In this system, the quantity of heat energy stored is proportional to the density, specific heat, volume and variation of temperature of the storage material. Density and specific heat of the substance used, that affects the required volume are factors that mainly determines the performance of a storage system. Sensible TES systems usually requires large size and the temperature fluctuations caused from the sensible addition and extraction of energy are the main disadvantages. If large temperature fluctuations are permitted, then the storage size can be correspondingly reduced. However, the storage size of sensible TES systems will be higher, when compared to other storage technologies. Storage materials with large thermal capacities can be used to reduce the plant size. Apart from occupying large space and large costs, a large storage size also causes large thermal losses. In general, sensible TES systems consists of inlet/outlet devices, storage medium and a container, usually a tank. These tanks must not only retain the storage material but also prevent thermal energy losses. The presence of a thermal gradient across storage tank is highly recommended. The sensible heat storage medium can be liquids, like water, oil based fluids, molten salts, etc., or solids like rocks, metals and others. Generally, solid media are usually used in packed beds and require a fluid to exchange the heat [Kousksou et al., 2014].

H.1.2.2 Latent Heat Storage

In latent TES systems, the thermal medium changes phase, also known as phase change material (PCM), during the energy storage process. For a given substance, the latent heat is generally much higher than sensible heat. Hence, smaller storage volumes are required and the temperature difference during operation is almost zero because the phase change occurs at nearly constant temperatures. Based on the state of phase change, the PCMs can be solid-solid PCMs, solid-liquid PCMs or liquid-gas PCMs. Each of these PCMs are most suitable based on the application. Usually, in solid-liquid PCMs, practical difficulties in applying the latent heat method arises due to density change, stability of properties under extended cycling and occasionally phase segregation and super-cooling of the phase change materials. Disadvantage of latent TES system is the low thermal conductivity of the

phase change materials that limits the extractable power from the energy storage system [Kousksou et al., 2014]. Merlin et al. [2016] conducted an experimental study on the performance of using an enhanced conductivity latent heat thermal energy storage for industrial WHR and the conclusive results are encouraging for application for industrial usage, however the long-term stability of the composite material requires thorough investigation to know the feasibility of the concept.

H.1.2.3 Thermochemical Energy Storage

The working principle of thermochemical reaction storage uses the heat collected to excite a reversible endothermic chemical reaction. By reversing this reaction, the stored heat energy can be recuperated, occasionally by means of a catalyst. A phenomenon of fixation or capture of a sorbate (gas or vapor) by a substance in condensed state (solid or liquid; called sorbent) is called Sorption. This phenomena also includes thermo-physical and thermo-chemical aspects. Sorption is the general term used for absorption and adsorption. Absorption is defined as a process in which a liquid or a gas enters a solid or a liquid, however for storage applications, this term is usually related to the absorption of a gas by a liquid (absorbent). Similarly, adsorption is the term used for the process of binding a gas onto a surface of a solid or porous material, in other words, an attachment of gas or liquid phase of a component to the surface of another substance [Kousksou et al., 2014].

H.2. Battery Energy Storage System

Due to limitations in available space, varying operating profile, susceptibility towards sea hazards and environmental factor, many of the described energy storage systems may not be suitable for marine application. Batteries, however have higher energy density than PHS, CAES, SMES, Flywheel, TES, capacitors and super-capacitors, making battery sets lighter and smaller, which is highly suitable for marine use considering the weight and volume limitations. The lifetime durability of such battery sets can go up to 20 years which is generally the lifetime of the vessel itself. BESS have very low self-discharge rate and high storage duration compared to SMES, flywheel, capacitor and super-capacitor.

Unlike these storage technologies with discharge time within minutes, batteries have a discharge time of up to several hours, making it suitable for daily usage in auxiliary consumption on-board vessels. The power rating of batteries can go up to 50 MW, significantly higher than flywheel, SMES and super-capacitors. Efficiency of battery sets are higher than hydrogen storage system (for fuel-cell) and TES [Chen et al., 2009; Ferreira et al., 2013] Battery technology is very mature for power quality, ride-through capability, emergency back-up power, load leveling, peak shaving, motor starting, standing reserve, uninterrupted power supply (UPS),network fluctuation suppression, end-user electricity and service reliability [Luo et al., 2015].

The available types of battery technologies are lead-acid, nickel cadmium (Ni-Cd), nickel-metal hydride (NiMH), sodium-sulphur (NaS), sodium nickel-chloride (Na-Ni-Cl or zebra) and lithium ion (Li-ion). Lead-acid battery is a mature technology, however it has poor low-temperature performance, low durability and environmental concerns due to the lead toxicity. Nickel cadmium (Ni-Cd) batteries are also a mature technology used for its robustness to deep discharges, a long life cycle, temperature tolerance, and a higher energy density than lead-acid, however the drawbacks are, cadmium is a highly toxic material, expensive, requires advanced monitoring during charge and discharge.

Nickel-metal hydride (NiMH) batteries are a variant of NiCd, but unlike NiCd, this technology has a higher energy density and is more environmentally friendly because of the non-toxicity property of the materials used. However, this type of battery sets have high self-discharge rate and the consists of rare earth materials, making it infeasible for large scale applications. Sodium-sulphur (NaS) batteries have a working temperature in the region of 300°C which is a major disadvantage due to the need to maintain this high operating temperature and this technology may also have corrosive problems that could hamper its reliability. Sodium nickel-chloride (Na-Ni-Cl or zebra) battery sets have fast response, robustness to full discharge and a very high energy density. However, the costs involved are very high and has a high self-discharge rate [Ferreira et al., 2013].

	Technologies							
	Lead-acid	Ni−Cd	NiMH	Li-ion	NaS	Zebra	VRB	ZnBr
Power rating (MW)	0.001−50	0−46	0.01 to ∼MW	0.1−50	0.05−34	0.001−1	0.005−1.5	0.025−1
Discharge duration (h)	h	s−h	s−h	0.1−5	5−8	min−8h	s−8h	s−4h
Gravimetric energy density (Wh/Kg)	30−50	50−75	30−110	75−250	150−240	100−140	10−75	60−85
Volumetric energy density (Wh/L)	50−80	60−150	140−435	200−600	150−240	150−280	15−33	30−60
Power density (W/Kg)	75−300	150−230	250−2000	100−5000	150−230	130−245		50−150
Efficiency	70−92%	60−70%	60−66%	85−90%	75−90%	∼90%	65−85%	75 %−80%
Durability (years)	5−15 (∼10)	5−20	3−15	5−20	15	8−14	10−20	5−20
Durability (cycles)	500−1200	1000−2500	200−1500	1000−10,000	2000−5000	2500−3000	13,000+	∼2000
Capital cost ($/KW)	300−600	500−1500		1200−4000	1000−3000	150−300	600−1500	700−2500
Capital cost ($/KWh)	200−400	800−1500		600−2500	300−500	100−200	150−1000	150−1000
Technological maturity level (1− lower to 5 − higher)	5	4	4	4	4	4	3	2
Availability	99.997%	99%+	99%+	97%+	Up to 99.98%	99.9%+	96−99%	94%

Figure H.7: General table of current battery technologies and their characteristics[Ferreira et al., 2013]

On the other hand, lithium ion battery sets have very high efficiency and reliability, good energy density and slow self-discharge rate with an availability of over 97%. Despite being costly for medium and large scale power, its deployment for wide spread usage for its properties is decreasing the costs and the energy density may reach up to 30 MWh. This technology has a good development and maturity level with an efficiency and power rating of 85-90% and up to 50MW, which is either equal or higher than the other battery types.

Moreover the durability of Li-ion in number of cycles [Ferreira et al., 2013] and cycle life is higher than other types of battery sets [Chen et al., 2009]. These battery sets also have higher efficiency, longer lifetime and larger charge-discharge cycles than NaS, NiCd and flow battery sets [Hall and Bain, 2008]. Figure H.7 contains the table showing the characteristics of current battery technologies and it can be observed that Li-ion battery technology is suitable for marine applications.

Bibliography

Angelo Algieri and Pietropaolo Morrone. Comparative energetic analysis of high-temperature subcritical and transcritical organic rankine cycle (orc). a biomass application in the sibari district. Applied Thermal Engineering, 36:236–244, 2012.

Wendy C. Andersen and Thomas J. Bruno. Rapid screening of fluids for chemical stability in organic rankine cycle applications. Industrial and Engineering Chemistry Research, 44:5560–5566., 2005.

Jesper Graa Andreasen, Andrea Meroni, and Fredrik Haglind. A comparison of organic and steam rankine cycle power systems for waste heat recovery on large ships. Energies, 10(4), 2017.

O. Badr, S. D. Probert, and P. W. O'Callaghan. Selecting a working fluid for a rankine-cycle engine. Applied Energy, 21:1–42, 1985a.

O. Badr, S. D. Probert, and P. W. O'Callaghan. Selecting a working fluid for a rankine-cycle engine. Applied Energy, 21:1–42, 1985b.

Francesco Baldi and Cecilia Gabrielii. A feasibility analysis of waste heat recovery systems for marine applications. Energy, 80:654–665, 2015.

Francesco Baldi, Cecilia Gabrielii, Francesco Melino, and Michele Bianchi. A preliminary study on the application of thermal storage to merchant ships. Energy Procedia-ELSEVIER, 2015a.

Francesco Baldi, Ulrik Larsen, and Cecilia Gabrielii. Comparison of different procedures for the optimisation of a combined diesel engine and organic rankine cycle system based on ship operational profile. Ocean Engineering, 110:85–93, 2015b.

Charlotte Banks, Osman Turan, Atilla Incecik, G. Theotokatos, Sila Izkan, Catherine Shewell, and Xiaoshuang Tian. Understanding ship operating profiles with an aim to improve energy efficient ship operations. Low Carbon Shipping Conference, London 2013, 2013.

Junjiang Bao and Li Zhao. A review of working fluid and expander selections for organic rankine cycle. Renewable and Sustainable Energy Reviews, 24:325–342, 2013.

F.J. Bayley. The saturated liquid reservoir for energy storage in hybrid vehicles. Proceedings of the IMechE automobile division southern centre conference on total vehicle technology challenging current thinking, 2001.

S. Bellolio, V. Lemort, and P. Rigo. Organic rankine cycle systems for waste heat recovery in marine applications. 2015.

Giovanni Benvenuto, Alessandro Trucco, and Ugo Campora. Optimization of waste heat recovery from the exhaust gas of marine diesel engines. Journal of Engineering for the Maritime Environment, 230 (1):83–94, 2016.

Paola Bombarda, Costante M. Invernizzi, and Claudio Pietra. Heat recovery from diesel engines: a thermodynamic comparison between kalina and orc cycles. Applied Thermal Engineering, 30: 212–219, 2010.

Erik-Jan Boonen. Advanced waste heat recovery for 4-stroke diesel engines onboard ships. TU Delft Master Thesis, 2009.

Haisheng Chen, Thang Ngoc Cong, Wei Yang, Chunqing Tan, Yongliang Li, and Yulong Ding. Progress in electrical energy storage system: A critical review. Progress in Natural Science, 19:291–312, 2009.

Huijuan Chen, D. Yogi Goswami, and Elias K. Stefanakos. A review of thermodynamic cycles and working fluids for the conversion of low-grade heat. Renewable and Sustainable Energy Reviews, 14(9):3059–3067., 2010.

CIMAC Congress. Energy Saving Technologies and New Analysis Methods in Cargo Ship Machinery Design. CIMAC Congress, Helsinki, June 6 - 10, 2016, page 2016|310, 2016.

Santiago Surez de la Fuente, David Roberge, and Alistair R. Greig. Safety and co2 emissions: Implications of using organic fluids in a ship's waste heat recovery system. Marine Policy, 2016.

Gokmen Demirkaya, Saeb Besarati, Ricardo Vasquez Padilla, Antonio Ramos Archibold, D. Yogi Goswami, Muhammad M. Rahman, and Elias L. Stefanakos. Multi-objective optimization of a combined power and cooling cycle for low-grade and midgrade heat sources. Journal of Energy Resources Technology, 134, 2012.

MAN Diesel and Turbo. MAN Diesel and Turbo. Thermo Efficiency System for Reduction of Fuel Consumption and CO2 Emission; 2014. 2014.

V. Eyring, H. W. Khler, A. Lauer, and B. Lemper. Emissions from international shipping: 2. impact of future technologies on scenarios until 2050. Journal of Geophysical Research Atmospheres, 110 (D17), 2005.

Helder Lopes Ferreira, Raquel Garde, Gianluca Fulli, Wil Kling, and Joao Pecas Lopes. Characterisation of electrical energy storage technologies. Energy, 53:288–298, 2013.

Alessandro Franco and C. Casarosa. Thermodynamic and heat transfer analysis of lng energy recovery for power production. Journal of Physics: Conference Series 547, 2014.

Axel Friedrich, Falk Heinen, Fatumata Kamakaté, and Drew Kodjak. Air pollution and greenhouse gas emissions from ocean-going ships: Impacts, mitigation options and opportunities for managing growth. International Council on Clean Transportation (ICCT), 2007.

S.M. Mousavi G, Faramarz Faraji, Abbas Majazi, and Kamal Al-Haddad. A comprehensive review of flywheel energy storage system technology. Renewable and Sustainable Energy Reviews, 67: 477–490, 2017.

Siemens Power Generation. Waste heat recovery with organic rankine cycle technology-power generation with the siemens orc-module. Siemens Power Generation *http://www.energy.siemens.com/mx/pool/hq/power-generation/steam-turbines/downloads/brochure-orc-organic-Rankine-cycle-technology_EN.pdf*, 2014.

Hugo Trienko Grimmelius. Condition monitoring for marine refrigeration plants based on process models. TU Delft Doctoral Thesis, 2005.

Mirko Grljusic, Vladimir Medica, and Nikola Racic. Thermodynamic analysis of a ship power plant operating with waste heat recovery through combined heat and power production. Energies, 7: 7368–7394; doi:10.3390/en7117368., 2014.

Peter J. Hall and Euan J. Bain. Energy-storage technologies and electricity generation. Energy Policy, 36:4352–4355, 2008.

Raymond W. Harrigan and William B. Stine. Solar energy fundamentals and design: With computer applications. Wiley, 1985.

T.C. Hung, T.Y. Shai, and S.K. Wang. A review of organic rankine cycles (orcs) for the recovery of low-grade waste heat. Energy, 22(7):661–667, 1997.

T.C. Hung, S.K. Wang, C.H. Kuo, B.S. Pei, and K.F. Tsai. A study of organic working fluids on system efficiency of an orc using low-grade energy sources. Energy, 35:1403–1411, 2010.

H. Ibrahim, A. Ilinca, and J. Perron. Energy storage systems - characteristics and comparisons. Renewable and Sustainable Energy Reviews, 12:1221–1250, 2008.

Fernandez-Seara J, Vales A, and Vazquez M. Heat recovery system to power an onboard nh3-h2o absorption refrigeration plant in trawler chiller fishing vessels. Applied Thermal Engineering, 18: 1189–1205, 1998.

Yunli Jin, Naiping Gao, and Tong Zhu. The study of dynamic process of orc variable conditions based on control characteristics analysis. Energy Procedia, 129:208–215, 2017.

Stéphanie Jumel, Michel Feidt, Van Long Le, and Abdelhamid Kheiri. Working fluid selection and performance comparison of subcritical and supercritical organic rankine cycle (orc) for lowtemperature waste heat recovery. European Council for an Energy Efficient Economy, 4(086):559–569, 2012.

A.I. Kalina. Generation of energy by means of a working fluid, and regeneration of a working fluid. United States Patent 4346561, pages Filed date: Aug.31, 1982., 1982.

A.I. Kalina. Combined cycle and waste heat recovery power systems based on a novel thermodynamic energy cycle utilizing low-temperature heat for power generation. The American Society of Mechanical Engineers (ASME), pages 83–JPGC–GT–3, 1983.

A.I. Kalina. Combined-cycle system with novel bottoming cycle. Journal of Engineering for Gas Turbines and Power, 106:ASME. 737–42., 1984.

M. N. Karimi, A. Dutta, A. Kaushik, H. Bansal, and S. Z. Haque. A review of organic rankine, kalina and goswami cycle. International Journal of Engineering Technology, Management and Applied Sciences, 3:90–105, 2015.

Abdullah Kececiler, H. Ibrahim Acar, and Ayla Dogan. Thermodynamic analysis of the absorption refrigeration system with geothermal energy: an experimental study. Energy Conversion and Management, 41:37–48, 2000.

Mohammed Khennich and Nicolas Galanis. Optimal design of orc systems with a low-temperature heat source. Entropy, 14:370–389, 2012.

T. Kousksou, P. Bruel, A. Jamil, T. El Rhafiki, and Y. Zeraouli. Energy storage: Applications and challenges. Solar Energy Materials & Solar Cells, 120:59–80, 2014.

Ulrik Larsen, Leonardo Pierobon, Fredrik Haglind, and Cecilia Gabrielii. Design and optimisation of organic rankine cycles for waste heat recovery in marine applications using the principles of natural selection. Energy, 55:803–812, 2013.

Ulrik Larsen, Oskar Sigthorsson, and Fredrik Haglind. A comparison of advanced heat recovery power cycles in a combined cycle for large ships. Energy, 74:260–268, 2014.

H. Lindstad and S. Sandaas. Emission and fuel reduction for offshore support vessels through hybrid technology. In: Conference Proceedings at Society of Naval Architects and Marine Engineers (SNAME) Annual Convention, 20-25 October 2014, Houston, USA., 2014.

Haakon Lindstad. Maritime shipping and emissions: A three- layered, damage-based approach. Ocean Engineering, 110:94–101, 2015.

Bo-Tau Liu, Kuo-Hsiang Chien, and Chi-Chuan Wang. Effect of working fluids on organic rankine cycle for waste heat recovery. Energy, 29:1207–1217, 2004.

Xing Luo, Jihong Wang, Mark Dooner, and Jonathan Clarke. Overview of current development in electrical energy storage technologies and the application potential in power system operation. Applied Energy, 137:511–536, 2015.

Pedro J. Mago, Louay M. Chamra, Kalyan Srinivasan, and Chandramohan Somayaji. An examination of regenerative organic rankine cycles using dry fluids. Applied Thermal Engineering, 28:998–1007, 2008.

MARPOL. Review of MARPOL Annex VI and the NOx Technical Code. Sub-Committee on Bulk Liquids and Gases (IMO) 12th Session Agenda Item 6, 2007.

Kevin Merlin, Jérôme Soto, Didier Delaunay, and Luc Traonvouez. Industrial waste heat recovery using an enhanced conductivity latent heat thermal energy storage. Applied Energy, 183:491–503, 2016.

Marcelo Gustavo Molina. Chapter 4: Dynamic modelling and control design of advanced energy storage for power system applications. Dynamic Modelling. ISBN 978-953-7619-68-8, 2010.

Michael J. Moran and Howard N. Shapiro. Fundamentals of engineering thermodynamics. 5th Edition, pages 325–372., 2004.

Tuong-Van Nguyen, Thomas Knudsen, Ulrik Larsen, and Fredrik Haglind. Thermodynamic evaluation of the kalina split-cycle concepts for waste heat recovery applications. Energy, 71:277–288, 2014.

Knut Erik Nielsen and Marta Molinas. Superconducting magnetic energy storage (smes) in power systems with renewable energy sources. IEEE International Symposium on Industrial Electronics, pages 2487–2492, 2010.

M.L. Parry, O.F. Canziani, J.P. Palutikof, P.J. van der Linden, and C.E. Hanson. Ipcc (2007) climate change 2007: Impacts, adaptation and vulnerability. Report of the Intergovernmental Panel on Climate Change, page Contribution of Working Group II to the Fourth Assessment, 2007.

Ram Darash Patel and Priti Shukla. Thermodynamics analysis and optimization for a combined power and refrigeration cycle. International Journal of Research in Aeronautical and Mechanical Engineering, 1(7):267–273, 2013.

Sylvain Quoilin, Martijn Van Den Broek, Sebastien Declaye, Pierre Dewallef, and Vincent Lemort. Techno-economic survey of organic rankine cycle (orc) systems. Renewable and Sustainable Energy Reviews, 22:168–186, 2013.

N. A. Rayner, P. Brohan, D. E. Parker, C. K. Folland, J. J. Kennedy, M. Vanicek, T. J. Ansell, and S. F. B. Tett. Improved analyses of changes and uncertainties in sea surface temperature measured in situ since the mid-nineteenth century: The hadsst2 data set. Journal of Climate, 19:446–469., 2006.

S. B. Riffat and Xiaoli Ma. Thermoelectrics: a review of present and potential applications. Applied Thermal Engineering, 23:913–935, 2003.

Kasper De Ruyck. Simulation of advanced engine room configurations with energy saving concepts. TU Delft Master Thesis, 2011.

Andrea Saltelli. Sensitivity analysis for important assessment. Risk Analysis, 22(3):579–590, 2002.

Heinrich Schmid. Waste heat recovery (whr): fuel savings with less emissions. Proceedings of the Green Ship Technology Conference, London, page Wartsila Corporation, 2004.

Gequn Shu, Youcai Liang, Haiqiao Wei, Hua Tian, Jian Zhao, and Lina Liu. A review of waste heat recovery on two-stroke ic engine aboard ships. Renewable and Sustainable Energy Reviews, 19: 385–401., 2013.

Dig Vijay Singh and Eilif Pedersen. A review of waste heat recovery technologies for maritime applications. Energy Conversion and Management, 111:315–328., 2016.

S. Solomon, D. Qin, M. Manning, Z. Chen, M. Marquis, K.B. Averyt, M. Tignor, and H.L. Miller. Ipcc (2007) climate change 2007: The physical science basis. Report of the Intergovernmental Panel on Climate Change [Summary for Policymakers], page Contribution of Working Group I to the Fourth Assessment, 2007.

Charles Sprouse and Christopher Depcik. Review of organic rankine cycles for internal combustion engine exhaust waste heat recovery. Applied Thermal Engineering, 51:711–722, 2013.

Douwe Stapersma. Diesel engines. NLDA and TUDelft, Volume 3(Chapter 13), 2010.

Wenqiang Sun, Xiaoyu Yue, and Yanhui Wang. Exergy efficiency analysis of orc (organic rankine cycle) and orc-based combined cycles driven by low-temperature waste heat. Energy Conversion and Management, 135:63–73, 2017a.

Zhixin Sun, Feng Wang, Shujia Wang, Fuquan Xu, and Kui Lin. Performance analysis of different orc configurations for thermal energy and lng cold energy hybrid power generation system. Earth and Environmental Science, 52:012024, 2017b.

Dr. Pieter Tans. Global monitoring division. Earth System Research Laboratory (ESRL) of National Oceanic & Atmospheric Administration (NOAA), page http://www.esrl.noaa.gov/gmd/ccgg/trends/; ftp://aftp.cmdl.noaa.gov/products/trends/co2/co2_gr_mlo.txt, 2016.

María Uris, José Ignacio Linares, and Eva Arenas. Techno-economic feasibility assessment of a biomass cogeneration plant based on an organic rankine cycle. Renewable Energy, 66:707–713, 2014.

H. van Putten and P. Colonna. Dynamic modeling of steam power cycles: Part ii- simulation of a small simple rankine cycle system. Applied Thermal Engineering, 27:2566–2582, 2007.

E.H. Wang, H.G. Zhang, B.Y. Fan, M.G. Ouyang, Y. Zhao, and Q.H. Mu. Study of working fluid selection of organic rankine cycle (orc) for engine waste heat recovery. Energy, 36:3406–3418, 2011.

S.G. Wang and R.Z. Wang. Recent developments of refrigeration technology in fishing vessels. Renewable Energy, 30:589–600, 2005.

Z. Q. Wang, N. J. Zhou, J. Guo, and X. Y. Wang. Fluid selection and parametric optimization of organic rankine cycle using low temperature waste heat. Energy, 40:107–115, 2012.

Wärtsilä. Product Guide Wartsila 50DF - 1/2012. WARTSILA Engines *http://www.wartsila-hyundai.com/data/project_guide/Project_guide3.pdf*, 2012.

Feng Xu, D. Yogi Goswami, and Sunil S. Bhagwat. A combined power/cooling cycle. Energy, 25: 233–246, 2000.

Haoshui Yu, Xiao Feng, , and Yufei Wang. Working fluid selection for organic rankine cycle (orc) considering the characteristics of waste heat sources. Industrial and Engineering Chemical Research, 55(5):1309–1321, 2016.

Jun Yuan, Szu Hui Ng, and Weng Sut Sou. Uncertainty quantification of co2 emission reduction for maritime shipping. Energy Policy, 88:113–130., 2016.

Xinxin Zhang, Maogang He, and Ying Zhang. A review of research on the kalina cycle. Renewable and Sustainable Energy Reviews, 16:5309–5318., 2012.